

7-259
D1-91
N 87-25256

INTRODUCTION

A broad range of channel and valley features are displayed on the surface of Mars. There is as great a range in morphology as in scale, from huge macro- and smaller meso-scale outflow channels such as Kasei Vallis and Ladon Valles respectively, to small scale valley networks such as Nirgal Vallis and Parana/Loire Valles. The Margaritifer Sinus quadrangle of Mars contains examples of all these types of systems, and has one of the best integrated and highest concentrations of valley networks on the entire planet (Carr 1979a; 1980b; Pieri 1979; Baker 1982). The quadrangle also displays a variety of other interesting geologic and geomorphic features, such as etched, chaotic and fretted terrain; ancient multi-ringed impact basins (Schultz et al. 1982b); possible relict polar deposits (Schultz 1984); ancient heavily cratered uplands; and smooth plains that display various crater densities.

Several possible Earth analogs have been examined in an effort to explain the origin of the various different scale channels seen of the Martian surface. The morphology and scale of the Channeled Scabland in eastern Washington is strikingly similar to the Martian outflow channels (Baker 1982). A catastrophic flood hypothesis similar in effect to that which formed the Channeled Scabland has been evoked as one possible mechanism for the creation of the outflow channels (Baker 1982; Murray et al. 1981; Carr 1979b; 1981; Masursky 1973). Boothroyd and Timson (1983) showed that braided rivers on the Arctic North Slope that frequently switch active channels, due to ice jams during ice drives, can result in morphologic features similar to those found within Martian meso-scale outflow channels such as Ladon Valles.

The smaller valley networks are the most diverse and least studied of the channel and valley features (Baker 1982). Several different theories have attempted to explain their formation, ranging from lava erosion (Carr 1974) to rainfall and surface runoff at an earlier time in Martian history (Masursky 1973; Masursky et al. 1977). Many workers (Sharp and Malin 1975; Sagan and Pieri 1979; Mutch et al. 1976; Carr 1979a; 1980a; 1981; Carr and Clow 1981; Pieri 1980a; 1980b; Murray et al. 1981; Baker 1982; Laity 1985; Laity and Pieri 1980; Mars Channel Working Group 1983; Higgins 1982; 1984) now feel that a combination of wet-sapping and resultant downstream fluvial action, after Sharp and Malin (1975), were the most probable formative processes.

The purpose of this paper is to: 1) present a larger scale (1:2,000,000), more detailed geologic map of the Margaritifer Sinus quadrangle than presently exists (Saunders 1979); 2) use crater counts and cross-cutting

relationships to consider the timing of various channel and valley forming events, their drainage basin evolution, and the interplay and relationship of the channels and valleys to each other and other geomorphic features in the quadrangle; 3) use crater counts to determine when peak periods of geomorphic and tectonic activity occurred in the region; 4) advance the theory of valley network formation through wet-sapping and downstream fluvial action by providing a detailed, quantitative and qualitative study of their drainage basins, densities, morphology and geologic setting, and comparing them to terrestrial drainage systems formed by similar processes; 5) develop a reasonable hypothesis for the geologic/geomorphic evolution of the quadrangle.

PHYSICAL SETTING

Location and Description

The Margaritifer Sinus quadrangle is located at the eastern end of Valles Marineris, approximately 1000 km NE of Argyre Planitia, between 0° and 30°S, 0° and 45°W (Fig. 1). The quadrangle is located within a broad trough known as the Chryse Lowland (Frey 1974; Saunders 1979), and has a distinct northward slope (Fig. 2). Surface materials consist mainly of heavily cratered terrain and intercrater or smooth plains (Mutch et al. 1976; Scott and Carr 1978; Saunders 1979), two of the older units on the Martian surface (Scott and Carr 1978; Saunders 1979; Murray et al. 1981). The quadrangle includes: (1) some of the best integrated and highest concentrations of valley networks on the planet (eg Samara, Parana/Loire Valles in the SE quadrangle) (Carr 1979a; 1980b; Baker 1982); (2) Eos Chasma (12S, 39W) and Capri Chasma (8S, 40W), marking the eastern end of Valles Marineris; (3) several meso-scale outflow channels, Ladon, Uzboi and Margaritifer Valles (22S, 28W); (4) Chaotic terrain (many locations) and fretted terrain (3S, 20W); (5) several ancient multi-ringed impact basins (Schultz and Glicken 1979; Saunders 1979); and (6) possible ancient polar deposits (Schultz 1984).

Physical Processes

The Margaritifer Sinus quadrangle is presently undergoing only minor morphologic modifications resulting mainly from eolian (Carr 1981; 1984; Greeley et al. 1982; Murray et al. 1981), cratering and mass movement events. A wide range of processes, including tectonism, cratering, volcanism, and channeling, have operated within the quadrangle at a much greater rate and scale in the past (Saunders 1979; Neukum and Hiller 1981; Schultz et al. 1982; Scott and Carr 1978). The result is that features formed at a relatively early period in the history of the planet can still be observed and studied today.

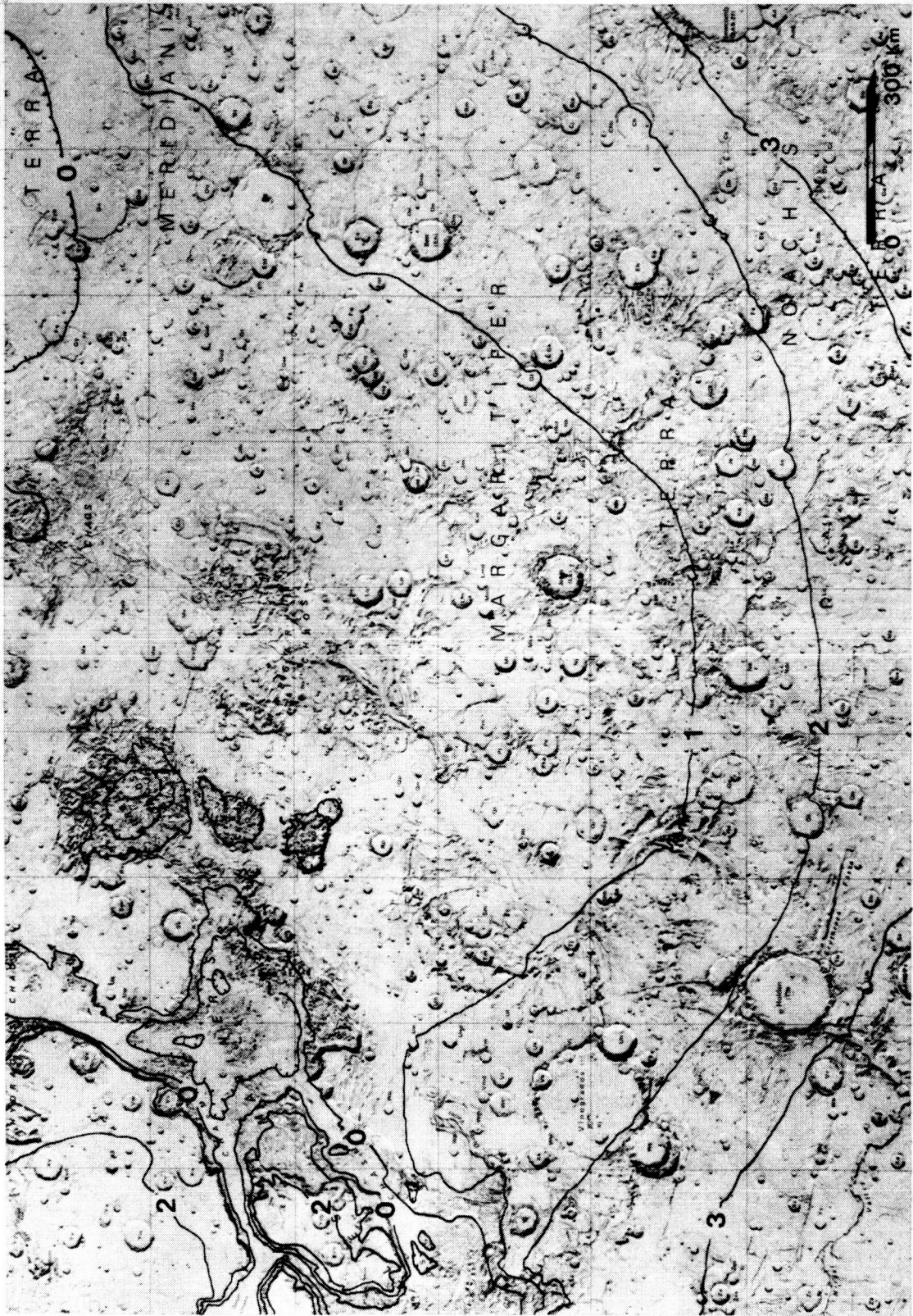
Fig. 1. Simplified geologic map of Mars between 65N and 65S showing the location of the Margaritifer Sinus quadrangle, selected channels, and other major features. Map modified from Baker (1982).

Fig. 2. Shaded relief map of Margaritifer Sinus with contours illustrating the distinct northward slope of the region and convergence towards the center of the quadrangle along the axis of the Chryse lowland trough. Contours from the topographic map of the Margaritifer Sinus quadrangle (USGS 1976). The contour interval is 1 km.

ORIGINAL PAGE IS
OF POOR QUALITY

M 58 15 22 R, 1960
1:250,000 (19)

Prepared for the
NATIONAL AERONAUTICS AND SPACE ADMINISTRATION
North



METHODS

Using approximately 400, mainly orthographic, Viking Orbiter Image negatives of the study area, contact prints were made to determine negative quality and precise location. All but the poorest quality were then printed to a scale of 1:2,000,000 and stereo pairs were selected. Certain high resolution sequences (about 50 m/pixel) were printed to a scale of 1:500,000 and assembled into mosaics. High quality negatives (200 m/pixel) of the area surrounding Samara and Parana/Loire Valles, in the Margaritifer Sinus SE and Argyre NE quadrangles, were printed to a scale of 1:1,000,000 and assembled into a mosaic. All of the above were then used in conjunction with published 1:2,000,000 photomosaics (USGS 1979a; 1979b; 1979c; 1979d; 1979e), and 1:5,000,000 geologic (Saunders 1979), shaded relief (USGS 1975; 1980), and topographic (USGS 1976) maps of the region to complete the 1:2,000,000 geologic map of the quadrangle. All work completed in the area since it was mapped by Saunders (1979), (Carr 1979b; 1980a; 1980b; Schultz and Glicken 1979; Shultz and Lutz-Garihan 1982; Schultz 1984; Pieri 1980a; Boothroyd 1983; Boothroyd and Grant 1984; 1985; Grant and Boothroyd 1984; Parker and Pieri 1985a; 1985b) was incorporated into the map. Methods employed for mapping were after Baker and Kochel (1979), Saunders (1979), Baker (1980a; 1980b; 1982), Boothroyd and Timson (1981), and Wise (1979).

Stereo pairs used for geologic mapping were also used to delineate drainage basin boundaries, after Boothroyd (1982). Work began in the Margaritifer Sinus SE and Argyre NE quadrangles along a major N-S trending basin boundary located at 9W (Boothroyd and Grant 1984), and extended towards the NW, encompassing all of Samara and Parana/Loire Valles, their associated sub-basins and internal-basins. Work continued westward to the Margaritifer Sinus SW quadrangle, mapped by Boothroyd (1982). A Bausch and Lomb zoom stereoscope was used for the mapping. The areas of the drainage basins were then measured using a polar planimeter and a table digitizer. All valley lengths visible within the basins at 1:1,000,000 scale and 200m/pixel resolution were measured using a table digitizer. Drainage densities, for Samara and Parana/Loire Valles, sub-basins, internal-basins, and selected areas within the drainage basins, were calculated and compared to values obtained for other Martian systems (Baker 1985) and terrestrial systems (Gregory and Gardiner 1975; Abrahams 1984). A further comparison, based on morphology, density, and geologic setting was made to terrestrial systems formed mainly by sapping processes (Higgins 1974; 1982; D'Amore 1983; 1984; Laity 1985; Laity and Pieri 1980; Pieri, Malin and Laity 1980).

1:1,000,000 and 1:2,000,000 photographs, various orthographic negatives, stereo pairs and crater counts were

used to determine the relative ages of units surrounding/covering Samara/Parana/Loire Valles, Margaritifer Chaos (10S, 21W), and Ladon Basin (18S, 30W). The possibility of flow out of Samara and Parana/Loire and the Ladon Basin into/through the Margaritifer Chaos was also examined in this manner.

After consideration of many papers concerning various approaches to methods of crater counting and the presentation of results (Hartmann 1965; 1969; Marcus 1968; Chapman et al. 1969; Murray et al. 1971; Soderblom et al. 1974; McGill 1977; McGill and Wise 1972; Crater Analysis Techniques Working Group 1978; Masursky et al. 1980; Neukum and Wise 1976; Neukum and Hiller 1981; Neukum et al. 1979; Hiller and Neukum 1979; 1980; Wise 1984; 1985; Wise and Milkowski 1980; Wise et al. 1979; Wise, personal communication 1984) the D.U. Wise method of dating local surfaces was chosen to complete the crater counts. This method utilizes small, homogeneous crater populations and is described fully in Appendix 1. The relative ages of surfaces are presented as the cumulative number of craters $\geq 1 \text{ km} \cdot 10^6 \text{ km}^{-2}$, derived by comparison to the standard curve of Neukum and Hiller (1981). Absolute ages were derived from the Lunar cratering vs. age curve (Neukum and Hiller 1981). The counts were completed using a table digitizer linked to a DEC VAX 11/780 computer at the Lunar and Planetary Institute, Houston, TX.. A program called 'STAMMER' written by Brian Fessler at the Lunar and Planetary Institute, was used for calculation of cumulative crater/size frequency plots (Appendix 2). Plots were obtained on a Digital VT 125 graphics terminal, and compared to the standard curve to obtain relative ages for the various surfaces. Edits and final copies of the plots were made using an updated version of the 'STAMMER' program (Appendix 2). The updated version was designed to run on a Prime/850 computer and a CalComp 1051 plotter at the University of Rhode Island Computer Center was used to plot the final cumulative crater size-frequency curves.

RESULTS

Geologic/Geomorphic Mapping

On the basis of its high valley network density and overall geomorphic diversity, the Margaritifer Sinus quadrangle was selected as the site for this study. A detailed geologic/geomorphic map of the entire quadrangle was completed at a scale of 1:2,000,000 (Figs. 3a-d). For the purposes of this paper, the map has been reduced and divided into quarters. A copy of the original map, in the form of a clear overlay and at a scale of 1:2,000,000, can be obtained from the author. The map explanation is presented in Table 1.

Relative ages have been assigned to selected surfaces within the quadrangle based on 102 crater counts completed (Table 2, Figs. 4a-d, a reduced version of the original 1:2,000,000 Fig., shows crater count locations). The individual crater counts are presented in Appendix 3 and a summary of all results is given in Figure 5. The results of the crater counts were used, where possible, to help define and correlate units and to locate contacts. The map unit correlation is shown in Figure 6. Relative ages are always given as the cumulative number of craters $>1\text{km} \cdot 10^6 \text{ km}^{-2}$ obtained by projection of the Neukum and Hiller Martian standard curve (1981). Tentative absolute ages have been assigned by simple comparison with the lunar standard curve. An introduction to, and general description of, the various units and terrain types described below can be found in Mutch et al. (1976), Murray et al. (1981), and Baker 1982.

Description of Units

Channel Features

Channels and Valley Networks (Ch)-Examples of varying scale include: macro-scale features such as Eos and Capri Chasma (see USGS 1980); meso-scale outflow channels, Uzboi and Ladon Valles (see USGS 1980); and various valley networks ranging in size and morphology from Nirgal Vallis to Parana/Loire Valles (see USGS 1980) to numerous small, poorly-integrated valley features found throughout the quadrangle.

Morphological descriptions of Eos and Capri Chasma can be found in Boothroyd and Timson (1981), Baker (1982), and Carr (1981; 1984). Descriptions of the meso-scale features, Uzboi and Ladon Valles are found in Florenski et al. (1975), Carr (1979b), Carr and Clow (1981), Pieri (1980a), Boothroyd (1983), Parker and Pieri (1985a; 1985b), and later in this paper. A further description of these features is not presented here.

Figs. 3a-d. Geologic/Geomorphic map of MC19. Approximately one quarter of the quadrangle is displayed in each of 3a-d: MC19NW in 3a; MC19SW in 3b; MC19SE in 3c; and MC19NE in 3d. The map explanation is given in Table 1. A copy of the original map at 1:2,000,000 can be obtained from the author.

Fig. 3a

FIG 3 GEOLOGIC/GEOMORPHIC MAP OF MARGARITIFER SINUS
SEE TABLE 1 FOR MAP EXPLANATION

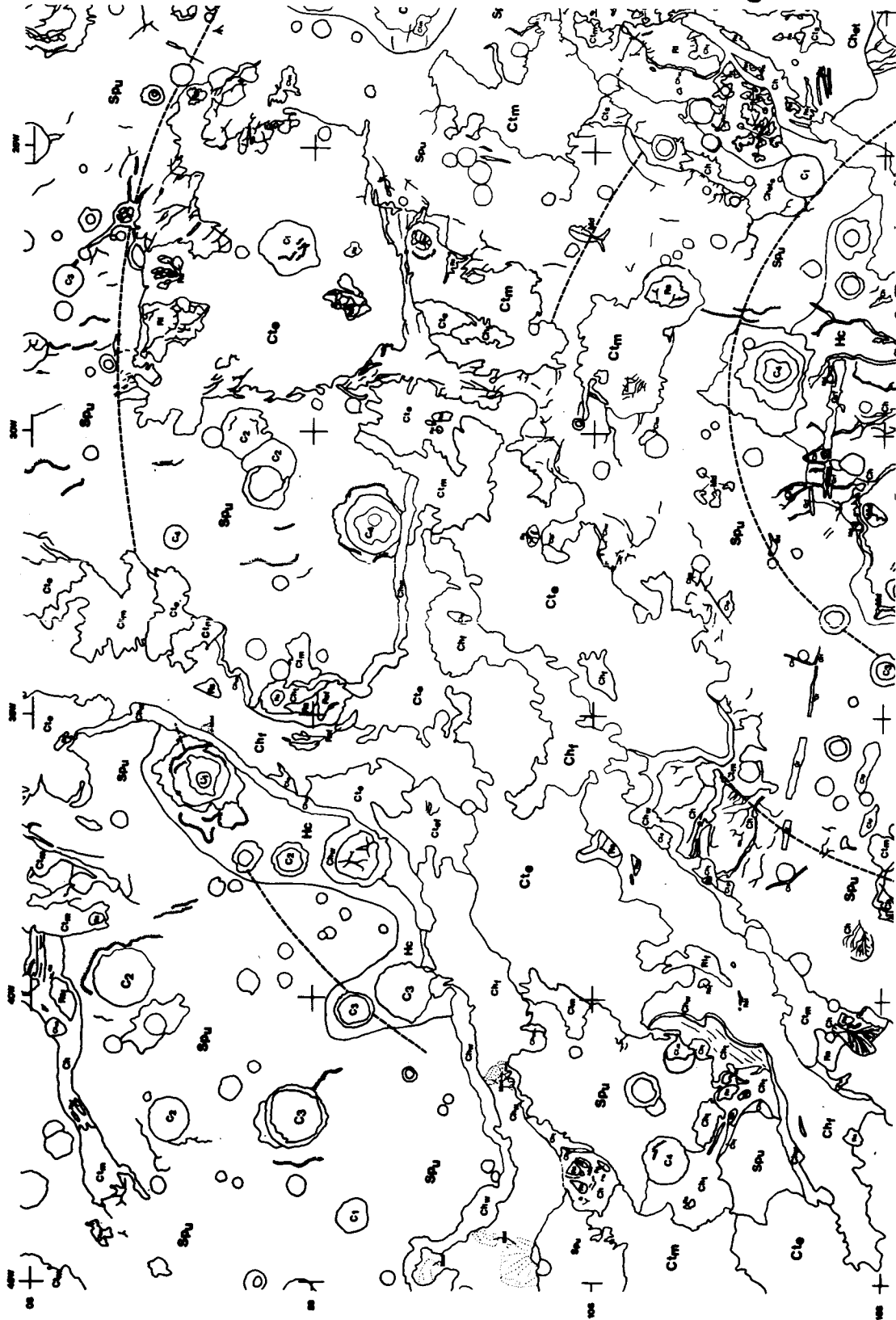


Fig. 3b

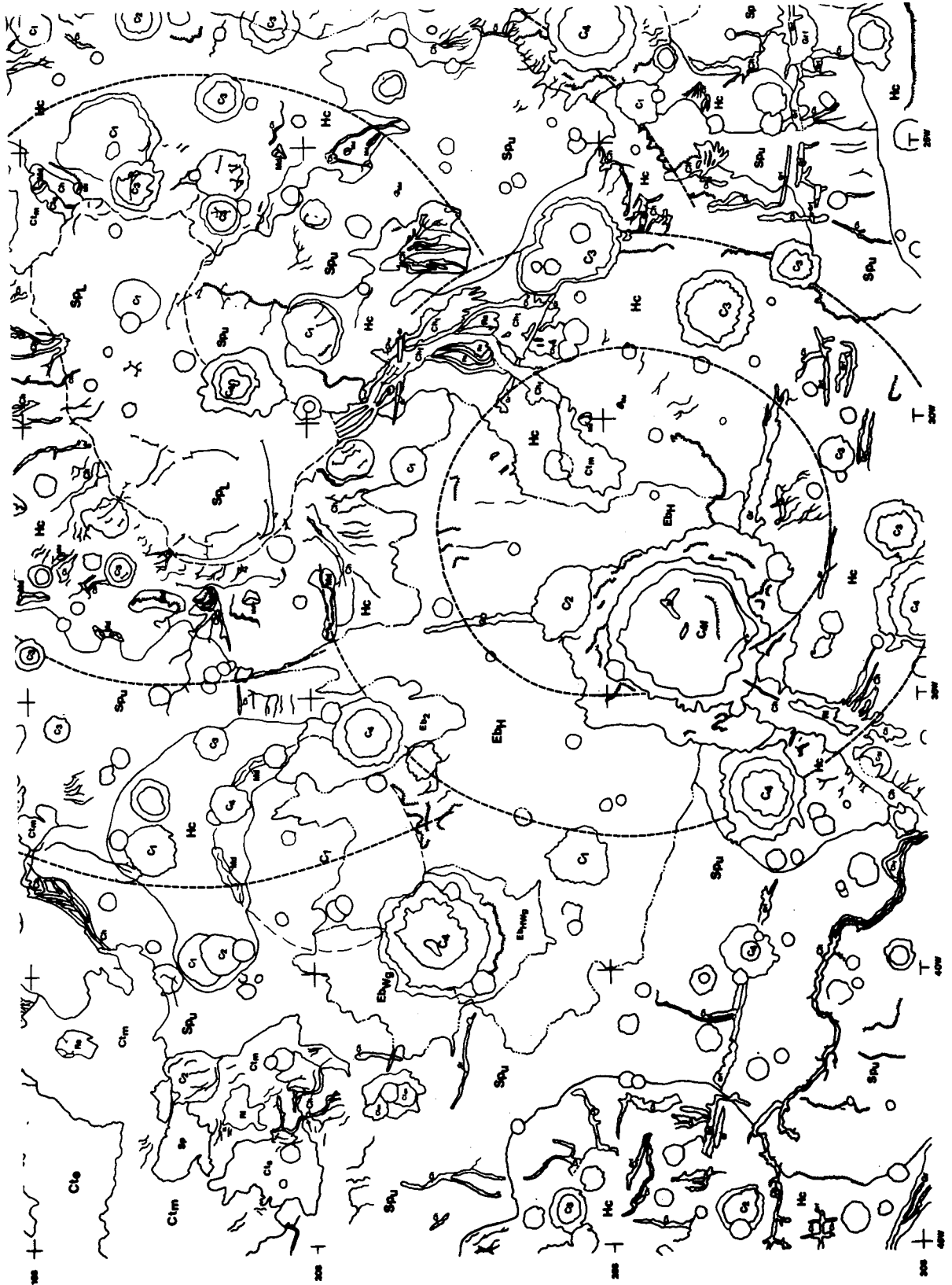


Fig. 3c

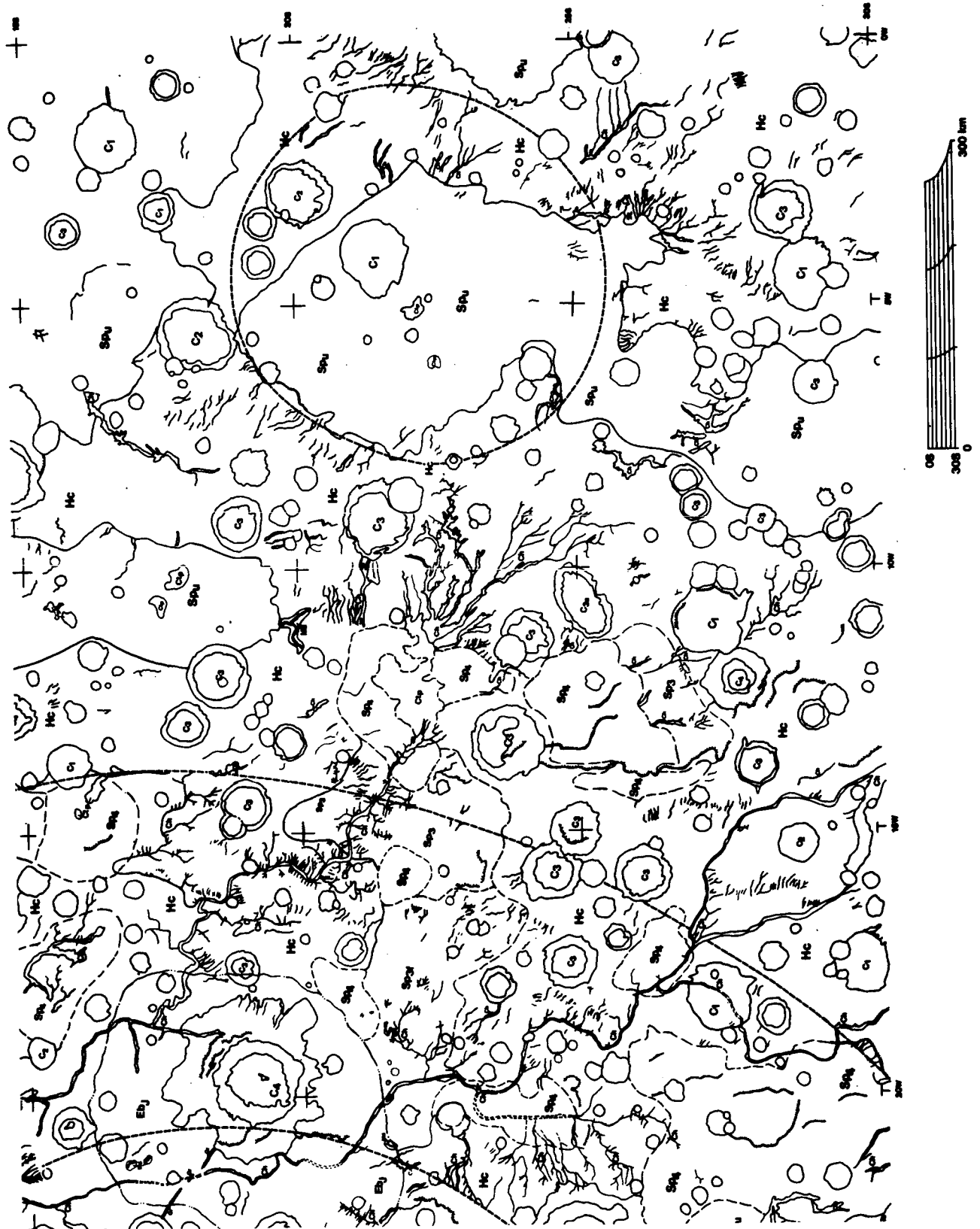


TABLE 1
GEOLOGIC/GEOMORPHIC MAP EXPLANATION

CHANNELS AND VALLEYS

- Ch Valley networks and channel features
Small valley networks
- Ch_w Channel walls
- Ch_f Channel floor
- Ch_t Terraces
- R_l Remnants, large
- R_s Remnants, small
- R_l_f Remnants, large, flow modified
- R_s_f Remnants, small, flow modified

CHAOTIC TERRAIN

- Ct_e Extreme collapse
- Ct_m Moderate collapse
- Ct_s Slight collapse
- Ct_p Positive relief chaotic deposits
- Ct_f Fretted terrain

SMOOTH PLAINS DEPOSITS

- Sp₄ Fourth resurfacing event (6000-2000)
- Sp₃ Third resurfacing event (14,000-8100)
- Sp_u Smooth plains, undifferentiated
- Sp_L Floor of Ladon Basin
- Sp_f Smooth plains, grooved
- Sp_p Relict polar deposits

CRATERS

- C₄ Youngest, fresh
- C₃ Subdued
- C₂ Degraded
- C₁ Extremely degraded
- C_f Craters, flow modified
- C_J Jones crater
- C_H Holden crater
- E_b Ejecta blanket, as labelled

MULTI-RINGED BASINS AND HEAVILY CRATERED TERRAIN

- Hc Hilly and heavily cratered terrain
-  Ancient multi-ringed impact basins (AMIB)
- Md Mount material

OTHER FEATURES

- Gr Grabens
- Gr_f Grabens, flow modified
-  Ridges
- Ed Eolian deposits (mantled areas and dunes)
- Mml Mass movement deposits
-  Fractures

Table 2.-- CRATER COUNTS: location, age and quality
(count refers to the image or photomosaic derived from)

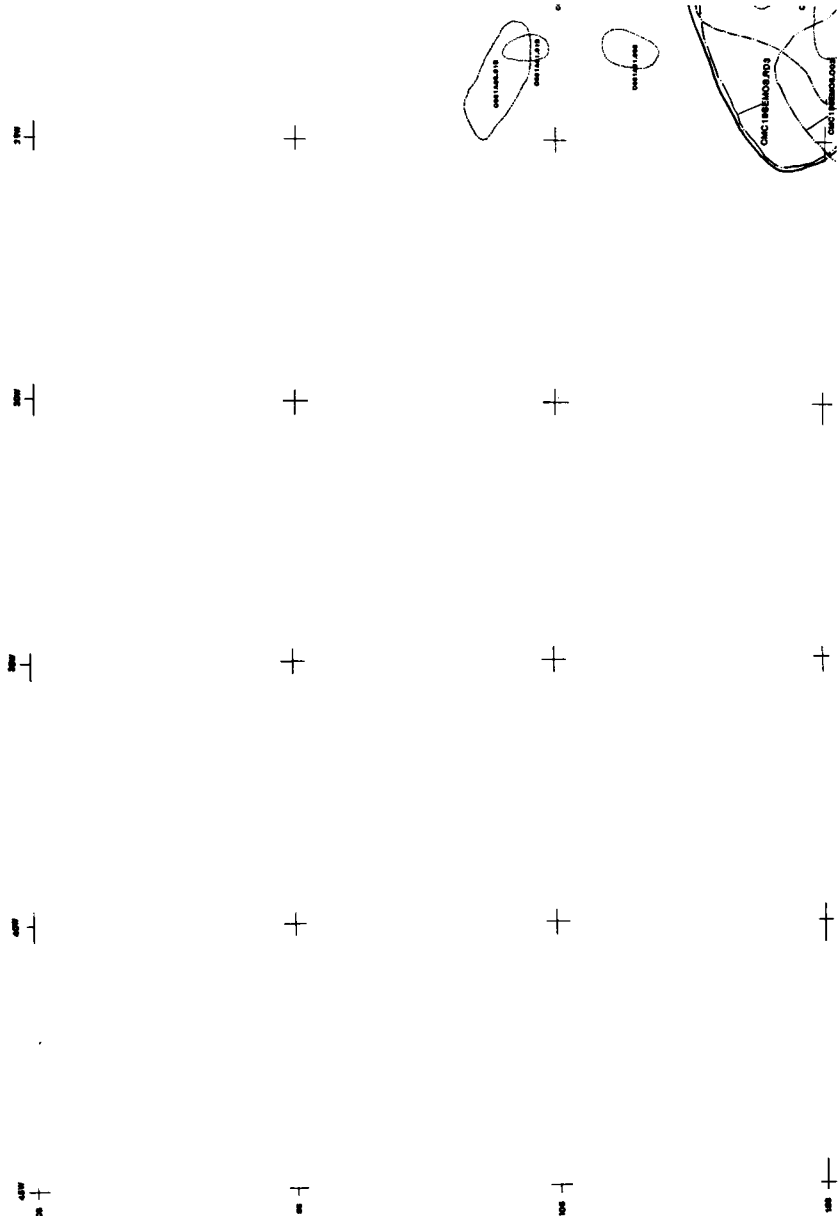
Crater Count	Location		Relative age (# >1km/10 ⁶ km ²)	Count quality	Number of Craters
	S Lat	W Long			
C084A38.001	28.5	21	5500	GOOD	18
C084A38.002	29	22	12500	FAIR	5
C084A39.01B	30	20.5	2000	GOOD	12
C084A39.01C	29	21	1600	GOOD	13
C084A40.01B	27	21	5400	FAIR	10
C084A40.002	27	18	3300	POOR	10
C084A40.003	27	21	3500	GOOD	12
C084A40.004	26	20	4000	POOR	9
C084A40.005	29	20	2200	POOR	20
C084A42.001	26	18	8700	GOOD	8
C084A42.01B	26	18	2600	GOOD	14
C084A42.02B	27	17	5200	POOR	10
C084A43.001	27	13.5	2500	POOR	22
C084A43.01B	26	3	4900	FAIR	10
C084A45.01B	25	13	3950	FAIR	15
C084A45.002	27	11	9000	FAIR	7
C084A45.02B	27	12	13800	FAIR	7
C084A46.016	22	13	5200	GOOD	11
C084A46.01D	22	14	10800	FAIR	7
C084A46.01E	21	13	10000	FAIR	8
C084A46.02B	23	13	12500	POOR	6
C084A47.01B	24	8	11500	POOR	28
C084A47.002	25	7.5	9500	FAIR	9
C084A47.02B	24	8.5	9000	POOR	15
C084A47.003	23	11	9500	POOR	15
C451A06.001	3	17	10000	POOR	5
C451A06.002	1N	17	6000	POOR	8
C451A07.001	2N	17	7000	POOR	4
C451A07.01B	2N	17	5000	POOR	5
C451A08.001	4	18	8000	POOR	6
C615A24.001	10	22	7100	POOR	9
C615A24.002	11	21	9000	POOR	8
C615A42.001	19	21	3400	POOR	4
C615A42.01B	20	22	3000	POOR	8
C615A43.001	21	18	3000	POOR	13
C615A43.002	23	18	10000	FAIR	11
C615A46.001	16	15	34000	POOR	5
C615A46.002	15	15	10000	FAIR	13
C615A46.003	17	14	5800	FAIR	7
C650A13.001	17	31	8500	POOR	7
C650A13.002	18	28	8900	POOR	18
C650A13.003	15.5	28	11000	POOR	18
C650A13.004	16	27	6200	POOR	15
C651A61.01B	9	23	7000	FAIR	6
C651A61.002	11	23	6700	FAIR	10
C651A63.001	14	22	4600	POOR	9
C651A63.01B	15	23	9000	GOOD	11
C651A64.001	16	27	10500	GOOD	7
C651A64.02B	16	25	8500	FAIR	9

Table 2 (cont'd)

C651A67.001	23	15	16000	FAIR	10
C651A67.002	22	18	7000	FAIR	8
C651A68.001	24	22	9000	FAIR	12
C651A68.002	25	21	9800	POOR	6
C651A85.001	10	21	5500	GOOD	7
C651A85.002	9	18	5000	FAIR	15
C651A86.01B	9	23	2375	POOR	5
C651A86.002	10	21	5000	POOR	8
C651A87.001	12	16	105000	POOR	111
C651A87.01B	13	16	110000	FAIR	17
C651A87.002	15	17	3100	FAIR	21
C651A87.003	14	15	13900	FAIR	29
C651A92.001	23	15	9000	POOR	23
CNC19SEMOS.001		MC19SE	8700	FAIR	64
CNC19SEMOS.002	16	23	11000	POOR	20
CNC19SEMOS.003	14	18	15300	POOR	8
CNC19SEMOS.004	22	23	10100	POOR	21
CNC19SEMOS.005	28	20	10000	FAIR	29
CNC19SEMOS.006	23	15	9500	FAIR	13
CNC19SEMOS.007	22	19	11000	POOR	9
CNC19SEMOS.008	25	6	11500	FAIR	6
CNC19SEMOS.009	20	10	9100	FAIR	16
CNC19SEMOS.010	25	10	10000	POOR	18
CNC19SEMOS.011	35	10	14000	FAIR	8
CNC19SEMOS.012	34	15	20000	POOR	10
CNC19SEMOS.013	34	7	11000	FAIR	10
CNC19SEMOS.014	31	7	15500	POOR	7
CNC19SEMOS.015	32	12	10000	POOR	12
CNC19SEMOS.016	29	13	10000	FAIR	28
CNC19SEMOS.017	31.5	18	11700	GOOD	13
CNC19SEMOS.018	28	16	12300	POOR	10
CNC19SEMOS.BK1	16	15	50000	GOOD	6
CNC19SEMOS.BK2	20	12	56000	POOR	8
CNC19SEMOS.BK3	25	9	48000	POOR	10
CNC19SEMOS.BK4	14	22	41000	POOR	12
CNC19SEMOS.BK5	22	22	47000	POOR	6
CNC19SEMOS.BK6	29	16	57000	FAIR	20
CNC19SEMOS.BK7	34	11	65000	POOR	9
CNC19SEMOS.BK8	27	21	40000	POOR	21
CNC19SEMOS.BK9	21	16	43000	FAIR	11
CNC19SEMOS.BK0	18	22	67000	POOR	7
CNC19SEMOS.BU1		MC19SE	120000	FAIR	18
CNC19SEMOS.BU2		MC19SE	92000	FAIR	26
CNC19SEMOS.BU3	18	22	170000	POOR	7
CNC19SEMOS.BU4	34	14	220000	GOOD	7
CNC19SEMOS.BU5	28	9	170000	POOR	26
CNC19SEMOS.BR1	18	12	1000000	GOOD	7
CNC19SEMOS.BR2	28	16	950000	FAIR	17
CNC19SEMOS.BR3	34	7	1000000	GOOD	7
CNC19SEMOS.BR4	18	22	850000	FAIR	9
CNC19SEMOS.RD1	27	10	300000	GOOD	39
CNC19SEMOS.RD2	26	20	198000	GOOD	16
CNC19SEMOS.RD3	16	19	210000	GOOD	18

Figs. 4a-d. Crater count locations in MC19. Approximately one quarter of the quadrangle is displayed in each of 4a-d: MC19NW in 4a; MC19SW in 4b; MC19SE in 4c; and MC19NE in 4d. The map explanation is given at the bottom of Fig. 4b. A copy of the original diagram at 1:2,000,000 can be obtained from the author.

FIG. 4 CRATER COUNT LOCATIONS



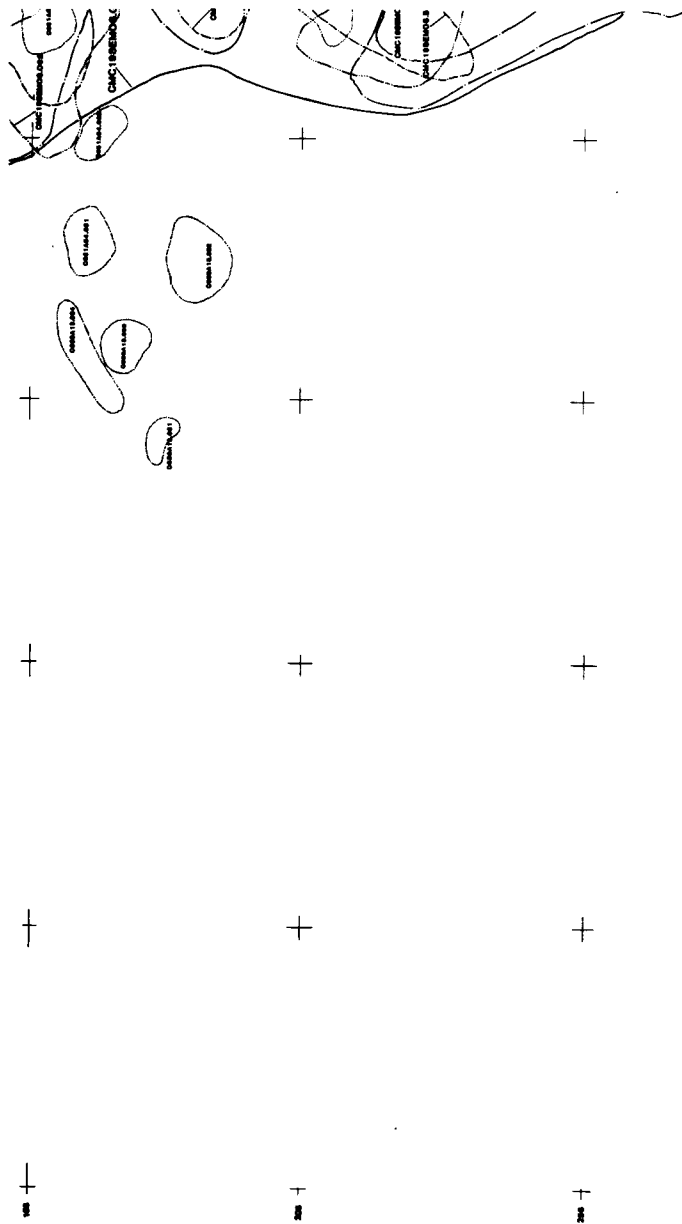
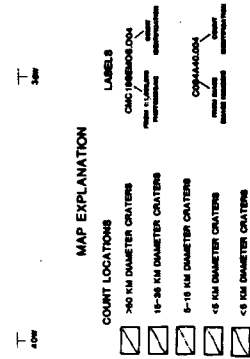
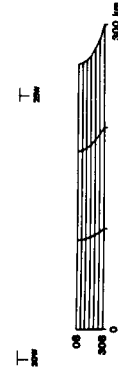


Fig. 4b



ORIGINAL PAGE IS
OF POOR QUALITY

ORIGINAL PAGE IS
OF POOR QUALITY

Fig. 4c

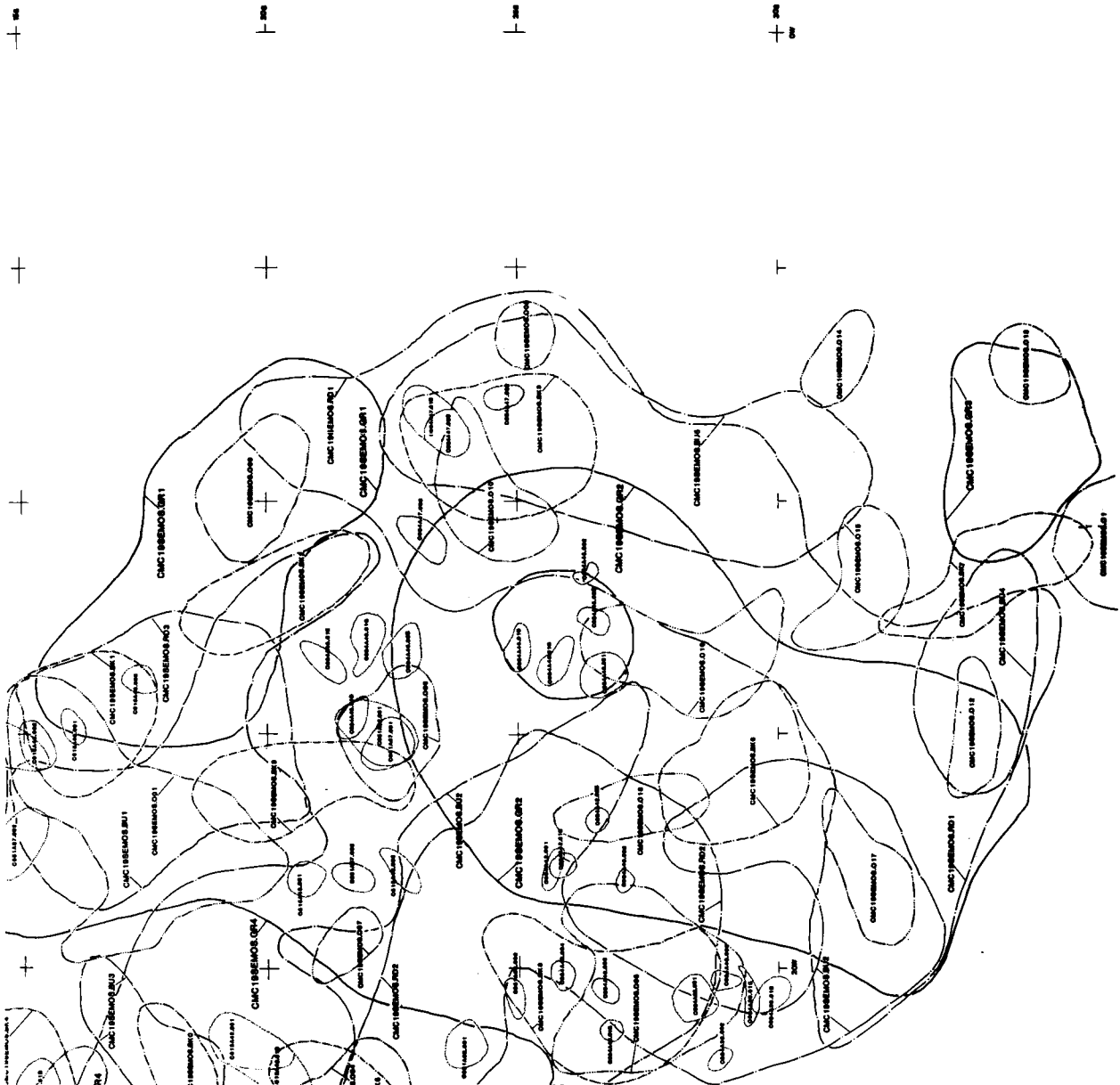
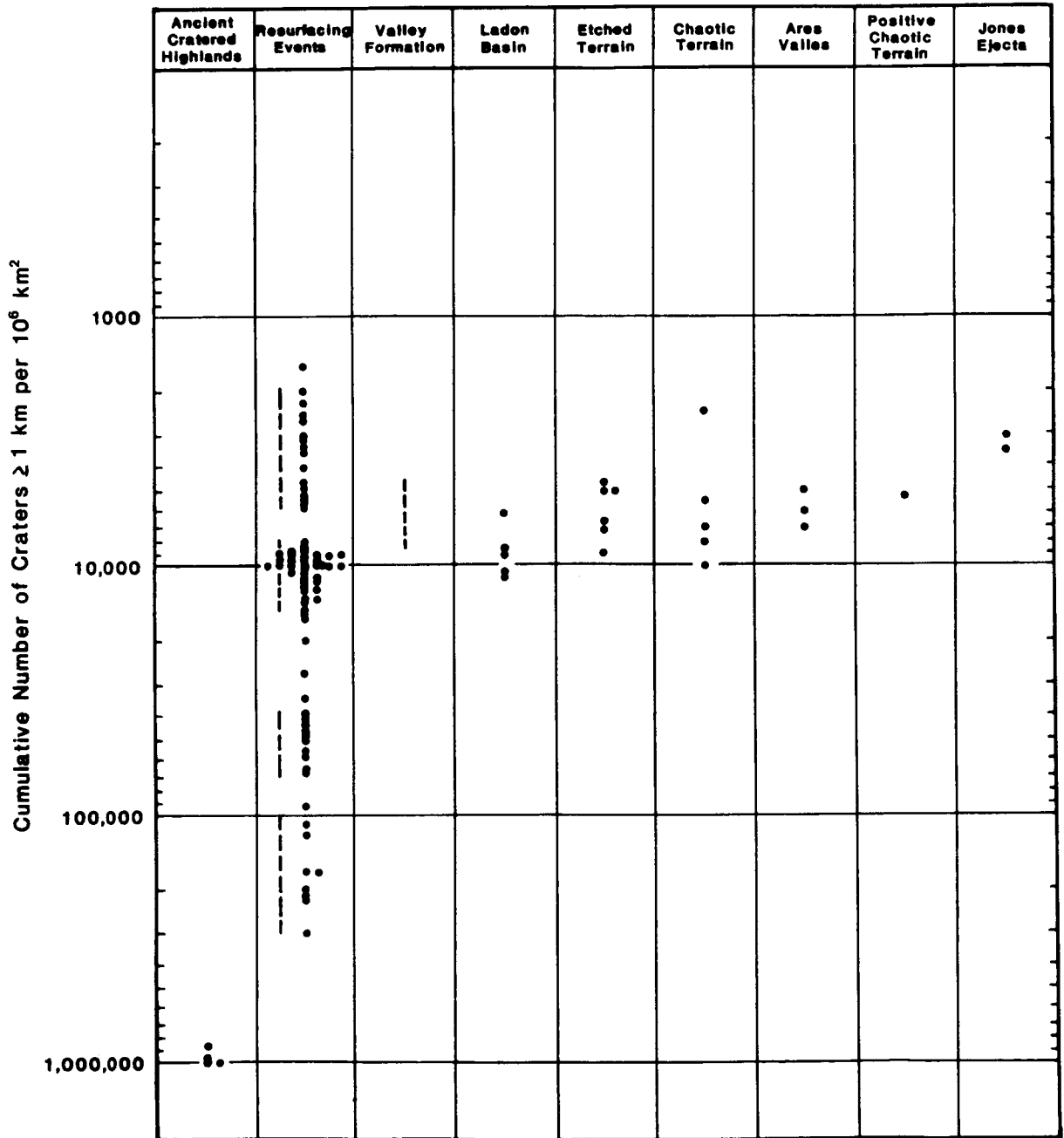


Fig. 5. Summary of all useable crater count data. Each point plotted represents the relative age of one crater count performed in the terrain indicated (see Table 2 and Appendix 3 for individual cumulative crater size-frequency curves, locations, and assigned relative ages). Time intervals of formation of various features and terrain were determined by using the range of relative ages obtained for that feature. Most likely times of resurfacing (dashed vertical lines) were determined by identifying distinct clusters of the relative age values that were obtained by performing crater counts on various homogeneously cratered surfaces (in a specific crater size range). The time of valley formation in the region (dashed vertical line) was determined by the cross cutting relationship of various dated surfaces incised by, and covering, the valleys.

Figure 5



ORIGINAL PAGE IS
OF POOR QUALITY

Fig. 6. Correlation of map units on the geologic/geomorphic map of MC19 (Figs. 3a-d), and comparison to the timing of major events across the planet. Correlations were made using the relative ages determined for various surfaces by crater counting, and cross-cutting relationships. Relative ages are given as the cumulative number of craters $> 1\text{km} \cdot 10^6 \text{ km}^{-2}$.

The morphology of the valley networks is similar to that observed across the planet, as described by the Mars Channel Working Group (1983). Valley walls appear cliff-like and most valley floors are flat, especially in the case of Nirgal and Loire Valles. The network tributaries usually have steep, cusped headward ends, best developed in Nirgal and Parana Valles. Valley widths average about 3 to 5 km for the larger systems, and range up to about 20 km at the widest point of Nirgal Vallis. Valley lengths range from about 10 km for small valleys and tributaries to 900 km for the Parana/Loire system to over 1200 km for the Samara Valles system. Some networks show interior channels, possibly indicating differential erosion of layered deposits and/or multiple flow events.

A relative age of 8,500 to 4,600 has been determined for the valley network systems in MC19SE on the basis of crater densities observed on surfaces incised by the networks and those covering them. This age is inferred for the other valley networks incised in surfaces for which no age was derived and is in general agreement with the age determined for valley networks by other workers (Carr 1979b; 1980a; Hiller and Neukum 1979; and Neukum and Hiller 1981; Baker and Partridge 1984b).

The meso-scale outflow channel features have a relative age of 11,000 to 6200 based on crater densities found in Ladon Basin. Chasma flow features are probably of a similar, but slightly younger age than the other flow features because some valley systems have been beheaded by the Chasma wall (Schultz 1982; Boothroyd 1982; 1983). With the exception of the Chasma, most other channel and valley features are located within the hilly and heavily cratered terrain. Two notable exceptions to this are Nirgal Vallis and a large unnamed valley network in MC19NE (Fig 3d) at 9S, 14W. It is important to note however, that both of these systems head in the hilly and heavily cratered terrain.

Where possible, sub-units have been assigned to further define features within the channels and valleys. Sub-units include: the bounding channel walls; the channel floor, to distinguish that part of the channel that was actually occupied by fluid; terraces, to indicate various locations and elevations occupied by fluid as downcutting progressed; and large (long axis greater than 50km) and small (long axis less than 50km) remnants. Remnants have been further subdivided into those that have been submerged and modified by flow over the top, and those not modified by flow.

Etched Terrain (Ch_{et})-Etched terrain is present in the central part of the quadrangle near the foot of Samara, Parana/Loire, and Margaritifer Valles (Fig. 7). Crater densities display a wide range of values from 9,000 to 4,600. Numerous remnants are seen across the unit some of

Fig. 7. Photomosaic of etched terrain, with numerous remnants (R), in MC19 centered at 12S, 22W. Shows the relationship of Samara and Loire Valles, entering from the south, and Margaritifer Valles, to the etched terrain and Margaritifer Chaos to the north. The presence of distributaries (D) and flow modified remnants clearly associated with Margaritifer Valles, and the lack of same visibly associated with Samara and Loire Valles, suggests that flow out of Ladon Basin was the dominant factor in the formation of the etched terrain (651A61, 63, 64, 85, 86, 88).

ORIGINAL PAGE IS
OF POOR QUALITY



which may have been submerged and flow modified. Some low areas in the unit show slight collapse. The boundary along the west side and northeast corner is very subtle and its exact position is subject to question. Type locality: 11.5S, 21W and Figure 7.

Chaotic Features

Chaotic Terrain (Ct)-Chaotic terrain is located mainly in MC19NW (Fig 3a) and the eastern part of MC19NE (Fig. 3d, see also USGS 1980, and Fig. 7) where it appears as disordered areas of flat-topped, angular and occasionally rounded or flow modified blocks of material showing high local relief. A trend from flat-topped blocks towards the edge to angular and rounded blocks in the center is common. The terrain is located in depressions, that are sometimes closed, and are either scarp bounded or gradational with channel floors, fretted terrain or adjacent uplands. The deposits surrounding the chaotic terrain occasionally displays many fractures. Crater densities within Iani and Margaritifer Chaos display a range of values from 10,000 to 2375. Type localities: 0 to 10S and 15 to 30W.

Fretted Terrain (Ct_f)-A small area of fretted terrain exists in MC19NE at 3S, 19W (Fig. 3d). It grades into the adjacent uplands to the west and the chaotic terrain to the east. The fretted terrain occurs as undissected outliers of the adjacent uplands separated from each other by steep, flat-floored chasms or channels that are roughly aligned parallel to the east-southeast, west-northwest structural grain that is seen the area. Type locality: 3S, 19W.

Positive Relief Chaotic Deposits (Ct_r)-Positive relief chaotic deposits occur as small, commonly rounded, isolated patches mostly in MC19SE. These are best developed in Parana Basin between Parana and Loire Valles (22.5S, 12W, Fig. 3c). The chaos consists of numerous fairly flat-topped blocks that commonly display an outward facing scarp that forms the boundary with the adjacent terrain. The chasma between adjacent blocks are less well developed than in the fretted terrain and they do not appear to show a preferred orientation. A very tentative crater density of 5200 (based on a single count) was obtained for the positive chaotic deposits in the region of 22.5S, 12W, making it younger than the valleys in that area.

Smooth Plains

Smooth Plains Deposits (Sp)-Located throughout the quadrangle, smooth plains are seen as smooth to rolling surfaces that sometimes contain channels. These deposits are also present on many crater floors.

Crater densities, mainly from MC19SE (Figs. 3c, 4c), indicate that four resurfacing events occurred in the region. The earliest (300,000 to 100,000), was of wide regional extent and resulted in the first modification of the cratered highlands in the area. The second (70,000 to 40,000) and third (14,000 to 8,100) events were also of regional extent. The surface created by the third event, labelled Sp₃, is the youngest surface in the quadrangle dissected by the valley networks. It was dated mainly in MC19SE (Fig. 3c), but is probably of regional extent as surfaces displaying similar crater densities occur across the quadrangle. The youngest surface (6,000 to 2,000), labelled Sp₄, was also dated mainly in MC19SE (Fig. 3c). It occurs locally, filling basins, and always covers valley networks when present. Similar fill, not dated, occurs in other basins throughout the area. The Ladon Basin unit, mapped as Sp_L in Fig. 3b, displays a relative age of 11,000 to 6,200 based on the crater density of its surface. Areas mapped as smooth plains outside MC19SE and the Ladon basin are inferred to be associated with one or more of the above events and, unless otherwise specified, are labelled Sp_u (undifferentiated). Where two plains units are superimposed, only the top surface has been labelled. Grabens, wrinkle ridges, and fractures are located predominately within the smooth plains units. Type localities: 29S, 41W and 12S, 17W.

Relict Polar Deposits (Sp_r)—Relict polar deposits (described by Schultz 1984) occur as a distinct unit in the extreme northeastern corner of the quadrangle mapped as Sp_r (Fig. 3d). This unit partially and completely buries craters, and always covers valley networks that extend into the region. Inverted topography and pedestal craters are common.

Craters

Craters are classified on the basis of their morphology. For a given size range of craters, decreasing crater class number implies increasing age. However, within a given class, craters of differing sizes can be of differing ages (after Wise 1979). This is because smaller craters are more easily modified by resurfacing events than larger craters. Craters smaller than 10 km were not mapped and craters smaller than 30 km were not classified.

The youngest craters (C₄) are very fresh in appearance and usually display a central peak and a locally defineable ejecta blanket. The next class of craters (C₃) is subdued in appearance. This class of craters usually lacks a defineable central peak and proximal ejecta blanket. Their floors are usually quite smooth and show low local relief. Degraded craters (C₂) have been extensively modified and have floors that are only slightly lower than the adjacent

terrain. This class is the oldest/most modified that display complete rims. The oldest and/or most modified class of craters (C₁) are extremely degraded in appearance and display incomplete rims. Craters whose appearance has been modified by flow have the subscript 'f' following the usual classification, as is the case for Holden crater (Fig 3b, see also USGS 1980). Asymmetric craters, such as the one located at 25S, 11W (Fig. 3c), are the result of low angle (<10 degrees) impact events (Schultz and Lutz-Garihan 1982). They are denoted by the subscript 'a' following the normal classification.

Ejecta Blankets (Eb)—Ejecta blankets are mapped around some larger C₄ craters. Where defined, they are labeled according to the crater they are associated with.

Multi-Ringed Basins and Hilly and Heavily Cratered Deposits

Hilly and Heavily Cratered Terrain (Hc)—This terrain is located mainly in the southwest (Fig. 3b), southeast (Fig. 3c) and northeast (Fig. 3d) quarters of the quadrangle. Most valley networks are located within this unit. Large numbers of craters, approximately 50 km and larger, and of all morphologies are present. Very high calculated crater densities (1,000,000 to 100,000) characterize the unit. Areas that display numerous hills and scarps associated with ancient multi-ringed impact basins (Schultz et al. 1982) have been included in this unit. Grabens; ancient volcanic flows; and some channel, eolian, and mass movement deposits are also present. Type locality: 25S, 16W.

Ancient Multi-Ringed Impact Basins (—)—These features have been best described by Schultz et al. (1982). Three basins occur within the limits of the quadrangle: Ladon Basin, centered at 18S, 30W; Holden Basin at 26S, 32W (both in Fig. 3b); and Noachis/Newcomb A Basin located at 22.5S, 3W (Fig. 3c). The rings of these basins, identified by Schultz and Glicken (1979), Saunders (1979) and Schultz et al. (1982), are indicated on the map.

Mount Material (Md)—Mount material exists as isolated, degraded, generally elongate hills. They usually appear in somewhat arcuate patterns and often form the rings of multi-ringed impact basins. Type locality: 16 to 17S, 32 to 33W.

Other Features

Grabens (Gr)—Features interpreted as grabens occur mainly in MC19SW (Fig. 3b), the eastern edge of MC19SE (Fig. 3c), and the southern part of MC19NW (Fig. 3a). Their average trend is 100 degrees with a range between 90 and 110 degrees. The grabens are roughly parallel to the Valles Marineris system and radial to the Syria rise.

Flow modified grabens (Gr_f)-Many of the grabens have valley networks associated with them and have been flow modified.

Ridges ()-Almost all ridges mapped fall into two distinctly different categories. The first, and oldest, are those that define isolated arcuate sections of degraded multi-ringed impact basin rings, described by Schultz et al. (1982). Examples of this type of ridge are located at 26S, 25W and 20S, 21W (Fig. 3b, USGS 1980).

The second type of ridge strongly resembles lunar, volcanic, wrinkle ridges. These ridges occur throughout the quadrangle within smooth plains units. They are oriented predominantly N-S ± 10 degrees and are roughly concentric to the Tharsis region.

Eolian Deposits (Ed)-These deposits exist in numerous locations both as mantling deposits and dune fields. Many locations appear to be partially to completely buried by mantling deposits (e.g. the region just east of Osuga Valles, see USGS 1980). Dune fields occur mainly on crater floors (26S, 33.5W, Fig. 3b) and on the floors of Eos and Capri Chasma (Fig. 3a).

Mass Movement Deposits (Mml) All mapped locations consist of deposits derived from landslides, although other types of mass movement deposits probably exist. Landslide deposits have been observed on crater floors (27.5S, 36.5W, Fig. 3b) and on the floor of Eos and Capri Chasma (Fig. 3a).

Drainage Basins

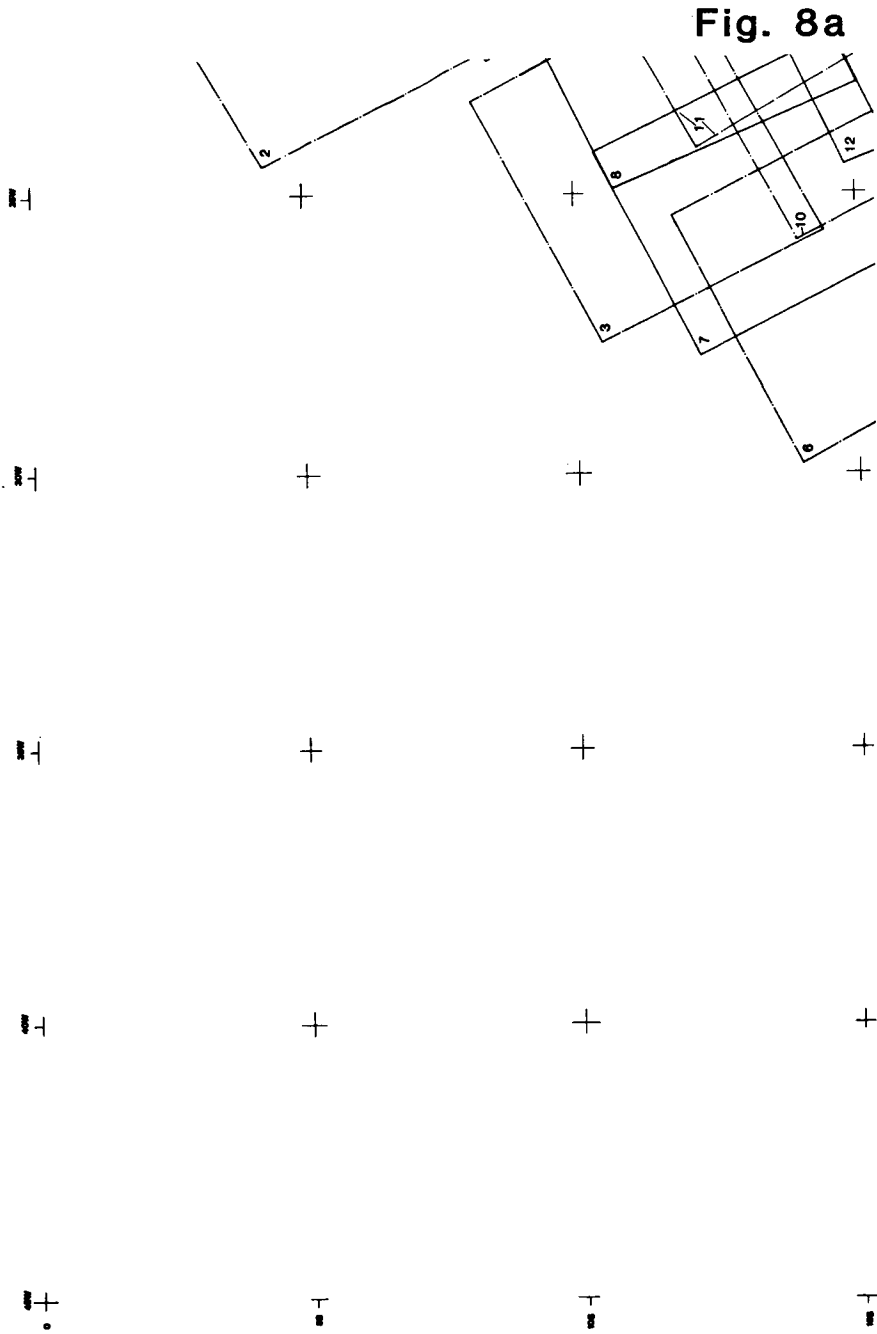
Drainage Basin Mapping

Drainage basin mapping, using stereo pairs of Viking Orbiter images after Boothroyd (1982), was conducted in MC19SE and MC26NE in the Samara and Parana/Loire Valles areas. Stereo pairs used for the drainage-basin mapping are shown in Appendix 4 (Table 6, Figs. 8a-d). The mapped area incorporates the entire drainage network of both systems, including sub-basins of major tributaries, and internal drainage basins between the major networks. Figures 9a-d shows the mapped region in MC19SE and MC26NE from a major N-S trending drainage divide at 9W (Figs. 9c,d), discussed by Boothroyd and Grant (1984; 1985) and Grant and Boothroyd (1984), westward to, and including, the locations in MC19SW (Fig. 9a,b) mapped by Boothroyd (1982). A copy of the original drainage basin map of the entire area, in the form of a clear overlay and at a scale of 1:2,000,000, can be obtained from the author.

Both Samara Valles and Parana/Loire Valles are fairly well integrated and extensive systems. Both have numerous

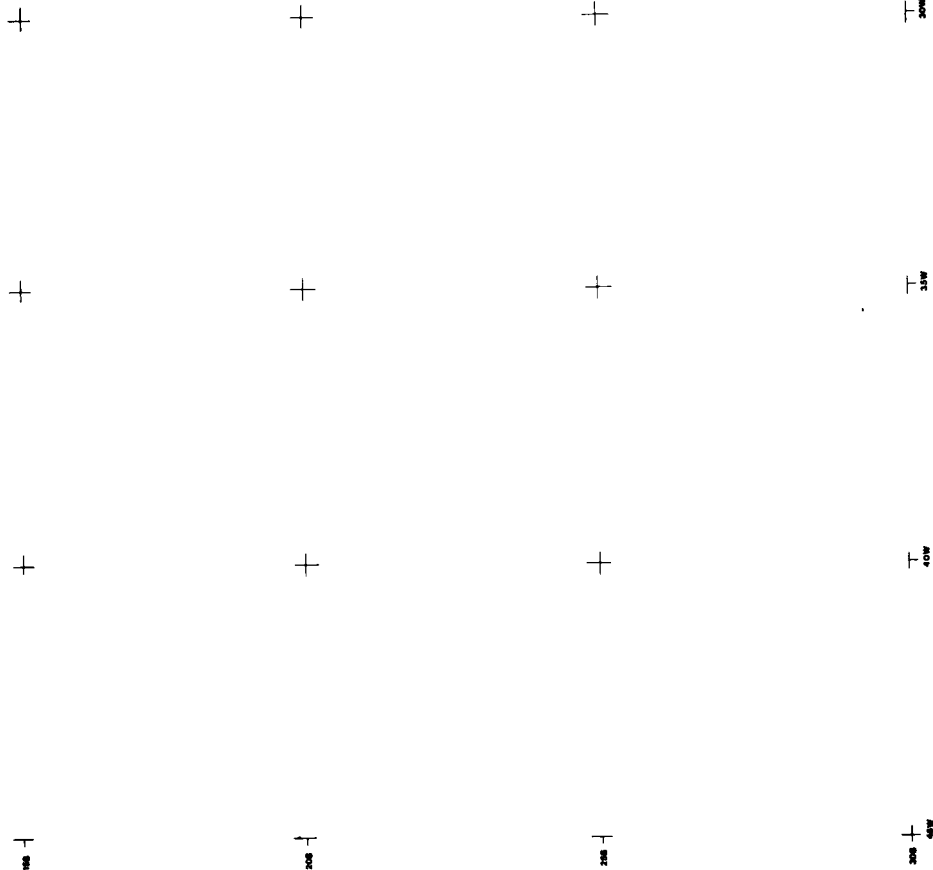
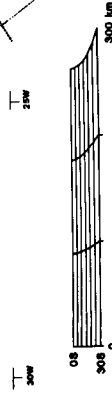
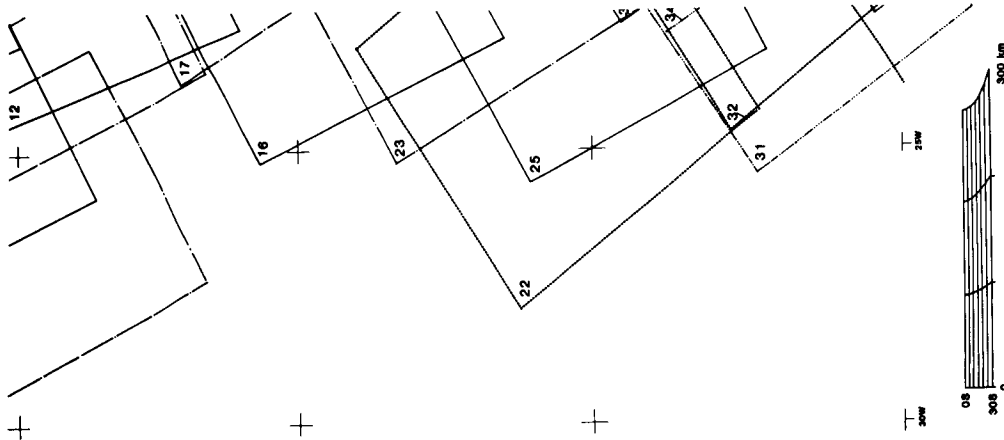
Figs. 8a-d. Stereo pairs used for drainage basin mapping in MC19. The footprints of the images making up the stereo pairs used are shown. Actual stereo pairs are listed in Table 6. Approximately one quarter of the quadrangle is displayed in each of 8a-d: MC19NW in 8a; MC19SW in 8b; MC19SE in 8c; and MC19NE in 8d. The map explanation is given at the bottom of Fig. 8b. A copy of the original diagram at 1:2,000,000 can be obtained from the author.

FIG 8 STEREO PAIR FOOTPRINT LOCATIONS



ORIGINAL MAP
OF POOR QUALITY

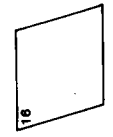
Fig. 8b



MAP EXPLANATION

- IMAGE FOOTPRINTS
- REV 084A FOOTPRINTS
 - REV 451A FOOTPRINTS
 - REV 579A FOOTPRINTS
 - REV 615A FOOTPRINTS
 - REV 650A FOOTPRINTS
 - REV 651A FOOTPRINTS

LABELS



NUMBERS IN UPPER LEFT HAND
CORNER OF FOOTPRINT
REFERS TO THE SPECIFIC IMAGE
NUMBER IN TABLE 8

SEE TABLE 8 FOR STEREO PAIR IMAGE NUMBERS

Fig. 8c

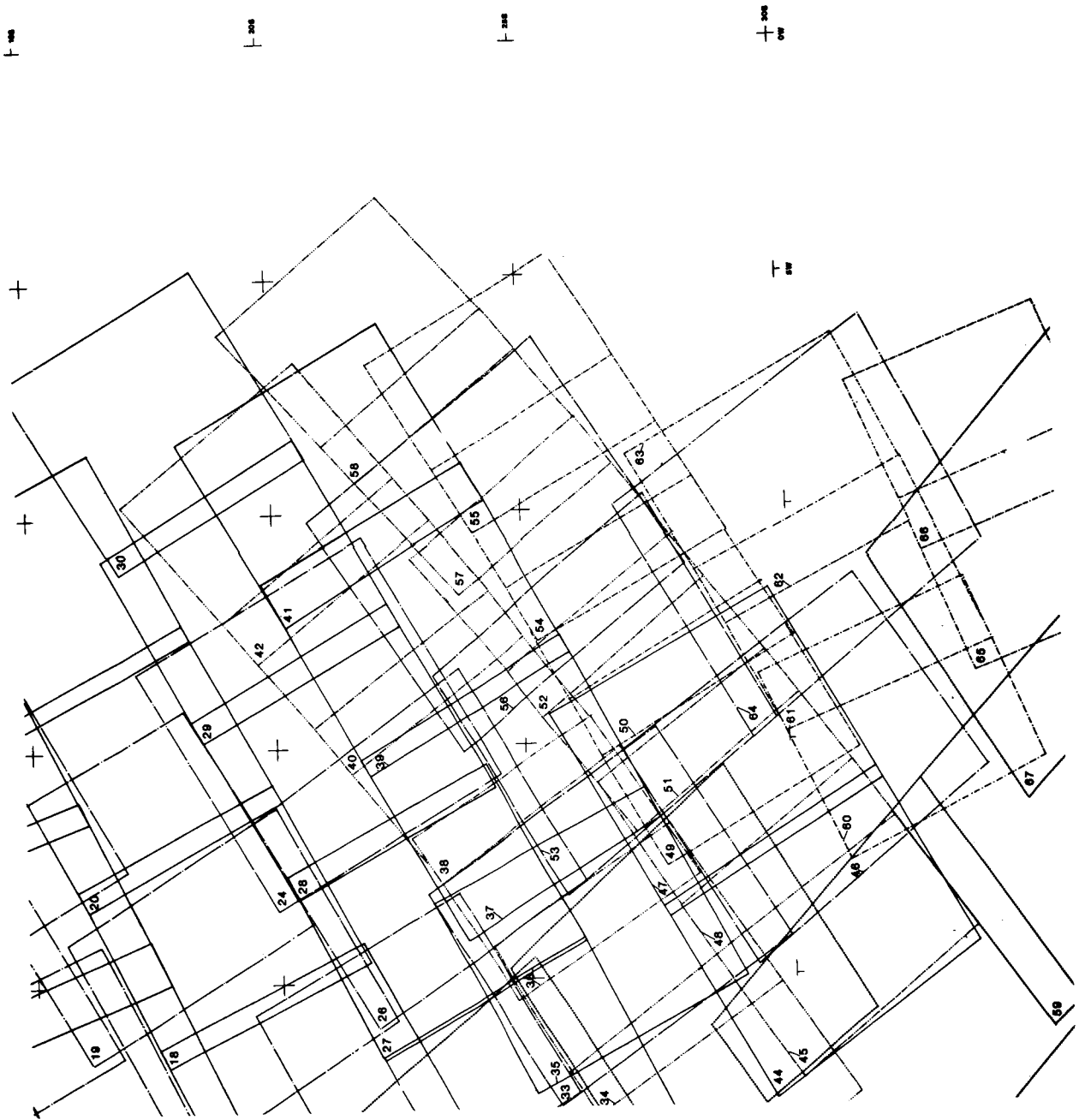
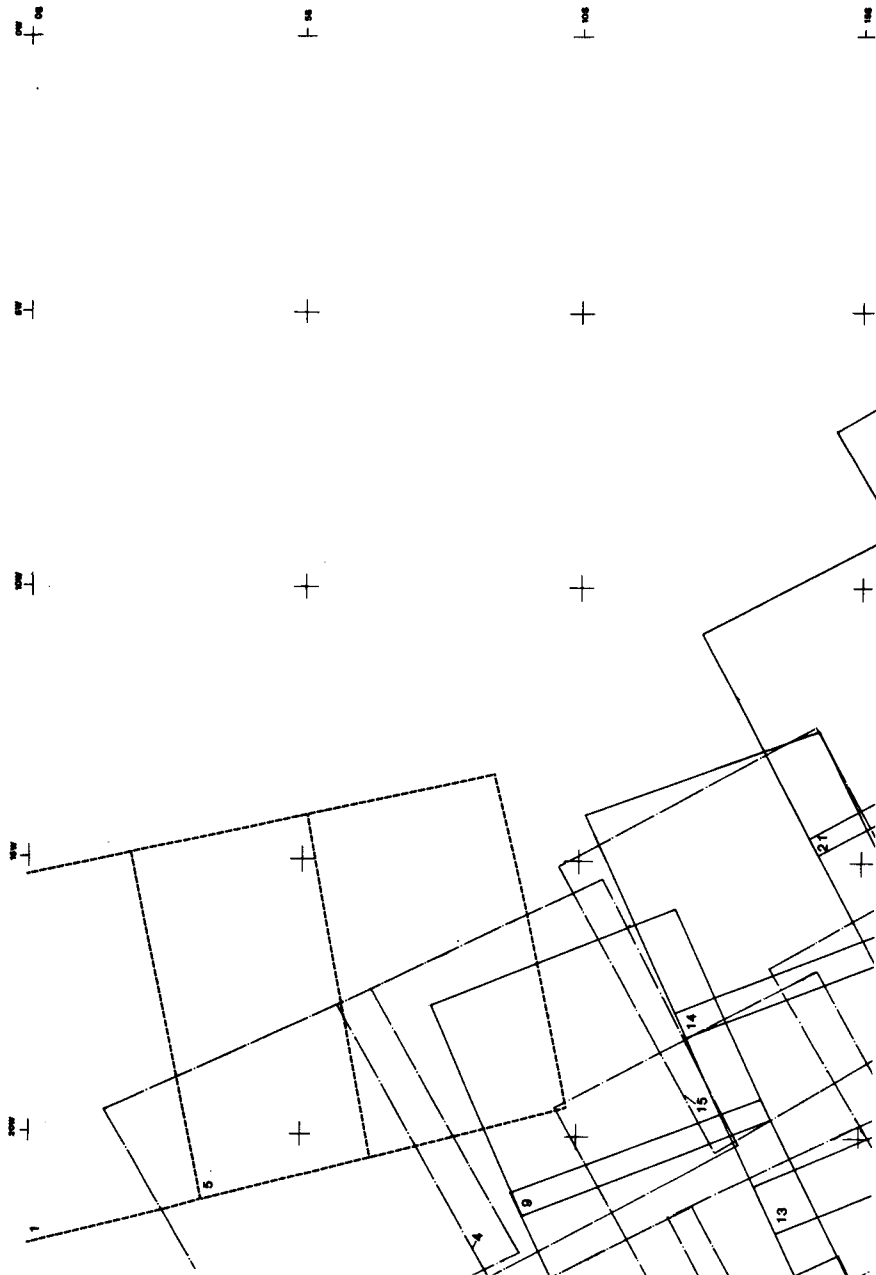


Fig. 8d



Figs. 9a-d. Drainage basins in MC19. Approximately one quarter of the quadrangle is displayed in each of 9a-d: MC19NW in 9a; MC19SW in 9b; MC19SE in 9c; and MC19NE in 9d. The map explanation is given at the bottom of Fig. 9b. A copy of the original diagram at 1:2,000,000 can be obtained from the author.

FIG 9 DRAINAGE BASINS IN MC19

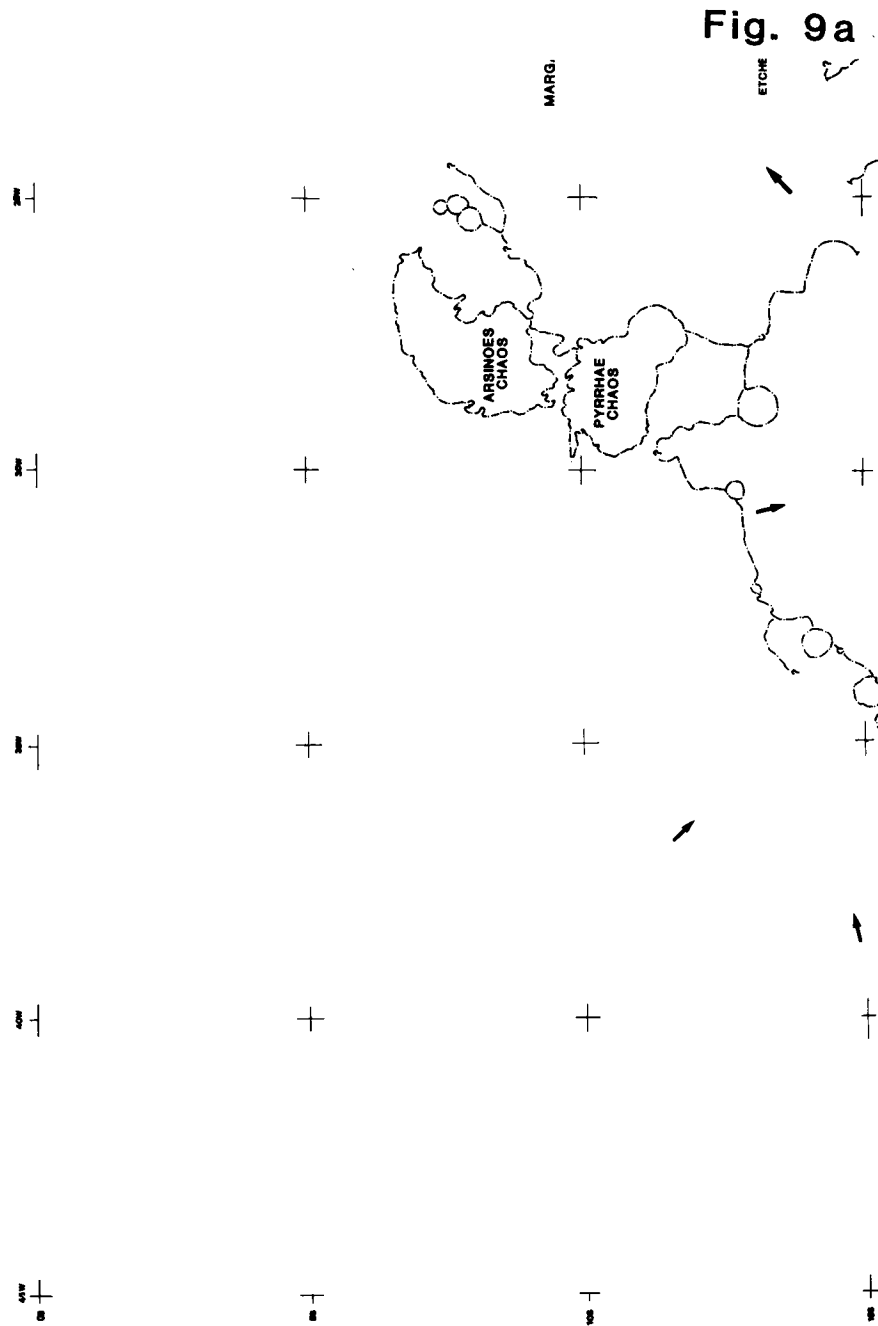


Fig. 9b

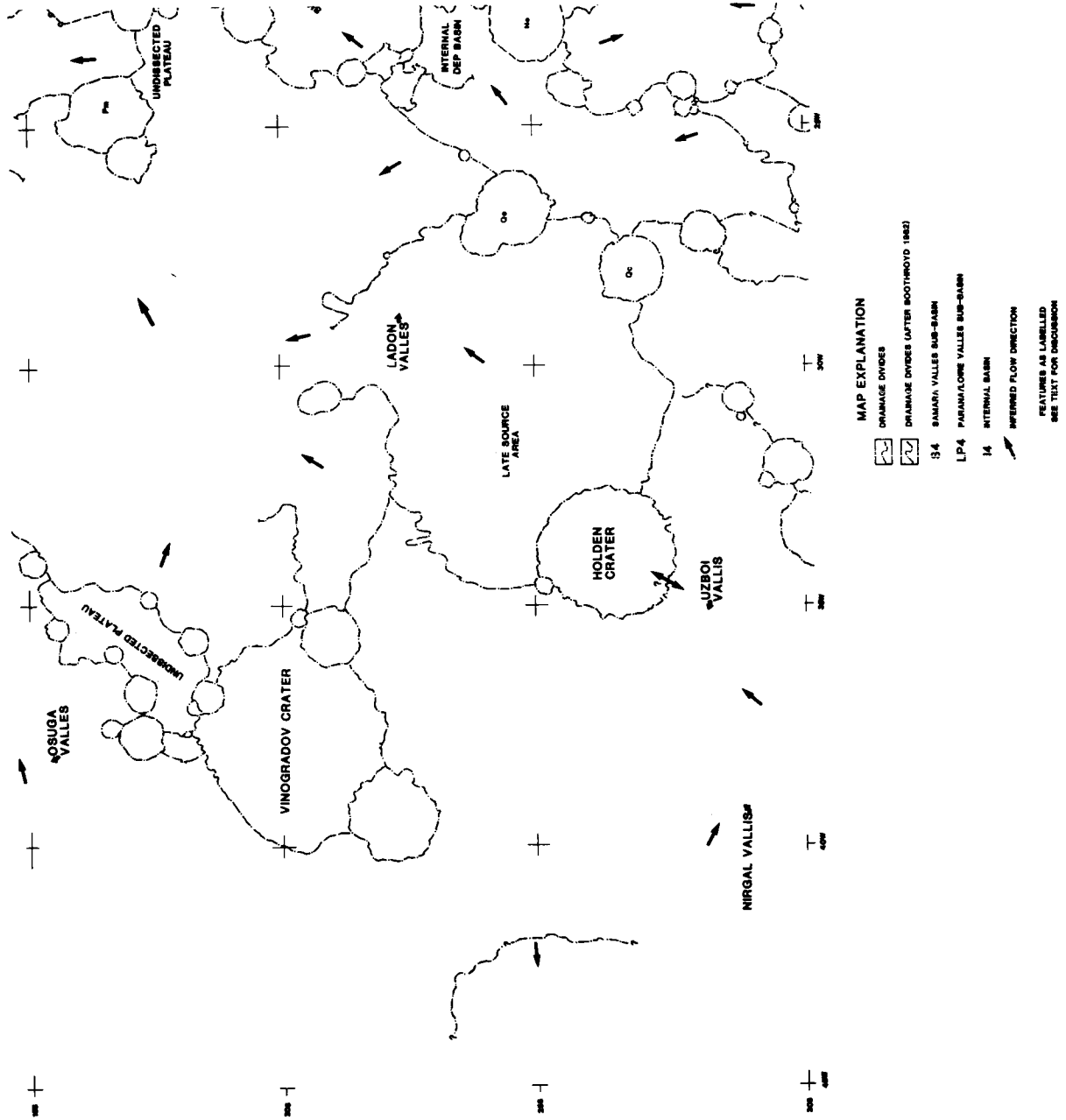


Fig. 9c

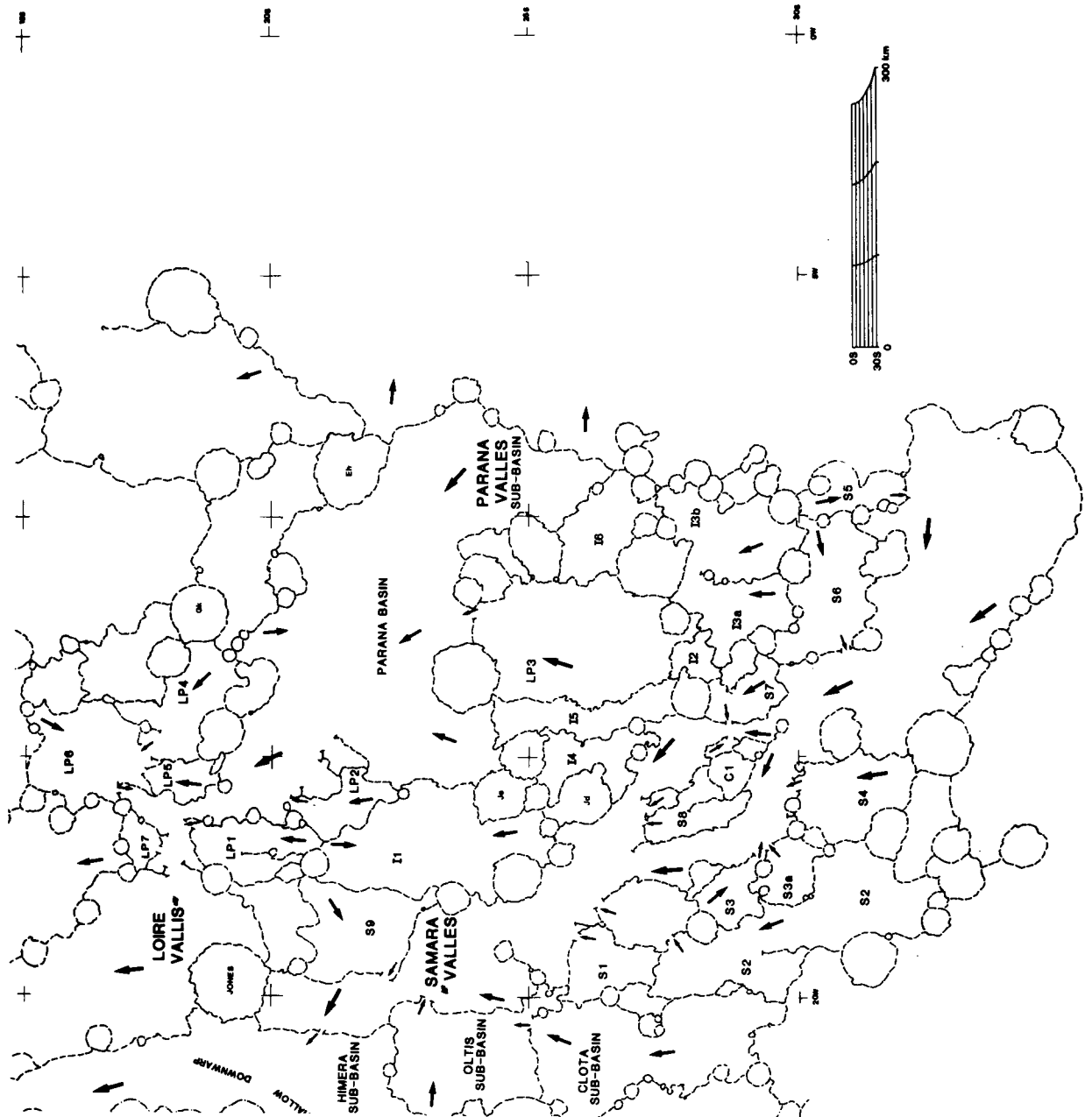
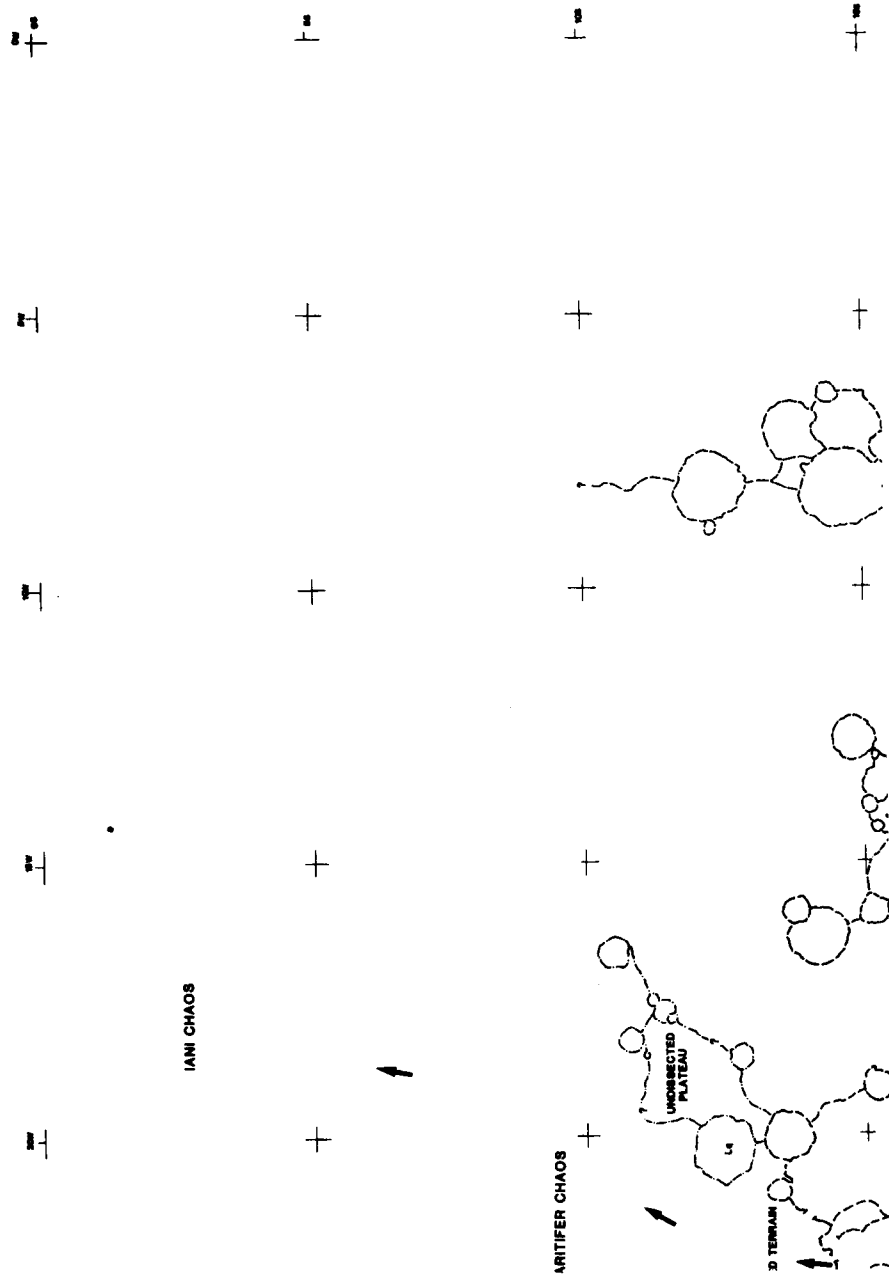


Fig. 9d



sub-basins, many of which are occupied by third or fourth order tributary valleys (Strahler stream order classification; Strahler 1952) that empty into the main trunk valley system. The locations of the major sub-basins and associated internal basins of these systems are given in Table 3, and are shown in Figs. 9c,d. The LP3 sub-basin and I2, I3a, and I3b internal basins are shown in Figure 10. Some sub-basins, notably southern Clota, S1, S5, S6, and LP3 (Fig 9c), have undergone post valley formation resurfacing that has partially to completely buried the existing valleys within them.

Drainage divides between basins and sub-basins are located: 1) along the rims of craters, such as the divide along the western side of the LP4 sub-basin; 2) along the crest of inferred wrinkle ridges, as for the divide around the western side of the LP3 sub-basin; 3) along the crest of rings of the ancient multi-ringed impact basins, as seen along the eastern Himeria sub-basin divide; and 4) as poorly defined lines crossing regions of low local relief as is the case for the divide along the southern edge of the Clota Valles sub-basin.

Drainage basin areas of Samara and Parana/Loire valleys, their major sub-basins and internal basins, were measured from the 1:1,000,000 photomosaic constructed for the region. The lengths of all valleys able to be identified at 200 m/pixel resolution were also measured (a reduced copy of the 1:1,000,000 photomosaic showing the measured valley segments is given in Fig. 11). Values obtained for total valley lengths were divided by the encompassing drainage basin area to obtain the drainage densities of the two systems, their major sub-basins, internal basins, and selected sections along the trunk valleys. Basin areas and densities are displayed in Table 4.

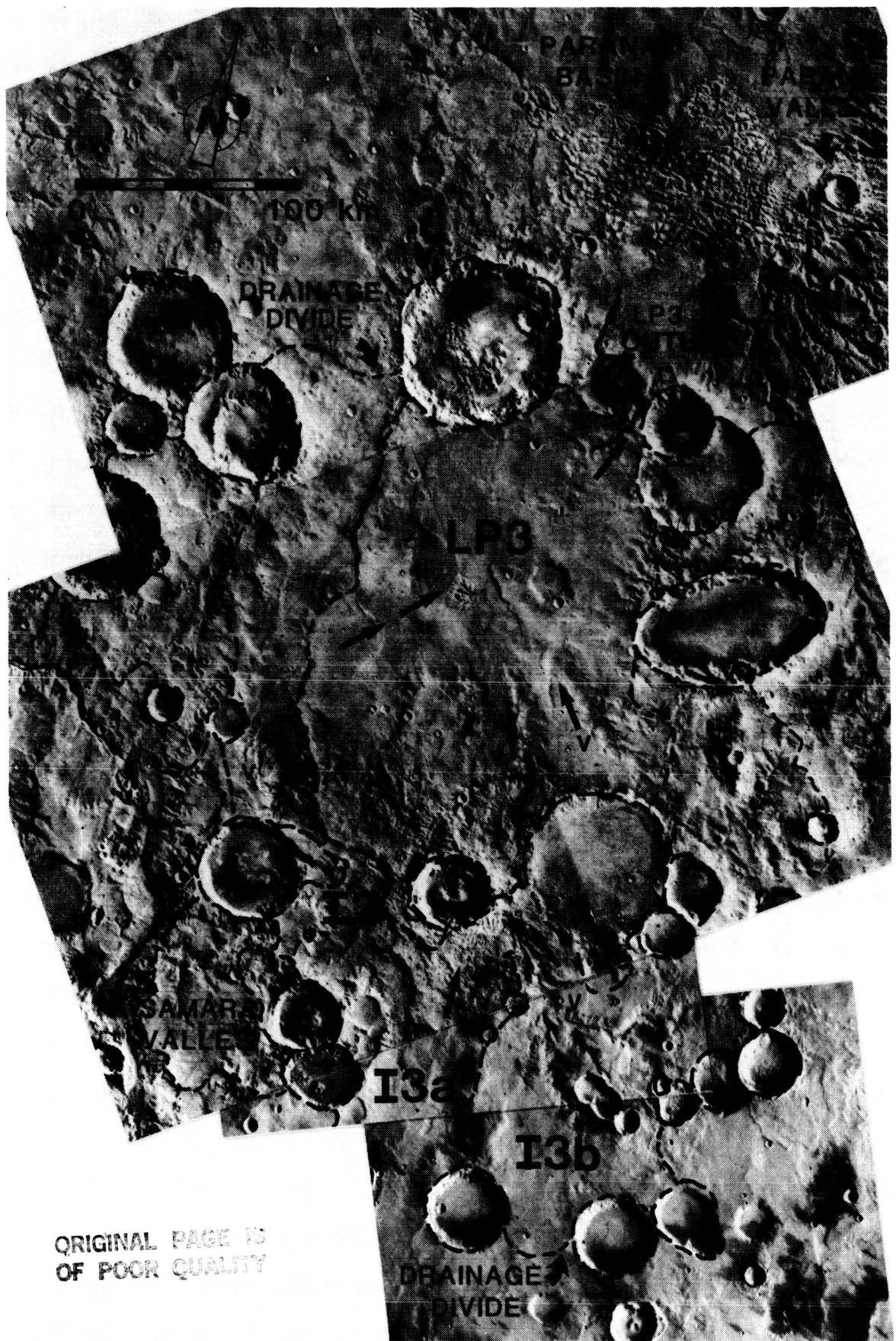
Drainage Basin Areas

From Table 4, the total drainage area of Samara Valles (313,295 km²) and Parana/Loire Valles (222,255 km²) are, respectively, approximately 0.5 and 0.33 that of the Colorado River, USA. Samara Valles sub-basins (Table 5) range in area from 52,528 km² for Himeria and 28,406 km² for S2 to 3,601 km² for S3 and 3,351 km² for S7. Sub-basins in Parana/Loire Valles (Table 5) range from 40,420 km² for Parana and 27,696 km² for LP3 to 3,690 km² for LP5 and 2,620 km² for LP7. Internal drainage basins (Table 4) range from 21,966 km² for I1 to 2,313 km² for I2. The majority of the Samara and Parana/Loire Valles sub-basins and associated internal basins are under 10,000 km², tending towards the lower end of the range of values presented above.

Table 3.-- SUB-BASINS, names and locations

SAMARA				PARANA/LOIRE				INTERNAL BASINS			
Sub-basin	S Lat	W Long	Location	Sub-basin	S Lat	W Long	Location	Sub-basin	S Lat	W Long	Location
Himera	21	22		Parana	23	9		I1	22	16.5	
Oltis	23.5	21		LP1	19.5	16.5		I2	28	12.5	
Clota	26.5	21		LP2	21.5	16		I3a	29	12	
S1	26.5	19		LP3	26	13		I3b	29	10	
S2	28.5-31	18-19.5		LP4	18.5	13.5		I4	26	15	
S3	28.5	18		LP5	18	15		I5	26	14	
S3a	29.5	17.5		LP6	16	15		I6	26	10	
S4	31	16		LP7	17.5	16.5		C1	29	15	
S5	31.5	9									
S6	31	11.5									
S7	29	13.5									
S8	28	16									
S9	21	18									

Fig. 10. Section of MC19SE centered at 275, 12W. Dashed lines outline sub-basin LP3 of Parana Loire Valles. A drainage divide along the the rim and ejecta blanket of crater Gb at the southern edge of LP3, separates drainage in the sub-basin from drainage in three internal basins to the south (I2, I3a, I3b). Several short valley segments are present in the southern half of LP3 (V) and well developed northward flowing segments exist in I3a and I3b (V). Paleoflow (arrows) was to the north out into Parana Basin. (OB4A43, 44, 45, 46, 579A44, 45).

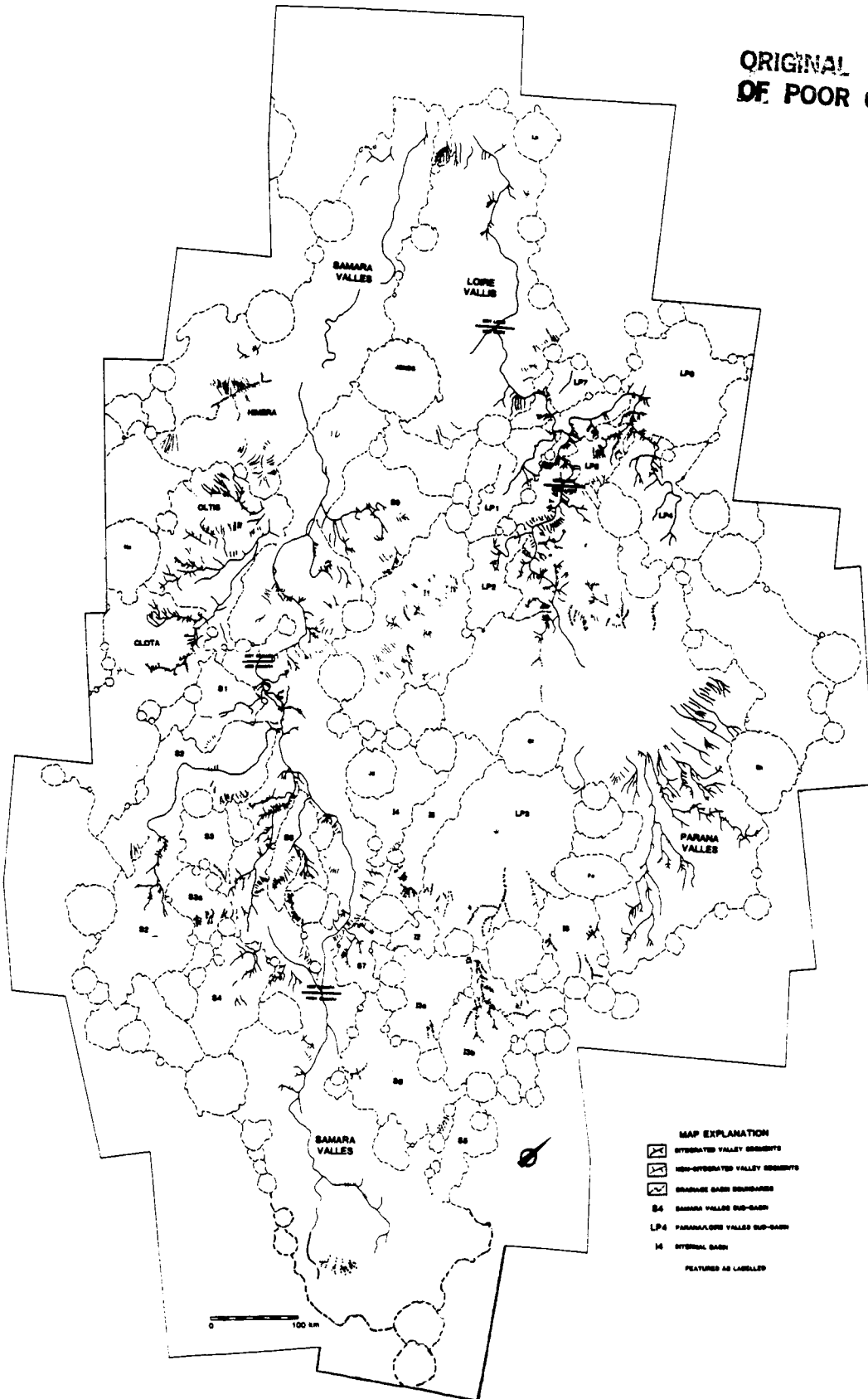


ORIGINAL PAGE IS
OF POOR QUALITY

Fig. 11. All valley segments measured for use in the calculation of drainage densities for Samara and Parana/Loire Valles, portions of their trunk valleys, all sub-basins and internal basins. Integrated valley segments are indicated by a solid line. Non-integrated valley segments are assumed to have been integrated in the past, and are indicated by a dashed line. Post valley formation resurfacing and valley burial was probably responsible for the present disintegrated appearance of some segments. A copy of the original figure at 1:1,000,000 can be obtained from the author.

FIG 11 VALLEY SEGMENTS MEASURED FOR DRAINAGE DENSITY CALCULATIONS

ORIGINAL PAGE IS
OF POOR QUALITY



Drainage Densities

Overall drainage densities of Samara and Parana/Loire Valles (Table 4) are quite similar with Samara Valles having an average density of $0.034 \text{ km}\cdot\text{km}^{-2}$ and Parana/Loire Valles an average density of $0.039 \text{ km}\cdot\text{km}^{-2}$. Loire Valles has a density of $0.032 \text{ km}\cdot\text{km}^{-2}$ and Parana Valles has a density of $0.070 \text{ km}\cdot\text{km}^{-2}$. Sections along the trunk portions of these large systems display a range of densities. The highest values, 0.043 and $0.067 \text{ km}\cdot\text{km}^{-2}$, are found along central portions, between the third and fourth rings of Ladon Basin. Slightly lower values, eg 0.016 and $0.022 \text{ km}\cdot\text{km}^{-2}$, are found in proximal and distal reaches. Samara Valles sub-basins (Table 5) have an average density of $0.039 \text{ km}\cdot\text{km}^{-2}$, with a range from $0.075 \text{ km}\cdot\text{km}^{-2}$ for S8 to $0.013 \text{ km}\cdot\text{km}^{-2}$ for S6. Parana/Loire sub-basins display slightly higher drainage density values (Table 5), averaging $0.054 \text{ km}\cdot\text{km}^{-2}$ and ranging from $0.107 \text{ km}\cdot\text{km}^{-2}$ in LP5 to $0.018 \text{ km}\cdot\text{km}^{-2}$ in LP1.

TABLE 4.-- DRAINAGE SYSTEMS, areas and densities

Location (basin)	Area (km ²)	Integrated Channels (km)	Integrated Density (km/km ²)	Additional Channels (km)	Total Density (km/km ²)
COMPLETE DRAINAGE SYSTEMS					
Samara	313,295	8616.7	0.028	2033.1	0.034
Parana/Loire	222,255	7378.1	0.033	1247.0	0.039
Loire	181,835	4547.5	0.025	1247.0	0.032
Parana	40,420	2830.6	0.070	--	0.070
SAMARA TRUNK VALLEY SECTIONS					
Proximal	56,874	834.5	0.015	84.3	0.016
Mid	33,300	2220.0	0.067	--	0.067
Mid/Dist	28,465	948.8	0.033	196.4	0.040
Dist	52,528	509.6	0.010	1002.1	0.028
LOIRE TRUNK VALLEY SECTIONS					
Proximal	22,023	1408.9	0.022	25.9	0.022
Mid	19,255	670.8	0.035	162.4	0.043
Distal	32,898	707.5	0.034	476.3	0.045
INTERNAL DRAINAGE BASINS					
I1	21,966	--	--	596.9	0.027
I2	2,313	--	--	18.4	0.008
I3A	8,081	--	--	57.4	0.007
I3B	11,583	--	--	608.1	0.053
I4	6,529	--	--	41.3	0.006
I5	7,471	--	--	127.1	0.017
I6	5,304	--	--	140.0	0.026
C1	2,136	--	--	95.2	0.045

AVERAGE INTERNAL BASIN DRAINAGE DENSITY = 0.0236

TABLE 5.-- SUB-BASINS, areas and densities

Location (sub- basin)	Area (km ²)	Integrated Channels (km)	Integrated Density (km/km ²)	Additional Channels (km)	Total Density (km/km ²)
SAMARA VALLES SUB-BASINS					
Himera	52,528	509.6	0.010	1002.1	0.028
Oltis	18,090	1149.5	0.064	91.7	0.069
Clota	23,509	631.3	0.027	38.1	0.029
S1	6,794	113.0	0.016	25.1	0.020
S2	28,406	602.6	0.021	147.5	0.026
S3	3,601	--	--	--	--
S3a	3,544	--	--	189.4	0.053
S4	8,320	236.6	0.028	--	0.028
S5	5,578	--	--	--	--
S6	9,009	--	--	118.3	0.013
S7	3,351	242.9	0.073	--	0.073
S8	7,077	533.4	0.075	--	0.075
S9	12,997	379.5	0.029	140.2	0.040
PARANA/LOIRE SUB-BASINS					
Parana	40,420	2830.6	0.070	--	0.070
LP1	7,686	136.5	0.018	--	0.018
LP2	5,225	191.1	0.037	--	0.037
LP3	27,696	71.2	0.003	526.0	0.022
LP4	9,910	396.4	0.040	--	0.040
LP5	3,690	338.9	0.092	56.4	0.107
LP6	12,589	335.0	0.027	--	0.027
LP6a	2,708	212.8	0.079	--	0.079
LP7	2,620	21.9	0.083	--	0.083

Average Samara Sub-Basin Drainage Density = 0.0386

Average Parana/Loire Sub-Basin Drainage Density = 0.0537

Average Internal Basin Drainage Density = 0.0236

DISCUSSION

Interpretation of Map Units

Channel Features

Channels and Valley Networks (Ch)—All the various scale channel and valley features have been shaped by fluid erosion. The source of this fluid varied for the different scale features. For the macro-scale features within Eos and Capri Chasma, the source was most likely the adjacent chaotic terrain (Carr 1979; Carr and Clow 1981; Murray et al. 1981; Baker 1982). Parker and Pieri (1985b) suggested that the catastrophic flow of water out of Argyre Planitia carved the Uzboi/Holden/Ladon system. Valley network formation by sapping processes and associated downstream fluvial activity was first hypothesized by Sharp and Malin (1975). As summarized by the Mars Channel Working Group (1983) this is currently the popular theory of formation held by most workers today, and will be further discussed in this study.

Etched Terrain (Ch_e)—The etched topography was created by the removal of surface material through fluidal activity. This flow was associated with discharge mainly from Margaritifer Valles and, to a lesser extent, Samara and Parana/Loire Valles. The eroded material was transported downslope to the north and east.

Chaotic Features

Chaotic Terrain (Ct)—The chaotic terrain represents the remains of a previously overlying surface that collapsed after water was catastrophically released from below and removed support (Saunders 1979; Carr 1979b). Carr (1979b) suggested that extremely high pore pressure in confined aquifers could lead to breakout and the catastrophic release of water, thus forming the chaotic terrain. He demonstrated that this process could repeat itself several times over an extended period of time. This would help explain the wide range of crater densities observed in the terrain. Errors in the measurement of crater densities, due to poor negative resolution (<260 km/pixel for much of Iani and Margaritifer Chaos) and difficulties in determining whether a crater is within the chaotic terrain, or on the pre-collapse surface, may be partially responsible for the large range of density values for the chaotic terrain.

Fretted Terrain (Ct_f)—The fretted terrain in MC19NE (Fig. 3d) is not typical of the fretted terrain described elsewhere by Sharp (1973). It is most probably the incompletely developed edge of the adjacent chaotic terrain to the east, and was formed in a similar manner.

Positive Relief Chaotic Deposits (Ct_r)-As previously suggested by Boothroyd and Grant (1985) the positive relief chaotic features may be similar to very large scale terrestrial pingos. It is unclear whether or not these features are still evolving at present.

Smooth Plains

Smooth Plains Deposits (Sp)-Volcanic, fluid and eolian deposits of various ages that partially to completely cover the Hc unit. Locations mapped as smooth plains that display high crater densities (about 100,000) have a deficiency of small diameter craters, and large craters display almost exclusively C₁, C₂, and occasionally C₃ morphology. Other areas, partially buried by resurfacing, that display mainly C₂, C₃, and C₄ class craters and high cumulative crater densities (greater than 100,000), are labelled as part of the Hc unit. Deposition of channel eroded material in the area within Ladon Basin was responsible for the formation of the smooth plains unit there. Smooth plains units mapped are equivalent to unit P mapped by Saunders (1979).

Relict Polar Deposits (Sp_r)-The location mapped as relict polar deposits was classified as such by Schultz (1984) on the basis of its: 1) layered nature; 2) numerous pedestal craters; 3) location adjacent to an area of low thermal inertia; and 4) position relative to asymmetric crater orientations around the planet (Schultz and Lutz-Garihan 1982). Schultz (1984) suggested that the polar wandering which resulted in the deposits was the result of a relatively rapid mass redistribution somewhere on the planet. The development of the Syria Rise may represent such a situation (Schultz, personal communication 1984).

Multi-Ringed Basins and Hilly and Heavily Cratered Deposits

Hilly and Heavily Cratered Terrain (Hc)-The terrain that comprises this unit is the oldest in the quadrangle. The unit is quite thick and intensely brecciated by impact events. It is also locally volatile rich. The surface of the unit shows impact crater saturation in some locations, and incorporates terrain associated with the multi-ringed impact basins (Schultz et al. 1982). Similar to unit pc mapped by Saunders (1979) and units hc and Uic mapped by Wise (1979).

Ancient Multi-ringed Impact Basins (—)-These features are multi-ringed topographic basins formed by large meteorite impacts. Cross cutting relationships indicate that they are the oldest recognizable features in the quadrangle.

Mount Material (Md)-These generally elongate hills are the extremely degraded remnants of concentric ridges (rings)

created during the formation of the multi-ringed impact basins (Schultz et al. 1982).

Other Features

Grabens (Gr)-All grabens in Margaritifer Sinus are tensional features. Parker and Pieri (1985) have associated their formation with the development of the fault system radial to Tharsis and the initiation of formation of Valles Marineris, thus giving them a relative age of about 10,000 to 5,500 from Wise et al. (1979).

Flow Modified Grabens (Gr_f)-Development of these grabens was synchronous with development of the other grabens. Flow modification associated with valley network development was immediately post graben formation, based on cross-cutting relationships and the relative ages of the two features.

Ridges (~~~~)-The first type of ridge is associated with multi-ringed impact basin rings. The second type of ridge, of compressional origin, is probably associated with Tharsis evolution. Parker and Pieri (1985a) suggested that the preferential location of the second type of ridge within smooth plains units was due regional compression that caused buckling in the relatively rigid plains deposits overlaying less competent regolith. Wise et al. (1979) derived a relative age of 10,000 to 5,000 for similar features located in the Tharsis region.

Eolian Deposits (Ed)-All post Sp₄ mantled and buried surfaces appear to be a result of eolian deposition. All dune fields also appear to be of eolian origin.

Geometry and Relationship of Large Scale Features

The NW portion of the quadrangle (see USGS 1980) is dominated by Eos and Capri Chasma and related chaotic terrain (Carr 1979; Carr and Clow 1981; Murray et al. 1981; Baker 1982). These workers have suggested that the catastrophic release of fluid from the chaotic terrain caused the flow features observed in the chasma and the connected outflow channels further to the north. Recession of the southern wall of Eos Chasma has caused the beheading of several southward flowing valley networks along the chasma edge (Schultz et al. 1982, Boothroyd 1983). The position of the chaotic terrain throughout the area (see Fig. 3a,b and USGS 1980) is probably controlled by a structural zone of weakness that enhanced permeability and collapse, associated with the region of overlap of the rings of the Ladon and Chryse multi-ringed impact basins (Schultz and Glicken 1979, Schultz et al. 1982).

The Ladon and Holden multi-ringed impact basins (Schultz et al. 1982) are clearly the dominant structural controls in

the SW portion of the quadrangle (Fig. 3b). Almost all mount material in the region is associated with the basins (Saunders 1979; Schultz and Glicken 1979; Schultz et al. 1982), and valley networks located there tend to show an exterior radial centripetal pattern (after Pieri 1980a) with segments of the systems commonly being deflected parallel to a ring just before crossing it. The drainage pattern in most of MC19SW is roughly centered on the Ladon impact basin, the largest of the three, and which has been the site of considerable fluvial deposition (Boothroyd 1982; Parker and Pieri 1985a).

A large segmented system consisting of Uzboi, Holden and Ladon Valles crosses the quadrangle from the SW to the NE. Ladon Valles (Fig. 12) has isolated terraces at different levels that were abandoned as the channel downcut (Boothroyd 1982; 1983; Parker and Pieri 1985a). Where Ladon Valles passes one of the impact basin rings before debouching into Ladon Basin, its course is changed from the NE to the NW indicating the structural influence of the Ladon impact basin on the system (Parker and Pieri 1985b).

The entire Uzboi/Holden/Ladon system was initially through flowing into Ladon Basin (Florenski 1975; Pieri 1975; Boothroyd 1982), however, Holden crater, now superimposed on the central part of the system, appears to have interrupted the late stage flow. Close examination of Margaritifer Valles at the NE margin of Ladon Basin (Fig. 7) shows that it drains the basin, and empties into the etched terrain just south of Margaritifer Chaos (as had been suggested by Florenski et al. 1975, and Boothroyd and Grant 1984). This indicates that the Uzboi/Holden/Ladon system may once have been through flowing to the northeast.

Nirgal Vallis (see USGS 1980), a tributary network to Uzboi Vallis, has received considerable attention because of its conspicuous sinuosity and unusual morphology (Milton 1973; Schumm 1974; Weihaupt 1974; Sharp and Malin 1975; Baker 1980b; 1982). Schultz et al. (1982) suggested a source area for the system along a ring of the Holden Basin. Milton (1973) described the lower half of Nirgal Vallis as being most similar to a sinuous lunar rille, with the upper half similar to the entrenched arroyo systems in the southwestern USA. Because the system is internally coherent Milton felt a two-fold method of genesis, e.g. lava tube collapse and subsequent headward extension by fluvial processes was unlikely. Sharp and Malin (1975) hypothesized that because Nirgal Vallis is probably not located in a region of youthful volcanic features, and because the overall morphology resembles that of terrestrial systems formed by sapping and runoff, sapping and associated fluidal activity was most likely the principal agent of formation. This is the generally accepted theory today.

Fig. 12. Ladon Valles (MC19SW centered at 22.5S, 29W) is part of a large, segmented, northward flowing system comprised of Uzboi/Holden and Ladon Valles. The system empties into Ladon Basin to the north of Ladon Valles, and may have been through flowing out of Ladon Basin into the etched terrain (Fig. 7) further to the NE. At least five different levels of terraces can be indentified in Ladon Valles (1 is oldest, 5 is youngest) that were created as the system evolved. A small region of chaotic terrain to the SW of Ladon Valles probably served as a late source area after interruption of the Uzboi/Holden flow by the Holden impact event. The course of Ladon Valles changes from the NE to the NW as it crosses the first (FRH) and second (SRH) rings of the Holden, and the second (SRL) ring of the Ladon multi-ringed impact basins. This is a result of the structural influence imparted on the system by the multi-ringed basins. Figure is slightly modified from that of Boothroyd (1982; 1983) (611A32, 650A16).



The influence of the Ladon impact event extends well out into MC19SE (Fig. 3c and USGS 1980), where a fourth poorly defined ring may be present (Schultz and Glicken 1979; Schultz et al. 1982; Schultz, personal communication 1985). The fourth ring is defined by widely spaced ridges concentric about the center of the basin. Other evidence favoring the existence of a fourth ring comes from morphological changes in Samara and Parana/Loire Valles (Fig. 3c), observed as they cross its hypothesized position (Schultz et al. 1982). Between the fourth and third rings of Ladon Basin, Samara and Parana/Loire Valles display many short tributaries that usually enter the trunk valley at very large junction angles, commonly 90 degrees (Schultz et al. 1982). The drainage density along this reach is the greatest that the two systems display (Tables 4 and 5). This is also the zone where tributaries with the highest drainage densities (with the exception of Parana Valles) enter the systems (Fig. 9c,d, Table 5). The plains and cratered terrain between the Ladon third and fourth rings in MC19SE are highly dissected by numerous short, poorly-integrated valleys, giving the area a grooved appearance. Inside the third ring and outside the fourth ring Samara and Parana/Loire Valles display a subdued morphology with relatively low densities and poorly integrated tributaries. Schultz et al. (1982), and Schultz (personal communication 1985) postulated that the observed change in valley number and density between the two rings was due to the presence of a thick blanket of volatile rich ejecta emplaced during the Ladon impact event. In the immediate vicinity of crater Jones, both Samara and Parana/Loire valles are partially to completely buried by ejecta from the Jones impact event (Fig. 13).

Samara and Parana/Loire Valles are classified as well integrated longitudinal stem valley networks after Pieri (1980a). Samara heads in the Argyre NE quadrangle (MC26NE) and flows across MC19SE. Just before crossing the fourth ring of Ladon basin, Samara Valles splits as it crosses an ancient ridge (Fig. 14), rejoining at the edge of the fourth ring. The more western of the two Samara valleys is higher than the eastern. This may be due to an impact crater in the western valley that appears to have dammed the flow, resulting in deposition upstream, and forcing flow to be diverted into the deeper eastern Samara valley. At the point that the two valleys diverge, several incised interior channels described by Pieri (1980a) can be seen in eastern Samara Valles (Fig. 14).

After crossing the fourth and third rings of Ladon Basin, Samara Valles enters a gentle northward trending downwarp known as the Himera Basin. At this point Himera Valles joins the system (Boothroyd and Grant 1985). After entering Himera Basin, Samara Valles trends in a more northerly direction along the axis of the Chryse lowland trough (Fig.

Fig. 13. Jones Crater, located just outside the third ring of the Ladon multi-ringed impact basin (TRL) at 19S, 20W. Ejecta from the crater has partially buried sections (P) of Samara and Loire Valles and completely buried sections (C) of Samara Valles and a graben located NW of the crater (651A65).

ORIGINAL PAGE IS
OF POOR QUALITY.

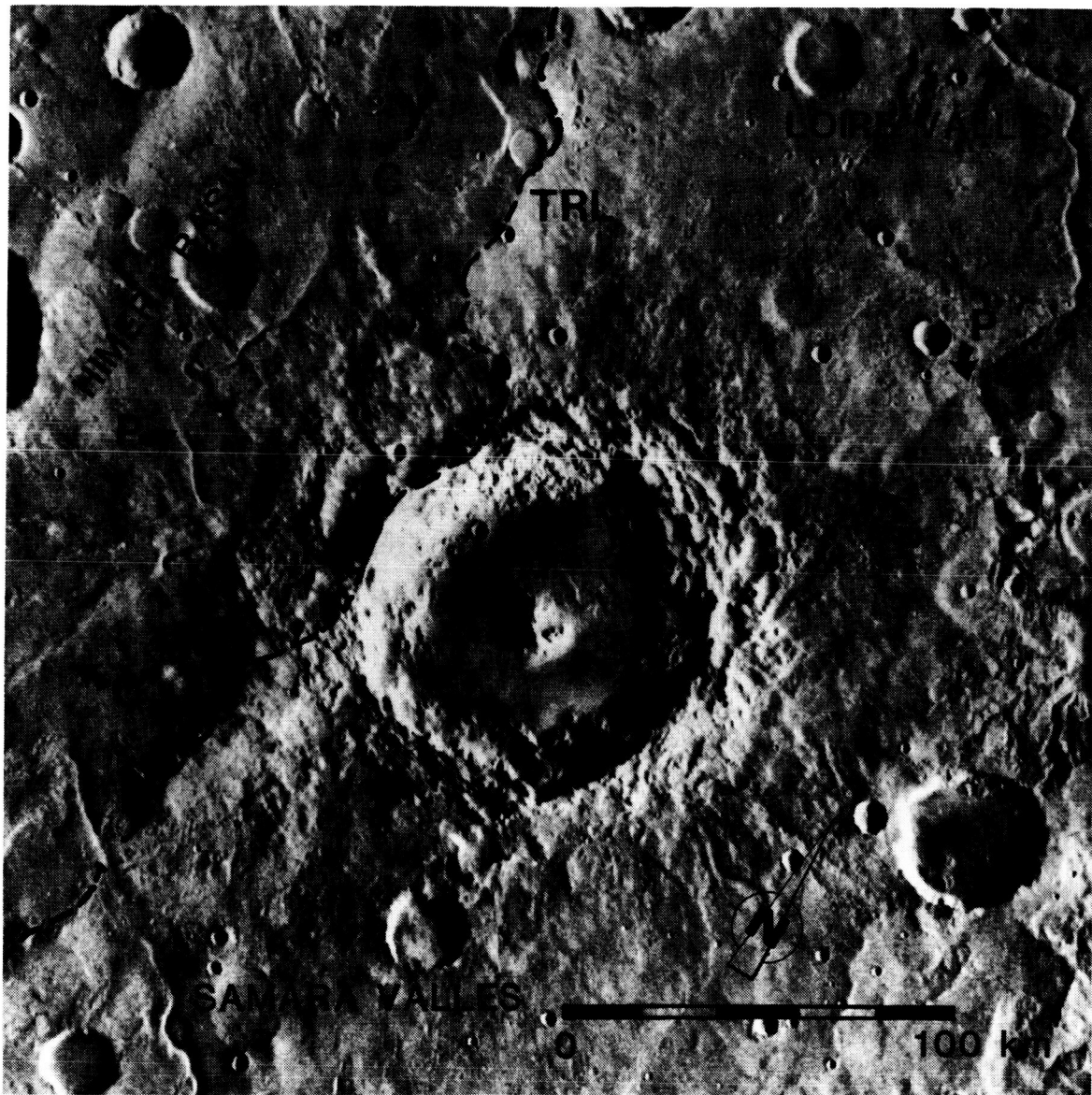


Fig. 14. Split in Samara Valles as it crosses an ancient NE trending ridge centered at 28.5S, 15W. The eastern valley is deeper than the western valley, possibly due to damming of the western channel by the crater at (C), resulting in deposition behind it (D), and the diversion of all flow into the eastern valley. The eastern valley shows several interior terraces and a deep central channel (I) at 29.5S, 14W. This may be due to multiple flow events and/or the differential erosion of the underlying units at that location. The material comprising the ancient ridge (dated by crater counting) is some of the oldest terrain in the quadrangle (relative age 1,000,000 to 850,000). Drainage basins are depicted by dashed lines, and large arrows indicate the flow direction. Positive relief chaotic deposits (Ct_r) exist along the eastern valley (084A41).



2). The system debouches into etched terrain just south of Margaritifer Chaos, close to Margaritifer Valles.

The Parana/Loire Valles system parallels Samara Valles to the northeast. This system is comprised of two separate, but connected sub-systems, Parana Valles and Loire Vallis, and is treated as one system (Boothroyd and Grant 1985). Parana Valles (Fig. 15 and USGS 1980) is a digitate network (after Pieri 1980; Mars Channel Working Group 1983) bounded to the east by the Noachis/Newcomb A multi-ringed impact basin (22.5S, 3W), described by Schultz et al. (1982). Parana Valles shows one of the highest drainage densities on the Martian surface (Baker 1982). This may in part be due to the presence of a thick volatile rich layer associated with the ejecta lithofacies of Noachis/Newcomb A basin to the east, similar to that between the third and fourth rings of the Ladon Basin (Schultz et al. 1982; Schultz, personal communication 1985). Parana Valles drains to the northwest into Parana basin, located within a very degraded impact basin (Fig. 15) that displays positive relief chaos features similar to very large scale pingos (Boothroyd and Grant 1985).

Loire Vallis heads in Parana basin (Fig. 15), thus Parana and Loire Valles are connected and were probably through flowing (Boothroyd and Grant 1985). Loire Valles is a longitudinal stem valley that drains in a northwesterly direction along its entire course, finally debouching into etched terrain at the axis of the Chryse lowland trough close to Samara Valles and Margaritifer Valles (Figs. 2, 7). Between the third and fourth rings of the Ladon impact basin, Loire Valles displays a wide flat-bottomed profile with tighter incised meander bends than Samara Valles. Short high angle tributaries entering into Loire Vallis along this section tend to be more numerous and better developed than along the same section of Samara Valles (Fig. 3c).

The etched terrain that Margaritifer Valles and Samara and Parana/Loire Valles empty into is shown in detail in Figure 7. The unit lies along the axis of the Chryse lowland trough and is bounded on the west, south and east by relatively higher terrain (Fig. 7). The northern boundary has been engulfed by collapse features associated with Margaritifer Chaos. Remnants appear to be unmodified by flow over their tops. However, fluidal erosion from flow out of the three systems was probably responsible for removal of the material between the remnants.

Margaritifer Chaos and Iani Chaos (Fig. 7 and USGS 1980) lie to the north of the etched terrain; Ares Valles outflow channel heads along the northern edge of chaotic terrain. The relationship between Ares Valles, the chaotic terrain,

Fig. 15. Relationship between Parana Valles, Parana Basin and Loire Vallis. Parana Valles heads along a drainage divide (dashed line) located at the crest of a ring of the Noachis multi-ringed impact basin. It drains to the NW, emptying into Parana Basin (22S, 12W). Loire Vallis heads in Parana Basin with paleoflow to the NW, roughly parallel to Samara Valles. Because Loire Vallis heads in Parana Basin, and because the relative ages of the two valley networks are similar (based on crater counts), they can be treated as one system. Positive relief chaotic features (Ctp) are present in Parana Basin (084A46, 47, 48, 615A45).



ORIGINAL PAGE IS
OF POOR QUALITY

etched terrain and flow out of Ladon Basin, Samara and Parana/Loire Valles will be discussed later in the paper.

Besides Margaritifer and Iani Chaos, MC19NE shows several large unnamed valley networks (Fig. 3d and USGS 1980). These networks drain to the north and west and may possibly empty into Iani Chaos. Poor image resolution and thick mantling in the region by relict polar deposits prevent definitive mapping.

The northeastern most corner of MC19NE (Fig. 3d) is the site of a thick blanket of relict polar deposits (Schultz 1984) that completely covers all valley networks and some very large craters (Fig. 16). The deposit may have been created by migration of the pole relative to the stationary spin axis of the planet (Schultz 1984). Because the relict polar deposits always cover the valley networks, Schultz (1984) determined they are younger than the networks. He suggests that by basal melting and/or trapping by impact ejecta or flood basalts, volatiles in the deposits could accumulate in the underlying megaregolith.

Drainage Basin Evolution

Period of Formation

The period of formation for the major valley networks in the quadrangle, Samara and Parana/Loire Valles, was between 8,500 and 4,600 based on the crater densities of surfaces incised by the valleys and those covering them. Figures 9a-d shows the drainage basins for these two systems. The combined drainage area of Samara and Parana/Loire valles is 84% that of the Colorado River in the southwest USA (Table 4). Coupled with the fact that each major sub-basin is drained by at least a third or fourth order system (Strahler stream order classification, Strahler 1952), and the extensive, well integrated nature of these networks becomes evident.

Several of the sub-basins of the two systems underwent extensive resurfacing after formation by the fourth or youngest dated resurfacing event that partially to completely buried parts of the networks. Examples are Clota Valles, S1, S3a, S5, S6, and LP3 (Figs. 17, 18). The formation of some impact craters has also deranged and buried valley segments that were probably once integrated parts of the larger valley network systems.

Figure 10 shows an area in MC19SE centered at 27S, 12W. A sub-basin of the Parana/Loire system (LP3) is in the central portion of the figure. The southern half shows several internal drainage basins (I2, I3a and I3b) separated from LP3 by a drainage divide running E-W along the rim of a

Fig. 16. An example of the typical appearance of relict polar material located in the NE corner of MC19NE described by Schultz (1984). Figure is centered at 1N, 1.5W. Pedestal craters (P) are common, indicating the removal of material around them since their formation (615A36).

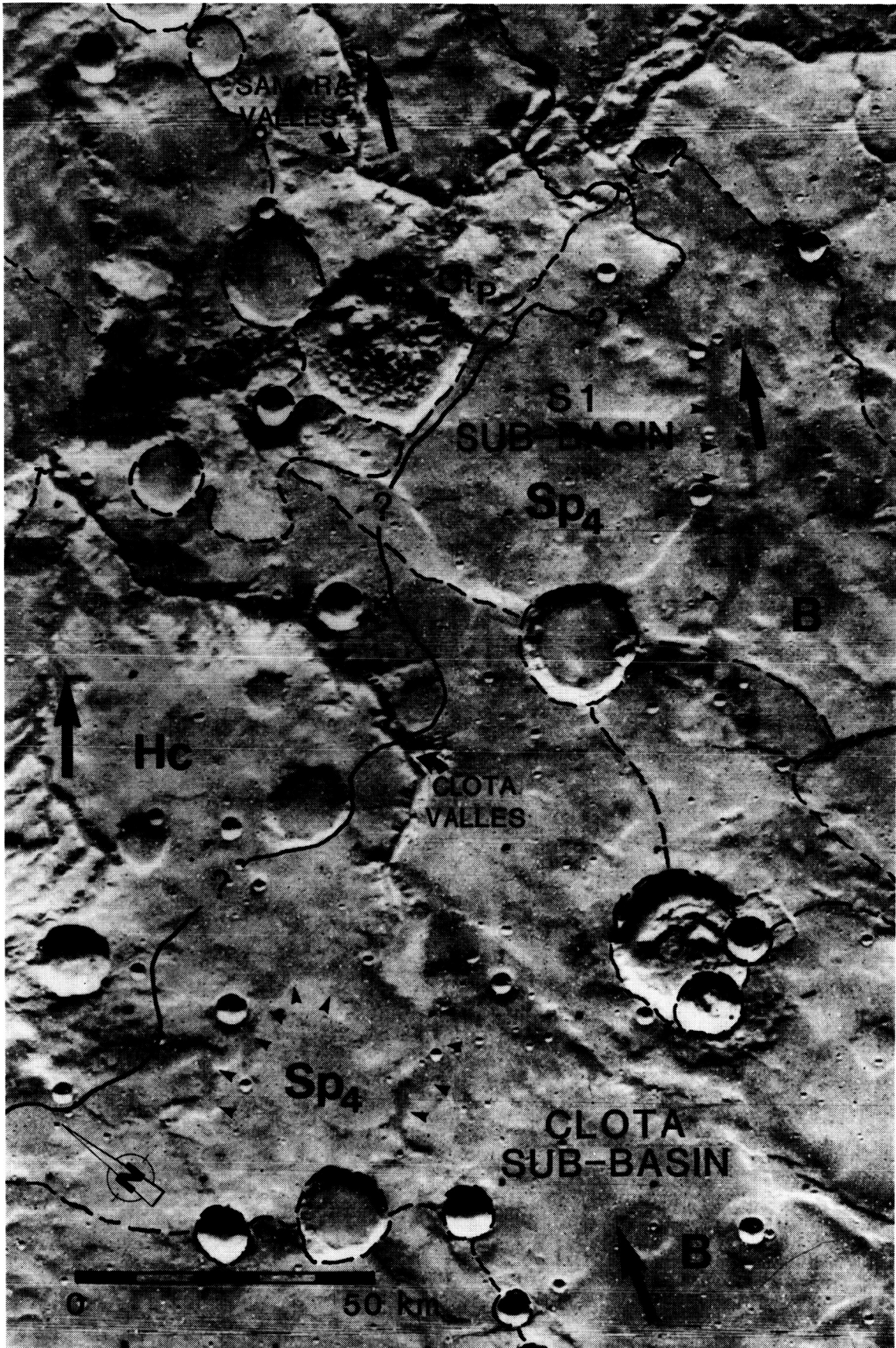
ORIGINAL PAGE IS
OF POOR QUALITY



Fig. 17. LP3 sub-basin of the Parana/Loire drainage system, centered at 26S, 13W. The area shown is the same as the central portion of Figure 10. Valley segments (VS) and some craters (C) are present in the southern 1/3 of the sub-basin that have been partially to completely buried by material associated with the Sp₄ resurfacing event in the northern 2/3 of the sub-basin. The contact between the Sp₃ and Sp₄ material was located using crater counts and is shown as a solid line. Dashed lines show the location of drainage divides. Flow in the sub-basin (large arrows) was to the north and out into Parana Basin via the small, partially filled, outlet shown (084A43, 45).



Fig. 18. Clota Valles and S1 sub-basins of Samara Valles centered at 27S, 21W. Valley segments (small arrows) in both sub-basins have been partially buried by material associated with the Sp₄ resurfacing event. The contact between the Sp₄ and the older material to the north was located using crater counts and is drawn as a solid line. Any valley segments in the southern part of either of these two sub-basins (B) have been completely buried by Sp₄ material. The dashed lines represent the position of drainage divides and the large arrows indicate the flow direction. Positive relief chaotic features are labelled Ct_p (084A40).



class C₄ crater. The regional slope of the area shown in the figure is to the north, determined by stereographic mapping. Figure 19a, a sketch of the area in Fig. 10, shows numerous short northward flowing valley segments incised into the Sp₃ surface (14,000 to 8,100) can be seen in the southern third of LP3 (Figs. 10, 19a) that are completely buried by the Sp₄ unit (6,000-2,000) further to the north (Fig. 19a). A short segment of almost completely buried valley marks the outlet of LP3 into Parana Basin. The I3a and I3b internal drainage basins are also occupied by fairly well developed valley segments indicating paleoflow to the north, that terminate at the southern edge of class C₄ crater Gb where buried by its ejecta (Fig. 19a).

It seems likely that the valley segments in LP3 were once part of a more extensive integrated valley system that drained the entire area and emptied into Parana Basin (Fig. 19b). This drainage has since been completely mantled, except along the southern edge of LP3, by basin fill associated with the last resurfacing event (Sp₄). It also seems likely that internal basins I3a and I3b were once connected to and a part of the LP3 drainage before interruption by the crater Gb impact event. Figure 19b shows a reconstructed drainage pattern for LP3, I3a and I3b before valley burial by the fourth resurfacing event in the northern part of LP3, and before the crater Gb impact event. Drainage was probably much more extensive and better integrated in the past than observed today (Fig. 19b). Similar modifications, mainly burial after valley formation (6,000-2,000), have affected other sub-basins and sections of the trunk systems. Locations include Clota Valles (Fig. 18), S3a, the headward section of Samara Valles, S5, S6, and the northern edge of Parana Basin (Fig. 15).

The presence of several terrace levels in Samara Valles at 29.55, 14.5W (Fig. 14), first identified by Pieri (1980a), indicate that multiple flow events may have occurred there, each resulting in incision below a given terrace level. Another possibility is that the terraces represent differential erosion of material deposited by various resurfacing events. This could have happened as the channel was downcut continuously or during multiple flow events. A stronger case for differential erosion of the strata deposited by resurfacing events can be made for an area on the eastern side of Loire Valles at 20S, 15W (Fig. 20). At this location, headward erosion by small tributaries of Loire Vallis was at different rates on different levels, with the headwall receding more rapidly than any beds below it. Differential erosion may have been due to differences in the composition, porosity and thickness of the various beds.

Samara and Parana/Loire Valles and their associated sub-basins are extensive and well integrated systems, and may

Figs. 19a-b. Figures 19a, b are sketch maps of the area shown in Figure 10, containing the LP3 sub-basin of Parana/Loire Valles and I2, I3a, and I3b internal basins. Several short valley segments are present in the southern half of LP3 (V) and well developed, northward flowing, valley segments exist in I3a and I3b (V) (Fig. 19a). Drainage in LP3 was to the north out into Parana Basin. Much post valley resurfacing (Sp_4) has occurred in the northern 2/3 of LP3 (Fig 19a). The resurfacing appears to have buried all valley segments in that area. Surviving valley segments in the southern 1/3 of the sub-basin are incised into the Sp_3 surface. Valleys in I3a and I3b terminate where buried at the edge of ejecta (E) from crater Gb (Fig. 19a). Figure 19b is a reconstruction of drainage in Parana/Loire sub-basin LP3 before partial valley burial in the northern section by Sp_4 material and interruption of the southern drainage by crater Gb. Existing valley segments in Figure 19b are shown as solid lines, dotted segments are inferred. Drainage divides in Figs. 19a, b are depicted as dashed lines. Arrows show paleoflow direction. See text for further discussion.

Figure 9A

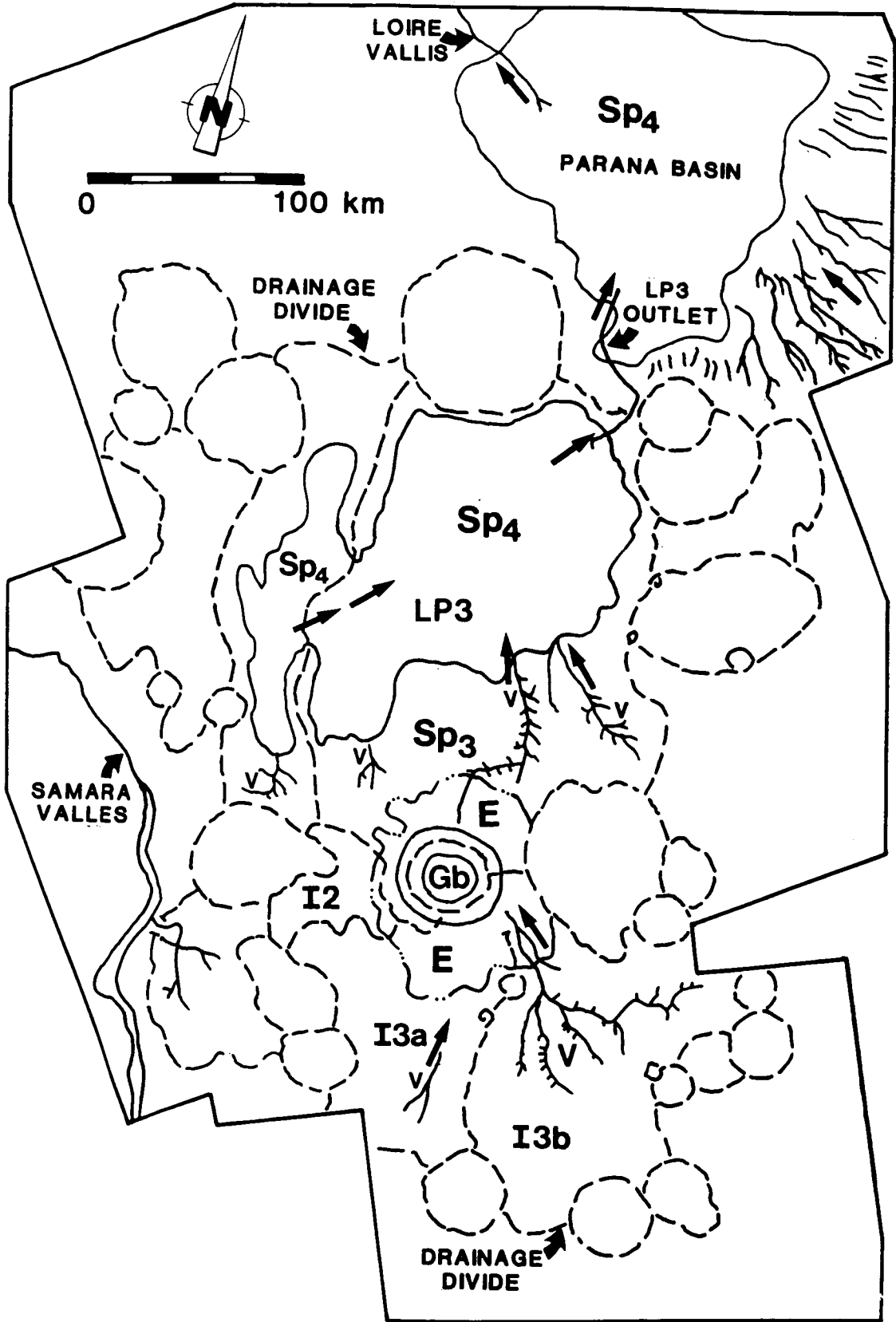


Figure 9B

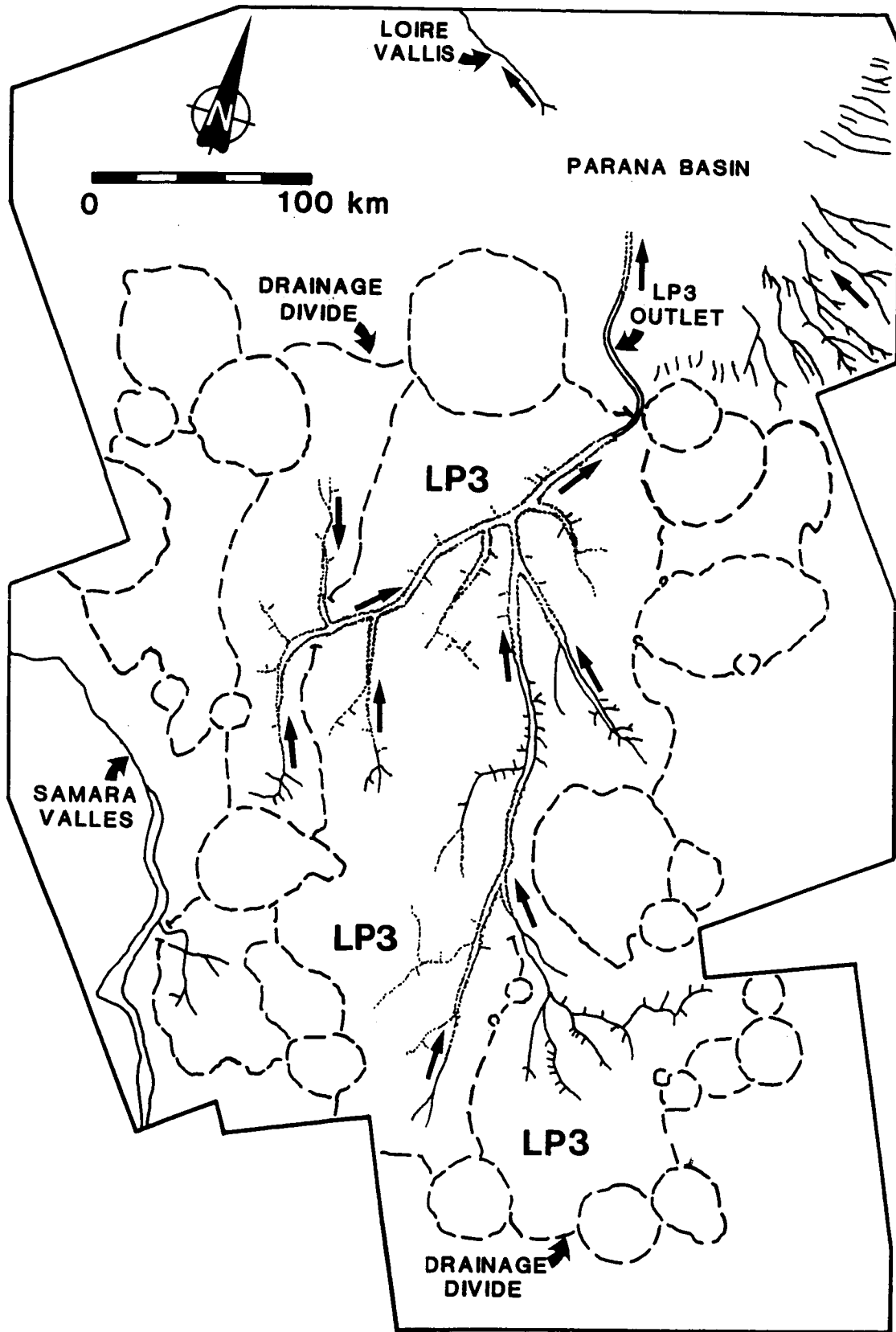


Fig. 20. Headward and middle portions of Loire Vallis with Parana Basin to the SE. The arrowheads in the north central part of the figure show the location where differential erosion of layers in the substrate may have occurred. The geomorphic contact between smooth plains and the heavily cratered terrain is shown by the solid line. The geologic contact between Sp₃ and Sp₄ (in Parana Basin and along the western edge of the photograph), as determined by crater counts, is shown by the dashed/dotted line (615A45).



have been even more extensive and better integrated in the past. Because of this, a relatively long period during which climatic conditions were favorable for network formation must have existed to permit their development. This implies that valley formation, once initiated, was probably more or less continuous throughout the 8,500 to 4,600 (3.73 to 3.6 BYBP) period determined for their formation.

Evidence for an extended period of conditions favorable to valley formation argues against the possibility that a single catastrophic event was responsible for their formation. It seems unlikely that events such as the creation of Argyre Planitia, though huge in scale, could have modified conditions regionally or possibly planetwide for such an extended period of time (probably on the order of 100 million years based on crater counts). A more appealing scenario would be one where a sustained event, capable of affecting conditions on such a large scale, was responsible for the period of valley formation. A possibility of such an event was the period of activity in the Tharsis region associated with the creation of the Syria Rise. This appears to have been mainly a tectonic event that began at about 15,000 and peaked in activity from 10,000 to 5,000 (Wise et al. 1979). The timing of this event is right, however any relationship to the valleys and the creation of conditions favorable to their formation remains unclear and may warrant further investigation.

Valley Network Drainage Densities

Drainage density, the measure of the total valley length/basin area (Gregory and Walling 1973; Baker 1982), is one of the most useful variables in the analysis of drainage basins because it measures the stream density, a fundamental feature of fluvial drainage basins (Gregory and Gardiner 1975; Baker 1982; Abrahams 1984). Simplistically, drainage density is the measure of the basin efficiency in removing excess precipitation in the form of surface runoff (Patton and Baker 1976). Despite its value, few studies have focused on drainage density for several reasons, including the time consuming nature of derivation (Gregory and Gardiner 1975). Only one study besides this one has quantitatively examined the drainage density of Martian valley networks (Baker and Partridge 1984a; Baker 1985), and to date, no drainage density data has been located for terrestrial systems formed by sapping processes.

At the macroscale relevant for Mars (Baker 1985), terrestrial drainage densities are climate controlled (Gregory and Gardiner 1975; Abrahams 1984) and are dependent on mean annual precipitation, its seasonality (Gregory and Gardiner 1975) and intensity (Gregory 1976). Drainage densities are lowest in arid regions (mean annual

precipitation (<180 mm), increase to a maximum in semiarid regions (mean annual precipitation >180mm but <380mm), decrease again in humid areas due to vegetation cover (mean annual precipitation >500mm but <1,000mm) and finally increase to a second maximum in superhumid areas (mean annual precipitation >1,500mm but <3,000mm) (Abrahams 1984).

The drainage densities determined for Samara and Parana/Loire Valles (Table 4) are remarkably similar for both systems ($0.034 \text{ km} \cdot \text{km}^{-2}$ for Samara and $0.039 \text{ km} \cdot \text{km}^{-2}$ for Parana/Loire). This suggests that the mechanism that created the valleys was operating at similar rates during formation of both systems. It further suggests that the substrate beneath the two systems is of fairly uniform composition and that equivalent amounts of fluid, whether of meteoric or subsurface origin, were available to both during formation.

The range of drainage density values observed for the sub-basins and various trunk portions of Samara and Parana/Loire Valles (Table 4 and 5) is probably due to local variations in the amount of resurfacing that has occurred since valley formation and/or local variations in the substrate and amount of fluid available. The Clota Vallis sub-basin shows extensive post valley resurfacing limited mainly to the southern 2/3 of the basin. The observed drainage density of the entire sub-basin is $0.029 \text{ km} \cdot \text{km}^{-2}$, however, if only the northern third of the basin is considered, the density becomes $0.049 \text{ km} \cdot \text{km}^{-2}$. Other sub-basins and portions of the trunk valleys displaying low density values may have been affected in a similar manner.

Mid trunk portions of Samara and Loire Valles and all of Parana Valles may be incised into thick, volatile rich lithofacies associated with ejecta from the multi-ringed impact basins (Schultz et al. 1982; Schultz, personal communication 1985). As discussed above, the presence of this material may be responsible for the higher density values.

The drainage density values calculated for Samara and Parana/Loire Valles are almost an order of magnitude lower than values reported by Baker and Partridge (1984a) and Baker (1985) for 24 Martian valley networks. This difference is due to differences in the technique used to derive the values. Baker and Partridge (1984a) and Baker (1985) used the headward extent of tributaries to define the limit of the drainage basins of the valley networks, not the topographic limit. Because of this, undissected basin between tributaries and above the headward extent of the tributaries was not included in the basin area and resulted in the higher drainage density values. Because the topographic drainage basin areas were utilized for density calculations in this study, the values obtained can be

compared better to terrestrial examples than those obtained by Baker and Partridge (1984a) and Baker (1985).

All drainage density values obtained for the Martian systems are well below those observed for terrestrial systems formed by surface runoff in even the most arid climates (Gregory and Gardiner 1975; Abrahams 1984), suggesting that other processes, such as spring sapping, were responsible for their formation. Unfortunately, drainage density values for terrestrial systems formed by sapping process are unavailable for comparison to Martian values.

Valley Network Genesis

The general characteristics of the valley networks in MC19 are similar to those described by others for networks elsewhere on the planet. The networks in MC19 all head in, and in most cases are located completely within, old heavily cratered terrain. Pieri (1979) and Carr (1979a) noted a similar distribution of networks in MC19 and elsewhere; Carr and Clow (1981) calculated that over 99% of all valley networks were located within heavily cratered terrain. Tributary valleys either hang or appear as deep and wide as trunk valleys; the interfluvial areas between valleys are broad, flat, and undissected. Valley junction angles tend to show wide variability, but in general are low, a characteristic that has been well documented (Pieri 1980a; 1980b; Pieri and Sagan 1979) for other Martian systems. Drainage densities in MC19 and elsewhere are quite low (Baker 1982; 1985; this study), and all the valleys are scale variant (Mars Channel Working Group 1983). In summary, the valley networks in MC19 are morphologically typical of most Martian valley networks.

Pieri and Sagan (1979) compared all of the above mentioned Martian valley characteristics, plus sinuosity, presence of drainage basins, and drainage patterns among others, to characteristics of terrestrial systems. On this basis they concluded that genesis by headward sapping and associated down valley fluvial activity was most consistent with the observed Martian valley morphology. Formation of Martian valley networks by sapping and downstream fluvial activity was first suggested by Sharp and Malin (1975) and is the most popular theory for their formation today (Pieri and Sagan 1979; Pieri 1980a; 1980b; Pieri et al. 1980; Laity and Pieri 1980; Laity 1983; Laity and Malin 1985; Higgins 1982; Mars Channel Working Group 1983).

Laity and Malin (1985) define sapping as the process resulting in undermining and collapse of valley head and side walls, as a result of the reduction or complete loss of basal support due to enhanced weathering and erosion by concentrated fluid flow at a site of seepage. Examples of

terrestrial systems formed mainly by sapping are not easily located. This may be because many drainage systems whose early development was dominated by sapping processes have later been modified by surface runoff and can no longer be recognized (Higgins 1982; 1984). Baker (1982) suggests that systems formed by sapping simply have not received much attention in recent geomorphic research. Laity and Malin (1985) point out that most work that has been done on drainages formed by sapping has focused on small and micro scale systems (Higgins 1974; 1982; D'Amore 1983; 1984), although Higgins (1982; 1984) has suggested that the sapping process is scale independent.

Dunne (1980) developed a model for drainage networks formed by spring sapping. He cited the presence of a sloping water table with drainage towards a hydraulic sink (stream or sea level) as the most important conditions necessary for the initiation of sapping processes. Baker (1982) examined volcanic valleys in Hawaii that have formed by sapping. He noted that the high permeability of the surface materials there has inhibited network development by fluvial action and has thus allowed sapping processes to dominate.

One of the best examples of a terrestrial drainage system formed by sapping processes exists in the Glen Canyon region of the Colorado Plateau, southwestern USA. Because the region contains numerous canyons that are strikingly similar in appearance and scale to Martian valley networks it has recently been studied as a possible analog (Laity and Pieri 19780; Pieri et al. 1980; Laity 1983; Laity and Malin 1985). In addition to conditions outlined by Dunne (1980) and Baker (1982), Laity and Malin (1985) stated that the presence of beds dipping in accordance with the slope was very important in the development of valleys that most closely resemble those seen on Mars. Valleys in the Glen Canyon region that formed where the beds dipped away from the regional slope more closely resemble valleys formed by surface runoff. They also stated the importance of a relatively easily weathered lithology. This allows rapid undermining of the headwall by groundwater, and facilitates the removal of talus following collapse. Laity and Malin (1985) concluded that gross geomorphic processes similar to those forming drainages on the Colorado Plateau may have operated during formation of the Martian valley networks.

Fanale (1976), Carr (1979b) and Baker (1982) among others, have suggested that a thick permafrost layer covers the surface of Mars to a depth of 1 to 2 km. This is supported by numerous occurrences of inferred permafrost features. Saunders (1979) stated that in MC19 the ancient heavily cratered terrain was probably highly brecciated to a depth of at least 1 km. Locations undergoing later resurfacing have had a layer(s) of material deposited on top

of the ancient terrain. These overlaying units are probably thin in most locations, in comparison to the thickness of the ancient brecciated terrain beneath, and may consist of highly permeable lava and ash deposits. In MC19SE, the area between the third and fourth rings of Ladon basin probably contains an even thicker zone of intensely brecciated volatile rich regolith than surrounding areas. This is due to the probable presence of ejecta from the Ladon impact event (Schultz et al. 1982; Schultz, personal communication 1985).

Samara and Parana/Loire Valles in MC19SE have features indicating paleoflow directions accordant with the present regional slope in the area. This suggests that the Chryse lowland trough developed prior to the period of network formation. Material emplaced during resurfacing events prior to trough development would have been tilted to dip in accordance with the regional slope as the trough was formed.

It is apparent from the above discussion that the general conditions described by Dunne (1980), Baker (1982) and Laity and Malin (1985) as necessary for the initiation of sapping processes may be present on a regional scale in MC19SE. Creation of the Chryse lowland trough provided the necessary slope and hydraulic gradient towards the axis of the trough. It also caused the dip of beds on the flanks of the trough to be accordant with the regional slope. The presence of thick intensely brecciated regolith would provide the required permeability for ample groundwater flow. Even higher permeabilities would be expected between the third and fourth rings of Ladon Basin, the site of the most extensively developed sections for the networks. The intensely brecciated nature of the regolith probably also provided the required lithology for high erodeability and easy removal of debris. Regional thawing of the permafrost layer in locations with sufficient ground ice would probably have provided the necessary water to drive the system, although it remains unclear what process or event caused thawing to occur. Once started, sapping would have continued until conditions favoring their formation changed or until the groundwater supply was exhausted (assuming no recharge).

Samara and Parana/Loire Valles, in MC19SE, have extremely low drainage densities that argue strongly against formation by surface runoff. A morphological comparison of the two systems to terrestrial systems show that Samara and Parana/Loire most closely resemble terrestrial systems (e.g. the Glen Canyon region and the Gilf Kebir plateau in southwest Egypt) formed by sapping and associated downstream fluvial activity (Pieri and Sagan 1979). Geologically, the setting of Samara and Parana/Loire Valles appears to meet the general conditions described by Dunne (1980), Baker (1982), and Laity and Malin (1985) as important for network

development by sapping processes. Coupled with drainage density measurements and morphological evidence, and a strong case in favor of development by some sort of sapping process can be presented for Samara and Parana/Loire Valles. Similarities in scale, morphology and setting between Samara and Parana/Loire Valles and other valley networks in the region suggests that sapping processes may have been the dominant mechanism of valley formation throughout the region.

Finally, as pointed out by Baker (1985) caution must be exercised when directly comparing terrestrial and Martian valleys. He states that caution is necessary because: the origin of terrestrial systems is not fully understood; conditions creating the Martian valleys were probably unique; only morphologic parameters can be examined in the case of the Martian networks; and the fact that terrestrial studies have focused on channel networks, whereas Martian studies examine relict valleys. This requires that any conclusion concerning valley genesis and formation must remain speculative in nature.

Geologic/Geomorphic Evolution

The: 1) geologic/geomorphic map constructed of the area (Figs. 3a-d); 2) crater counts, summarized in Figure 5; 3) geologic/geomorphic map unit correlation (Fig. 6); 4) cross-cutting and morphologic relationships; and 5) results of drainage basin mapping and density determination (Figs. 9a-d, 11, Tables 3, 4 and 5); were used to trace the geologic/geomorphic evolution of the Margaritifer Sinus quadrangle.

The Oldest Features and Terrain

The oldest recognizable features present (about 4.5 BYBP) in Margaritifer Sinus are the three multi-ringed impact basins, Ladon, Holden and Noachis, first described by Schultz and Glicken (1979) and Saunders (1979). The formation of these basins resulted in large topographic basins (e.g. Ladon Basin) and deep seated fracture systems that have persisted to the present. Schultz and Glicken (1979) and Schultz et al. (1982) also proposed that a structural zone of weakness associated with an area of overlap of the Ladon and Chryse Basin rings and of the presence of a thick volatile rich ejecta blanket from Ladon Basin may have led to collapse and formation of the chaotic terrain in MC19NW (Figs. 3a,d and USGS 1980). The impact basins have had considerable influence on some of the drainage patterns. A thick blanket of volatile rich ejecta beginning at the limit of excavation of Ladon Basin (Schultz et al. 1982) may be responsible for the relatively higher drainage densities along central portions of Samara and Loire Valles (between the third and fourth rings of the Basin). A similar situation may exist around Noachis/Newcomb A Basin in the area of Parana Valles. Thus the multi-ringed impact basins probably exert the dominant structural control in Margaritifer Sinus.

The oldest dated surface in the quadrangle (1,000,000 to 850,000 or about 4.4 to 4.5 BYBP) was created during the period of early intense bombardment that appears to have affected the entire inner solar system 4.5 to 4.0 BYBP before present (Murray et al. 1981). Where recognized (Figs. 4a-d), the surface is expressed by numerous, large (>50km) craters of various classes. Of the locations where the surface has been dated (Figs. 4a-d), it is best preserved along a broad ridge trending roughly SW-NE from central Samara Valles (29S, 16W to southern Parana Valles (24S, 11W), and in the area to the west of Jones Crater from about 14S to 20S. The surface has been labelled Hc on the basis of its large diameter craters and very high crater densities.

Periods of Resurfacing

Towards the end of the period of intense bombardment, the first dated resurfacing event occurred (4.3 to 4.1 BYBP). The event was probably volcanic in origin and appears to have been the earliest regional modification of the cratered highlands in MC19. Of the locations dated (Figs. 4a-d), the surface is best preserved: 1) along a wide swath through medial and distal Loire Vallis; 2) from Parana Valles SW into MC267NE; and 3) in central areas of MC19NE (from crater count C651A87.01B, Table 2, Appendix 3). Because the event took place during the period of intense bombardment, the surfaces created display high crater densities (300,000 to 100,000) with numerous large diameter craters (20 to 40 km), though smaller in size and fewer in number than the cratered uplands. Thus, the surface is usually mapped as unit Hc where present. Crater densities observed on this surface are similar to those noted by Wise et al. (1979) for the ancient cratered highlands in the Tharsis region.

The next dated resurfacing event took place at the end of the period of intense bombardment (just over 4.0 BYBP). The surface displays moderately high crater densities (70,000 to 40,000) with craters predominantly 5 to 15 km in diameter. This event was also volcanic in origin and regional in extent. The surface is best preserved in the area around 27S, 22W and at the foot of Samara and Loire Valles. At some locations the unit has been almost completely buried by later events. The creation of this surface was concurrent with the end of the crustal destruction of the northern part of Mars (Wise et al. 1979). The unit has been mapped as Hc where superimposed on older, incompletely buried, higher density surfaces, and as Sp₂ where the older material has been completely buried.

The third period of resurfacing was the last to occur before development of the valley networks and was the last to affect the quadrangle on a regional scale. Whenever this unit is present, valley networks are always incised into it. The surface displays crater densities of 14,000 to 8,100 (about 3.75 to 3.8 BYBP) and has been dated at numerous locations in MC19SE, and MC26NE (Fig. 4c). Where thick enough to bury older terrain completely it is labelled as Sp₃. Emplacement of this unit coincided with creation of the Lunae Planum lava plains (from Wise et al. 1979).

Development of the Chryse lowland trough was prior to the initiation of valley network and channel formation (before about 3.8 BYBP). This can be inferred by observing that the paleoflow indicators of direction in the major channels and valleys are generally concordant with the present day regional slope of the area, as first pointed out by Saunders (1979). Several exceptions to this are the interior and

exterior radial centripetal drainage systems on hills surrounding multi-ringed impact basins.

Peak Geomorphic and Tectonic Activity

A peak in geomorphic and tectonic activity occurred in MC19 from 10,000 to 5,000 (3.75 to 3.6 BYBP), concurrent with peak Tharsis tectonic activity (Wise et al. 1979). This period saw the development of major channels and valleys, the etched terrain, and chaotic terrain. Development of grabens and wrinkle ridges also occurred at this time.

Meso-scale Outflow Channels - Channel and valley formation in the quadrangle may have begun with the development of the Uzboi/Holden/Ladon system between 11,000 and 6,200 (about 3.75 to 3.65 BYBP) and associated deposition in Ladon Basin. This event has been associated with flow out of Argyre Planitia (Parker and Pieri 1985b). The age of the system is not well constrained, being based on only five 'average' and 'poor' crater counts from the floor of Ladon Basin. The system may have developed contemporaneously with channel and valleys elsewhere in the region (8,500-4,600), or slightly earlier than the other systems. Earlier development may have been favored by local conditions associated with the Argyre impact event that hastened the release of fluid from that area. This may have occurred before conditions favorable to channel and valley formation were fully developed elsewhere in Margaritifer Sinus.

Flow in the Uzboi/Holden/Ladon system was interrupted as a result of the Holden crater impact event. The floor of Holden crater does show some evidence of flow modification and a relatively small valley crosses the southern crater rim from Uzboi Vallis into the crater (Fig. 21). The flow direction in this small valley has not been determined and it is possible that flow was out of Holden Crater southward into Uzboi Vallis due to a change in local slope associated with Holden crater. There is no evidence that the Uzboi/Holden/Ladon system was through flowing following the Holden impact event. No valleys breaching the northeast side of the crater and connecting with Ladon Valles are present, indicating that Holden Crater probably formed during the late stages of flow, between 9,000 and 6,000 (about 3.74 to 3.65 BYBP). Boothroyd (1982; 1983) and Parker and Pieri (1985b) have suggested that an area of chaotic terrain to the northeast of crater Holden (25.5S, 31W, Fig. 12) served as a late source area for Ladon Valles after interruption of the system by the Holden impact event.

Flow out of Ladon Basin to the northeast, via Margaritifer Valles appears to have been the dominant factor in development of the etched terrain centered at 12S, 22W

Fig. 21. Northern Uzboi Vallis, Holden crater, and small valley cutting across the rim of Holden crater (27.5S, 35W). The floor of Holden crater shows some evidence of flow modification (F), however, due to limited resolution, low slope, and high adjacent local relief, flow direction in the interior connecting channel could not be determined. It is possible that late flow in the channel was southward out of Holden crater, a result of a possible local change in slope associated with the impact. Flow in Uzboi Vallis further to the south (large arrows) is northward (467A18, 19, 20).

ORIGINAL PAGE IS
OF POOR QUALITY

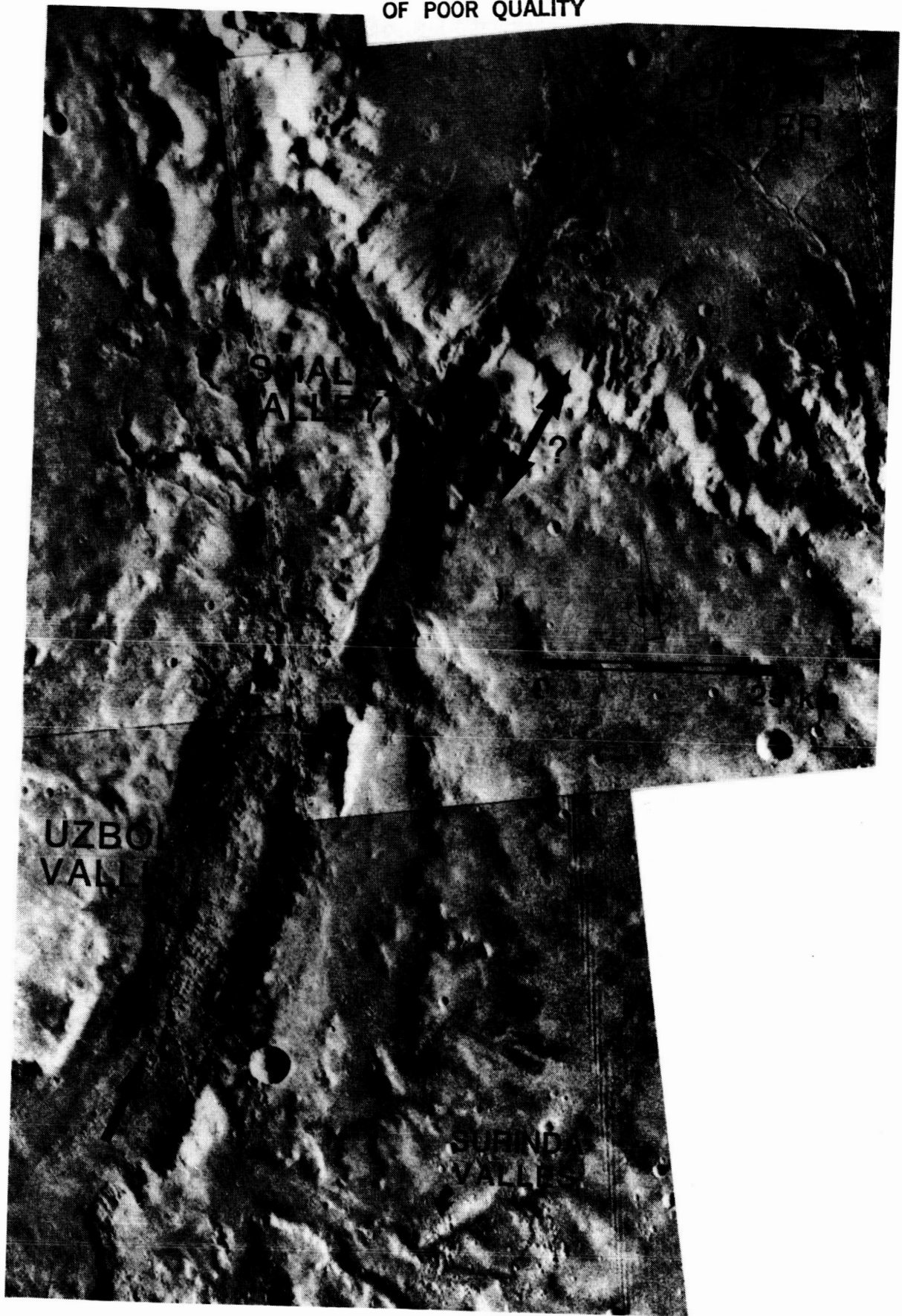


(Fig. 7). This is based on: 1) the large size of the meso-scale outflow channel in comparison to Samara and Parana/Loire Valles; 2) the relatively unmodified nature of several large distributaries clearly associated with Margaritifer Valles; and 3) the position of remnants throughout the system (Fig. 7). There is an apparent lack of distributary channels at the mouth of Samara and Parana/Loire Valles. Crater densities from within the etched terrain indicate a time of formation of 9,000 to 4,600, suggesting that flow out of Ladon Basin occurred at this time. This would mean that development of the Uzboi/Holden/Ladon/Margaritifer system actually may have been more contemporaneous with channel and valley formation elsewhere in the region (8,500 to 4,600) if flow was simultaneous in all segments of the system. But, if ponding in Ladon Basin occurred, release may have been associated with later flow into the Basin from the numerous small valley systems located mainly along its northern edge (see USGS 1980).

Valley Network Formation - The formation of the major valley systems in the quadrangle, Samara and Parana/Loire Valles, was between 8,500 and 4,600 (3.73 to 3.6 BYBP) and probably occurred over much of the time span. This age is based on numerous crater counts and is much better constrained than the age of the Uzboi/Holden/Ladon system. All valleys associated with Samara, Parana/Loire Valles and their tributaries are clearly incised into the unit associated with the third resurfacing event (14,000 to 8,100). A fourth unit, associated with a younger resurfacing event (6,000 to 2,000), and also well dated, always covers the valleys when present. The period of network formation can thus be narrowly constrained based upon the stratigraphic relationship of the networks to the two units. Flow out of Samara and Parana/Loire was into/through the etched terrain and out to the north. However, the lack of features in the etched terrain that can be confidently associated with flow from these valley networks further suggests that the terrain was shaped primarily by flow out of Ladon Basin.

It is possible that valley formation had ended completely by the time of the first occurrence of the fourth smooth plains unit (Sp₄, 6,000), however, because of the range of dates on this surface, and its local occurrence, a more intermediate value, such as 4,600, for the cessation of valley formation is probably more realistic. This suggests that the waning stages of valley formation in the region may have alternated with the initial phases of the last resurfacing event.

Tectonic Activity - The region was also tectonically active during the period 10,000 to 5,000. Almost all features labelled as grabens are approximately parallel to

Valles Marineris and radial to the Syria rise. Parker and Pieri (1985a) have associated these features with early development of Valles Marineris and are therefore probably part of the radial fault system of Tharsis. This would make them similar to grabens described by Wise et al. (1979) in the Tharsis area, thus assigning them an age of 10,000 to 5,500. The only exceptions to the graben orientation described above are a N-S trending graben associated with the Holden impact event (24S, 28.5W, Fig. 3b) and a graben system to the north of Ladon Basin (14S, 31W, see USGS 1980) that is arcuate in form and concentric about the center of Ladon Basin. It probably formed at the same time as the other grabens, but its trend was controlled by the Ladon fracture system.

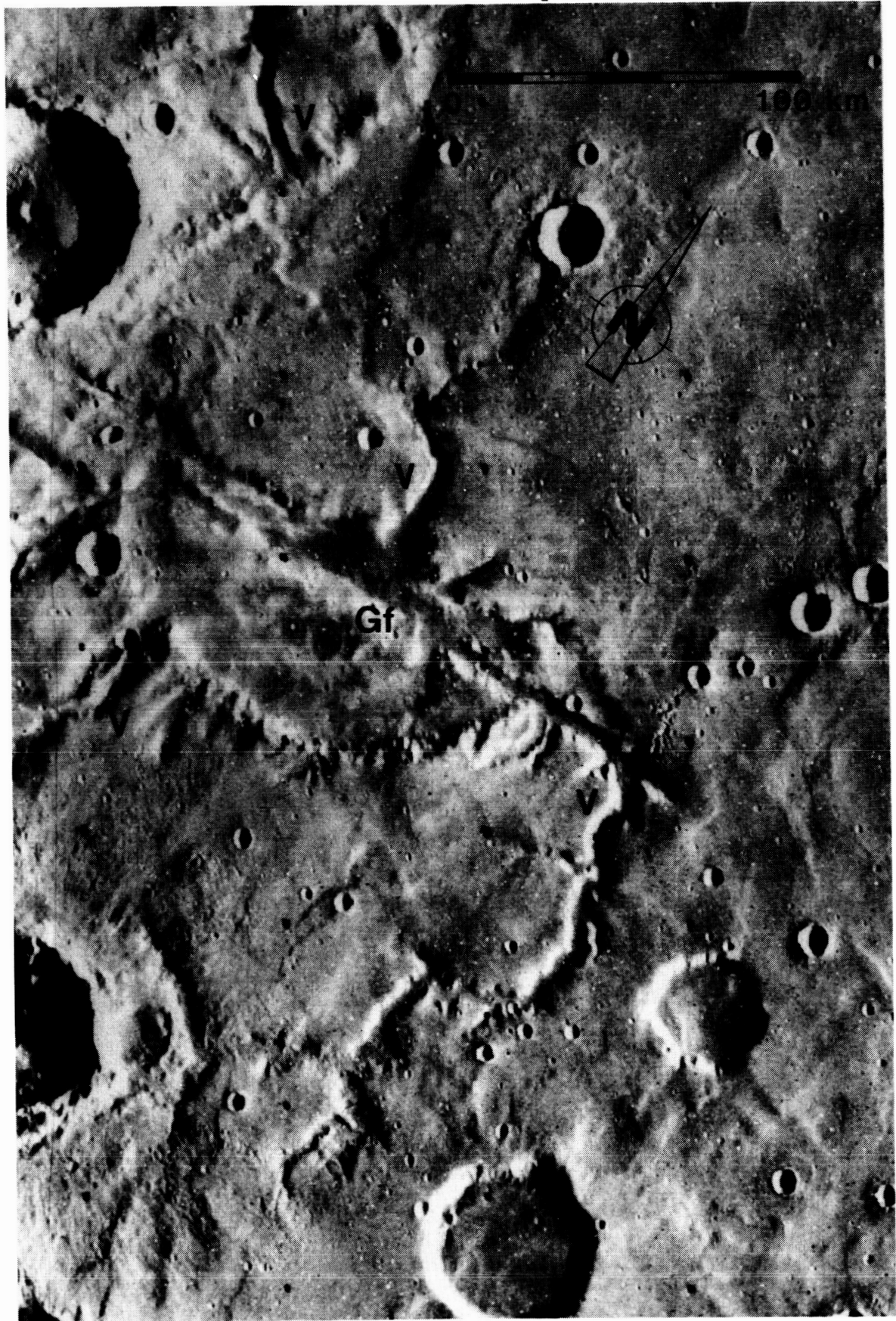
Many grabens have valley networks associated with them and have been flow modified (Fig. 22). Valley network development was definitely post, but probably just after graben formation, as the valleys always cut cross the grabens. Evolution of grabens at the same time that conditions favored valley formation would have created numerous seepage faces from which the valleys could then evolve through spring sapping and the headward extension of valleys, as suggested by numerous authors (Higgins 1974; 1982; Sharp and Malin 1975; Laity and Pieri 1980; Pieri et al. 1980; Mars Channel Working Group 1983; Laity 1983; Laity and Malin 1985).

Features interpreted as wrinkle ridges are oriented roughly N-S and are compressional features that may have formed when buckling occurred in rigid volcanic layers overlaying less competent regolith as described by Parker and Pieri (1985a). Because these features are oriented semi-concentric to the Tharsis region, they are inferred to be part of the semi-concentric system of wrinkle ridges described by Wise et al. (1979). This would assign an age of 10,000 to 5,000 to the wrinkle ridges in Margaritifer Sinus by analogy with those dated by Wise et al. (1979) closer to Tharsis.

Chaotic Terrain Formation - Development of the chaotic terrain in MC19NW and MC19NE (Figs. 3a,d and USGS 1980) was between 10,000 and 2,300 (3.75 to 3.1 BYBP). Initial development was post, but probably essentially synchronous with major channel and valley development and the formation of the etched terrain. The relative ages are based on cross-cutting relationships, as the chaotic terrain always interrupts valleys or etched terrain where they occur.

Chaotic terrain is located predominantly between the third and fourth rings of Ladon Basin, the proposed site of a thick layer of intensely brecciated, volatile rich regolith associated with the ejecta facies of Ladon Basin (Schultz et al. 1982). The region is also postulated to be

Fig. 22. Flow modified graben (Gf) and associated valley networks located at 28S, 23W. All valleys (V) drain into the graben and appear to have originated either along its walls or the walls of the degraded crater bisected by the graben (084A38).



a structural zone of weakness due to overlap of the rings of Chryse and Ladon multi-ringed impact basins and their associated deep seated fracture systems (Schultz and Glicken 1979 and Schultz et al. 1982). The nature of the regolith and presence of numerous fractures would have greatly improved permeability. Later development and thickening of a permafrost layer, after flow through the etched terrain during channel and valley formation, would have substantially increased the pore pressure in the regolith (Carr 1979b), further reducing support in this already structurally weak area. The result would have been the rapid collapse of the surface and the catastrophic outflow of fluid from the region (after Carr 1979b), resulting in the observed downslope flow features and outflow channels to the north. Collapse and outflow would have continued until pore pressures were reduced and the area became more stable, or until outflow had decreased to the point that freezing could occur thus resealing the aquifer (Carr 1979b).

It is possible that development of the chaotic terrain was periodic in nature. A period(s) of collapse may have been associated with each of the following events: 1) discharge from Ladon Basin via Margaritifer Valles (11,000 - 6,200); 2) discharge from Samara and Parana/Loire Valles (8,500 - 4,600); and 3) the continued eastward development of Valles Marineris toward Margaritifer Sinus, probably between 5,000 and 4,000 from Wise et al. (1979). Any chronological combination of these events may reflect reality, however, insufficient data precludes determination of the precise age relationships of these systems/features. Thus, the actual combination of events resulting in collapse, and the number of periods of collapse remains obscure. Following a period of collapse, redevelopment of the permafrost layer and/or later recharge of the aquifer by downslope migration of additional groundwater could have resulted in additional collapse unrelated to the above events (Carr 1979b).

Development of the positive relief chaotic features (5,200?) may also have begun during the period of peak geomorphic and tectonic activity (10,000 to 5,000). The nature and origin of these features, and whether or not they are actively evolving at present, remains obscure. As suggested by Boothroyd and Grant (1985) these features resemble large scale pingos and may or may not have formed in similar manner.

The fretted terrain in MC19NE (Fig. 3d) is inferred to be the incompletely developed edge of the chaotic terrain. It probably occurred during the waning stages of collapse and outflow, either during the initial period of collapse or a possible later period of collapse.

The orientation of the chasma or channels between undissected remnants in the fretted terrain appears to be somewhat structurally controlled (Fig. 3d). However, the orientation of fractures associated with the multi-ringed basins, and the orientation of fractures inferred to be associated with the early opening of Valles Marineris (10,000 to 5,000) is similar. It can not be determined, therefore, which, if either, set of fractures controls the chasma orientation.

A fourth period of resurfacing, between 6,000 and 2,000 (about 3.65 to 2.5 BYBP) began as the period of channel and valley formation was nearing its end. This event was probably of volcanic origin and occurred locally, filling basins. The unit is the youngest dated in the quadrangle and is mapped as Sp₄. Emplacement coincided with the building of Alba and Uranis Patera (Wise et al. 1979), and at the time of enlargement of Valles Marineris eastward.

Post Channel and Valley Formation Activity

Following the period of channel formation the relict polar deposits described by Schultz (1984) in the NE corner of MC19NE (Figs. 3d, 16) were emplaced. The relationship of those deposits to the adjacent Iani Chaos is unknown due to poor image coverage and resolution. Although undated, an age between 4,500 and 2,000 (3.5 to 2.5 BYBP) appears reasonable, based on the stratigraphic relationship of the unit to the valleys and other smooth plains units.

Jones Crater (19S, 20W) was formed sometime after the peak period of geomorphic and tectonic activity. Ejecta associated with the crater partially to completely covers all valleys and grabens present (Fig. 13). Two tentative crater counts performed on the Jones ejecta blanket have yielded an age of 3,500 to 3,000 (about 3.4 BYBP) for the crater, making it one of the youngest dated features in the quadrangle.

Eolian mantling following the Sp₄ event may account for significant deposits around the quadrangle. Numerous locations display a subdued appearance as a result of this mantling, and in some locations the complete burial of features may have occurred. Thus, eolian mantling, occurring after the Sp₄ event, may represent a separate, undated, resurfacing event in some locations. Eolian dune formation and mass movement have probably occurred throughout the history of the planet. Present day locations of these features include crater floors and the floors of Eos and Capri Chasma. Dunes probably exist in other locations not mapped, such as on the plains units, and mass movement has probably occurred anywhere there was sufficient relief.

CONCLUSIONS

1) The oldest recognizable features in Margaritifer Sinus, based on cross-cutting relationships, are the three multi-ringed impact basins, Ladon, Holden, and Noachis, first described by Schultz and Glicken (1979) and Saunders (1979). These basins have remained as the dominant structural control in Margaritifer Sinus to the present.

2) The oldest dated surface in Margaritifer Sinus (1,000,000 - 850,000 craters $> 1 \text{ km} \cdot 10^6 \text{ km}^{-2}$) was created during the period of early intense bombardment (4.5 to 4.0 BYBP). Since that time numerous events, including four resurfacing events of volcanic, fluid or eolian origin, have occurred.

a) The earliest resurfacing event (300,000 - 100,000) was of regional extent and was the first modification of the ancient highlands in the area.

b) The second event (70,000 - 40,000) was also of regional extent and coincides with the crustal destruction of the northern third of Mars.

c) The third event (14,000 - 8200) was the last of regional extent and is the youngest surface dissected by valley networks. This event coincided with the end of emplacement of the Lunae Planum lava plains.

d) Following the third event, the peak period of geomorphic activity occurred from 10,000 - 5000 (3.75 - 3.6 BYBP) concurrent with peak Tharsis tectonic activity.

e) The fourth resurfacing event (6000 - 2000) occurs locally, filling basins, and always covers valley networks when present. Emplacement was contemporaneous with the opening of Valles Marineris.

f) Following the last resurfacing event, geomorphic activity has resulted in: 1) eolian deposits that mantle, and sometimes completely bury, features in some locations; 2) the formation of relict polar material; 3) the possible continued development of positive relief chaotic features; 4) the Jones impact event; and 5) mass movement and eolian dune deposits.

3) During the peak period of geomorphic activity the following events related to fluid release occurred: a) the development of Uzboi/Holden/Ladon Valles with deposition in Ladon Basin (11,000 - 6,200); b) the formation of Samara and Parana/Loire Valles in MC19SE (8,500 - 4,600); c) flow out of Ladon Basin via Margaritifer Valles and, to a limited extent, flow out of Samara and Parana/Loire Valles that created etched terrain (9,000 - 4,500) at their confluence;

and d) initial development of Margaritifer and Iani Chaos (10,000 - 2,300), which was immediately post channel and valley formation.

4) Channel and valley formation may have begun with development of the Uzboi/Holden/Ladon system (11,000 - 6,200). However, if ponding in Ladon Basin did not occur and flow in Uzboi/Holden/Ladon was continuous into the etched terrain, dates within the etched terrain (9,000 - 4,600) suggest that development actually was contemporaneous with channel and valley formation elsewhere (8,500 - 4,600).

5) Development of Margaritifer and Iani Chaos (10,000 - 2,300) may have been periodic in nature. A period of collapse associated with each of the following events is possible: a) discharge from Ladon Basin; b) discharge from Samara and Parana/Loire Valles (8,500 - 4,600); and c) development of Valles Marineris into Margaritifer Sinus (around 5,000 - 4,000). Any chronological combination of these events may reflect reality, however, insufficient age data prevents the actual combination of events and number of periods of collapse from being determined. Additional periods of collapse, unrelated to these events, may have occurred in the manner described by Carr (1979b).

6) Samara and Parana/Loire Valles are extensive well-integrated fluvial systems with a combined drainage area of 535,550 km², 84% of that of the Colorado River in the southwestern USA. As a result of resurfacing episodes after valley formation and impact events, some valley burial and network derangement has occurred indicating that these systems were more extensive in the past.

7) The extensive, well-integrated nature of Samara and Parana/Loire Valles and their sub-basins requires a relatively long period of favorable climatic conditions to have existed to allow their evolution. Once initiated, valley creation was probably continuous throughout the interval (8,500 - 4,600).

8) Development of Samara and Parana/Loire Valles was most likely a result of sapping processes because: a) the geologic setting of the two systems appears to meet the general conditions described by Dunne (1980), Baker (1982) and Laity and Malin (1985) as important for the initiation of terrestrial network development by sapping processes; b) drainage densities for Samara (0.034 km·km⁻²) and Parana/Loire Valles (0.039 km·km⁻²) are well below those observed for terrestrial systems formed by surface runoff; and c) morphologically, Samara and Parana/Loire Valles most closely resemble terrestrial systems formed by sapping and associated downstream fluvial activity (Pieri and Sagan 1979).

9) The similarity in drainage density values between Samara and Parana/Loire valleys suggests that the mechanism that created the valleys was operating at similar rates during formation of the two systems. It further suggests that the substrate beneath the two systems is of fairly uniform composition and that equivalent amounts of fluid, whether of meteoric or subsurface origin, were available to both systems on a regional scale.

10) The range of density values that is observed for the sub-basins and various trunk portions of Samara and Parana/Loire Valles is probably because of: a) local variations in the amount of resurfacing that has occurred after valley formation thus masking original higher drainage densities; and b) variations in substrate and the amount of fluid available on a local scale.

REFERENCES CITED

- ABRAHAMSON, A.D., 1984, Channel networks: A geomorphological perspective: Water Res. Research, v. 20, p. 161-188.
- BAKER, V.R., 1980a, Geomorphic mapping of dry valley systems on Mars: Reports of the Planetary Geology Program, NASA Tech. Memo. B1776, p. 54-56.
- BAKER, V.R., 1980b, Nirgal Vallis: Reports of the Planetary Geology Program, NASA Tech. Memo. B2385, p. 345-347.
- BAKER, V.R., 1982, The channels of Mars: Austin, Texas, University of Texas press, 198p.
- BAKER, V.R., 1985, Paleohydrologic implications of valley networks on Mars: Reports of the Planetary Geology Program, NASA Tech. Memo. B7563, p. 313-315.
- BAKER, V.R. AND KOCHER, R.C., 1979, Martian channel morphology: Maja and Kasei Valles: Jour. Geophys. Research, v. 84, p. 7961-7983.
- BAKER, V.R. AND PARTRIDGE, J.B., 1984a, Morphometry of small valley networks on Mars: p. 23-24, in Lunar and Planetary Science XV, Lunar and Planetary Institute, Houston, Texas.
- BAKER, V.R. AND PARTRIDGE, J.B., 1984b, Pristine and degraded segments of small valley networks on Mars: p. 25-26, in Lunar and Planetary Science XV, Lunar and Planetary Institute, Houston, Texas.
- BOOTHROYD, J.C., 1982, Ancient fluvial drainage systems: Margaritifer Sinus area, Mars: Reports of the Planetary Geology Program, NASA Tech. Memo. B5127, p. 209-212.
- BOOTHROYD, J.C., 1983, Fluvial drainage systems in the Ladon Basin area: Margaritifer Sinus area, Mars: Geol. Soc. America Abstracts with Programs, v. 15, p. 530.
- BOOTHROYD, J.C. AND TIMSON, B.S., 1981, Geomorphic mapping of Capri Chasma: Reports of the Planetary Geology Program, NASA Tech. Memo. B4211, p. 302-304.
- BOOTHROYD, J.C. AND TIMSON, B.S., 1983, The Sagavanirktok and adjacent river systems, Eastern North Slope, Alaska: An analog for ancient fluvial terrain on Mars: p. 74-79, in Permafrost: Fourth International Conference, Proceedings, National Academy Press, Washington, DC, 1524p.

- BOOTHROYD, J.C. AND GRANT, J.A., 1984, Fluvial drainage systems: Margaritifer Sinus and Argyre (NC,NE) quadrangles, Mars: Reports of the Planetary Geology Program, NASA Tech. Memo. 86246, p. 182-184.
- BOOTHROYD, J.C. AND GRANT, J.A., 1985, Fluvial drainage basins and valley networks: Eastern Margaritifer Sinus, Mars: Reports of the Planetary Geology Program, NASA Tech. Memo. 87563, p. 316-318.
- CARR, M.H., 1974, The role of lava erosion in the formation of Lunar rilles and Martian channels: Icarus, v. 22, p. 1-23.
- CARR, M.H., 1979a, Distribution of small channels on Mars: Reports of the Planetary Geology Program, NASA Tech. Memo. 80339, p. 337.
- CARR, M.H., 1979b, Formation of Martian flood features by the release of water from confined aquifers: Jour. Geophys. Research, v. 84, p. 2995-3007.
- CARR, M.H., 1980a, Fluvial history of Mars: Reports of the Planetary Geology Program, NASA Tech. Memo. 82385, p. 342-344.
- CARR, M.H., 1980b, Survey of Martian fluvial features: Reports of the Planetary Geology Program, NASA Tech. Memo. 81776, p. 265-267.
- CARR, M.H., 1981, The surface of Mars: New Haven, Conn., Yale University Press, 232p.
- CARR, M.H., 1984, Mars: p. 207-263, in Carr, M.H. (ed.), The geology of the terrestrial planets, NASA SP-469: NASA, Washington, D.C., 317p.
- CARR, M.H. AND CLOW, G.D., 1981, Martian channels and valleys: Their characteristics, distribution and age: Icarus, v. 48, p. 91-117.
- CHAPMAN, C.R., POLLACK, J.B. AND SAGAN, C., 1969, Analysis of the Mariner-4 cratering statistics: The Astronomical Journal, v. 74, p. 1039-1051.
- CRATER ANALYSIS TECHNIQUES WORKING GROUP, 1978, Standard techniques for presentation and analysis of crater size-frequency data: NASA Tech. Memo. 79730, 21p.
- D'AMORE, D.W., 1983, Hydrogeology and geomorphology of the Great Sanford Outwash Plain, York County, Maine: Tech. Report No. 3, Boston, Mass., Boston University Dept. of Geology.

- D'AMORE, D.W., 1984, Branch Brook in York County Maine: Formation and maintenance of a drainage network by groundwater sapping: p. 370-380, in Hanson, L.S. (ed.), Geology of the coastal lowlands, Boston, MA, to Kennebunk, ME: 76th Annual NEIGC Guidebook, 1984.
- DUNNE, T., 1980, Formation and controls of channel networks: Progress in Phys. Geog., v. 4, p. 211-239.
- FANALE, F.P., 1976, Martian volatiles: Their degassing history and geochemical fate: Icarus, v. 28, p. 179-202.
- FLORENSKI, C.P., BASILEUSKI, A.T., KUZMIN, R.O. AND CHERNAYA, I.M., 1975, Geomorphic analysis of some Martian surface images from the Mars 4 and 5 automatic stations: Icarus, v. 26, p. 219-229.
- FREY, H., 1974, Surface features on Mars: Ground-based albedo and radar compared with Mariner-9 topography: Jour. Geophys. Research, v. 79, p. 3907-3916.
- GRANT, J.A. AND BOOTHROYD, J.C., 1984, Geomorphic mapping and delineation of drainage basin boundaries: Margaritifer Sinus (SE) quadrangle, Mars: Geol. Soc. America Abstracts with Programs, Northeastern Section, v. 16, p. 19.
- GREELEY, R., LEACH, R.N., WILLIAMS, S.H., WHITE, B.R., POLLACK, J.B., KRINSLEY, D.H. AND MARSHALL, J.R., 1982, Rate of wind abrasion on Mars: Jour Geophys. Research, v. 87, p. 10,009-10,024.
- GREGORY, K.J., 1976, Drainage networks and climate: p. 289-315, in Derbyshire, E. (ed.), Geomorphology and climate: London, John Wiley and Sons Press, 514p.
- GREGORY, K.J. AND WALLING, D.E., 1973, Drainage basin form and process: A geomorphological approach: New York, John Wiley and Sons, 458p.
- GREGORY, K.J. AND GARDINER, V., 1975, Drainage density and climate: Z. Geomorph. N.F., v. 19, p. 287-298.
- HARTMANN, W.K., 1965, Terrestrial and Lunar flux of large meteorites in the last two billion years: Icarus, v. 4, p. 157-165.
- HARTMANN, W.K., 1973, Martian cratering, 4, Mariner 9 initial analysis of cratering chronology: Jour. Geophys. Research, v. 78, p. 4096-4116.
- HIGGINS, C.G., 1974, Model drainage networks developed by ground-water sapping: Geol. Soc. America Abstracts with Programs, v. 6, p. 794-795.

- HIGGINS, C.G., 1982, Drainage systems developed by sapping on Earth and Mars: *Geology*, v. 10, p. 147-152.
- HIGGINS, C.G., 1984, Piping and sapping: Development of landforms by groundwater outflow: p. 18-58, in LaFleur, R.G. (ed.), *Ground water as a geomorphic agent, The Binghamton Symposia in Geomorphology: International Series*, no. 13: Boston, Mass, Allen and Unwin, Inc., 389p.
- HILLER, K. AND NEUKUM, G., 1979, Ages of Martian volcanoes and erosional features: *Reports of the Planetary Geology Program, NASA Tech. Memo. 80339*, p. 173-175.
- HILLER, K. AND NEUKUM, G., 1980, Time sequence of martian geologic features: *Reports of the Planetary Geology Program, NASA Tech. Memo. 81776*, p. 119-121.
- LAITY J.E., 1983, Diagenetic controls on groundwater sapping and valley formation, Colorado Plateau, revealed by optical and electron microscopy: *Physical Geography*, v. 4, p. 103-125.
- LAITY J.E. AND PIERI, D.C., 1980, Sapping processes in tributary valley systems: *Reports of the Planetary Geology Program, NASA Tech. Memo. 81776*, p. 295-297.
- LAITY, J.E. AND MALIN, M.C., 1985, Sapping processes and the development of theater-headed valley networks on the Colorado Plateau: *Geol. Soc. America Bull.*, v. 96, p. 203-217.
- MARCUS, A.H., 1968, Martian craters: Number density: *Science*, v. 160, p. 1333-1335.
- MARS CHANNEL WORKING GROUP, 1983, Channels and valleys on Mars: *Geol. Soc. America Bull.*, v. 94, p. 1035-1054.
- MASURSKY, H., 1973, An overview of geological results from Mariner 9: *Jour. Geophys. Research*, v. 78, p. 4009-4030.
- MASURSKY, H., DIAL, A.L., Jr. AND STROBELL, M.E., 1980, Martian channels - A late Viking view: *Reports of the Planetary Geology Program, NASA Tech. Memo. 82385*, p. 184-187.
- MASURSKY, H., BOYCE, J.M., DIAL, A.L., SCHABER, G.G. AND STROBELL, M.E., 1977, Classification and time of formation of Martian channels based on Viking data: *Jour. Geophys. Research*, v. 82, p. 4016-4038.

- MCGILL, G.E., 1977, Craters as "fossils": The remote dating of planetary surface materials: Geol. Soc. America Bull., v. 88, p. 1102-1110.
- MCGILL, G.E. AND WISE, D.U., 1972, Regional variations in degradation and density of Martian craters: Jour. Geophys. Research, v. 77, p. 2433-2441.
- MILTON, D.J., 1973, Water and processes of degradation in the Martian landscape: Jour. Geophys. Research, v. 78, p. 4037-4047.
- MURRAY, B.C., MALIN, M.C. AND GREELEY, R., 1981, Earthlike planets: San Francisco, Calif., W.H. Freeman press, 387p.
- MURRAY, B.C., SODERBLOM, L.A., SHARP, R.P. AND CUTTS, J.A., 1971, The surface of Mars: 1. Cratered terrains: Jour. Geophys. Research, v. 76, p. 313-330.
- MUTCH, T.A., ARVIDSON, R.E., HEAD, J.W., III, JONES, K.L. AND SAUNDERS, R.S., 1976, The geology of Mars: Princeton, New Jersey, Princeton University Press, 400p.
- NEUKUM, G. AND WISE, D.U., 1976, Mars: A standard crater curve and possible new time scale: Science, v. 194, p. 1381-1387.
- NEUKUM, G. AND HILLER K., 1981, Martian ages: Jour. Geophys. Research, v. 86, p. 3097-3121.
- NEUKUM, G., HILLER, K. AND HENKEL, J., 1979, Martian absolute time scales: Reports of the Planetary Geology Program, NASA Tech. Memo. 80339, p. 170-172.
- PARKER, T.J. AND PIERI, D.C., 1985a, Geomorphology and geology of the southwestern Margaritifer Sinus and Argyre regions of Mars-1: Geological and geomorphological overview: Reports of the Planetary Geology and Geophysics Program, NASA Tech. Memo. 87563, p. 361-363.
- PARKER, T.J. AND PIERI, D.C., 1985b, Geomorphology and geology of the southwestern Margaritifer Sinus and Argyre regions of Mars-3: Valley types and distribution: Reports of the Planetary Geology and Geophysics Program, NASA Tech. Memo. 87563, p. 367-368.
- PATTON, P.C. AND BAKER, V.R., 1976, Morphometry and floods in small drainage basins subject to diverse hydrogeomorphic controls: Water Res. Research, v. 12, p. 941-952.
- PIERI, D.C., 1979, Global distribution of Martian valley systems: Reports of the Planetary Geology Program, NASA Tech. Memo. 80339, p. 353-356.

- PIERI, D.C., 1980a, Geomorphology of Martian valleys: p. 1-60 in Advances in Planetary Geology, NASA Tech. Memo. B1979, 326p.
- PIERI, D.C., 1980b, Geomorphology of valley networks on Mars: Speculations on their origins: p. 82-87, in Planetary Water: Proceedings of the Third Colloquium on, Niagra Falls, N.Y., October, 27-29, 1980, 189p.
- PIERI, D.C. AND SAGAN, C., 1979, Origin of Martian valleys: Reports of the Planetary Geology Program, NASA Tech. Memo. 80339, p. 349-352.
- PIERI, D.C., MALIN, M.C. AND LAITY, J.E., 1980, Sapping: Network structure in terrestrial and martian valleys: Reports of the Planetary Geology Program, NASA Tech. Memo. 81776, p. 292-294.
- SAUNDERS, S.R., 1979, Geologic map of the Margaritifer Sinus quadrangle of Mars: USGS Map I-1144 (MC-19).
- SCHULTZ, P.H., 1984, Polar wandering on Mars and the distribution of water-ice through time: p. 71-73, in "Water on Mars" Workshop Abstracts Volume, 1984.
- SCHULTZ, P.H. AND GLICKEN, H., 1979, Impact crater and basin control of igneous processes on Mars: Jour. Geophys. Research, v. 84, No. B14, p. 8033-8047.
- SCHULTZ, P.H. AND LUTZ-GARIHAN, A.B., 1982, Grazing impacts on Mars: A record of lost satellites: Jour. Geophys. Research, v. 87, p. A84-A96.
- SCHULTZ, P.H., SCHULTZ, R.A. AND ROGERS, J., 1982, The structure and evolution of ancient impact basins on Mars: Jour. Geophys. Research, v. 87, No. B12, p. 9803-9820.
- SCHUMM, S.A., 1974, Structural origin of large Martian channels: Icarus, v. 22, p. 371-384.
- SCOTT, D.H. AND CARR, M.H., 1978, Geologic map of Mars: USGS Map I-1083.
- SHARP, R.P., 1973, Mars: troughed terrain: Jour. Geophys. Research, v. 78, p. 4063-4072.
- SHARP, R.P. AND MALIN, M.C., 1975, Channels on Mars: Geol. Soc. America Bull., v. 86, p. 593-609.
- SODERBLOM, L.A., CONDIT, C.D., WEST, R.A., HERMAN, B.M. and KRIEDLER, T.J., 1974, Martian planetwide crater distributions: Implications for geological history and surface processes: Icarus, v. 22, p. 239-263.

- STRAHLER, A.N., 1952, Hypsometric (area-altitude) analysis of erosional topography: Geol. Soc. America Bull., v. 63, p. 1117-1142.
- U.S. GEOLOGICAL SURVEY, 1975, Shaded relief map of the Argyre quadrangle Mars: USGS Map I-923 (MC-26).
- U.S. GEOLOGICAL SURVEY, 1976, Topographic map of the Margaritifer Sinus quadrangle Mars: USGS Map I-975 (MC-19).
- U.S. GEOLOGICAL SURVEY, 1979a, Controlled photomosaic of the Argyre NE quadrangle Mars: USGS Map I-1193 (MC-26NE).
- U.S. GEOLOGICAL SURVEY, 1979b, Controlled photomosaic of the Margaritifer Sinus SW quadrangle of Mars: USGS Map I-1209 (MC-19SW).
- U.S. GEOLOGICAL SURVEY, 1979c, Controlled photomosaic of the Margaritifer Sinus SE quadrangle of Mars: USGS Map I-1210 (MC-19SE).
- U.S. GEOLOGICAL SURVEY, 1979d, Controlled photomosaic of the Margaritifer Sinus NW quadrangle of Mars: USGS Map I-1381 (MC-19NW).
- U.S. GEOLOGICAL SURVEY, 1979e, Controlled photomosaic of the Margaritifer Sinus NE quadrangle of Mars: USGS Map I-1382 (MC-19NE).
- U.S. GEOLOGICAL SURVEY, 1980, Shaded relief map of the Margaritifer Sinus quadrangle Mars: USGS Map I-1293 (MC-19).
- WEIHAUPT, J.G., 1974, Possible origin and probable discharges of meandering channels on the planet Mars: Jour. Geophys. Research, v. 79, p. 2073-2076.
- WISE, D.U., 1979, Geologic map of the Arcadia quadrangle of Mars: USGS Map I-1154 (MC-3).
- WISE, D.U., 1984, Kasei Vallis of Mars: Dating the interplay of tectonics and geomorphology: Geol. Soc. America Abstracts with Programs 1984, v. 16, no. 6, p. 699.
- WISE, D.U., 1985, Kasei Vallis of Mars: Dating the interplay of tectonics and geomorphology: Reports of the Planetary Geology Program, NASA Tech. Memo. 87563, p. 512.

- WISE, D.U. AND MILKOWSKI, G., 1980, Dating methodology of small, homogeneous crater populations applied to the Tempe-Utopia Trough region of Mars: Reports of the Planetary Geology Program, NASA Tech. Memo. 81776, p. 122-124.
- WISE, D.U., GOLOMBECK, M.P. AND MCGILL, G.E., 1979, Tharsis province of Mars: Geologic sequence, geometry, and a deformation mechanism: *Icarus*, v. 38, p. 456-472.

APPENDIX 1

Crater Counting Methodology

Theory

The D.U. Wise method of dating local surfaces was employed to complete crater counts on various surfaces within MC19. This method uses relatively small areas displaying a homogeneous distribution of craters in some size range (Wise et al. 1979; Wise and Milkowski 1980). Most other methods of crater counting utilize relatively larger areas in an effort to build a large statistical base (Wise and Milkowski 1980). These other methods are effective when applied to single age surfaces, however, the method becomes ineffective in regions affected by multiple resurfacing events (Wise et al. 1979).

Lava flooding, mantling or erosion, occurring as resurfacing events, preferentially destroys smaller craters, due to their small volume and area, and usually only partially destroys larger craters. The result is an alteration in the crater size frequency distribution on surfaces affected by a resurfacing event(s), the extent of which being dependent on flow magnitude, thickness and frequency of occurrence, so that it represents at least two crater populations (Figs. 23a-d) (Neukum and Hiller 1981; Wise and Milkowski 1980). Each resurfacing event will affect crater populations in a similar manner, completely burying small craters and sometimes all craters in some locations, and leaving larger craters or patches of larger craters partially buried that represent an older surface and show through the cover material.

As pointed out by Neukum and Wise (1976) Neukum and Hiller (1981) and Wise and Milkowski (1980) a cumulative crater size-frequency plot performed on a large area affected uniformly by a resurfacing event will show flattening in the smaller crater sizes (Fig. 23a) or yield a curve with two segments parallel to the standard curve, but separated by a distinct bump. In the second case, one segment represents all the larger craters that survived the resurfacing event. Projection of the Martian standard curve (Neukum and Hiller 1981) through this segment to 1 km may yield a valid cumulative crater number for the older surface. The other segment represents the crater history of the surface following the resurfacing event. Projection to 1km for this section will yield only an approximate age for the resurfacing event. A crater size-frequency plot derived from an area affected by multiple resurfacing events will display numerous bumps that will prevent reliable ages for the various surfaces from being determined.

Even in an area affected by only one resurfacing event problems arise. If resurfacing did not uniformly affect the area, as often is the case, the larger surviving craters may only be visible in patches. A crater size frequency plot from such a location would result in a curve that is flat

Fig. 23. Fig 23a is a cumulative crater size-frequency plot obtained by counting all craters present in an area centered on 12S, 16W (see Fig. 4 and Table 2 for the location of count C651AB7.001). The curve is noticeably flat for craters less than 10 to 15 km in diameter, and it displays several bumps and different slopes. This is most likely the result of one or several periods of resurfacing. Comparison with the Martian standard curve (Fig. 25) would yield only one age for this curve, based on the largest craters, as that portion of the plot most closely matches the slope of the standard curve. Close examination of the region shows that three distinct size ranges of craters are present. Using the method of dating local surfaces and the three crater size ranges present, three plots (Fig. 23b-d), each representing a period of resurfacing, have been generated. Each curve yields a relative age that corresponds to events dated elsewhere in the quadrangle: Fig. 23b to the Sp₁ event (age 110,000); Fig. 23c to the Sp₄ event (age 3,100); and Fig. 23d to the Sp₃ event (age 13,900).

Fig. 23a

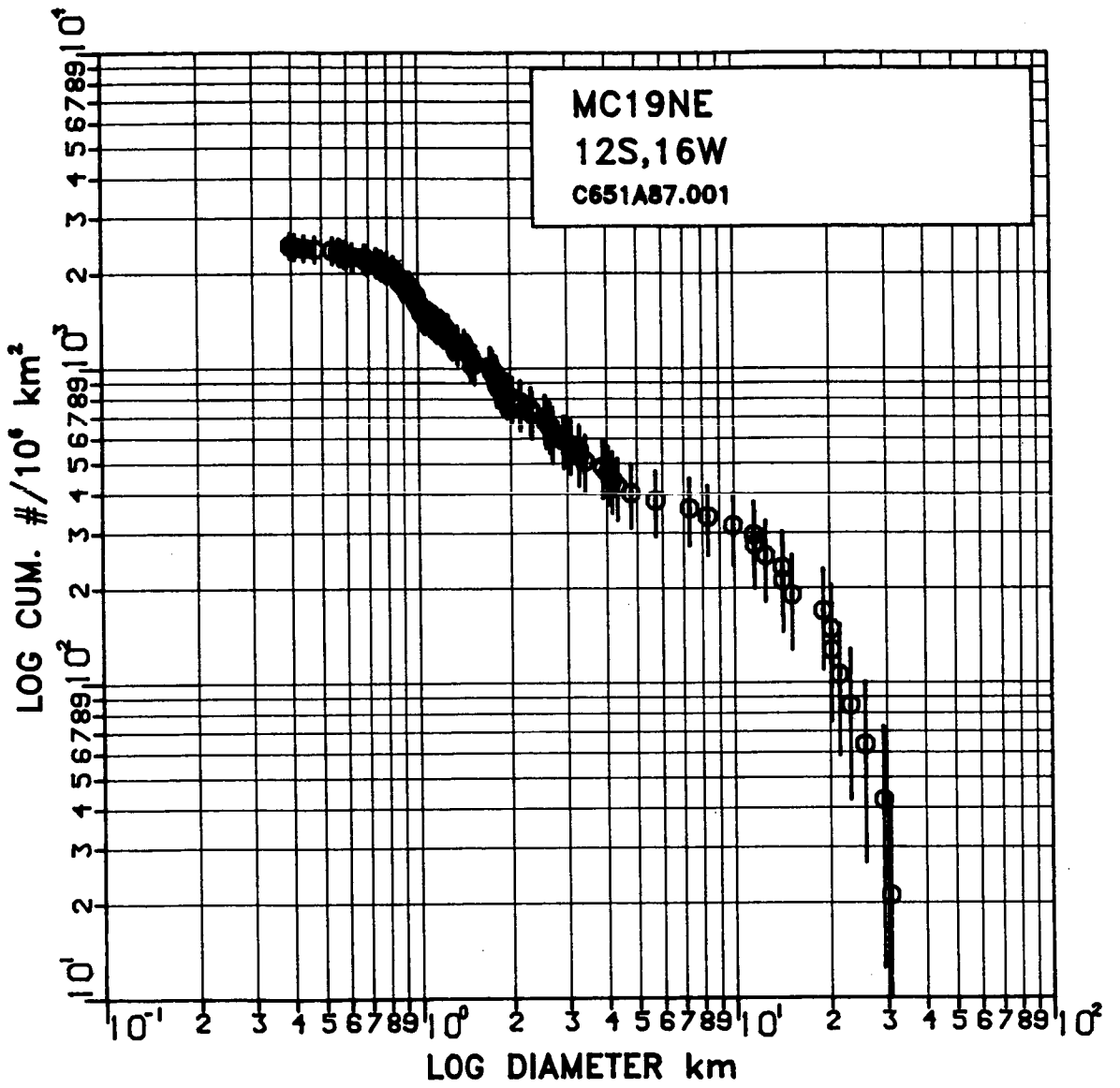


Fig. 23b

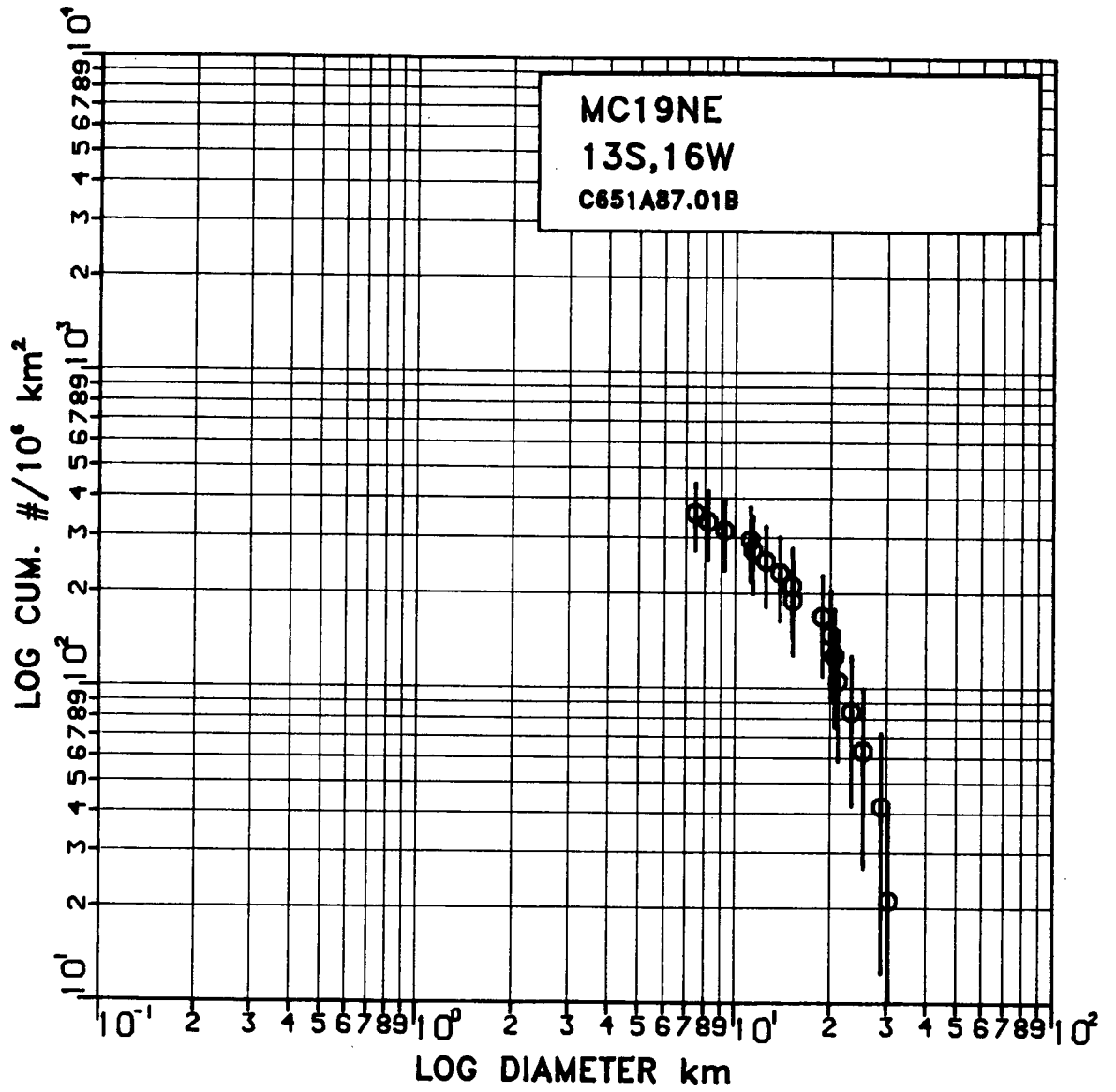
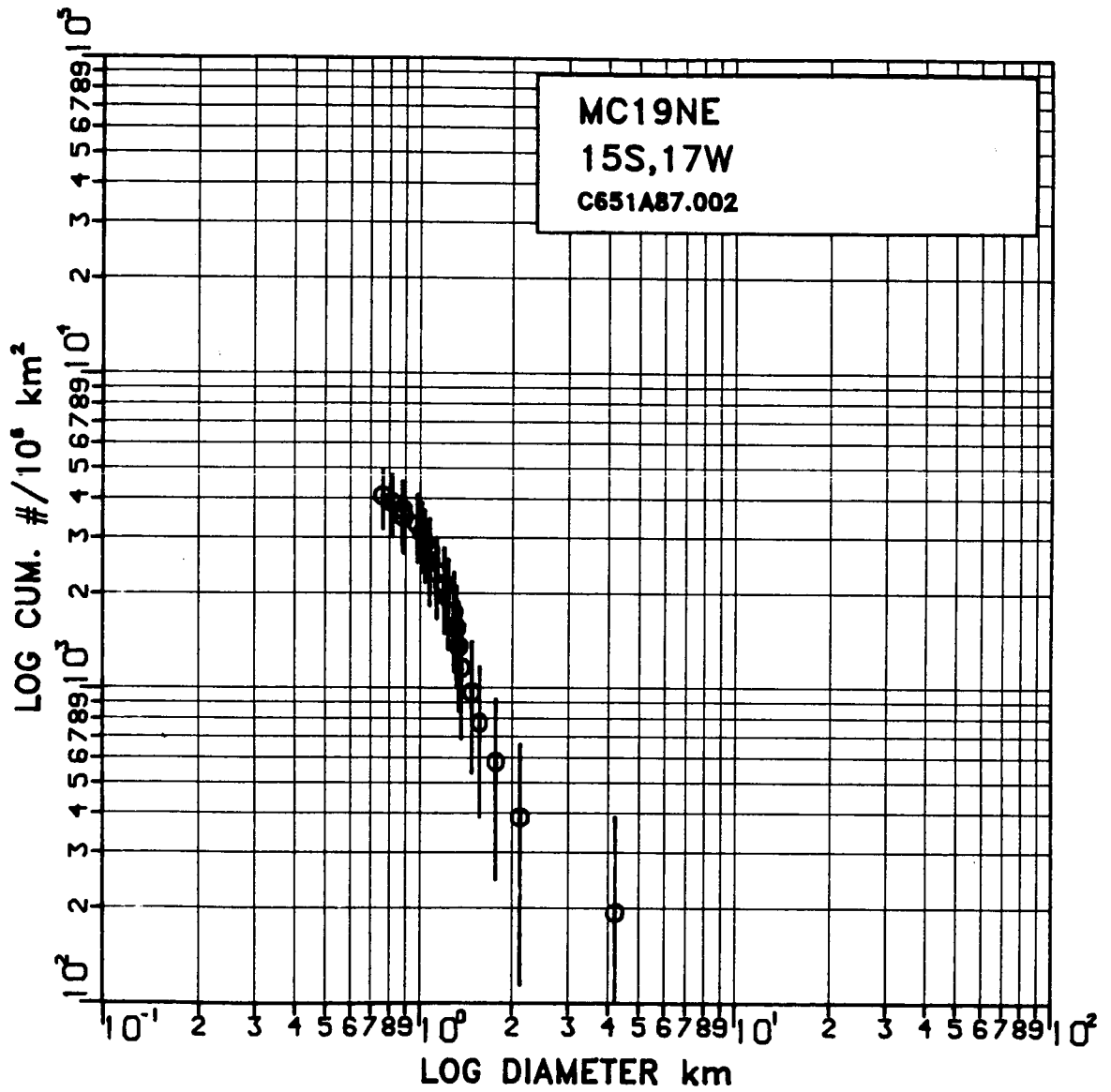


Fig. 23c



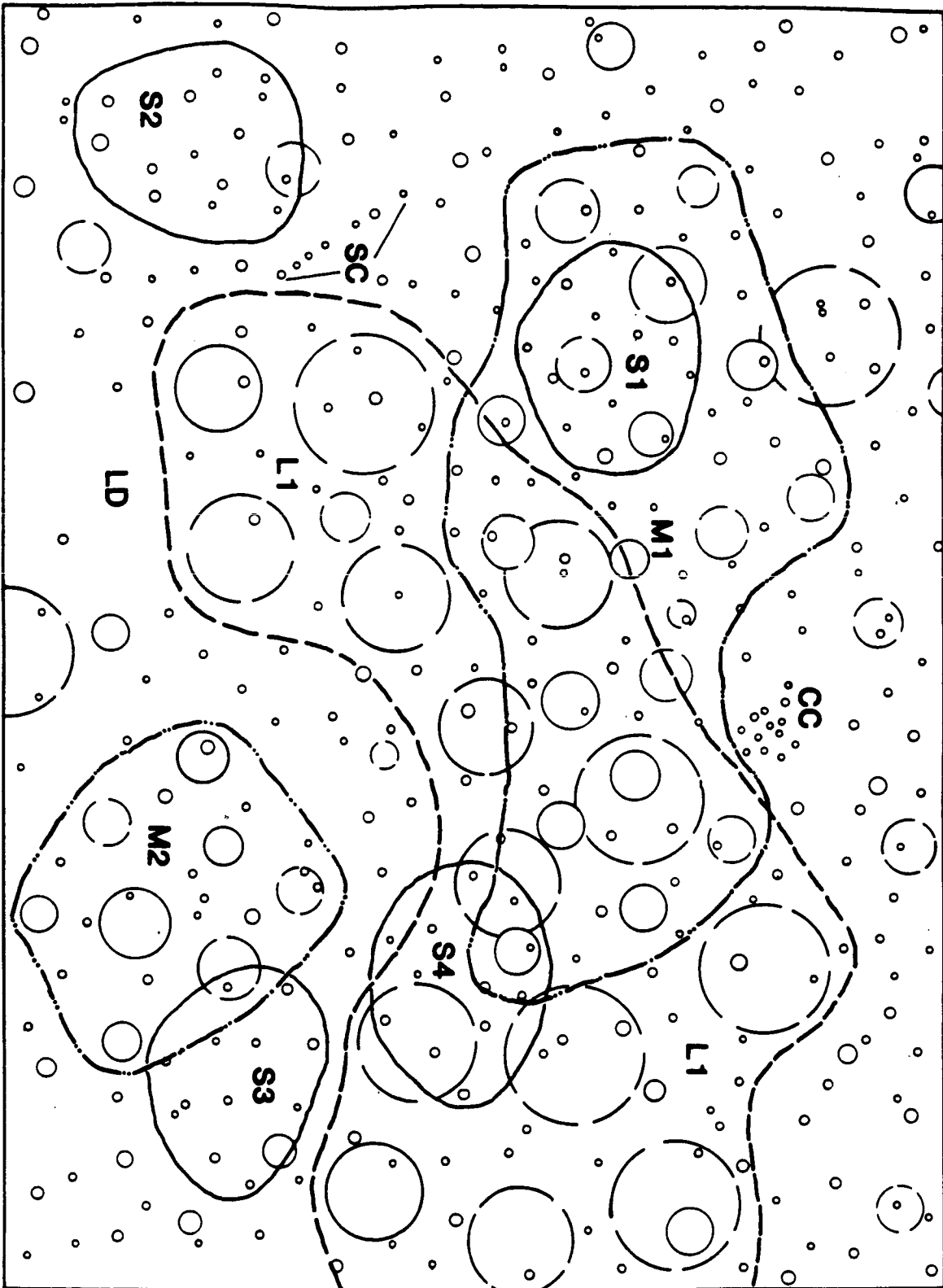
even for the larger diameter craters because local distributions of the larger craters would end up being averaged over the entire area of the count. This may prevent derivation of a reliable age for the older, partially buried surface. In both cases where a single resurfacing event affects an area the age determined for the time of resurfacing by projection through the segment parallel to the standard curve in the smaller crater diameters will be artificially high. Because the large craters from the old surface have been included in the plot, they become part of the cumulative frequency, causing all the smaller diameter craters to plot at artificially large cumulative values.

The method of dating local surfaces differs from the method described above in that small (on average 40 +/- 30 craters per count), homogeneous populations of craters in a given size range are utilized (Wise and Milkowski 1980). A homogeneously cratered area is one that would yield similar crater counts for randomly selected sub-areas within it (Wise et al. 1979). Areas that should be avoided when employing this method include those with: 1) anomalous crater concentrations, both high and low; 2) locations displaying numerous potential secondary craters; 3) linear rays of craters; and 4) some multiple craters. Figure 24 shows an idealized drawing of a hypothetical area that is homogeneously cratered in various locations by several size ranges of craters. Outlined are locations in the various size ranges that would be selected to perform crater counts. Figure 24 also shows areas that should not be counted due to the presence of anomalous crater distributions. The selected areas show the craters chosen for each count. Care must be taken to avoid counting craters partially buried and not incised into the surface being considered. Where not apparent, this is accomplished by examining the morphological characteristics of the crater such as crater class, rim characteristics, etc.. The presence of craters from older surfaces in a cumulative size-frequency plot of an area would shift the curve vertically upwards as a result of contamination from older crater populations.

By selecting areas to be counted in this manner, each cumulative crater size-frequency plot completed will be related to a specific geologic unit (Wise and Milkowski 1980). This technique allows the dating of the different periods of resurfacing by examining the locations of different homogeneous size populations of craters in an area. Each count will result in a cumulative crater size-frequency curve that is parallel to the standard curve and can be projected to a 1 km crater number using the standard curve of Neukum and Wise (1976). By projection to a 1km crater number, numerous curves from different size ranges of craters can be compared on a common base and the ages of the various surfaces determined. The method of local surfaces

Fig. 24. Idealized sketch of a hypothetical cratered surface. Three size ranges of craters are present, designated as small (S), medium (M), and large (L). Craters of subdued morphology are designated by a dashed outline. Only the small crater size range is present uniformly across the figure. As a result, a crater count performed over the entire area might resemble the one in Figure 23a. Areas that might be selected for crater counts using the method of local surfaces are shown for each size range. The large craters are homogeneously distributed over the area labelled L1 and enclosed by the dashed line. The medium size range of craters is homogeneously distributed in two separate areas (M1 and M2), so two counts could be performed, each enclosed by a dashed and dotted line. Numerous locations show a homogeneous distribution of craters in the small size range. Possible count locations in this size range (S1-S4), enclosed by a solid line, are only a few of those possible. Only craters on the surface represented by each size range should be included in a count on that surface. Areas to avoid include crater clusters (CC), low crater density areas (LD) and possible secondary craters (SC).

Figure 24



avoids the problem of smearing of the data, such as can occur when using large areas, due to an unequal distribution of various size crater populations across an area counted. The problem is eliminated by defining count locations on the basis of the presence of a homogeneous distribution of craters in some size range(s).

Because the number of craters in any one count completed using this method is small, individual counts are not statistically significant (Wise and Milkowski 1980), and should not be heavily relied on. However, when numerous counts are performed at various locations on the surface of the same unit, a consistently recurring age is a good indicator of the correct age.

As pointed out by Wise and Milkowski (1980), this method of crater counting requires that the geologic analyses and crater measurements be done simultaneously in an effort to explain the appearance of each plot. Each curve should also be re-examined to determine if the craters selected are actually on the surface in question, on an older partially buried surface, or part of a younger surface covering the area. This technique allows the surfaces of various specific units to be dated when it is not possible to do so by counting craters of various size populations over a large area (Wise and Milkowski 1980). A further discussion of the method of dating local surfaces can be found in Wise and Milkowski (1980), Neukum and Wise (1976), Neukum and Hiller (1981) and Wise et al. (1979).

Figure 23a shows count number C651A87.001, performed in MC19NE. This area has been affected by at least one resurfacing event. For all crater sizes $< 10 - 15$ km the curve is noticeably flattened and has several bumps in it. Comparison of this plot to the Martian standard curve would yield the relative age of the oldest surface in the area at best. Closer examination of this location shows that three size ranges of craters are present. Three separate counts (Figs. 23b-d), using the method of local surfaces, were performed in the same region as Figure 23a. Each count considered only craters in one of the three size ranges present, and only in the areas where they were homogeneously distributed. Interpretation of these three curves revealed that three resurfacing events have affected this area. Comparison with the standard curve of Neukum and Wise (1976) shows that these events correspond to the Sp_1 (Fig. 23b, age 110,000), Sp_2 (Fig. 23c, age 13,900), and Sp_4 (Fig. 23d, age 3100) events.

Technique

Areas were selected across MC19 that, when dated, would show the age relationships between the channel and valley features, the etched terrain at their confluence and

Margaritifer and Iani Chaos further to the north. For the Uzboi/Holden/Ladon system the floor of Ladon Basin was selected for crater counts and relative age determinations. Numerous locations, mainly in MC19SE and MC19NE, were selected in an effort to determine the relative ages of Samara and Parana/Loire Valles based on the ages of surfaces that the valleys were incised into and those covering the networks. Other counts were performed in this same area to determine the age of the ancient cratered highlands and the timing and extent of the resurfacing events that have occurred. All counts were used to help determine the geologic evolution of MC19. Crater counts were also performed in the etched terrain, within Margaritifer and Iani Chaos and on the floor of Ares valles to determine their age relationships to to each other and to other features in Margaritifer Sinus.

After selecting the types of terrain and the features where counts would be performed, the highest quality orthographic images of them (Table 2) were selected (resolution about 200m/pixel). These images, along with the 1:1,000,000 photomosaic of MC19SE were then checked to determine scale accuracy using the following spherical trigonometric formula:

$$\cos(a) = \cos(90 - \delta_2) \cos(90 - \delta_1) + \sin(90 - \delta_2) \sin(90 - \delta_1) \cos(\lambda_2 - \lambda_1)$$

where $\cos(a)$ is the cosine of distance between adjacent corners of the photograph or image in degrees, δ_1 = the latitude and δ_2 = the longitude of two adjacent corners of the photograph or image. To get $\cos(a)$ into degrees, its inverse was taken. This was then multiplied by the average number of km/degree on Mars (calculated to be 59.07 km/degree) to derive the actual distance between corners of the image or photograph in kms. This was then compared to the bar scale given on the images to determine the percent error in scale. All images examined were found to have less than 1% error in scale. The assembled 1:1,000,000 photomosaic of MC19SE was found to have a scale error of generally less than 1%. The 1% error in the scale of the images and photographs was considered negligible, therefore the scale on the images was utilized for crater and area measurements. The calculated scale was used for crater and area measurements done from individual negatives because of the large scale enlargement.

The 1:1000,000 photomosaic was then examined for specific areas with homogeneous crater populations in some size range(s). Measurements in areas displaying homogeneous populations of craters 5 km and larger in diameter were done directly from the 1:1,000,000 photomosaic. Some measurements were also made from the photomosaic in areas showing a homogeneous crater distribution in the range of 2

to 5 km in diameter. Measurements taken off individual images used for crater counts were made for areas showing a homogeneous crater distribution in diameters less than 5 km in diameter.

To perform crater counts in areas located on individual images, the following procedure was used. The images were enlarged using an overhead projector so that small diameter craters (about 0.75 to 5 km) could more accurately be measured. The projector was placed at least 7-8 m from a wall where a piece of tracing paper had been taped. An image was then taped in the center of the projector and projected onto the tracing paper. The scale of the enlarged image was determined by measuring the distance between the same two corners of the enlarged negative that were used in the original scale calculation and comparing it to the calculated value. Distortion due to the projector was considered and found to be 1% or less. A tracing of all craters on the image and/or the area of interest on the photomosaic was then made and the position of valleys, grabens, chaos, etc, were marked for later ease of location identification. Craters of various sizes partially buried by resurfacing events, and craters of questionable quality (see Theory section), were marked accordingly for later identification. This procedure was repeated for all the images used. The image tracings were then examined to locate those areas displaying homogeneous crater populations in some size range(s).

Locations selected to perform crater counts on both the 1:1,000,000 photomosaic and tracings of the individual negatives were defined by a loosely fitting line drawn around the selected craters that was placed in an effort to preserve the homogeneous crater distribution (Table 2, Fig. 24). This was done by placing the line about one half the observed distance between craters beyond the outermost craters in the group to be counted (Fig. 24). Placement of the line was such that narrow embayments and peninsulas were not created as this would not reflect a homogeneous crater distribution. For count locations chosen on the photomosaic the placement of the line averaged about 0.5 to 1.5 cm beyond the limit of the craters to be counted. Locations on the negative tracings have the line placed 1 to 3 cm beyond the outermost craters. This difference in the distance of line placement is due to the much larger scale of the negative tracings.

The last step before actual area and crater measurement was the labeling of all areas to be counted so that they could be easily referred to later. Individual craters within the count area were, in most cases, also numbered to prevent them from being overlooked or counted twice.

Measurement of the area of each crater count location was done at least twice and then averaged to derive a more accurate value. Areas were derived using both a Digital Polar Planimeter and a plane table digitizer. Measurement of individual crater diameters was performed twice on each crater across two different diameters approximately 90 degrees apart. These two values were then averaged to derive an accurate diameter for each crater. Diameter values were obtained using a plane table digitizer or by hand measurement and were calculated to the nearest 0.1 mm.

The values obtained for the area and crater diameters for each crater count location were used in a program called 'STAMMER' written by Brian Fessler at the Lunar and Planetary Institute, Houston, TX, USA, to derive a logarithmic plot of the cumulative crater size-frequency distribution (Figs. 23a-d, Appendix 3). Each plot has been normalized so that it displays the log of the cumulative number of craters $\cdot 10^6 \text{ km}^{-2}$ vs. log of the crater diameter (obtained by dividing 1,000,000 km by the actual area of the count and multiplying it times the cumulative frequency of each crater in the area measured). The counts were normalized to allow easy comparison of the plots to the Martian standard crater curve (Neukum and Hiller 1981) so that relative ages could be derived, and to provide a common base for inter-comparison of the plots. Each point on a plot represents the cumulative number of craters of that diameter and larger for that count. The confidence interval for each point on the plot was calculated using the following formula and is explained below:

Confidence interval = (cum.freq +/- square root of the cum.freq.) $\times 10^6 \text{ km}^2$ / Area of the count

The value for the cumulative frequency of each crater within the area measured +/- the square root of that value, was multiplied times the quantity (1,000,000 km^2 divided by the actual measured area of the crater count). This derives the confidence interval based on the normalized area (1,000,000 km^2) of the count.

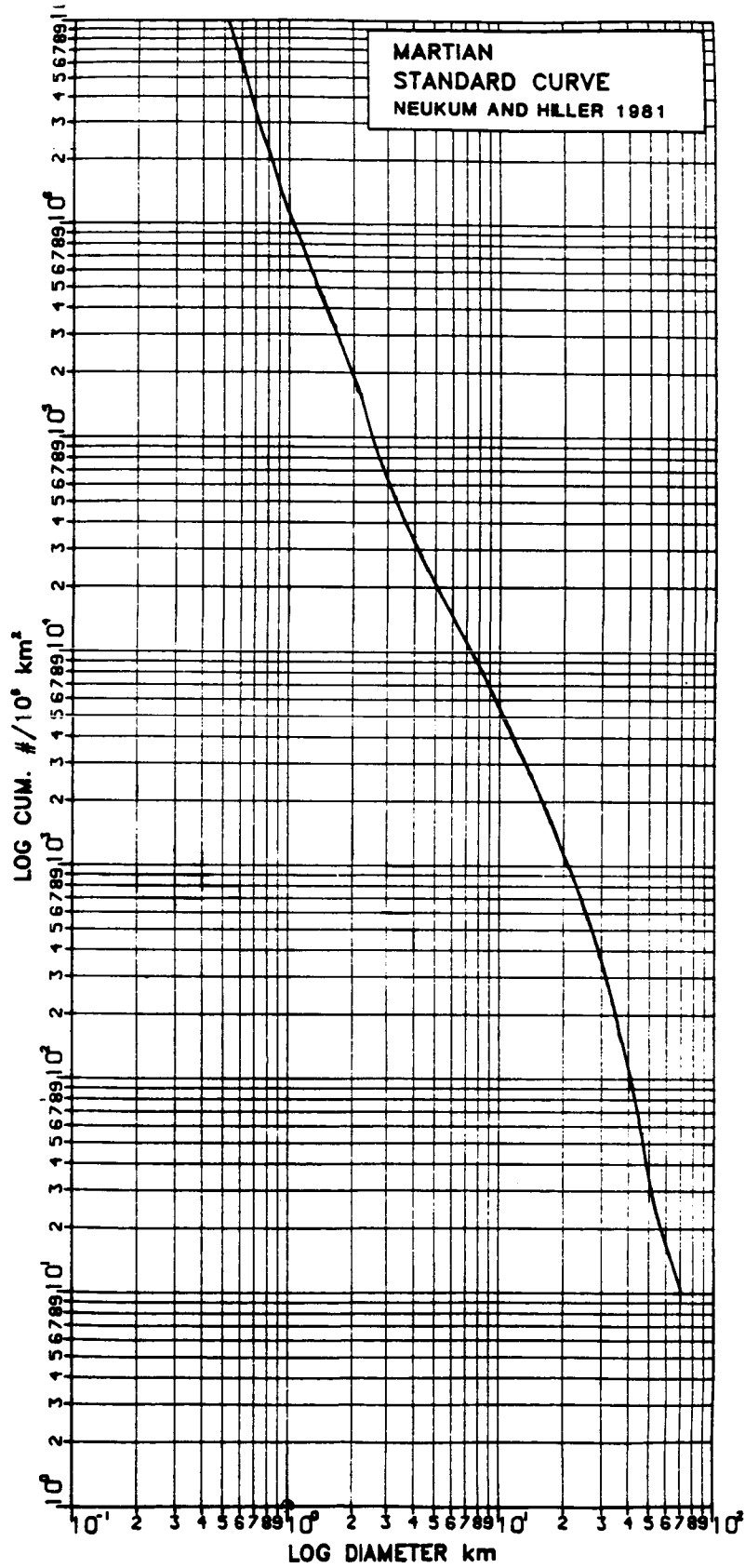
The Martian standard crater curve (Neukum and Hiller 1981, Fig. 25) was used to project the data to obtain a 1 km crater number. This was done for each plot and the resultant cumulative number of craters $\geq 1 \text{ km} \cdot 10^6 \text{ km}^{-2}$ has been used as a relative time standard throughout the study (after Neukum and Wise 1976; Wise 1979; Wise et al. 1979; Wise and Milkowski 1980; and Neukum and Hiller 1981).

Each crater count was compared to photographs of the count location. This was done to locate any errors in crater selection and to see how the derived relative age of the count compared to the geology of the region and other counts located on similar and different surfaces. Anomalous

Fig. 25. The Martian standard crater curve reproduced from Neukum and Hiller (1981). A copy of the standard curve at the same scale as the plots in Appendix 3, included in the original thesis, can be obtained from the author.

Figure 25

ORIGINAL PAGE IS
OF POOR QUALITY



curves due to error in crater selection or measurement were edited and replotted. Anomalous curves with no identifiable cause for their abnormalities (such as strange slope, numerous bumps in the curve, or poor relative age determination) were discarded altogether. All replotted curves were generated using a second version of the 'STAMMER' program set up to run on the Prime computer with CalComp graphics subroutines. All useable counts were eventually replotted using the updated program to create a common format for all counts (Appendix 3).

All counts considered as useable (total of 102) are listed in Table 2, Figure 4a-d, and presented in Appendix 3. A point representing the relative age of each count vs the terrain where the count was performed (e.g. smooth plains, chaotic, etc,) was plotted in Figure 5 in an effort to determine periods of resurfacing and the time of formation of the various units and landforms present. Emphasis was placed on the relative ages determined for the best counts. For specific types of terrain (Ladon Basin, etched, chaotic, etc) the full range of ages derived for the unit have been used to assign the period during which the feature most likely formed. Periods during which resurfacing events occurred were defined by distinct clusters of relative ages (Fig. 5) for counts completed at locations inferred to have been resurfaced, and that could be correlated with geologically distinct units.

Absolute ages were assigned to the units by comparison of their relative ages with the lunar standard crater curve (Neukum and Hiller 1981). The lunar curve is probably a reasonable estimate of the crater flux at Mars and was therefore used for the age determinations.

APPENDIX 2

Computer Programs Used to Derive Logarithmic Cumulative Crater Size-Frequency Plots

Two versions of the same program called 'STAMMER', were used to derive cumulative crater size-frequency plots for each crater count location. Each version is presented in the following pages. Both programs are written in Fortran 77 and both create data files containing all calculations performed during execution that allow for later examination. The first version was written by Brian Fessler at the Lunar and Planetary Institute, Houston, TX. USA. It is designed to run on a Digital Vax 11/780 mainframe computer. Graphics for this version were written using DEC ReGIS (Remote Graphics Instruction set) graphics subroutines. Output was reviewed on a Digital VT125 Graphics terminal and hardcopies were obtained from a Digital Letterwriter 100 printer. Initial plots and edits were obtained at the Lunar and Planetary Institute in January 1985.

The second version of the 'STAMMER' program, listed after the first in the following pages, was a modification of the original that allowed the program to operate on the Prime/850 computer at the University of Rhode Island. Modifications were almost entirely within the graphics section of the program, the actual calculation part of the text was unaltered. The new version used Primos/Rev.19.3 Calcomp graphic subroutines to obtain hardcopies of the plots on a Calcomp 1051 printer. Source changes were completed by Dan Halloway at the URI Academic Computer Center and by the author. All final edits of the program and final copies of each log cumulative crater size-frequency plots are shown in Appendix 3.

PRECEDING PAGE BLANK NOT FILMED

```

C      ORIGINAL VERSION OF PROGRAM STAMMER
C      FOR CALCULATION OF CUMULATIVE CRATER
C      SIZE-FREQUENCY PLOTS
C      WRITTEN BY BRIAN FESSLER
C      AT THE LUNAR AND PLANETARY INSTITUTE
C      HOUSTON, TX, USA

```

```

PROGRAM STAMMER

```

```

REAL    DIAM(1000),DIAMCUM(1000),DIAMNUM(1000),NEWD,OLDD
REAL    FACTOR,AREA,CUMPER1D6(1000),CONFID(2,1000),Y(2)
REAL    MAXDIAM
REAL    LENGTH1,LENGTH2,LENGTH(200),MM,KM
CHARACTER INFILE*40,OUTFILE*40,TITLE*40

      WRITE(6,*) 'ENTER INPUT FILENAME:'
      READ(5,5) INFILE
5     FORMAT(A)

C     OPEN(UNIT=1,FILE=INFILE,STATUS='OLD',READONLY)

      WRITE(6,*) ' '
      WRITE(6,*) 'ENTER OUTPUT FILENAME:'
      READ(5,5) OUTFILE
C     OPEN(UNIT=2,FILE=OUTFILE,STATUS='NEW')

C     WRITE(6,*) ' '
C     WRITE(6,*) 'ENTER TITLE FOR GRAPH:'
C     READ(5,5) TITLE

      MAXDIAM=100.0

      READ(1,6) MM,KM    /* READ MAP SCALE (mm:km)
6     FORMAT(F2.0,1X,F)
      CONST=KM/MM

      CALL GETVALUE(AREA1,*99) /* GET AREA ESTIMATES AND AVERAGE
      CALL GETVALUE(AREA2,*99)
      AREA=((AREA1+AREA2)/2.0)*CONST**2

      N=0
7     CALL GETVALUE(LENGTH1,*8) /* GET LENGTH ESTIMATES AND AVERAGE
      CALL GETVALUE(LENGTH2,*99)
      N=N+1
      LENGTH(N)=((LENGTH1+LENGTH2)/2.0)*CONST
      GOTO 7

8     CALL SORT(LENGTH,N) /* SORT LENGTHS INTO DESCENDING ORDER

10    DO I=1,N           /* DETERMINE NUMBER OF CRATER DIAMETERS

```

```

NEWD=LENGTH(I)
IF (I.EQ.1) THEN
  OLDD=NEWD
  ICTR=1
  DIAM(ICTR)=NEWD
ENDIF
IF (NEWD.EQ.OLDD) THEN
  DIAMNUM(ICTR)=DIAMNUM(ICTR)+1.0
ELSE
  OLDD=NEWD
  ICTR=ICTR+1
  DIAM(ICTR)=NEWD
  DIAMNUM(ICTR)=1.0
ENDIF
ENDDO

```

```

20 WRITE(2,*) 'DIAMETER    CUMULATIVE FREQUENCY    NO. OF CRATERS'

```

```

DO I=1,ICTR          /* COMPUTE CUMULATIVE FREQUENCY
IF (I.EQ.1) THEN    /* OF CRATERS
  DIAMCUM(I)=DIAMNUM(I)
ELSE
  DIAMCUM(I)=DIAMNUM(I)+DIAMCUM(I-1)
ENDIF
WRITE(2,*) DIAM(I), '    ',DIAMCUM(I), '    ',DIAMNUM(I)
ENDDO

```

```

WRITE(2,*) ' '
WRITE(2,*) 'DIAMETER    CUM.FREQ.*1.E6/AREA    CONFIDENCE INTERVAL'

```

```

FACTOR=1.0D6/AREA

```

```

DO I=1,ICTR          /* COMPUTE CUMULATIVE FREQUENCY
  CUMPER1D6(I)=FACTOR*DIAMCUM(I) /* OF CRATERS PER 10**6 KM**2
  CONFID(1,I)=FACTOR*(DIAMCUM(I)+SQRT(DIAMCUM(I))) /* COMPUTE CONFID
  CONFID(2,I)=FACTOR*(DIAMCUM(I)-SQRT(DIAMCUM(I))) /* INTERVAL
  IF (CONFID(2,I).EQ.0.0) CONFID(2,I)=1.0
  WRITE(2,*) DIAM(I),CUMPER1D6(I),CONFID(1,I),CONFID(2,I)
ENDDO

```

```

CALL INIT_GRAPHICS()
CALL CLEAR_TEXT
CALL CLEAR_SCREEN
CALL DRAW_GRAPHPAPER('LOG',5,1,'LOG',5,1,'GRAY3')
CALL LNAXIS('XT',INFILE,,)
CALL LNAXIS('XB','LOG(DIAMETER (km))',0.001,MAXDIAM,.FALSE.)
CALL LNAXIS('YL','LOG(CUM.#/10**6 km**2)',
*1.0,100000.0,.TRUE.)

```

```

DO I=1,ICTR
  Y(1)=DIAM(I)
  Y(2)=DIAM(I)
  CALL PLOT_POINT(Y(1),CUMPER1D6(I),'L',7)
  CALL PLOT_DATA(2,Y,CONFID(1,I),'L','GRAY3',,1,,)
ENDDO

```

```

80      WRITE(6,*) 'ENTER HARDCOPY OPTION: 1) SMALL, 2)LARGE, 3)NONE'
      READ(5,*) IOPT

      IF (IOPT.EQ.1) THEN
        CALL COPY_VIEWPORT
        GOTO 80
      ELSE IF (IOPT.EQ.2) THEN
        CALL ZOOM(2,2)
        CALL COPY_VIEWPORT
        CALL NOZOOM
        GOTO 80
      ENDIF

      CALL CLEAR_SCREEN
      STOP

99      WRITE(6,*) '***UNEXPECTED END OF DATA***'
      STOP
      END

```

```

SUBROUTINE GETVALUE(VAL,*)

```

```

      REAL VAL
      CHARACTER LINE*80,NUM*10

1       READ(1,5,ERR=25,END=35) LINE
5       FORMAT(A)
      NUM(1:6)=LINE(33:38)
      NUM(7:10)=LINE(41:44)
      DECODE(10,15,NUM(1:10),ERR=25) VAL
15      FORMAT(E10.3)
      IF (VAL.EQ.0.0) GOTO 1
      RETURN

25      WRITE(6,*) '***ERROR DURING READ OR DECODE***'
      WRITE(6,*) LINE
      WRITE(6,*) NUM
35      RETURN 1
      END

```

```

SUBROUTINE SORT(ARRAY,N) /* DESCENDING
      REAL ARRAY(200)
      LOGICAL SORTED
      SORTED=.FALSE.

```

```

      DO WHILE (.NOT.SORTED)
        SORTED=.TRUE.
        DO I=1,N-1
          IF (ARRAY(I).LT.ARRAY(I+1)) THEN
            SORTED=.FALSE.

```

```
    TEMP=ARRAY(I)
    ARRAY(I)=ARRAY(I+1)
    ARRAY(I+1)=TEMP
  ENDIF
ENDDO
RETURN
END
```

```

C      UPDATED VERSION OF PROGRAM STAMMER
C      FOR CALCULATION OF CUMULATIVE CRATER
C      SIZE-FREQUENCY PLOTS
C      CHANGED TO OPERATE ON
C      THE PRIME/850 COMPUTER WITH
C      CALCOMP GRAPHICS SUBROUTINES
C      CHANGES IMPLEMENTED BY
C      DAN HALLOWAY AND JOHN GRANT

```

```

PROGRAM STAMMER

```

```

REAL    DIAM(1002),DIAMCUM(1000),DIAMNUM(1000),NEWD,OLDD
REAL    FACT,AREA,CUMPER(1002)
REAL    CONFID1(1000),CONFID2(1000)
REAL    MAXDIAM,XARRY(1002),BLOG(10)
REAL    LENGTH1,LENGTH2,LENGTH(200),MM,KM
CHARACTER INFILE*40,OUTFILE*40,PLOTFILE*40
CHARACTER*1 TEXT1(24),TEXT2(24),TEXT3(24)

WRITE(*,*) 'ENTER INPUT FILENAME:'
READ(*,5) INFILE
5  FORMAT(A)

OPEN(UNIT=101,FILE=INFILE,STATUS='OLD')

WRITE(*,*) ' '
WRITE(*,*) 'ENTER OUTPUT FILENAME:'
READ(*,5) OUTFILE

OPEN(UNIT=102,FILE=OUTFILE,STATUS='NEW')

WRITE(*,*) ' '
WRITE(*,*) 'ENTER PLOTFILE FILENAME:'
READ(*,5) PLOTFILE

MAXDIAM=100.0
DIAMNUM(1)=0.0
DIAMCUM(1)=0.0

READ(101,6) MM,KM    /* Read map scale (mm:km)
6  FORMAT(F3.0,1X,F6.3)
CONST=KM/MM

CALL GETVALUE(AREA1,*99) /* Get area estimates and average
CALL GETVALUE(AREA2,*99)
AREA=((AREA1+AREA2)/2.0)*CONST**2

N=0
7  CALL GETVALUE(LENGTH1,*8) /* Get length estimates and average
CALL GETVALUE(LENGTH2,*99)

```

```

N=N+1
LENGTH(N)=((LENGTH1+LENGTH2)/2.0)*CONST
GOTO 7

8   CALL SORT(LENGTH,N)   /* Sort lengths into descending order

10  DO 991 I=1,N          /* Determine number of crater diameters

      NEWD=LENGTH(I)

      IF (I.EQ.1) THEN
        OLDD=NEWD
        ICTR=1
        DIAM(ICTR)=NEWD
      ENDIF

      IF (NEWD.EQ.OLDD) THEN
        DIAMNUM(ICTR)=DIAMNUM(ICTR)+1.0
      ELSE
        OLDD=NEWD
        ICTR=ICTR+1
        DIAM(ICTR)=NEWD
        DIAMNUM(ICTR)= 1.0
      ENDIF
991  CONTINUE

20  WRITE(102,*) 'DIAMETER   CUMULATIVE FREQUENCY   NO. OF CRATERS'

      DO 992 I=1,ICTR      /* Compute cumulative frequency
        IF (I.EQ.1) THEN   /* of craters
          DIAMCUM(I)=DIAMNUM(I)
        ELSE
          DIAMCUM(I)=DIAMNUM(I)+DIAMCUM(I-1)
        ENDIF
        WRITE(102,*) DIAM(I),'   ',DIAMCUM(I),'   ',DIAMNUM(I)
992  CONTINUE

      WRITE(102,*) ' '
      WRITE(102,*) 'DIAMETER   CUM.FREQ.*1.E6/AREA   CONFIDENCE INTERVAL'

      FACT=1.0D6/AREA

      DO 993 I=1,ICTR      /* Compute Cumulative frequency
        CUMPER(I)=FACT*DIAMCUM(I)
        CONFID1(I) = FACT*(DIAMCUM(I)+SQRT(DIAMCUM(I)))
        CONFID2(I) = FACT*(DIAMCUM(I)-SQRT(DIAMCUM(I)))
        IF (CONFID2(I).EQ.0.0) CONFID2(I)=1.0

C   Output Diameter, Cumulative frequency and Confidence intervals

      WRITE(102,*) DIAM(I),CUMPER(I),CONFID1(I),CONFID2(I)
993  CONTINUE

C
C   Minimum values stored into data arrays at ICTR+1 locations.

```

```

C      Used to insure constant scaling when using packaged SCALG routines.
C      ICTR then incremented to accommodate extra elements.
C      Added minimum data point will NOT be plotted.
C
      CUMPER(ICTR+1) = 100.00
      DIAM(ICTR+1) = 0.10
      ICTR = ICTR + 1
C
C
C      Source changes to operate on PRIME/850--PRIMOS/REV.19.3
C      Calcomp graphic subroutine calls to create log. plot
C
C      Open plotfile for output
      CALL OPEN(120,PLOTFILE,20,'OUTPUT')
      CALL PLOTS(0,0,120)
C
C      Call Automatic Scaling Routines
      CALL SCALG(CUMPER,6.0,ICTR,1)
      CALL SCALG(DIAM,6.0,ICTR,1)
      CALL NEWPEN(3)
C
C      Draw and Annotate X-Axis
      CALL LGAXS(0.0,0.0,' ',-1,6.0,+0.0,DIAM(ICTR+1),0.5)
      CALL CENTER(STX,.14,';LOG DIAMETER #KM',17,6.0)
      CALL CHARS(STX,-0.50,.14,';LOG DIAMETER #KM',0.0,17)
C
C      Draw and Annotate Y-Axis
      CALL LGAXS(0.0,0.0,' ',1,6.0,90.0,CUMPER(ICTR+1),0.5)
      CALL CENTER(STX,.14,';LOG CUM. ># C;/10^6 #KM;"2',27,6.0)
      CALL CHARS(-0.40,STX,.14,';LOG CUM. ># C;/10^6 #KM;"2',90.0,27)
C
C      Complete a Box with X and Y Axis
C
      CALL PLOT(0.0,6.0,3)
      CALL PLOT(6.0,6.0,2)
      CALL PLOT(6.0,0.0,2)
C
C      Draw Grid on Log. Axis
C
      CALL NEWPEN(1)
      ETO10 = 0.4342945
      DO 11 I=1,9
11      BLOG(I) = ALOG(FLOAT(I))*ETO10
      FXMN = INT( ETO10 * ALOG(CUMPER(ICTR+1))+100.0001)-100
      BLMN = (ETO10 * ALOG(CUMPER(ICTR+1)))-FXMN)/.5-.0001
      FJ = 0.0

```

```

X = 0.0
DO 13 J = 1,3
  DO 12 I = 1,9
    Y = (BLOG(I)+FJ)/0.5
    IF (( Y .GT. 4.9 ) .AND. ( Y .LE. 5.9 )) THEN
      CALL PLOT(X,Y,3)
      CALL PLOT(X+2.75,Y,2)
      CALL PLOT(5.9,Y,3)
      CALL PLOT(6.0,Y,2)
    ELSE
      CALL PLOT(X,Y,3)
      CALL PLOT(X+6.0,Y,2)
    ENDIF
12    CONTINUE
    FJ = FJ + 1.0
13    CONTINUE

FJ = 0.0
Y = 0.0
DO 14 J = 1,3
  DO 15 I = 1,9
    X = (BLOG(I)+FJ)/0.5
    IF (( X .GE. 2.75 ) .AND. ( X .LE. 5.9 )) THEN
      CALL PLOT(X,Y,3)
      CALL PLOT(X,Y+4.9,2)
      CALL PLOT(X,5.9,3)
      CALL PLOT(X,6.0,2)
    ELSE
      CALL PLOT(X,Y,3)
      CALL PLOT(X,Y+6.0,2)
    ENDIF
15    CONTINUE
    FJ = FJ + 1.0
14    CONTINUE

C
C   Annotate Graph in Upper-right corner
C
C   Draw a Box to enclose the annotation
C
      CALL NEWPEN(3)
      CALL PLOT(2.75,5.9,3)
      CALL PLOT(2.75,4.9,2)
      CALL PLOT(5.9,4.9,2)
      CALL PLOT(5.9,5.9,2)
      CALL PLOT(2.75,5.9,2)
C
C   Prompt User for Annotation Information
C
      WRITE(*,102)
102    FORMAT(' ', ' Enter First-Text Array')
      READ(*,104)(TEXT1(I),I=1,24)
104    FORMAT(24A1)

```

```

        WRITE(*,103)
103    FORMAT(' ',' Enter Number of Chars in Text Array')
        READ(*,*)N

        CALL CHARS(3.0,5.60,.15,TEXT1,0.0,N)
C
C    Prompt User for Second Line of annotation
C
        WRITE(*,105)
105    FORMAT(' ',' Enter Second-Text Array')
        READ(*,104)(TEXT2(I),I=1,24)
        WRITE(*,103)
        READ(*,*)N

        CALL CHARS(3.0,5.30,.15,TEXT2,0.0,N)
C
C    Prompt User for Third Line of annotation
C
        WRITE(*,106)
106    FORMAT(' ',' Enter Third-Text Array')
        READ(*,104)(TEXT3(I),I=1,24)
        WRITE(*,103)
        READ(*,*)N

        CALL CHARS(3.0,5.05,.100,TEXT3,0.0,N)
C
C    Plot data points with confidence interval attribute
C
        XMIN = ETO10 * ALOG(DIAM(ICTR+1))
        YMIN = ETO10 * ALOG(CUMPER(ICTR+1))

        CALL NEWPEN(2)
        DO 88 I = 1,ICTR-1
            CUMPER(I) = ALOG(CUMPER(I))*ETO10
            DIAM(I) = ALOG(DIAM(I))*ETO10
            XPAGE = (DIAM(I)-XMIN)/0.5
            YPAGE = (CUMPER(I)-YMIN)/0.5
C
C    Plot symbols at data points
C
            CALL SYMBOL( XPAGE, YPAGE, 0.100, 1, 0.0, -1 )
C
C    Plot line representing confidence-interval
C
            YNEW = ((ETO10*ALOG(CONFID1(I)))-YMIN)/0.5
            CALL PLOT( XPAGE, YNEW, 3 )
            YNEW = ((ETO10*ALOG(CONFID2(I)))-YMIN)/0.5
            IF( YNEW .LT. 0 ) YNEW = 0.0
            CALL PLOT( XPAGE, YNEW, 2 )
C
88    CONTINUE
C    Close plotfile

```

```
CALL PLOT(0.0,0.0,999)
CALL CLOSE(120)
```

```
C      Close Data and Output files
```

```
      CLOSE(UNIT=101)
      CLOSE(UNIT=102)
      STOP
```

```
C
C
C
```

```
Abnormal termination error message
```

```
99      WRITE(*,*) '***UNEXPECTED END OF DATA***'
      STOP
      END
```

```
SUBROUTINE GETVALUE(VAL,*)
```

```
      REAL VAL
      CHARACTER LINE*80,NUM*10
```

```
1      READ(101,5,ERR=25,END=35) LINE
5      FORMAT(A)
```

```
      NUM(1:6)=LINE(33:38)
      NUM(7:10)=LINE(41:44)
      DECODE(10,15,NUM(1:10),ERR=25) VAL
15     FORMAT(E10.3)
      IF (VAL.EQ.0.0) GOTO 1
      RETURN
```

```
25     WRITE(*,*) '***ERROR DURING READ OR DECODE***'
      WRITE(*,*) LINE
      WRITE(*,*) NUM
35     RETURN 1
      END
```

```
SUBROUTINE SORT(ARRAY,N) /* Descending
```

```
      REAL ARRAY(200)
      LOGICAL SORTED
      SORTED=.FALSE.
```

```
97     IF (.NOT.SORTED) THEN
      SORTED=.TRUE.
      DO 991 I=1,N-1
      IF (ARRAY(I).LT.ARRAY(I+1)) THEN
      SORTED=.FALSE.
      TEMP=ARRAY(I)
      ARRAY(I)=ARRAY(I+1)
      ARRAY(I+1)=TEMP
```

```
991      ENDIF  
        CONTINUE  
        GO TO 97  
      ENDIF  
    RETURN  
  END
```

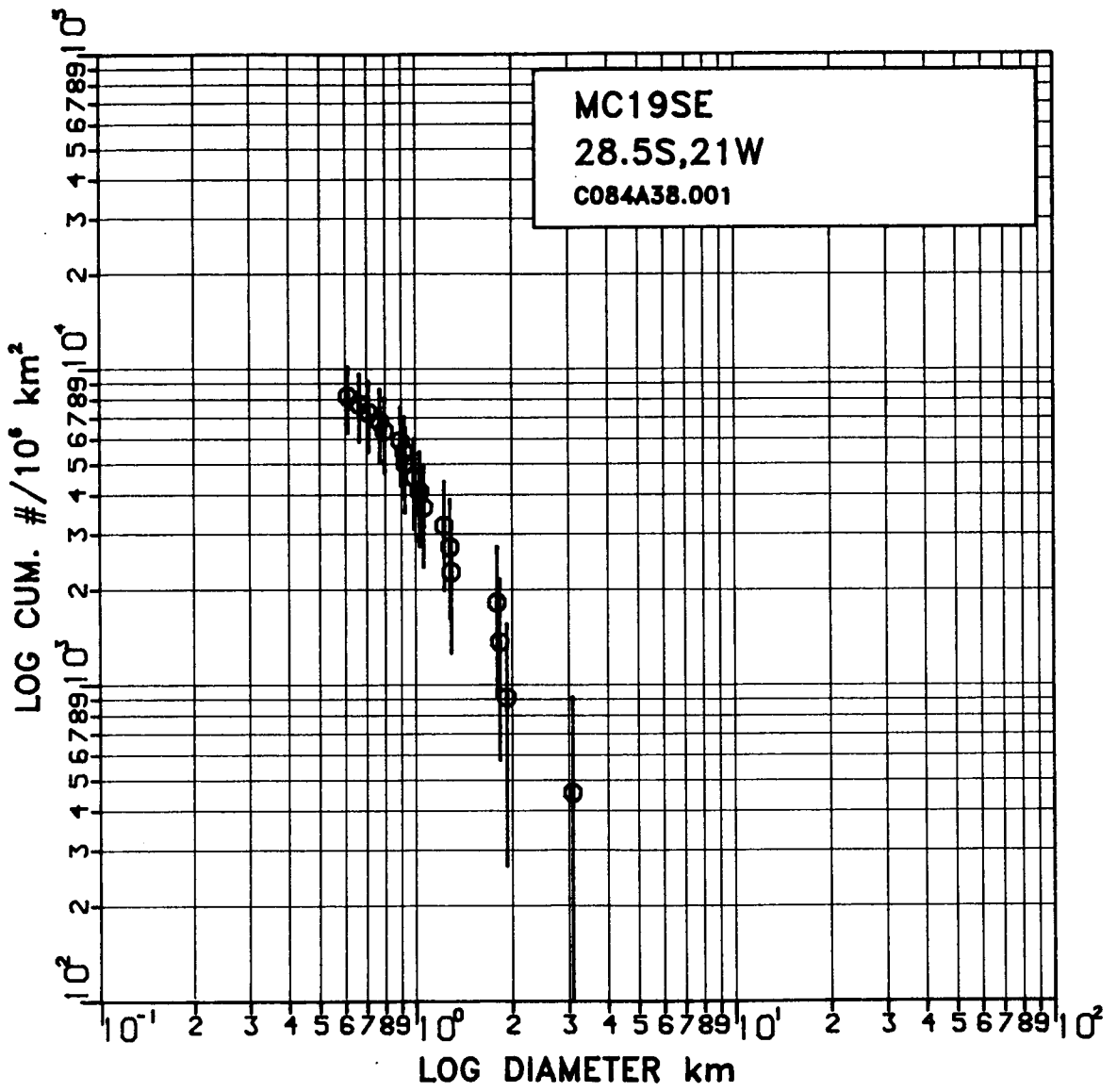
APPENDIX 3

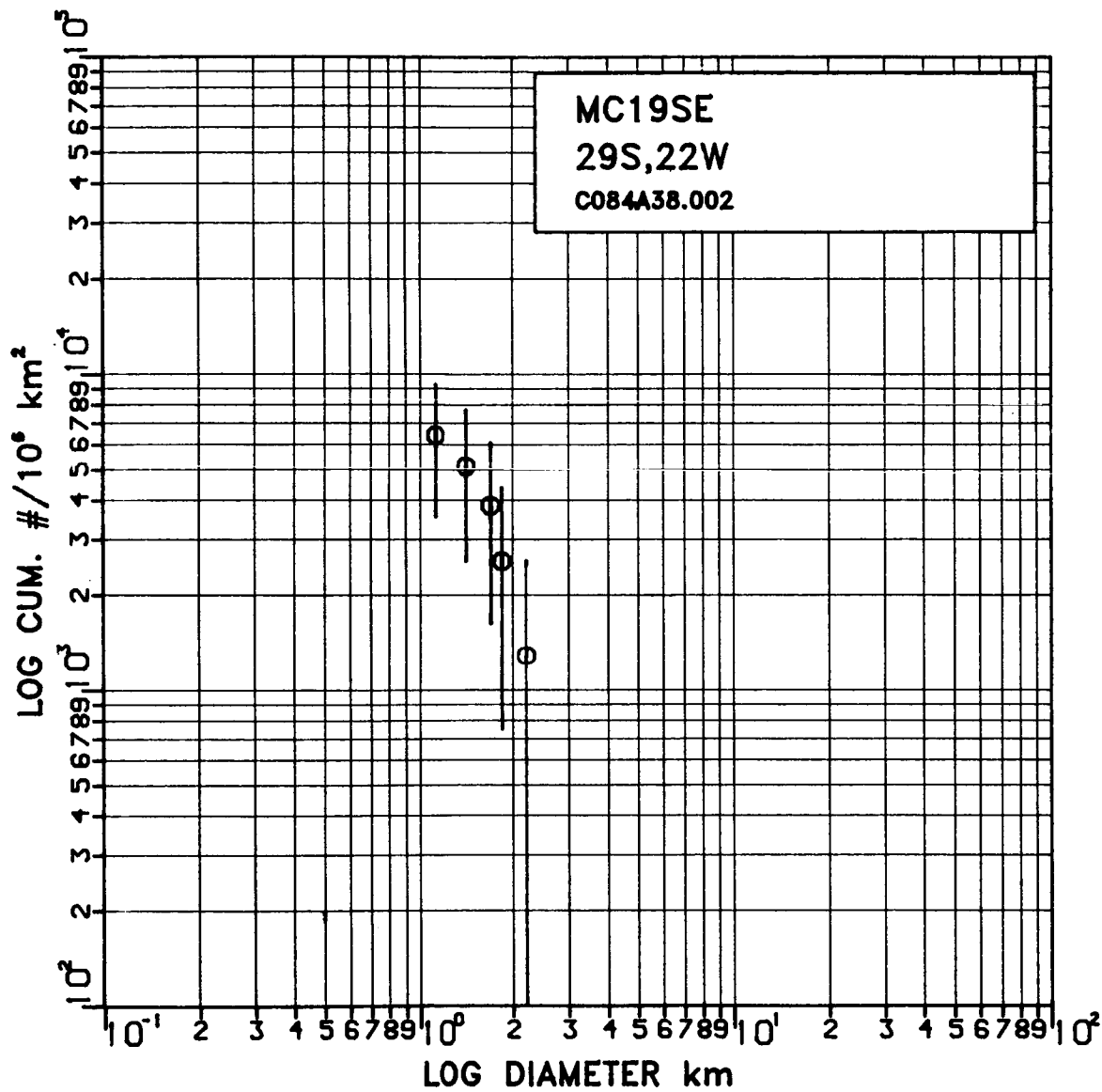
Crater Counts:

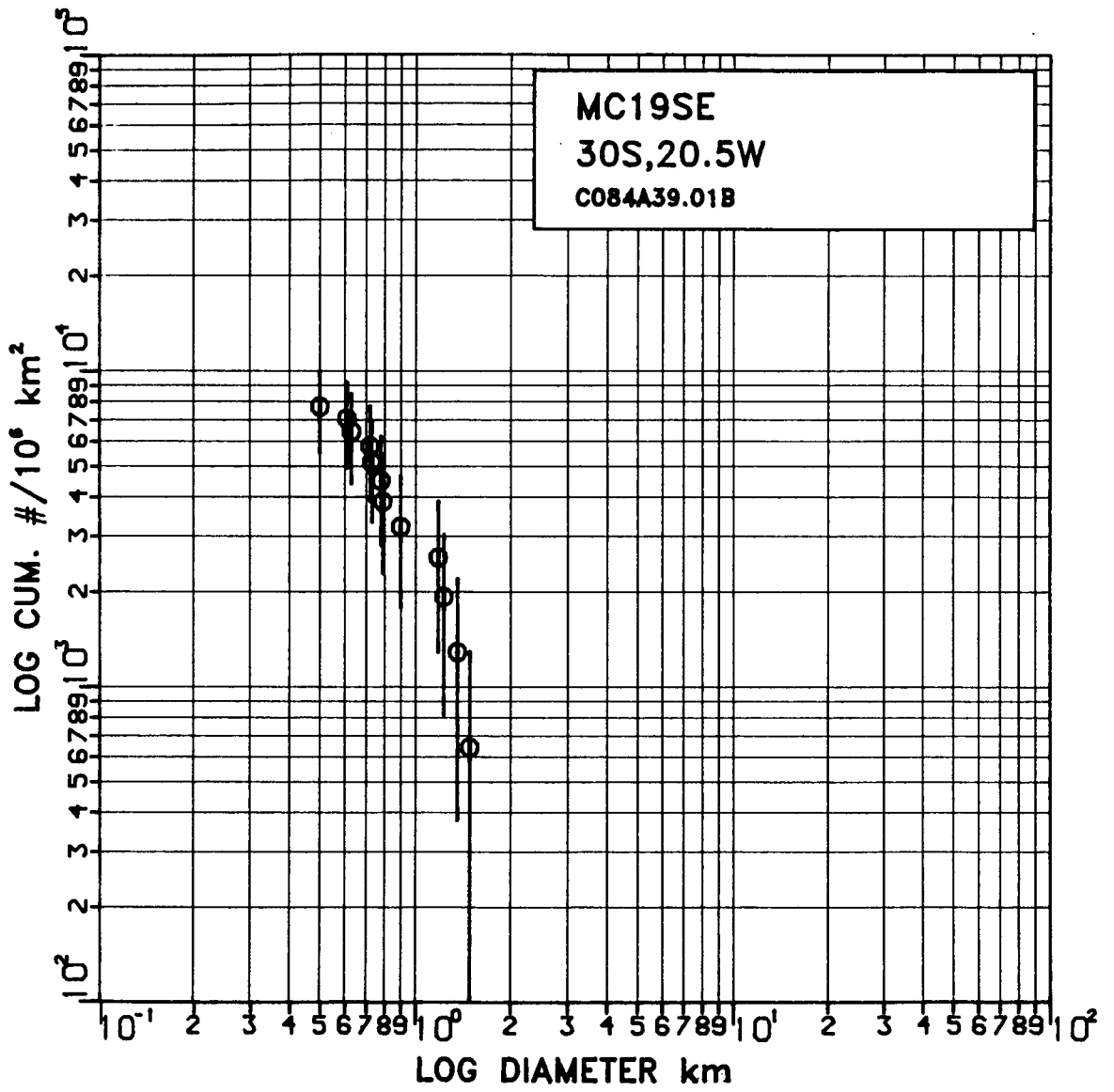
Logarithmic Cumulative Crater Size-Frequency Plots

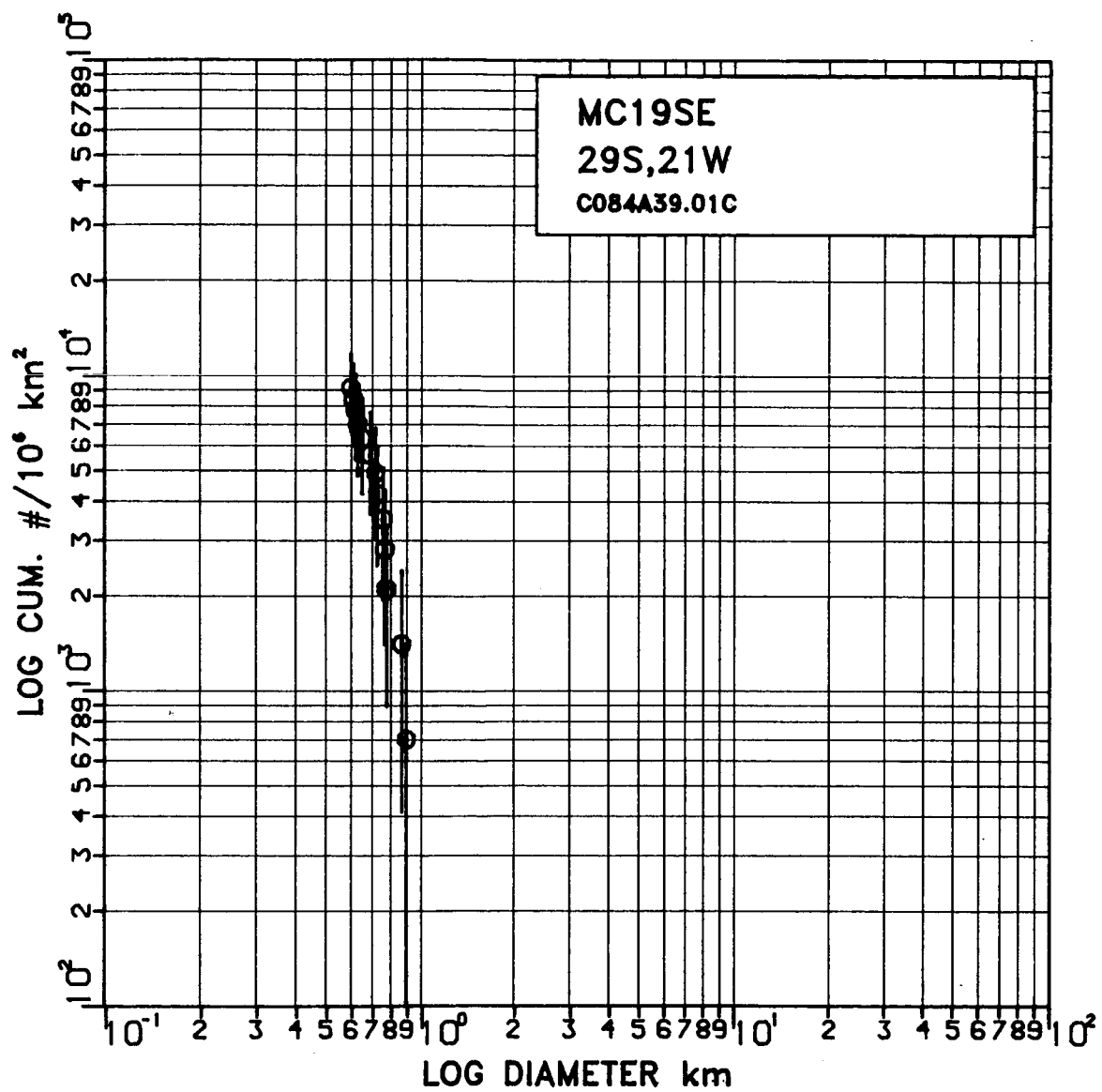
Each count is labelled in the top right hand corner of the plot. The first line of annotation refers to the quarter of MC19 or MC26 that the count was performed in. The second line describes the specific location of the count (place name) followed by the latitude and longitude of its center. The third line refers to the specific negative used for the count and the count number on the negative (e.g. C084A38.002 refers to count number two on the negative 084A38). Plots with CMC19SEMOS at the beginning of the third line of annotation refer to those counts taken from the 1:1,000,000 photomosaic constructed of MC19SE. The last three characters on the third line of these plots refers to the general size range of craters measured from the 1:1,000,000 photomosaic that were used to create the plot. See Table 2, Figs. 4a-d and the individual plots for the specific location and crater size range of individual counts.

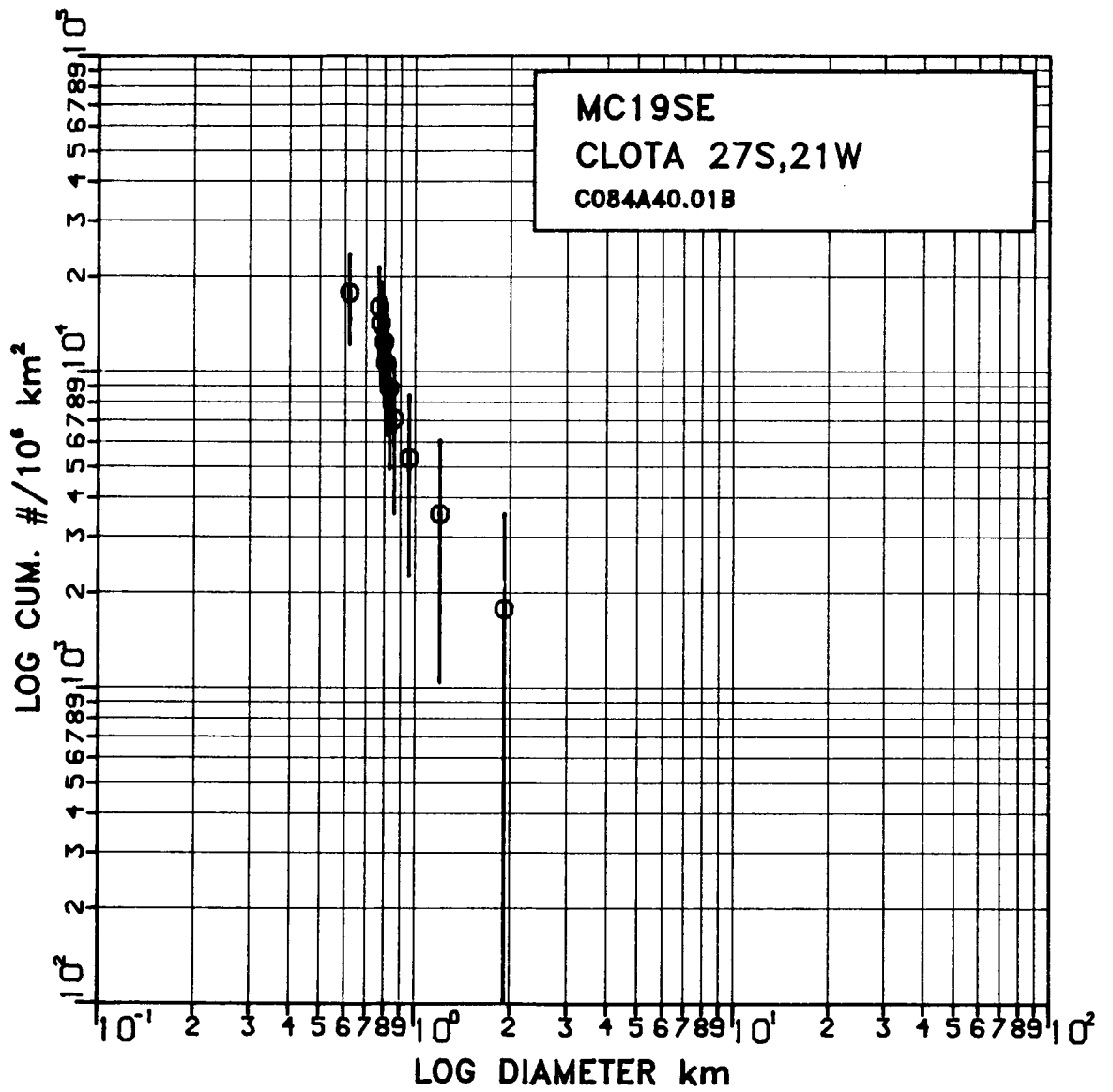
PRECEDING PAGE BLANK NOT FILMED

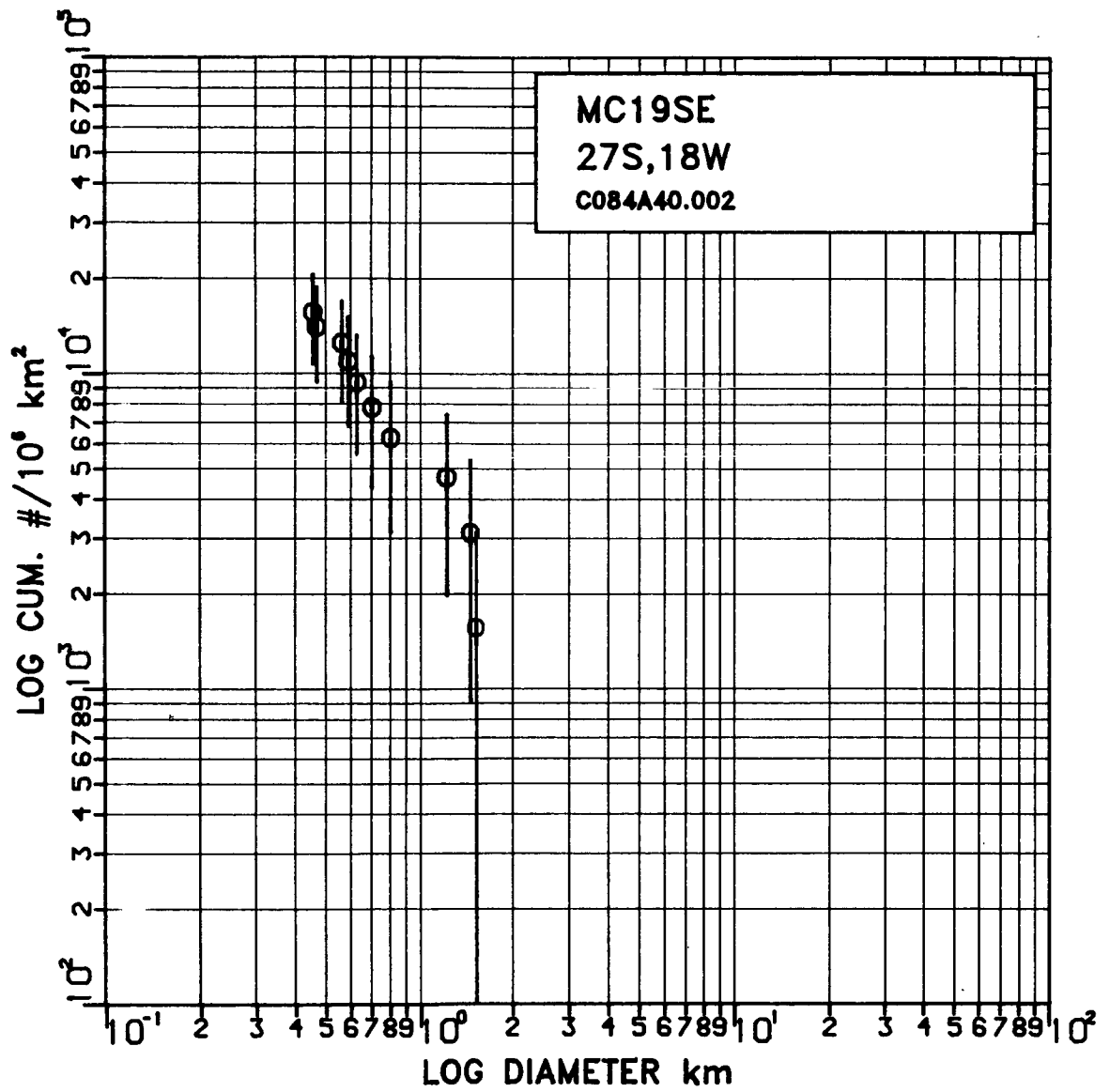


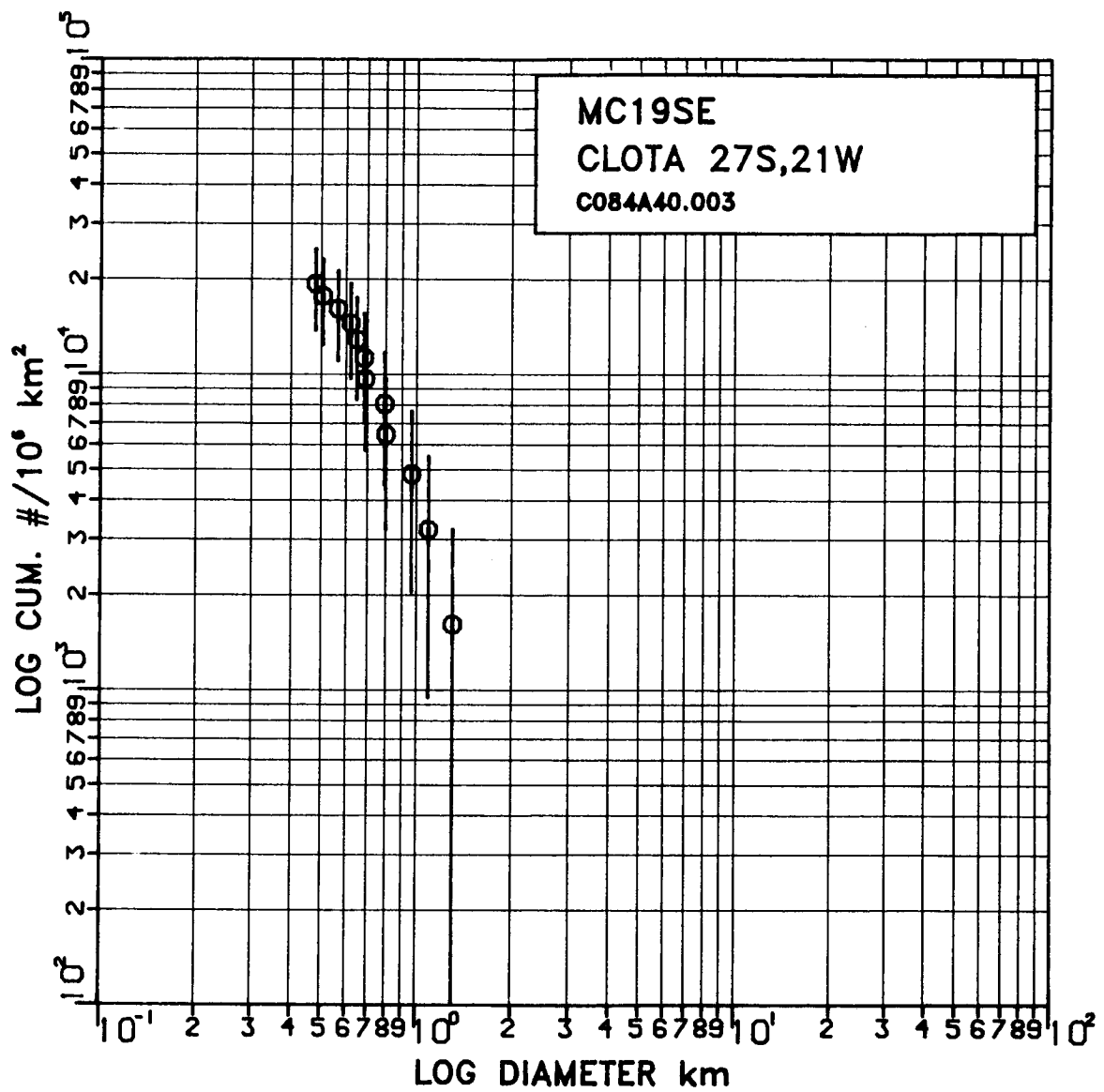


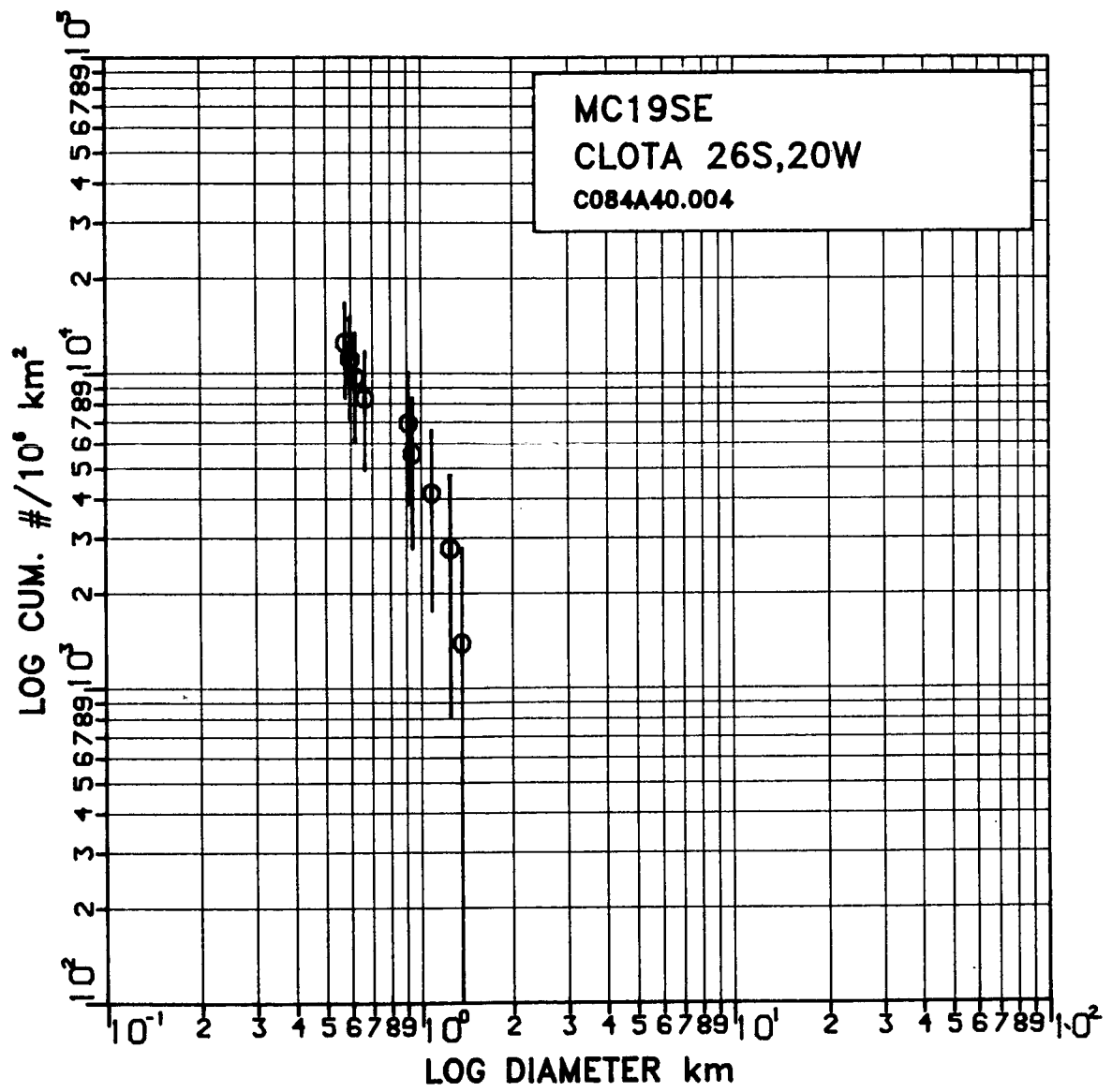


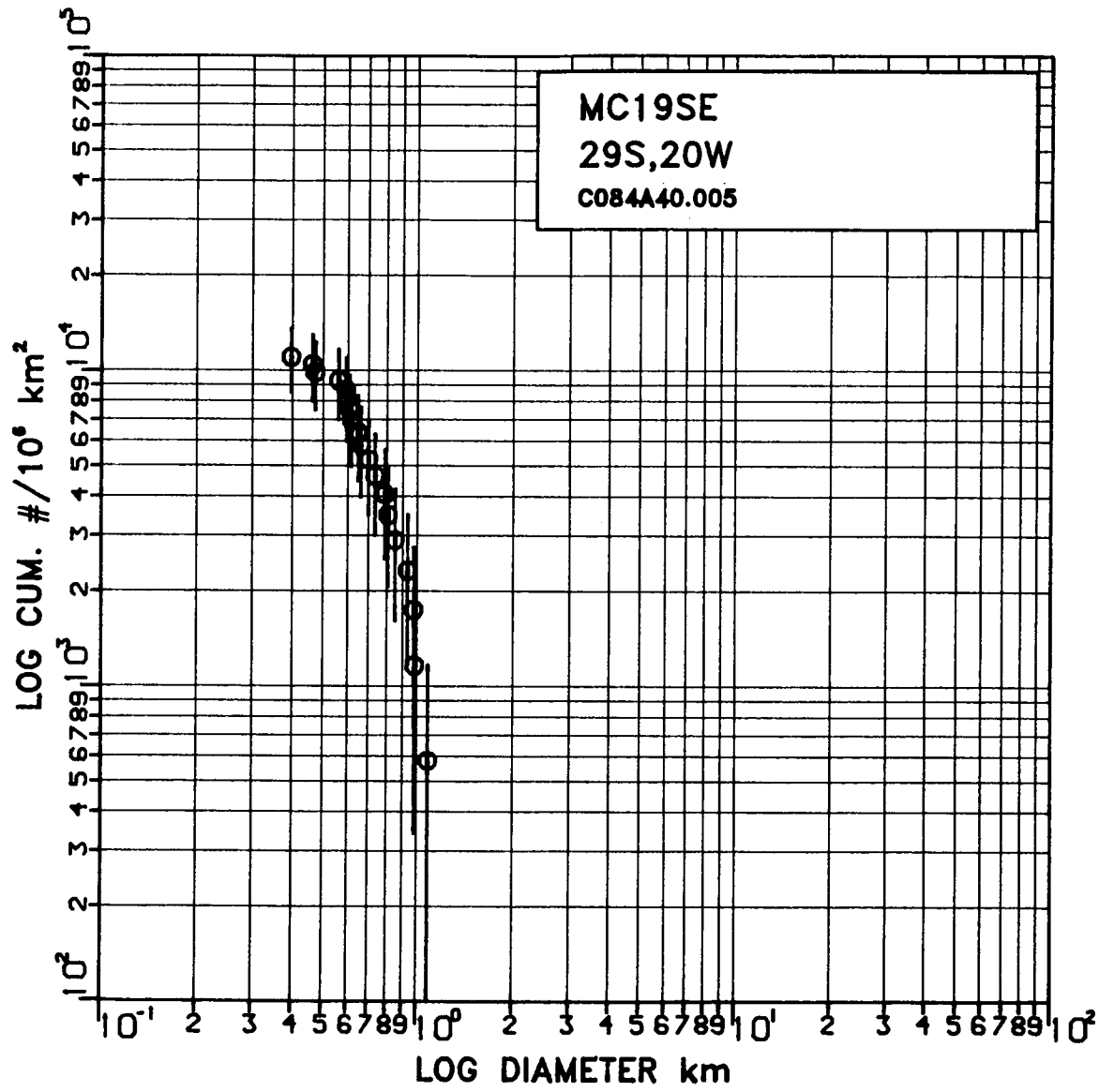


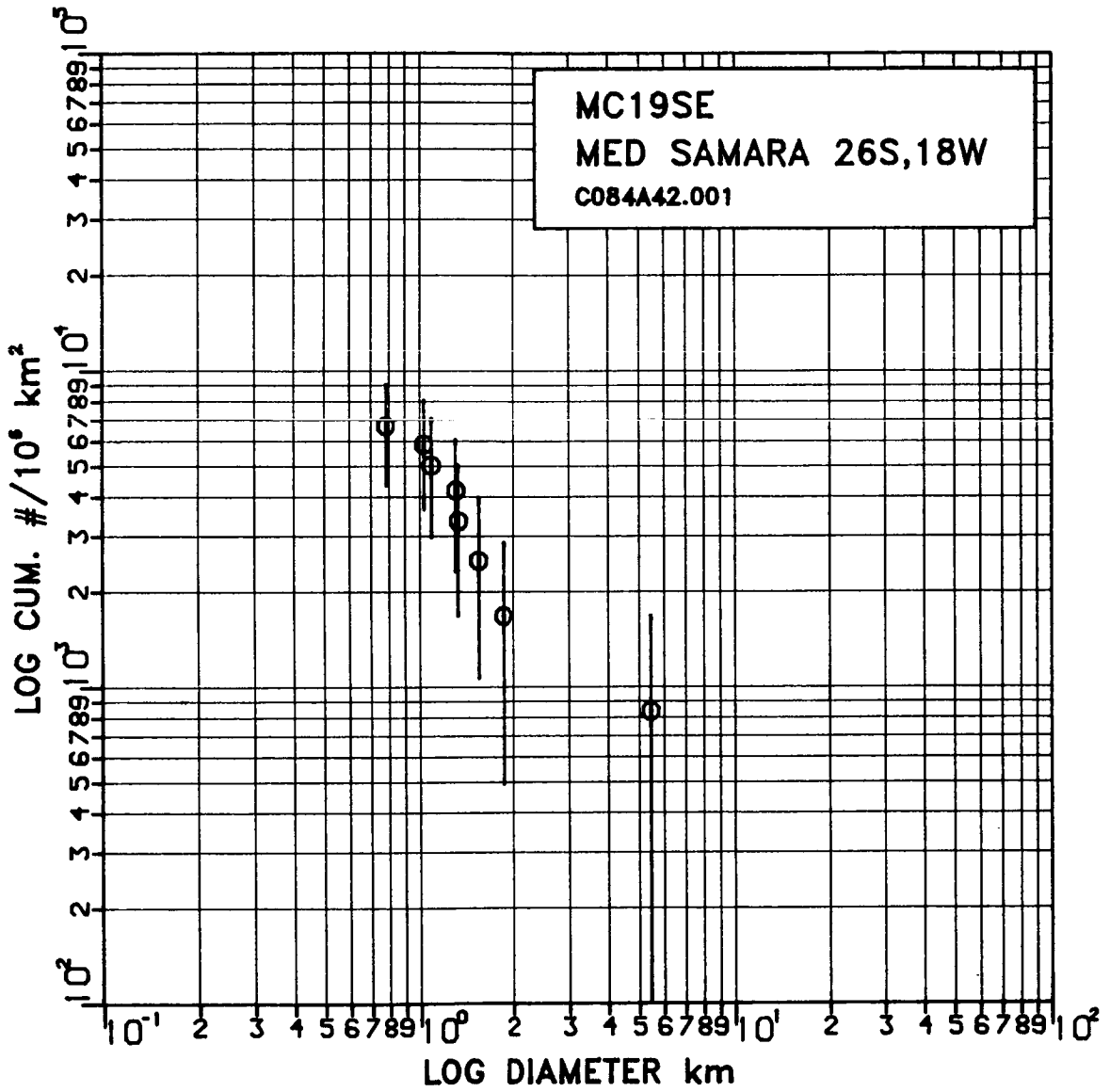


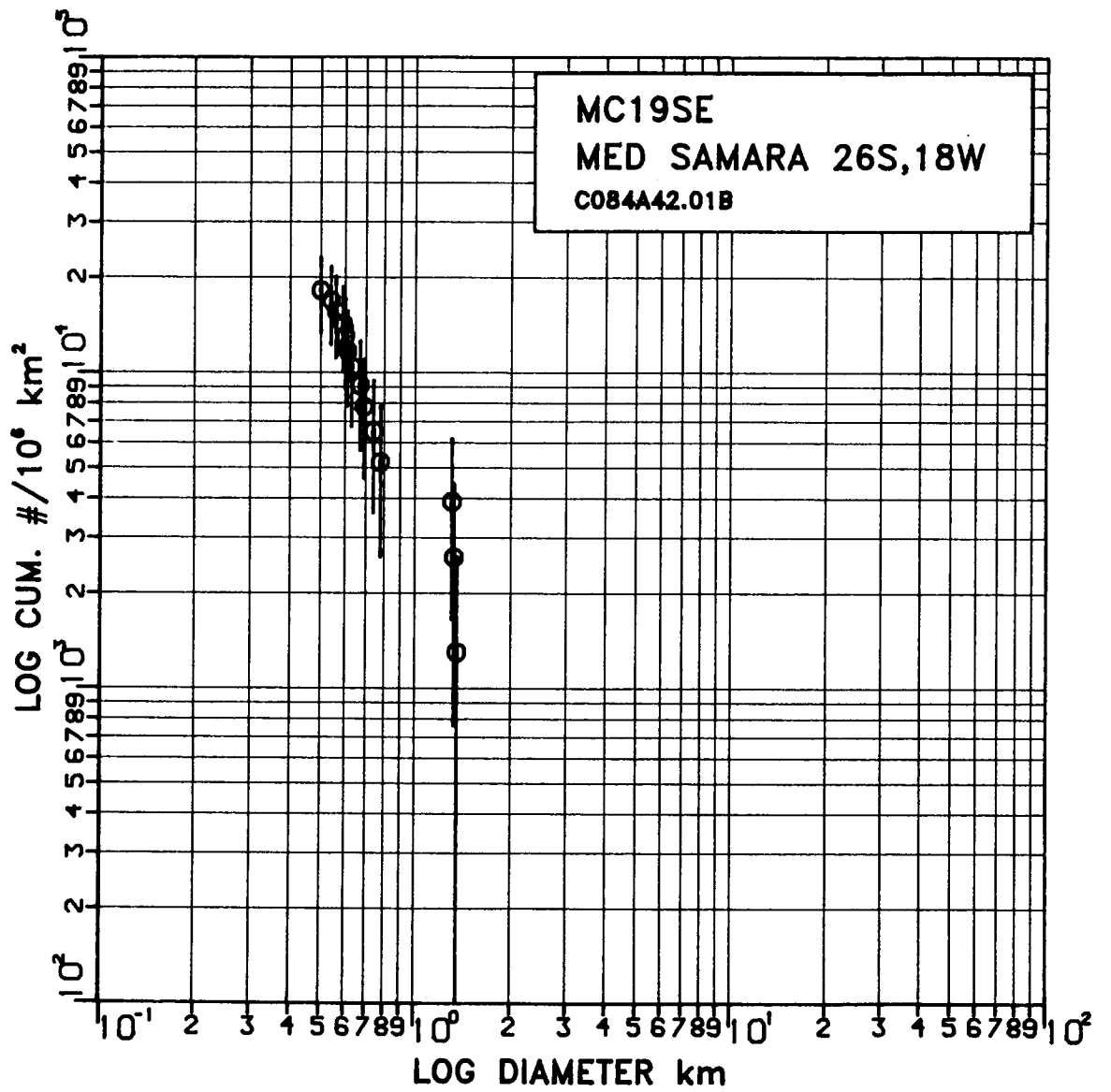


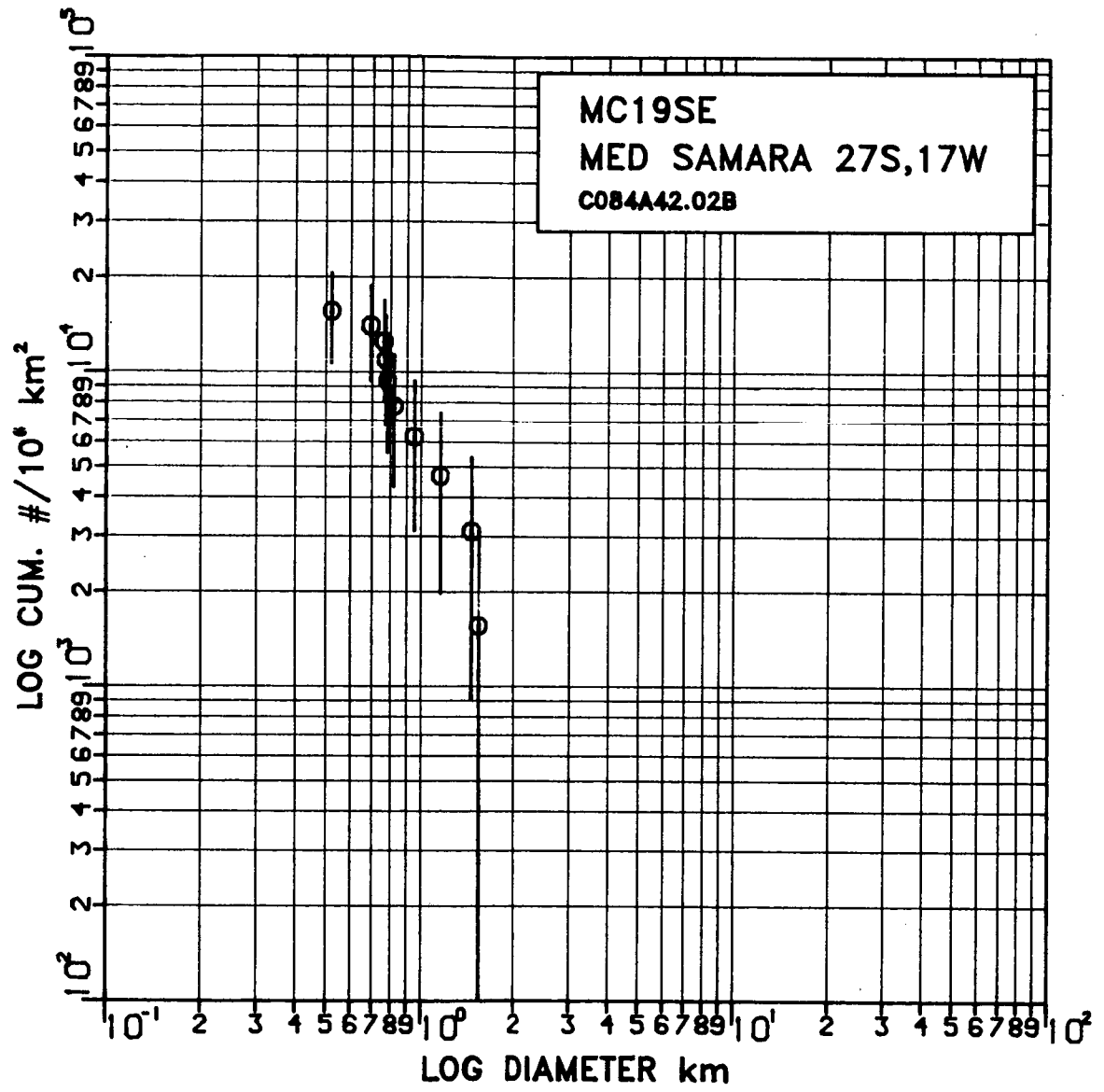


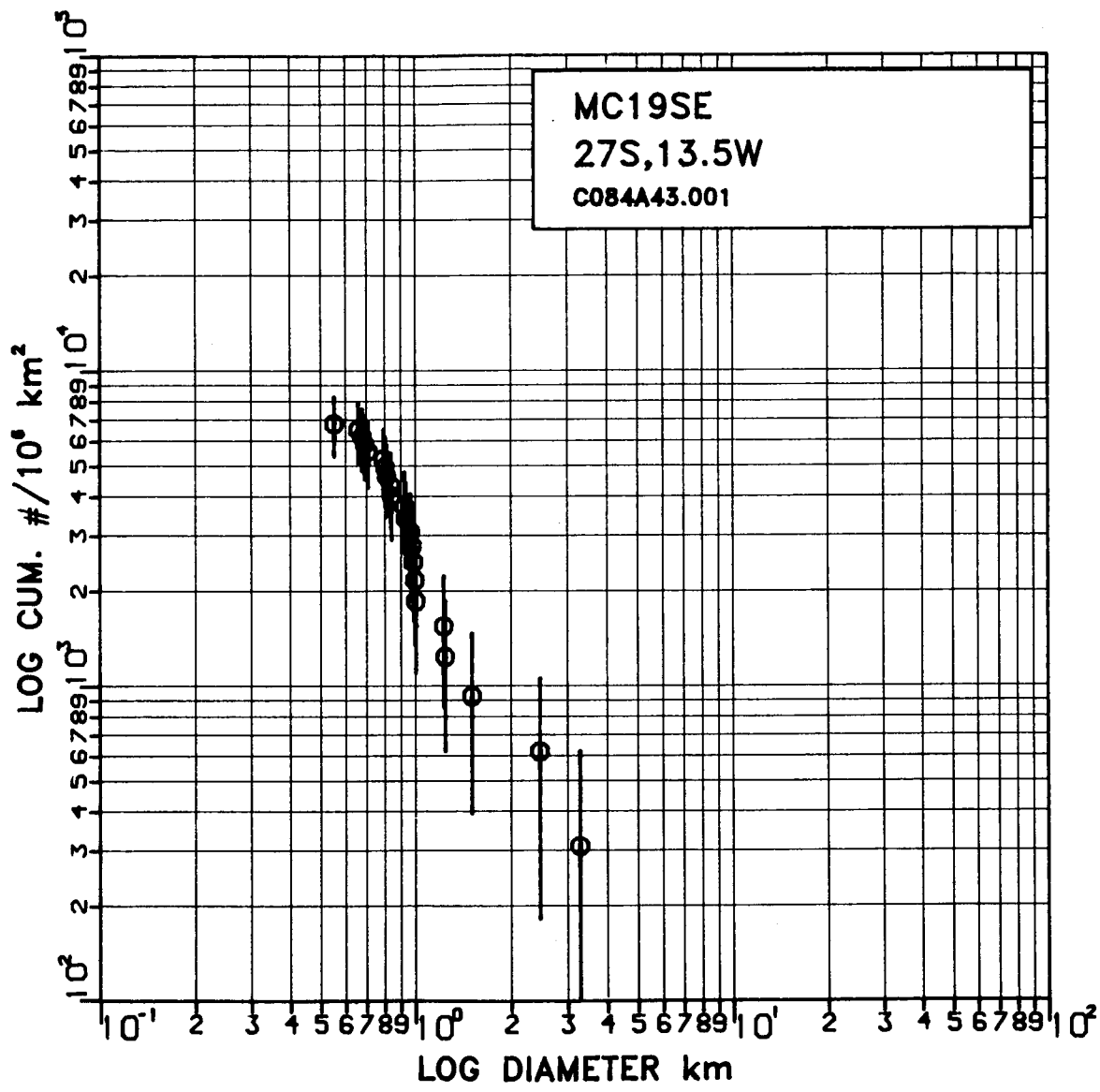


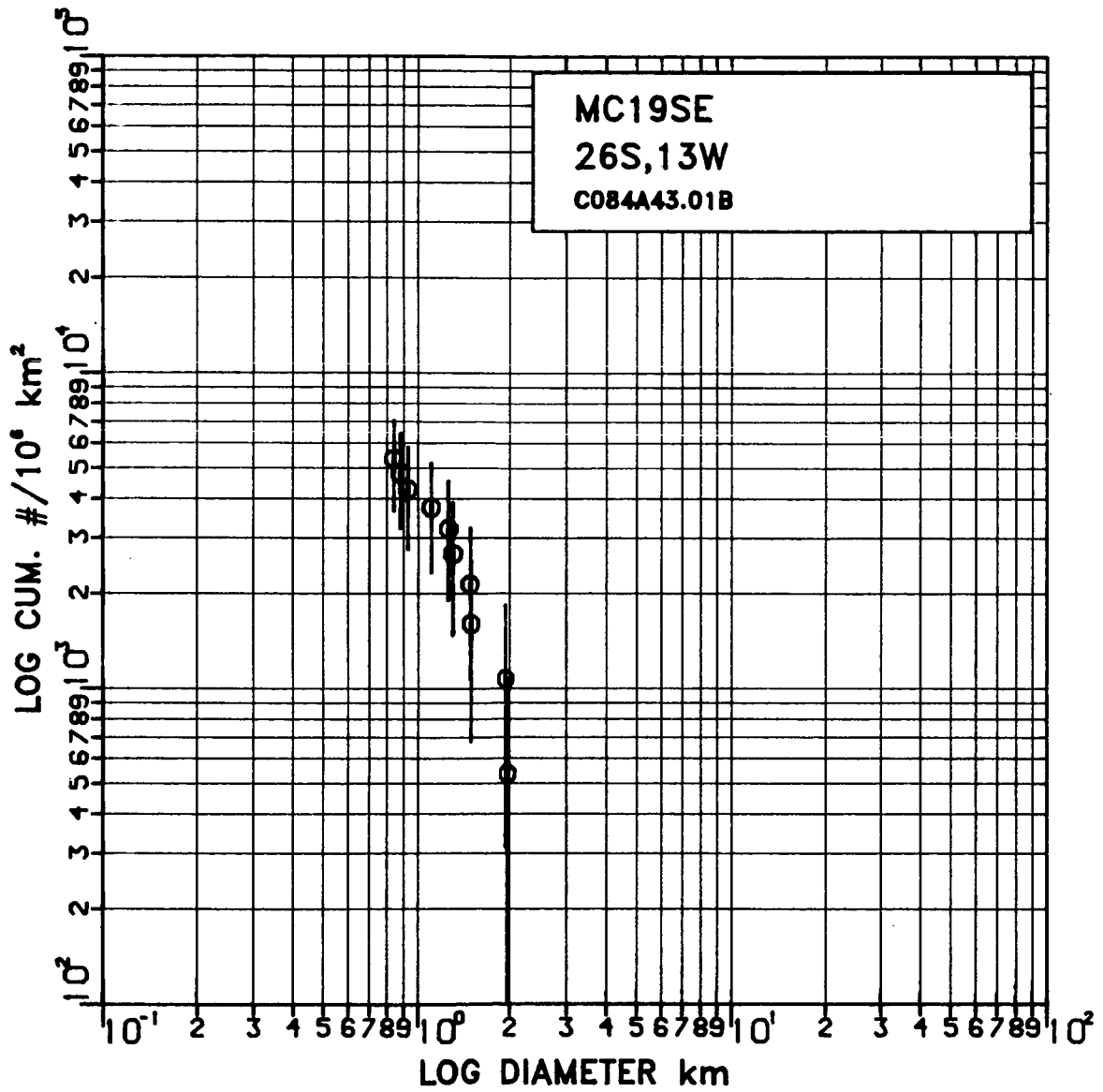


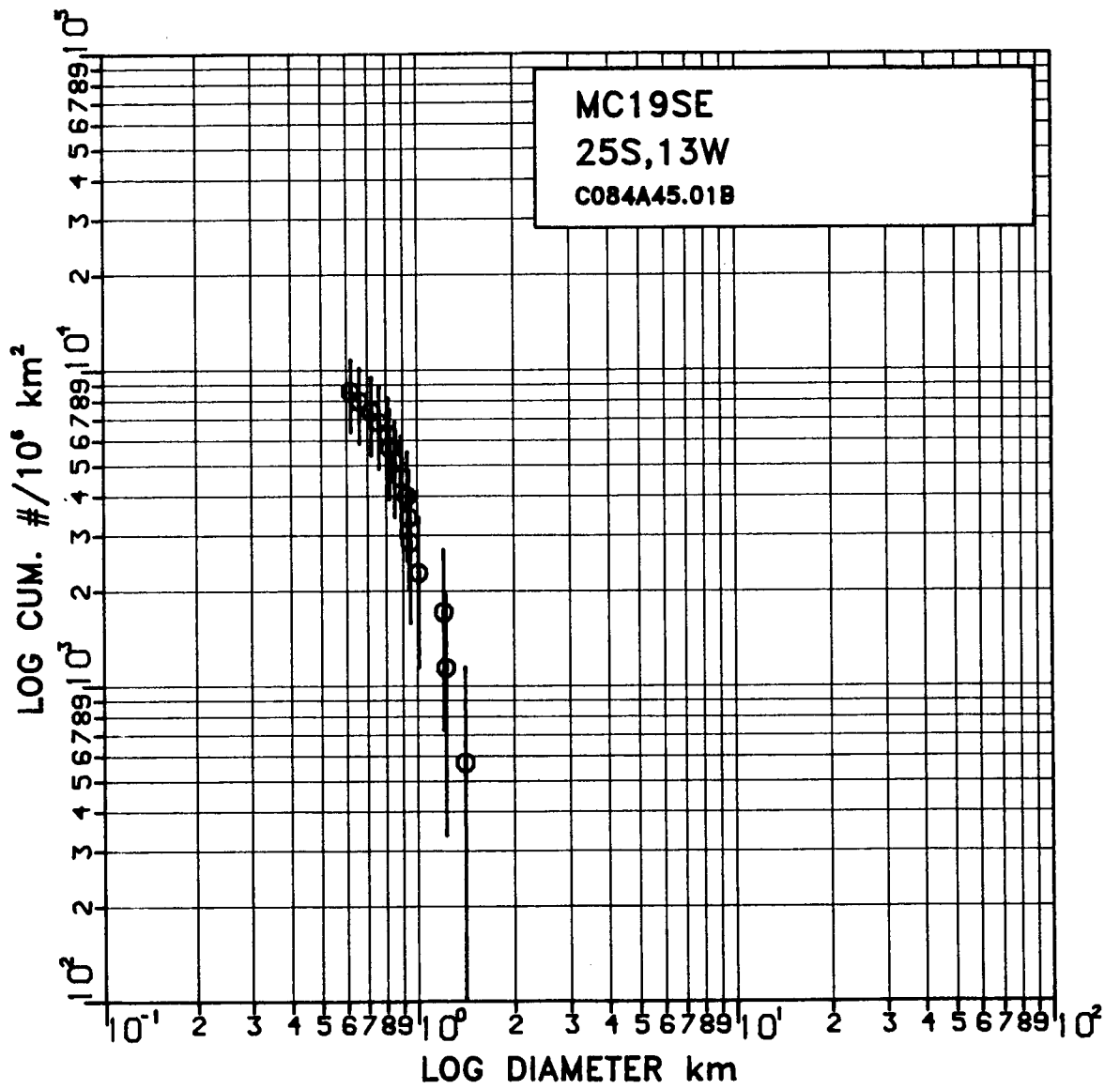


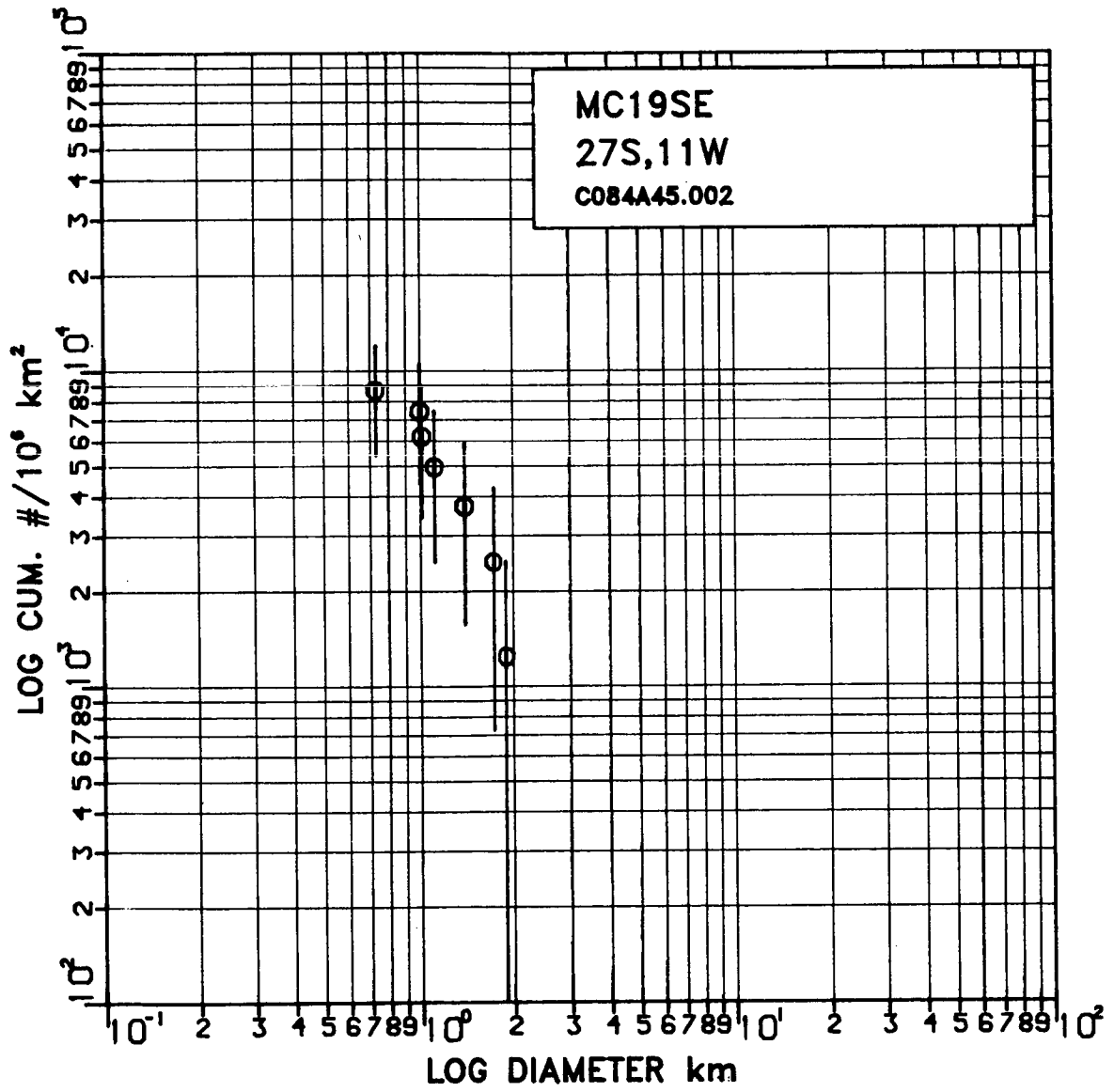


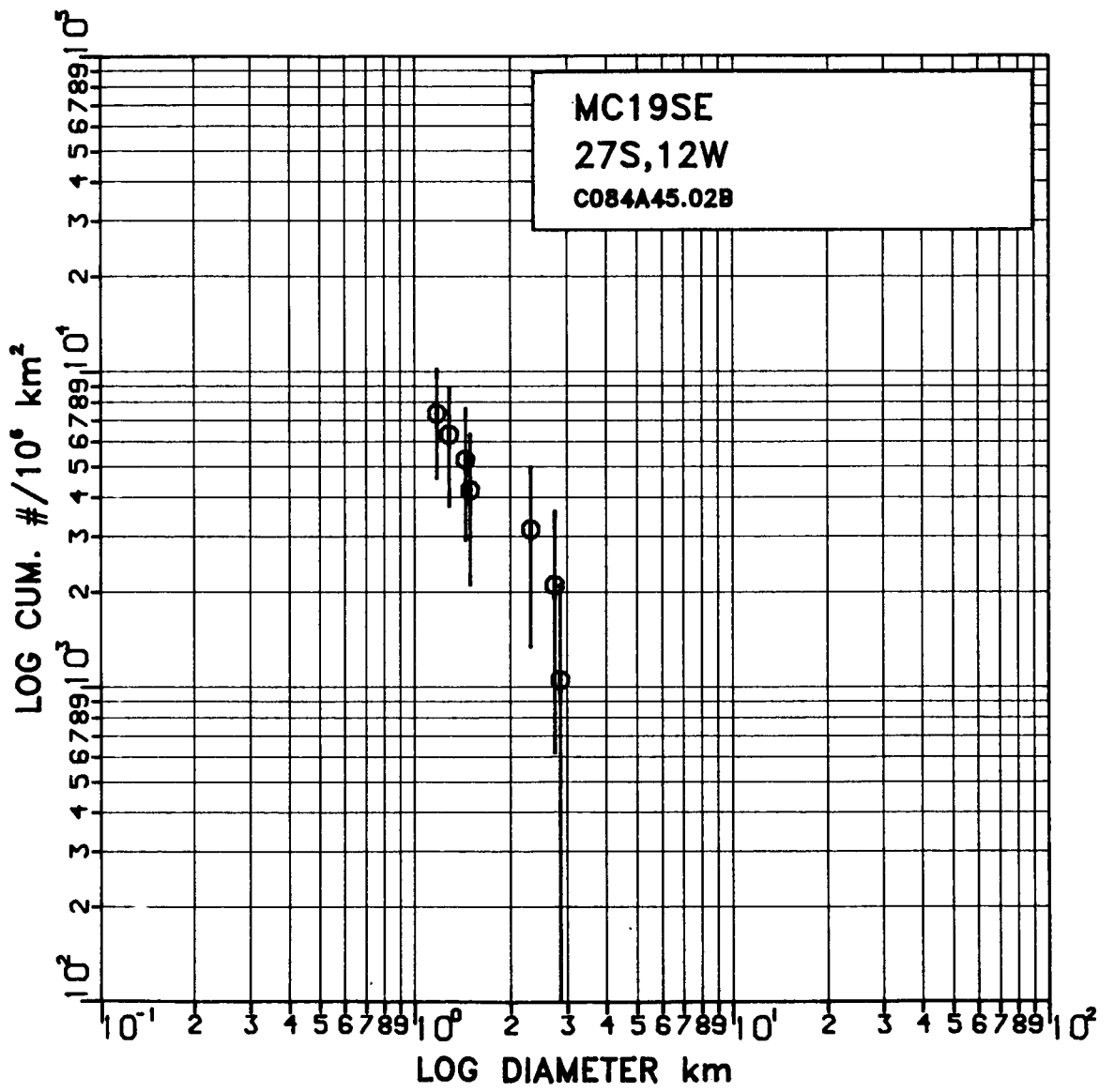


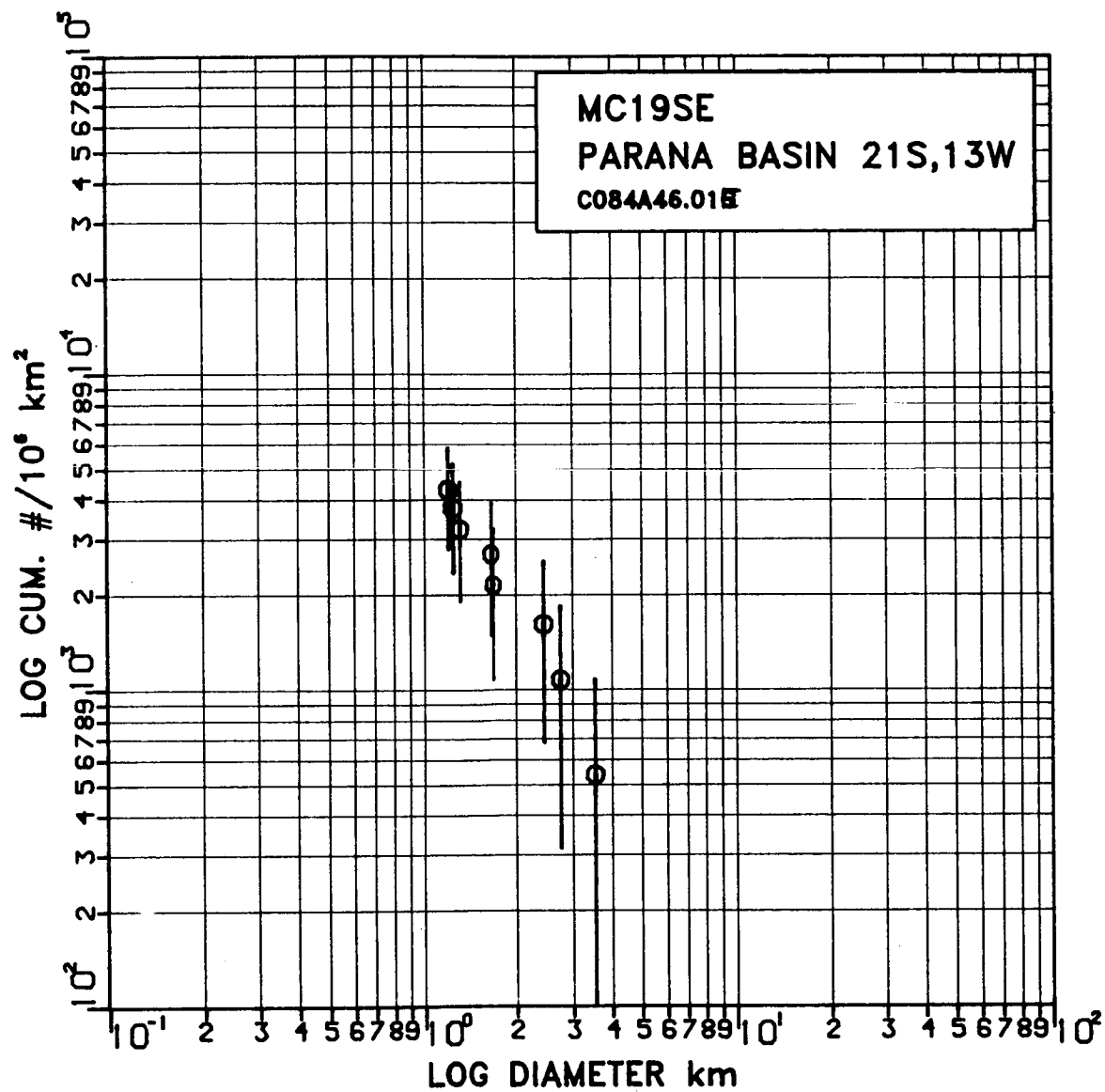


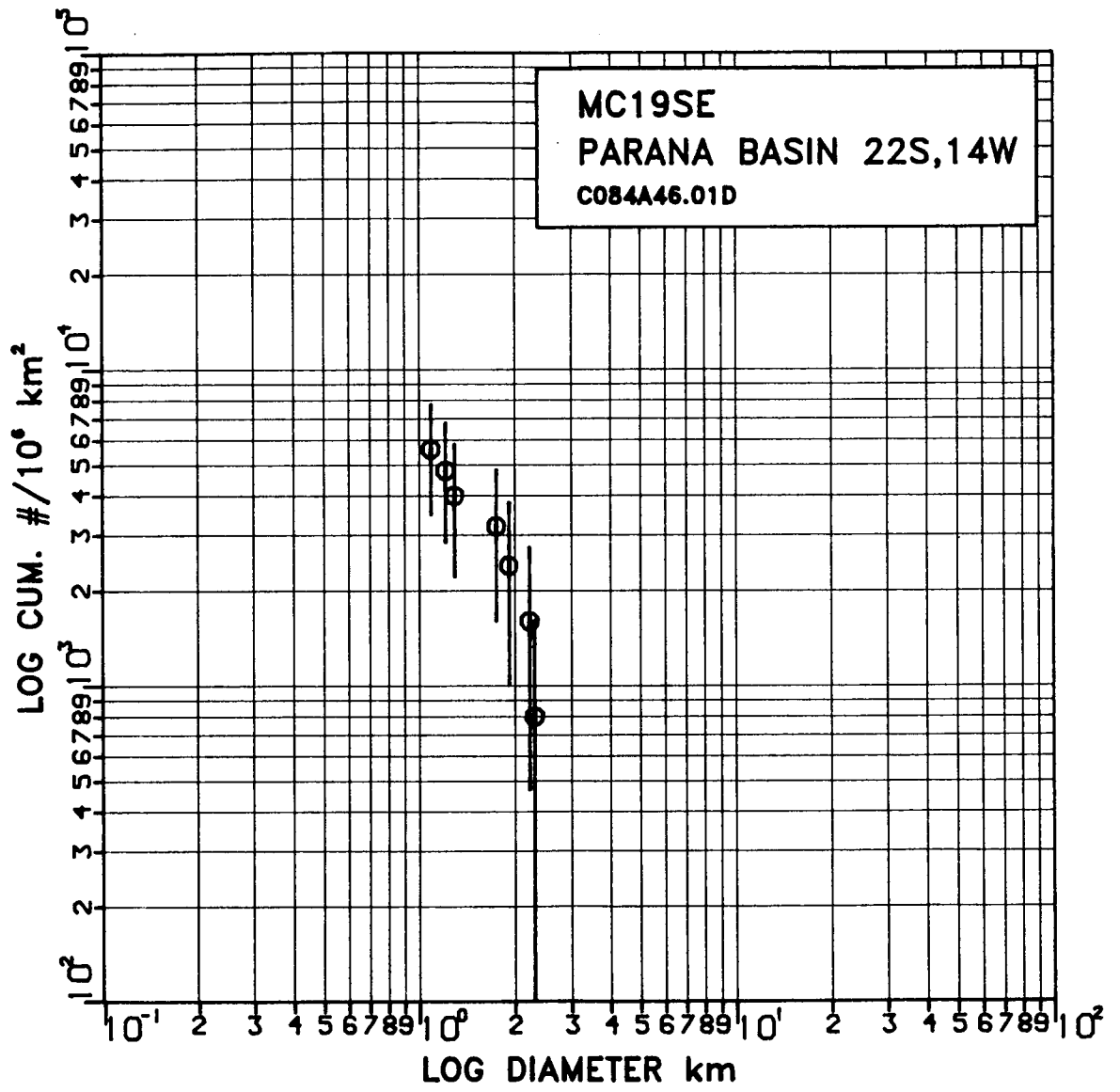


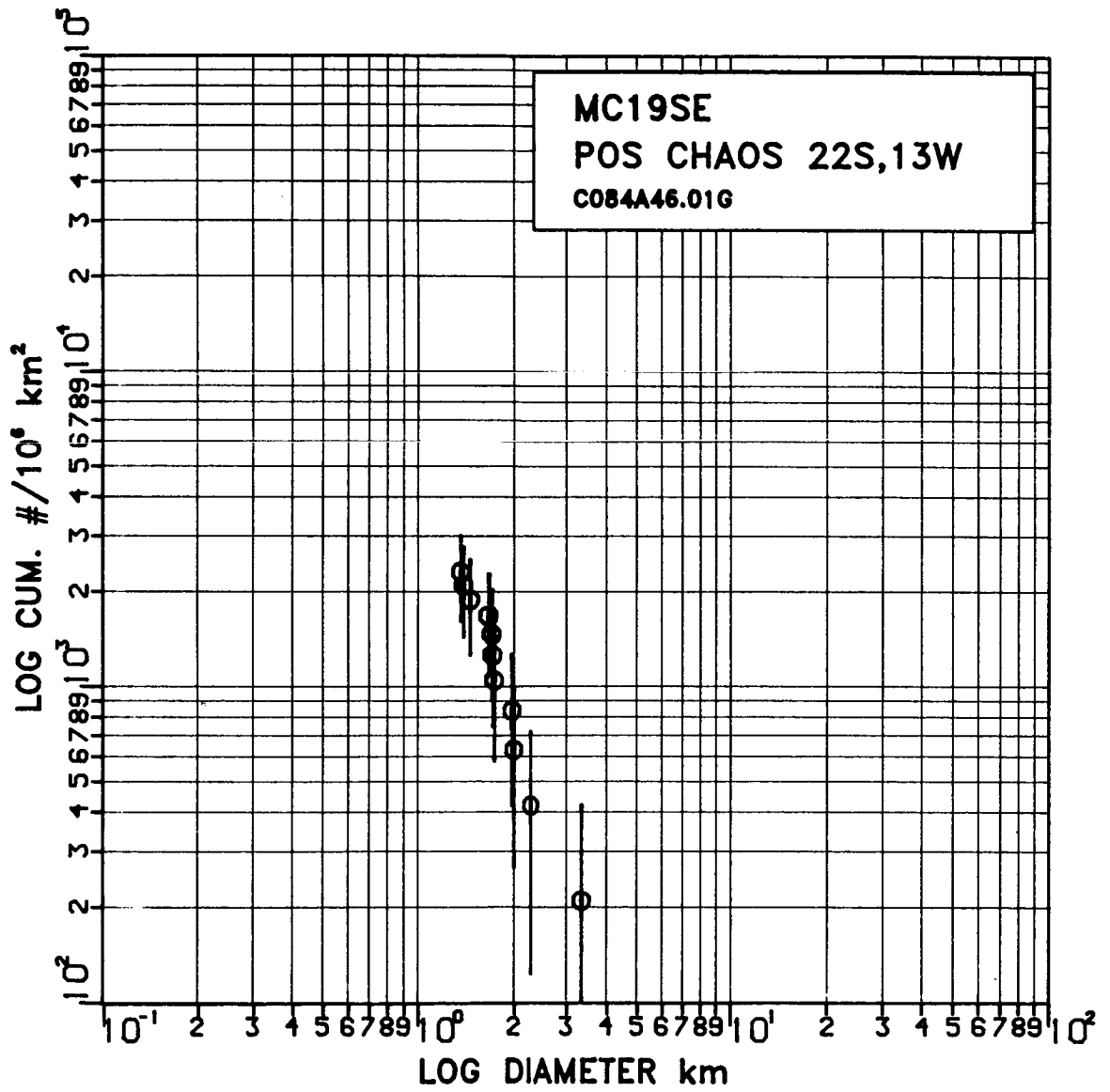


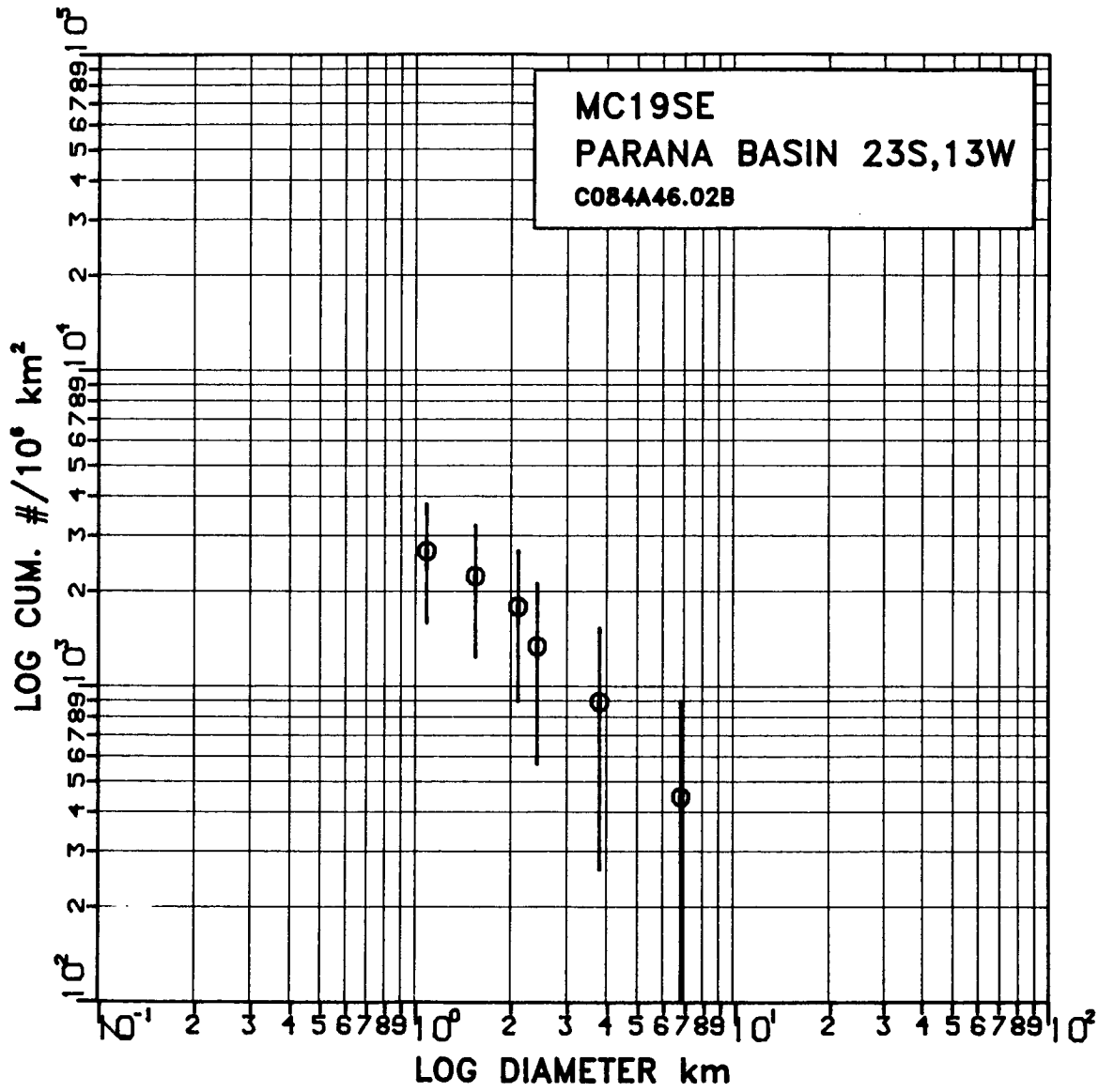


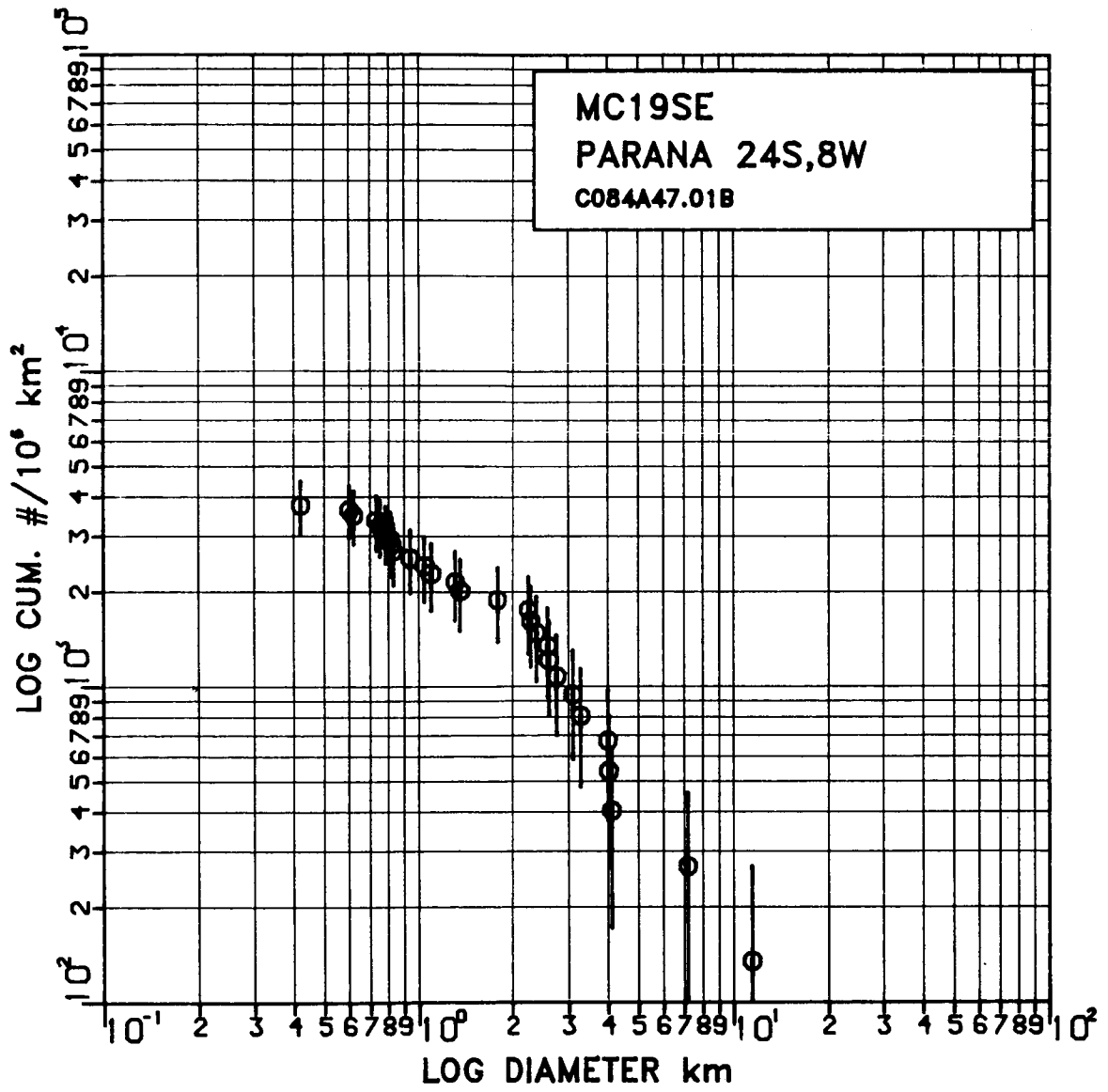


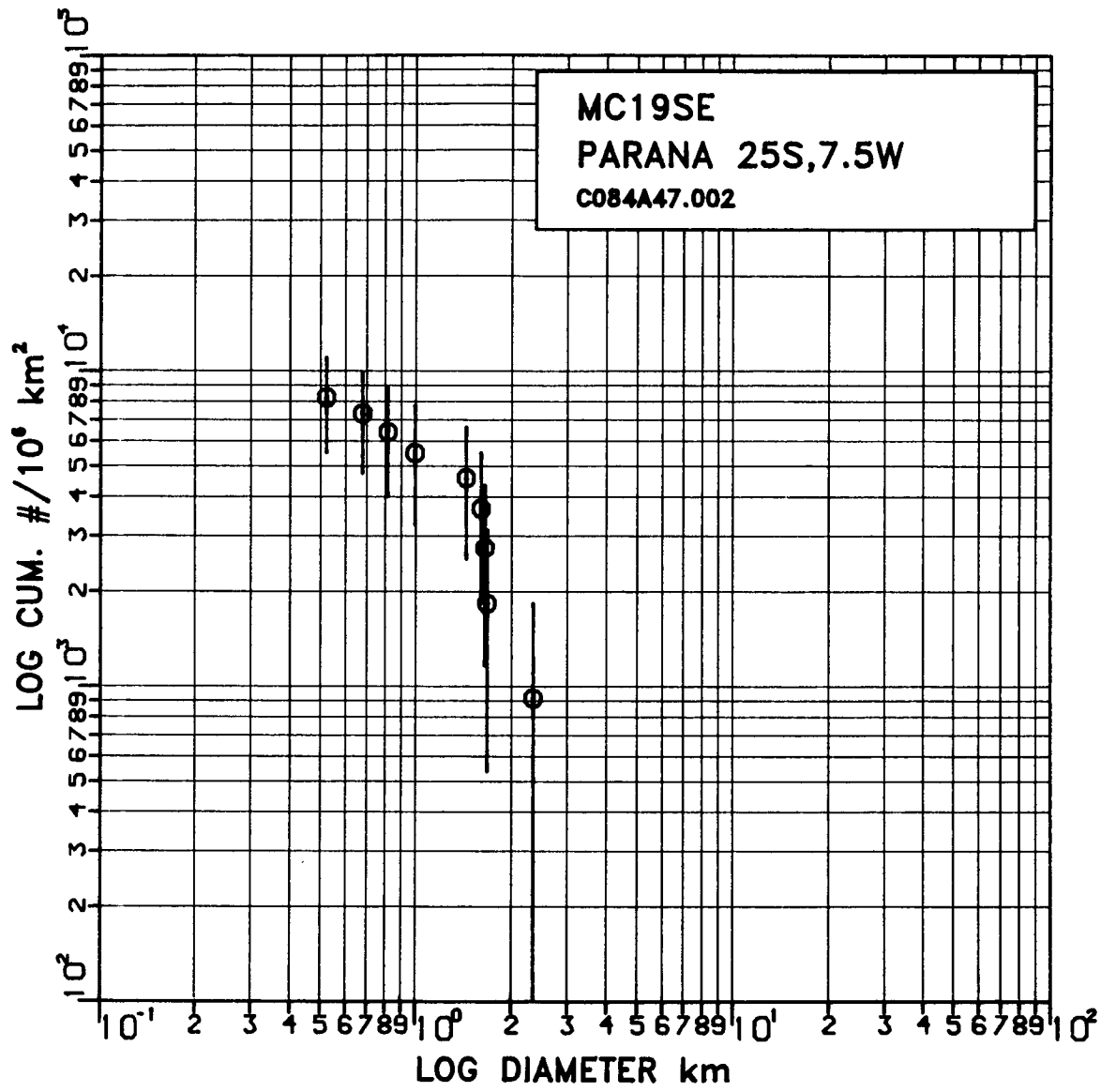


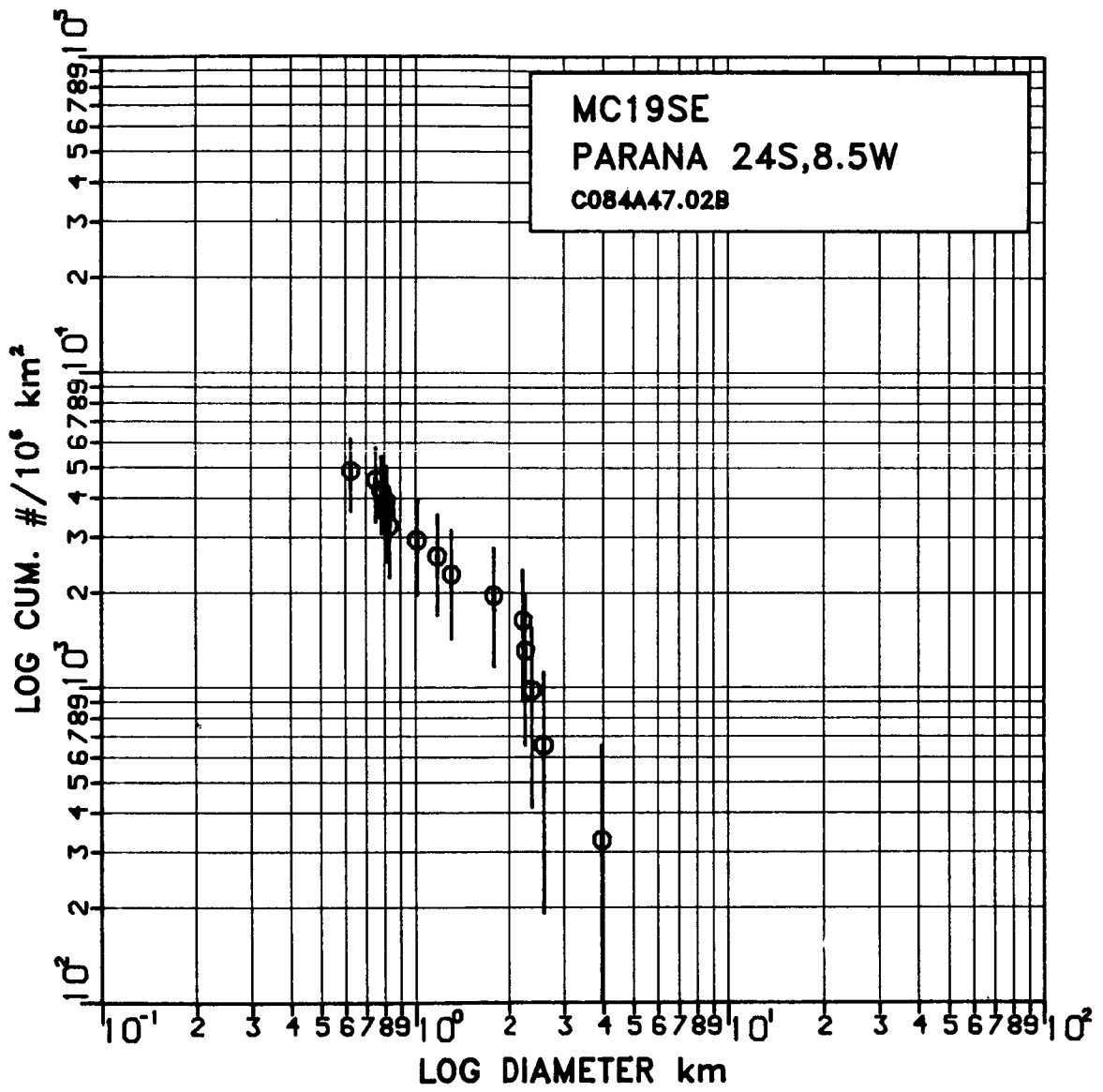


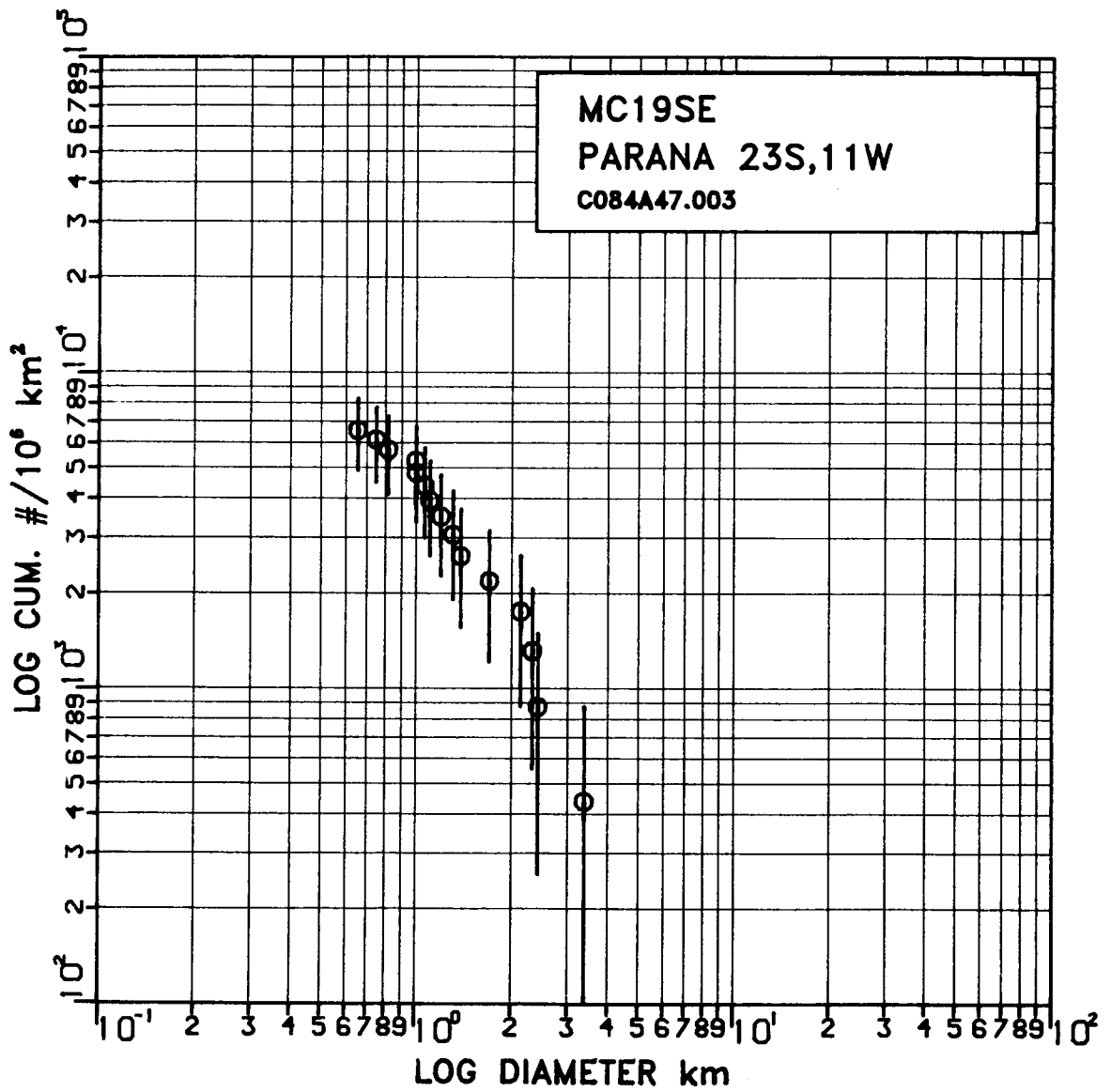


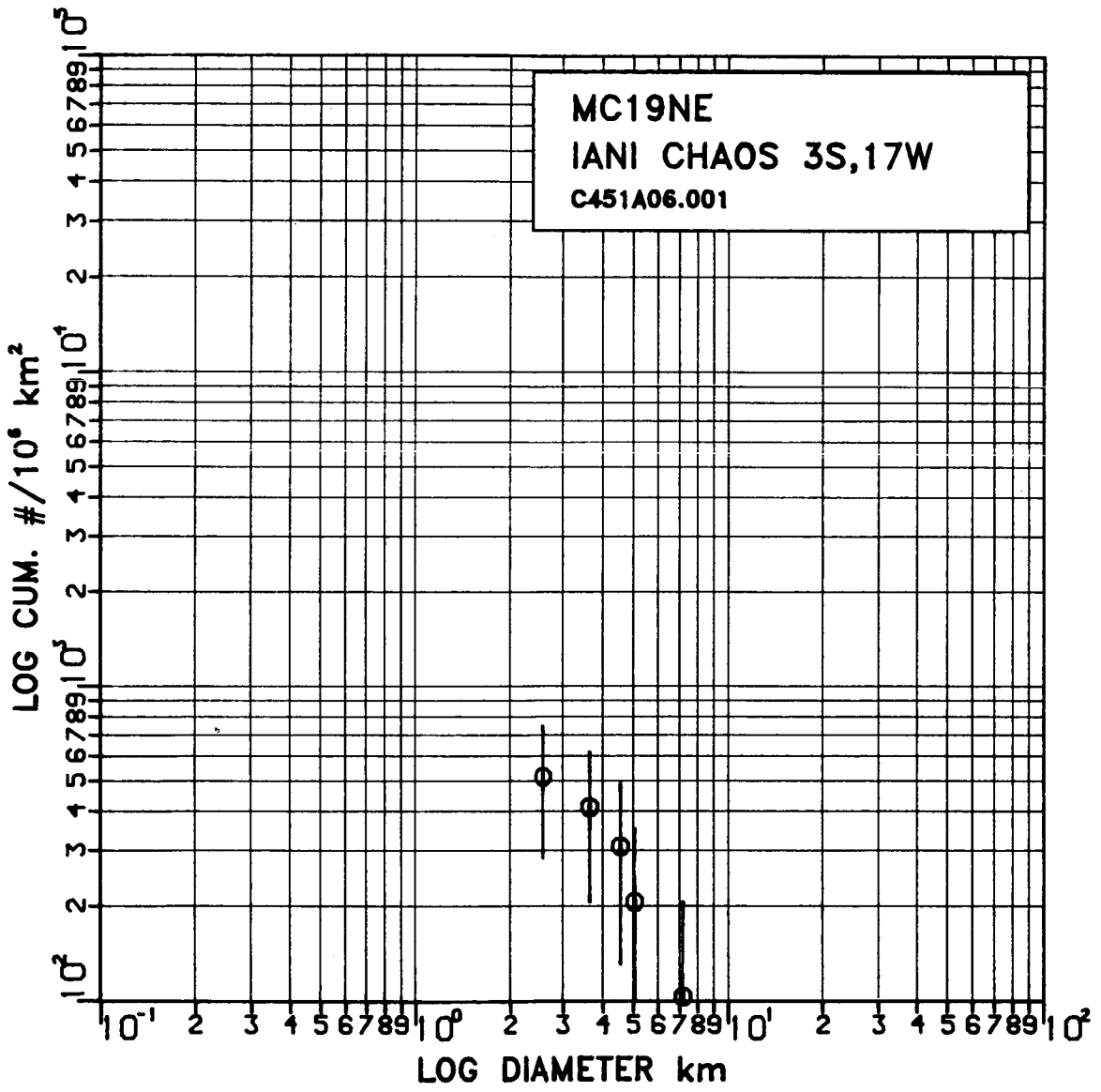


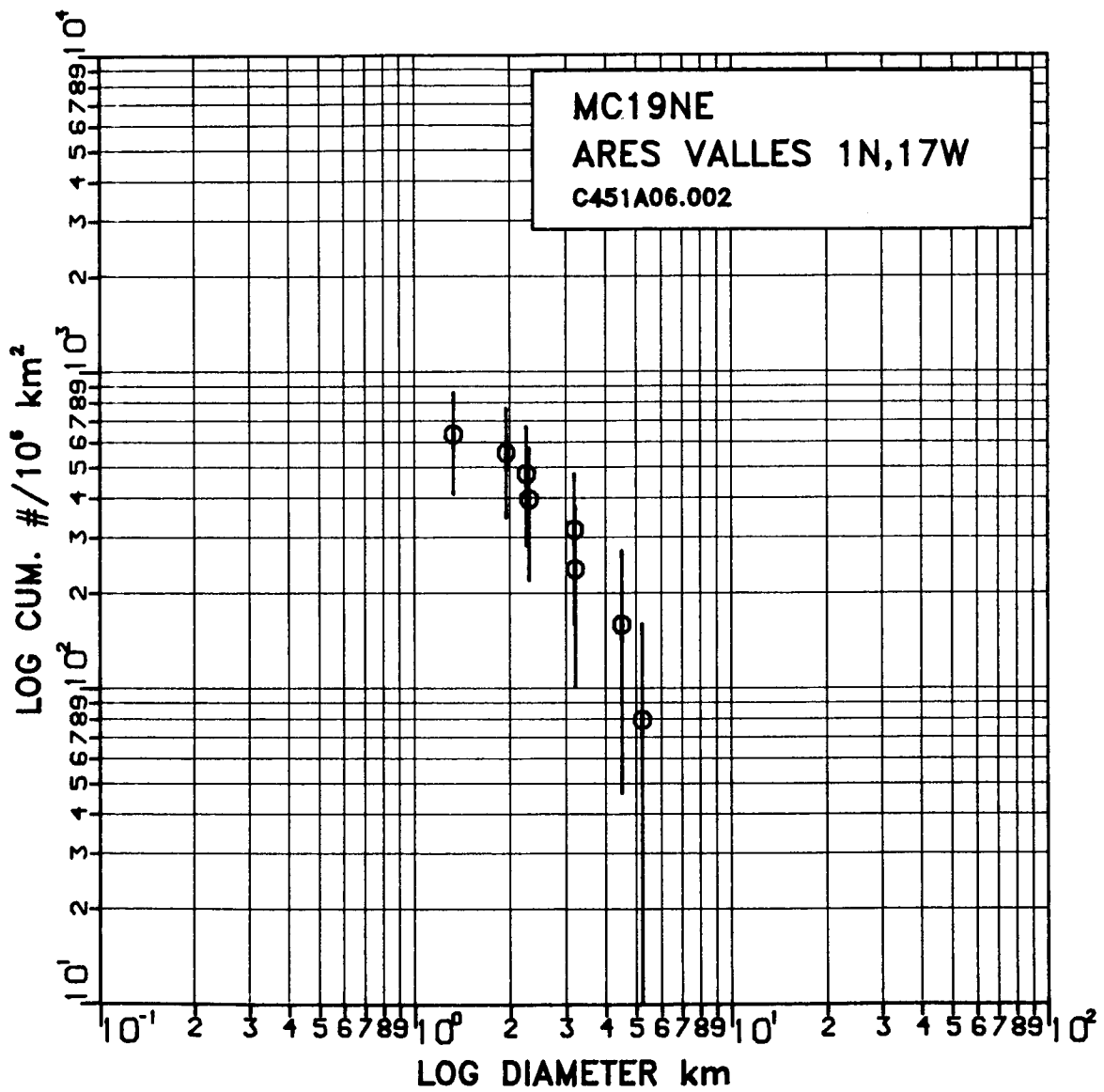


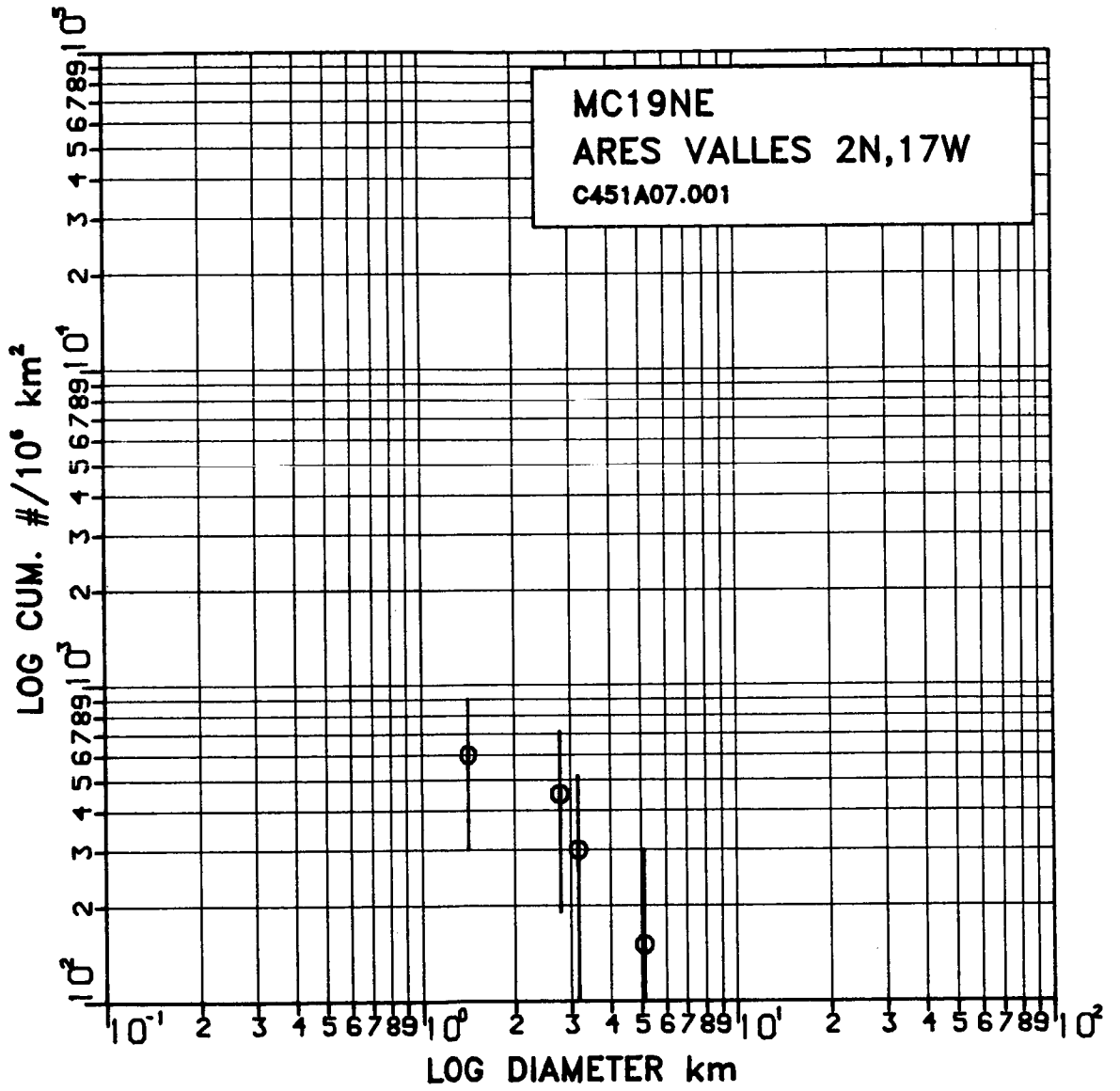


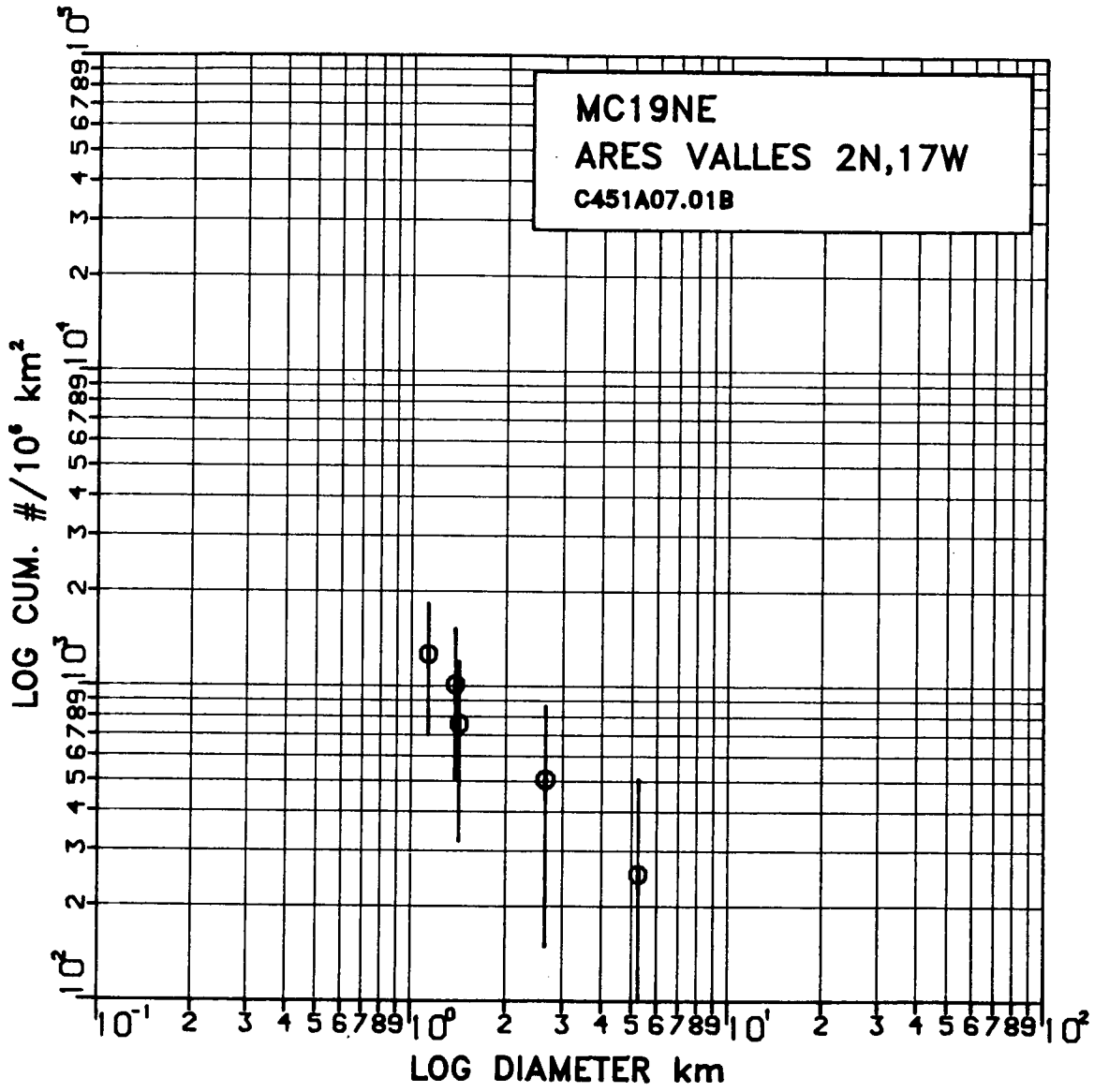


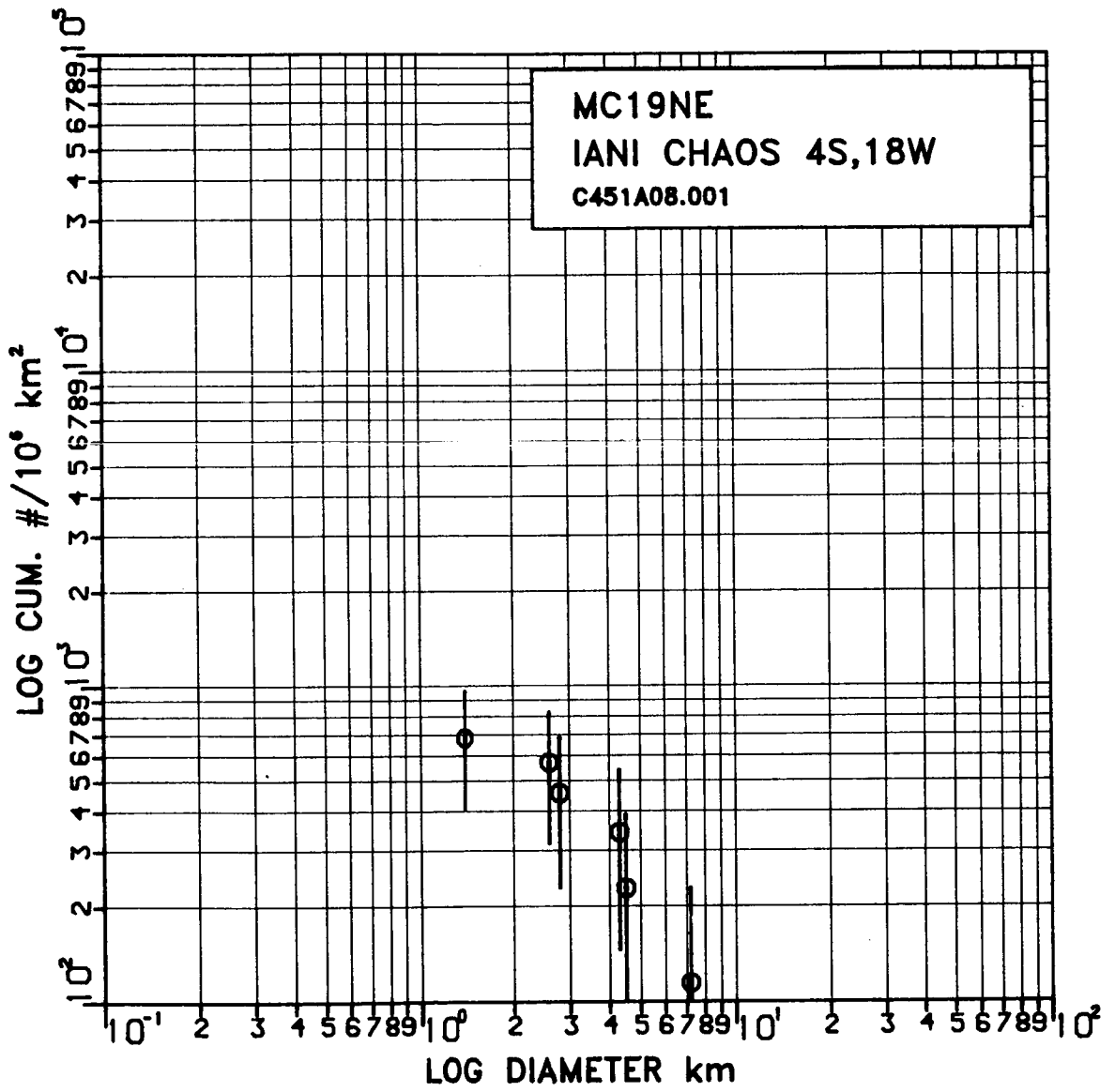


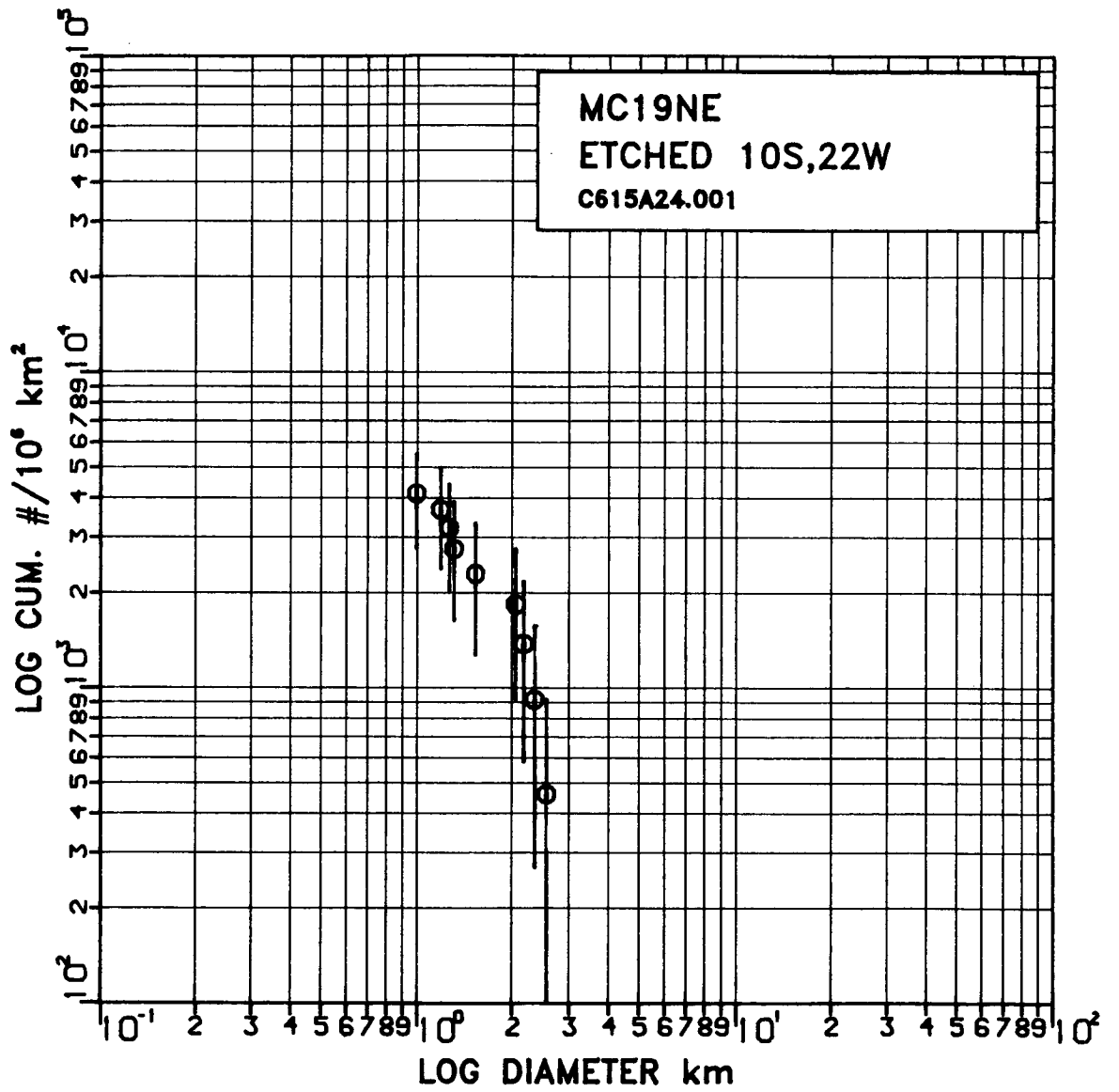


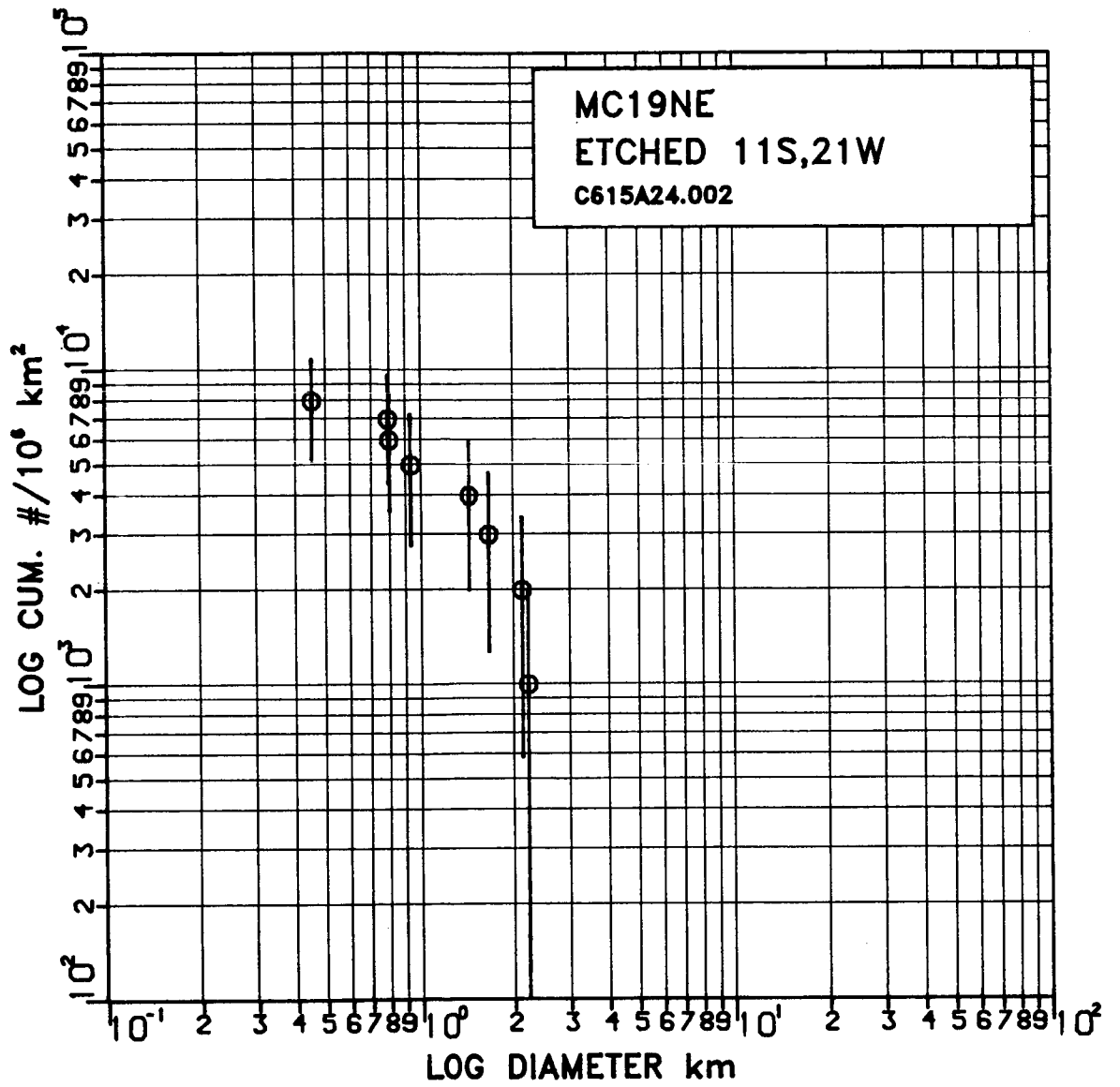


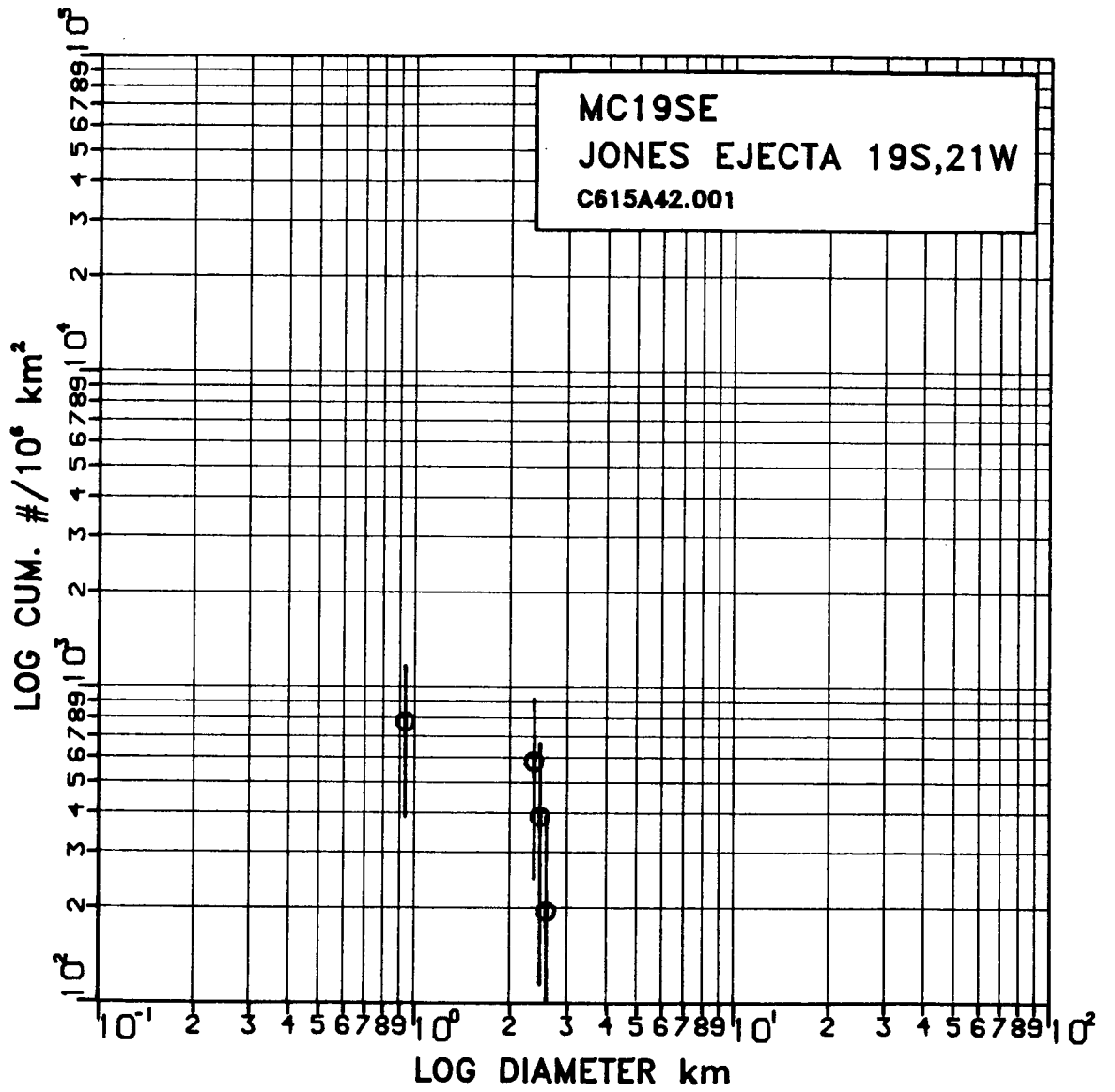


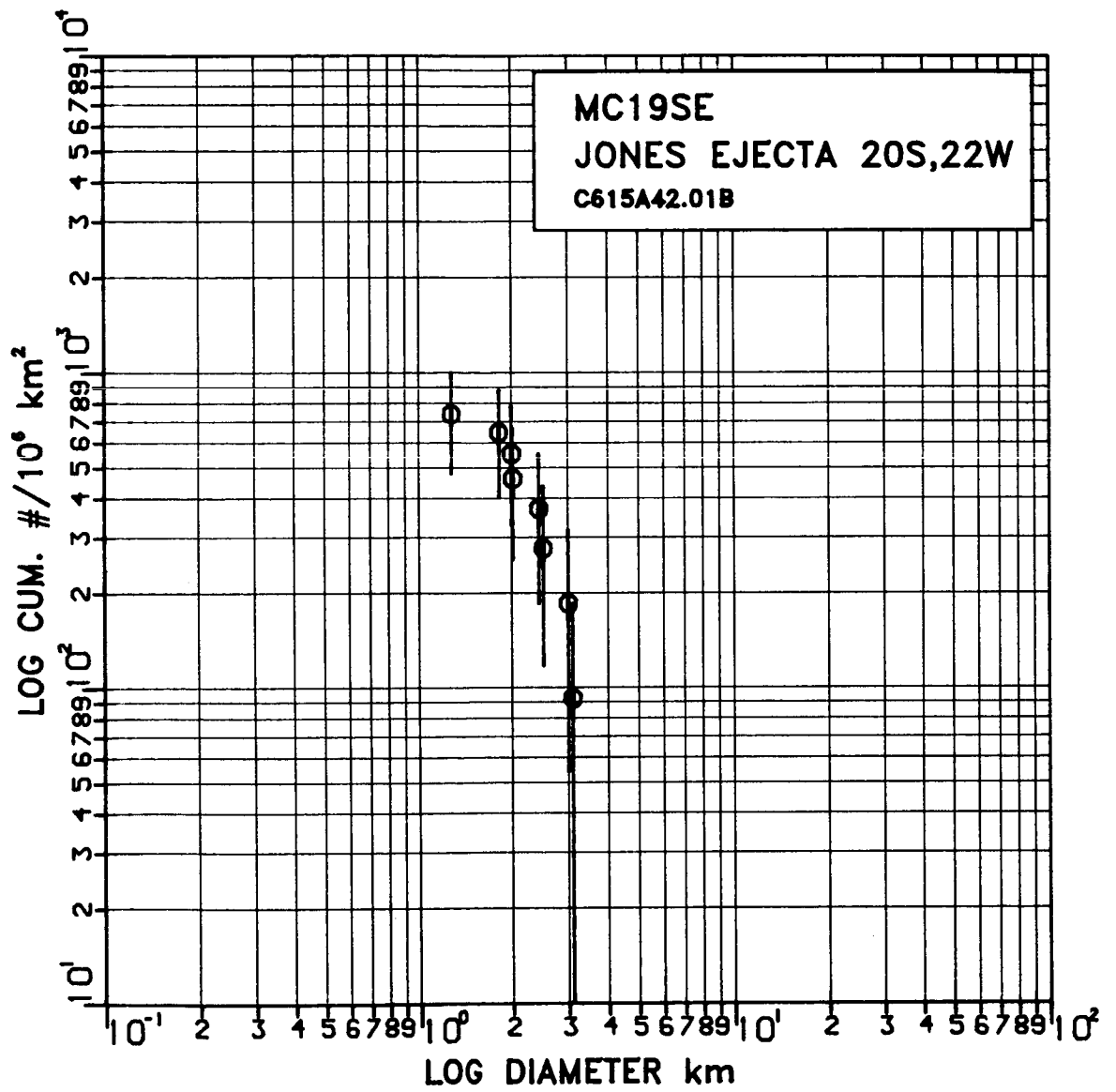


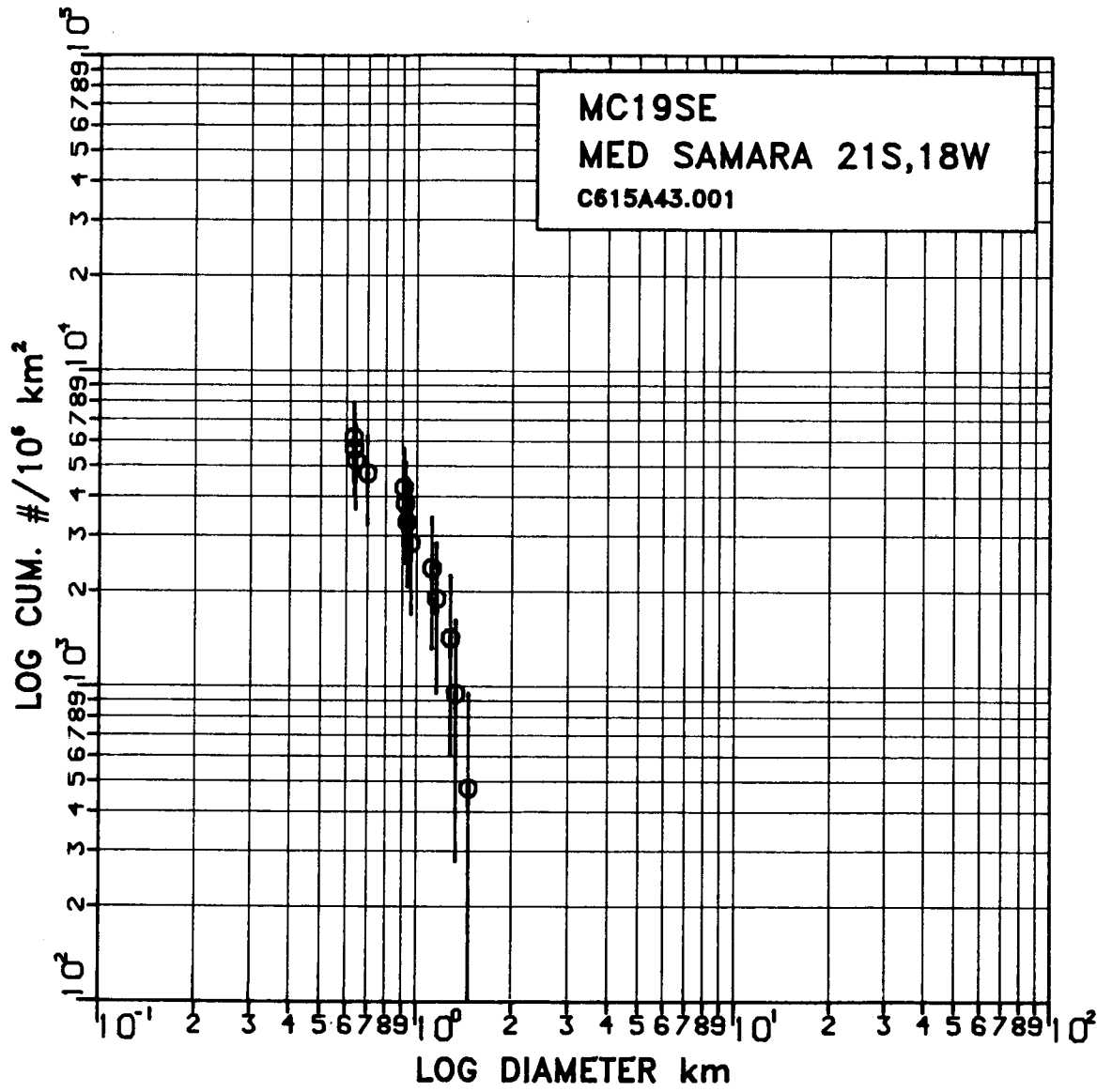


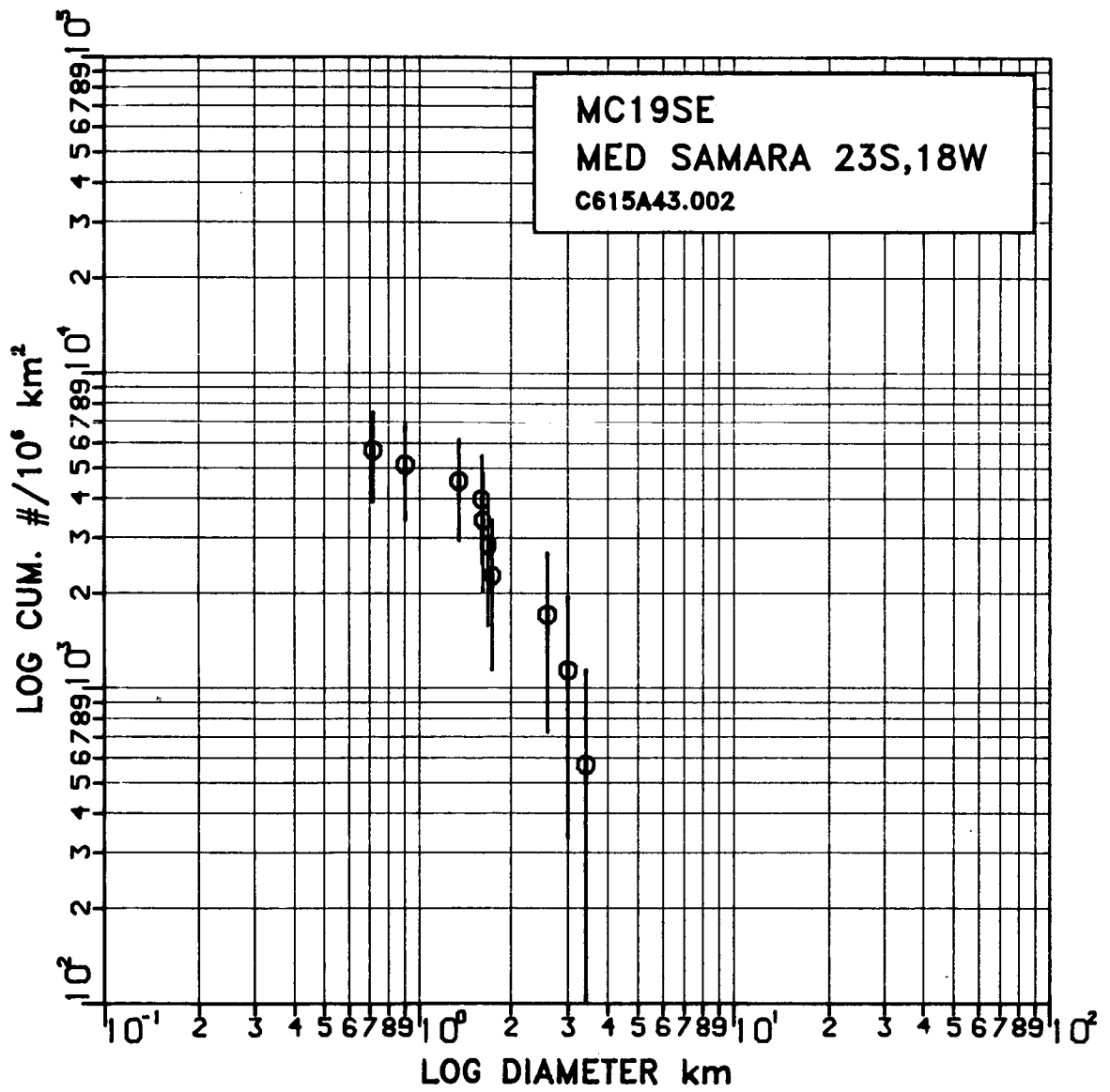


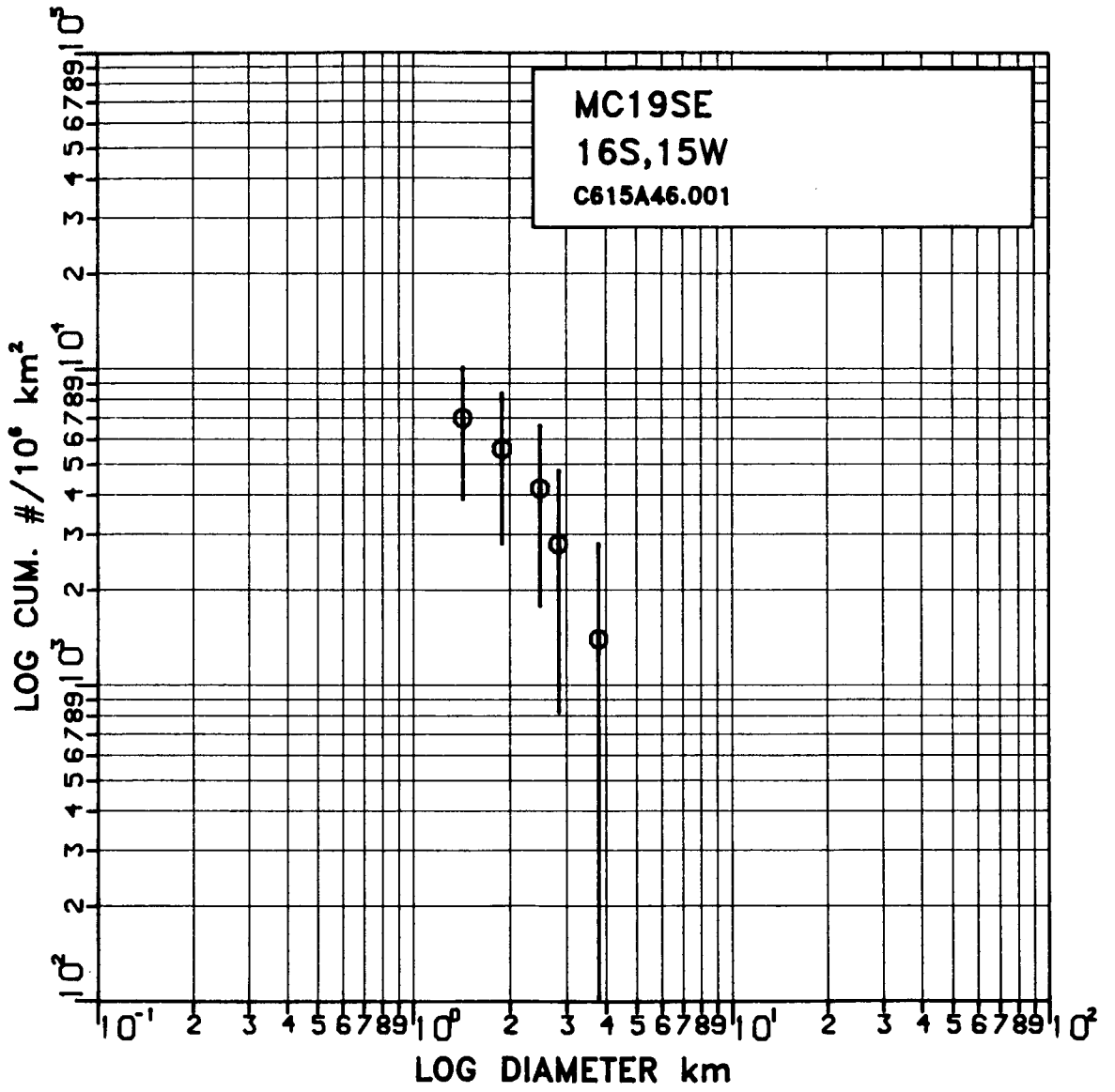


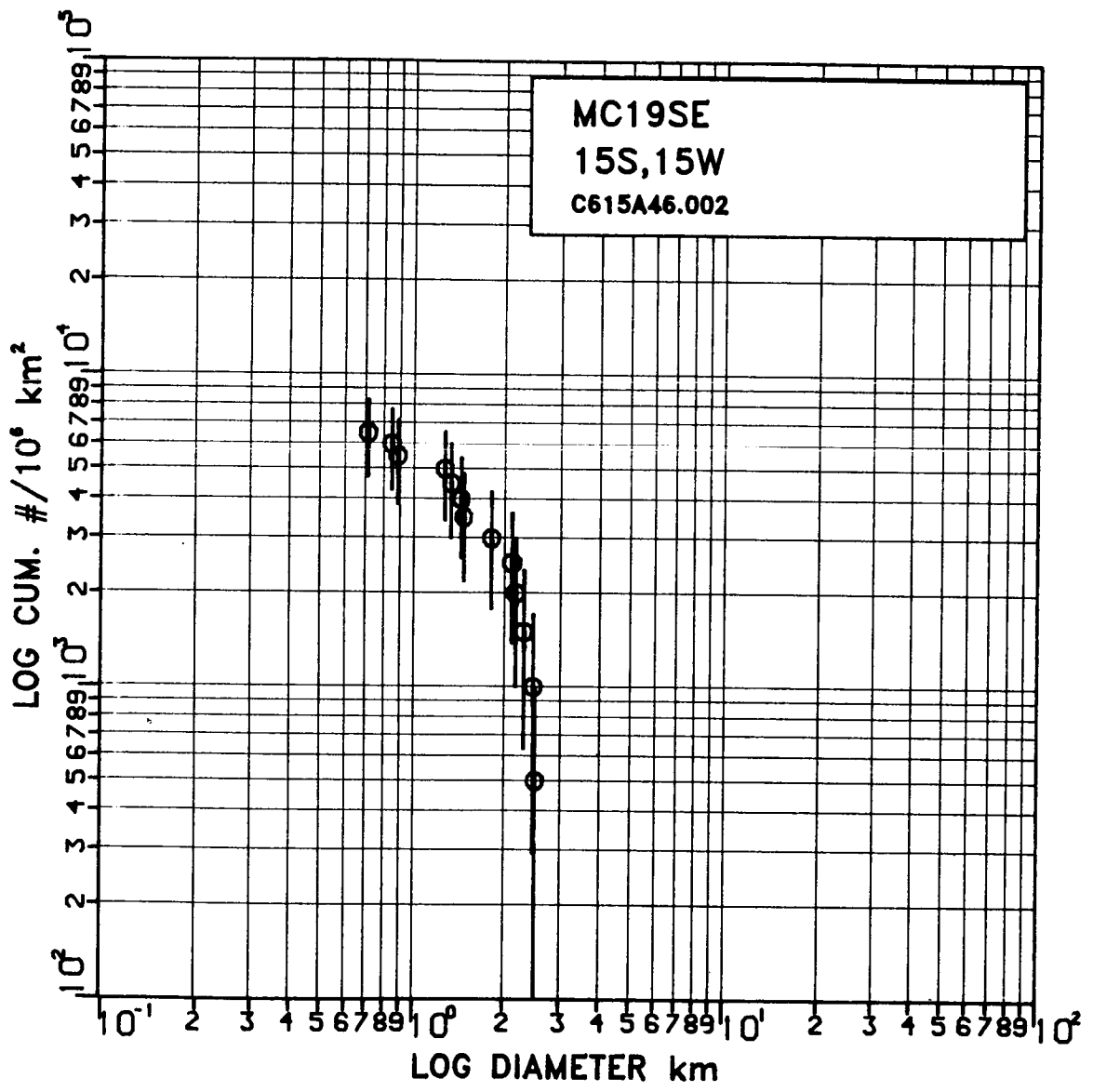


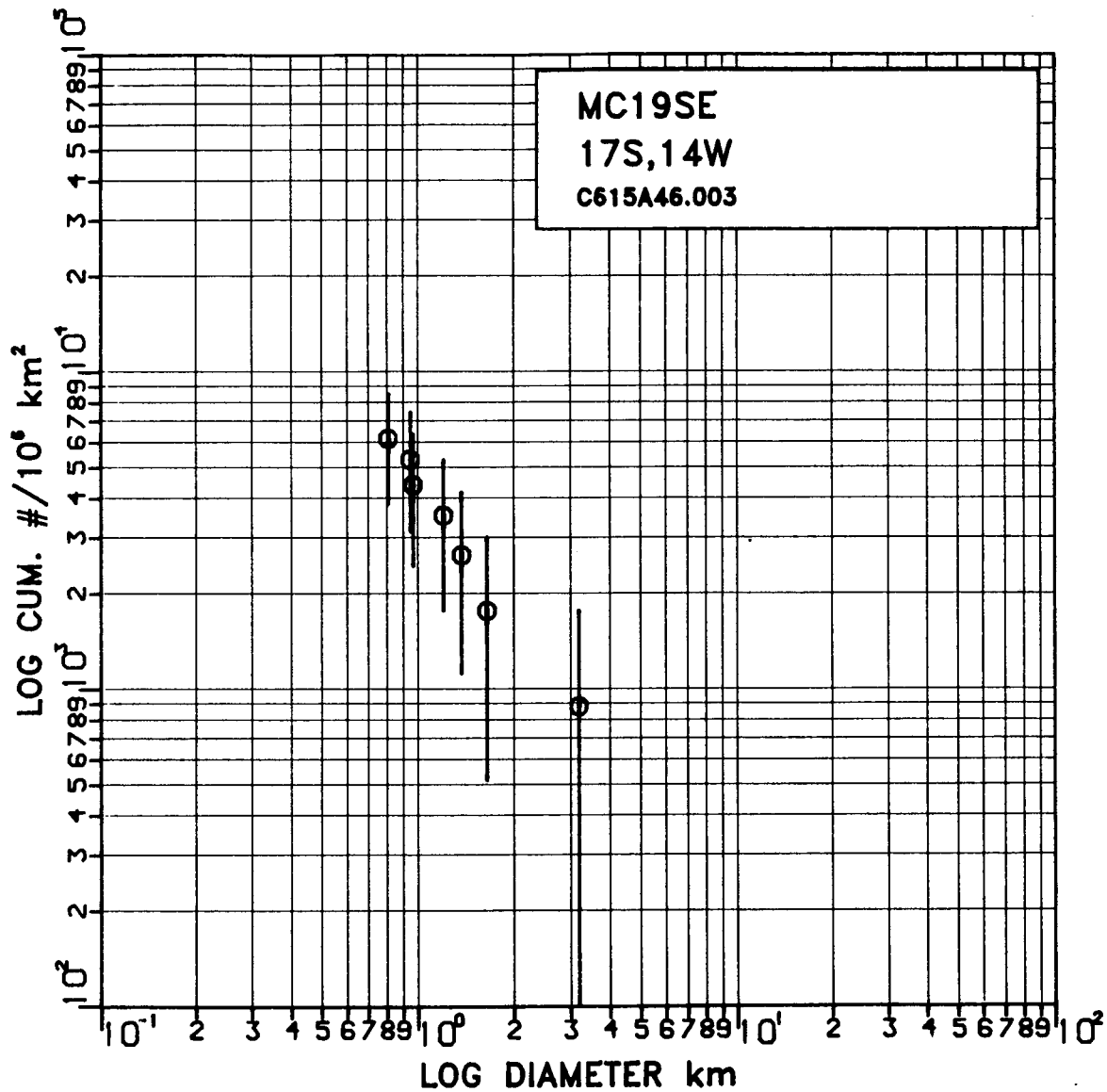


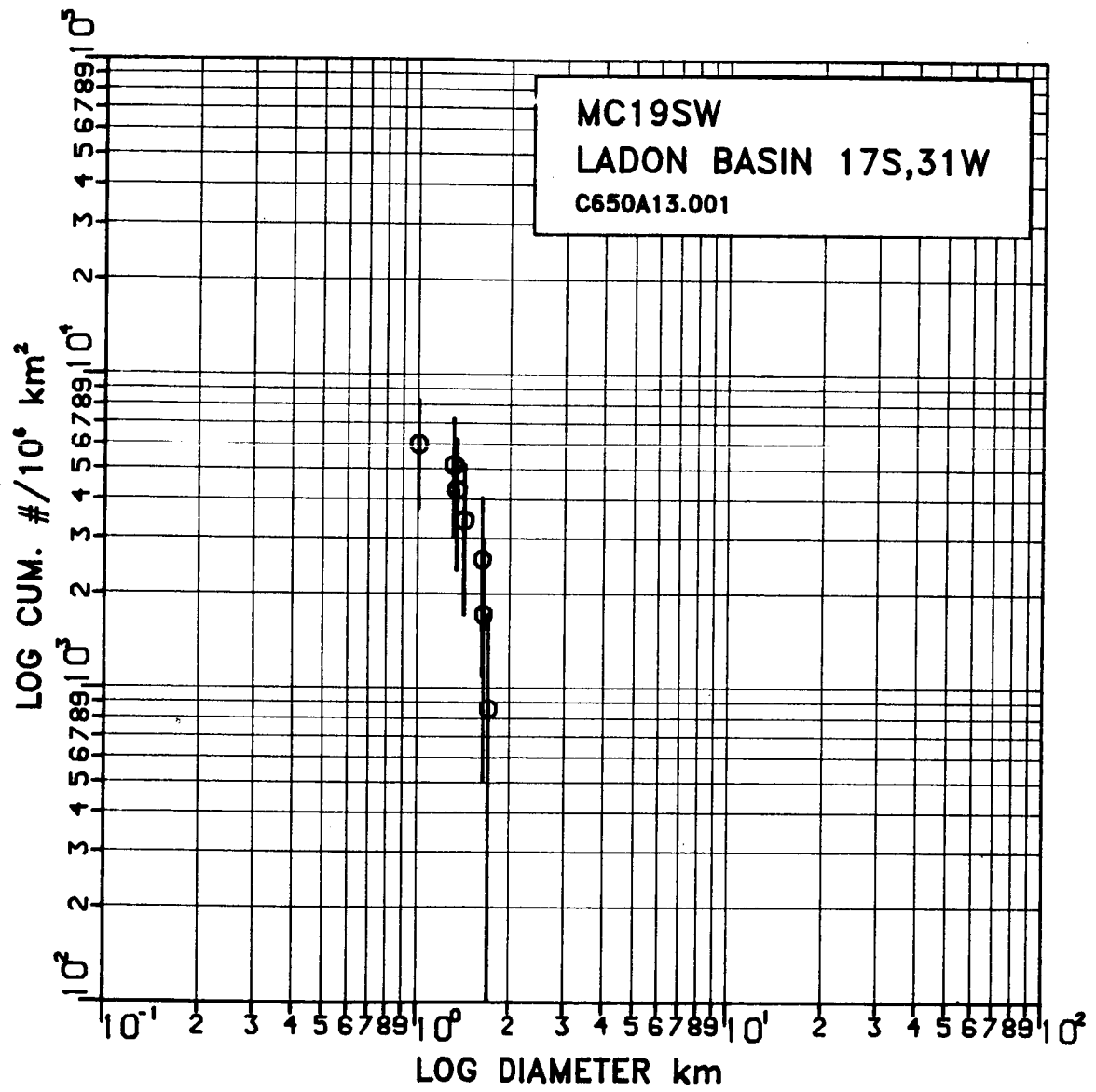


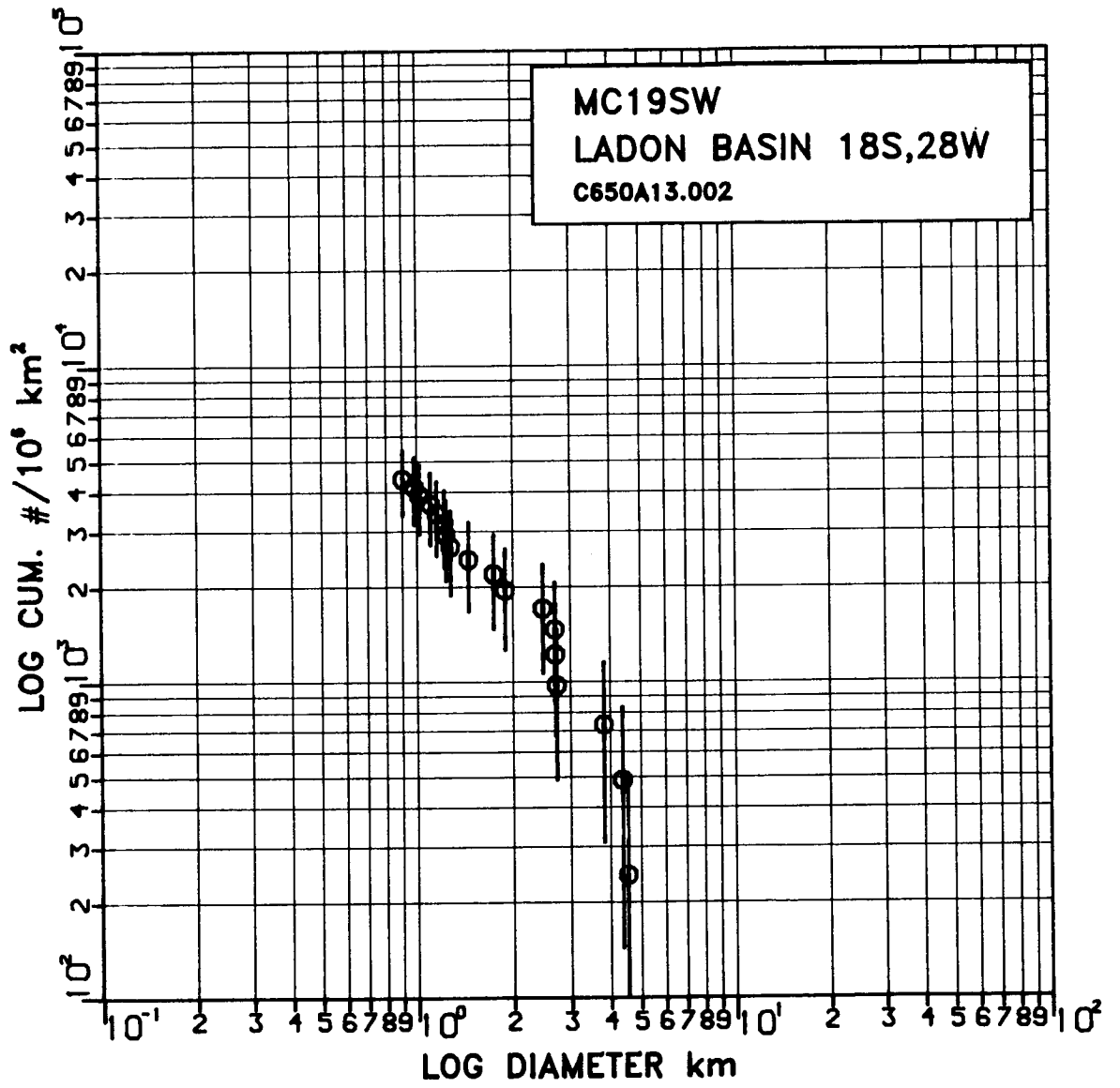


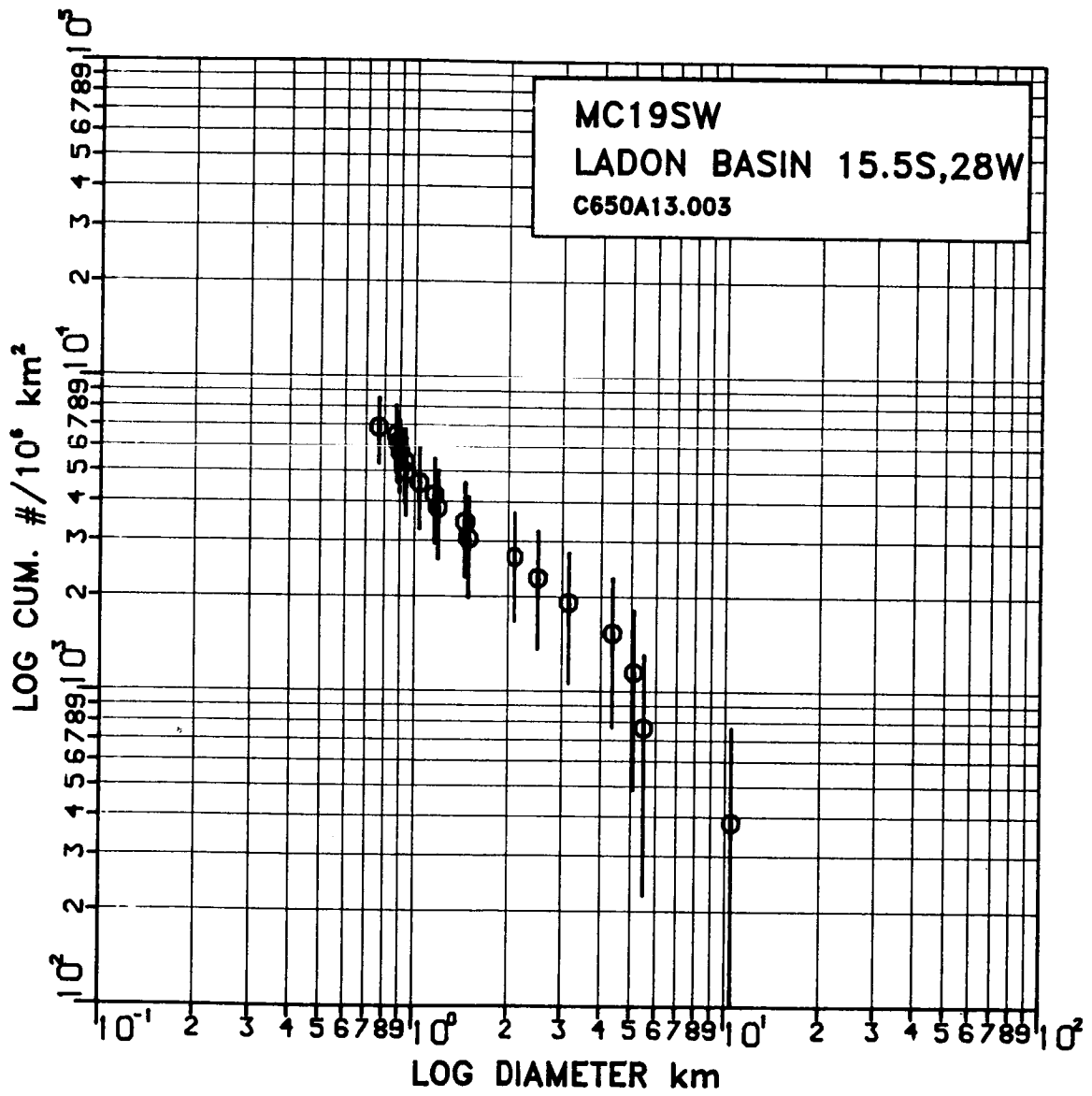




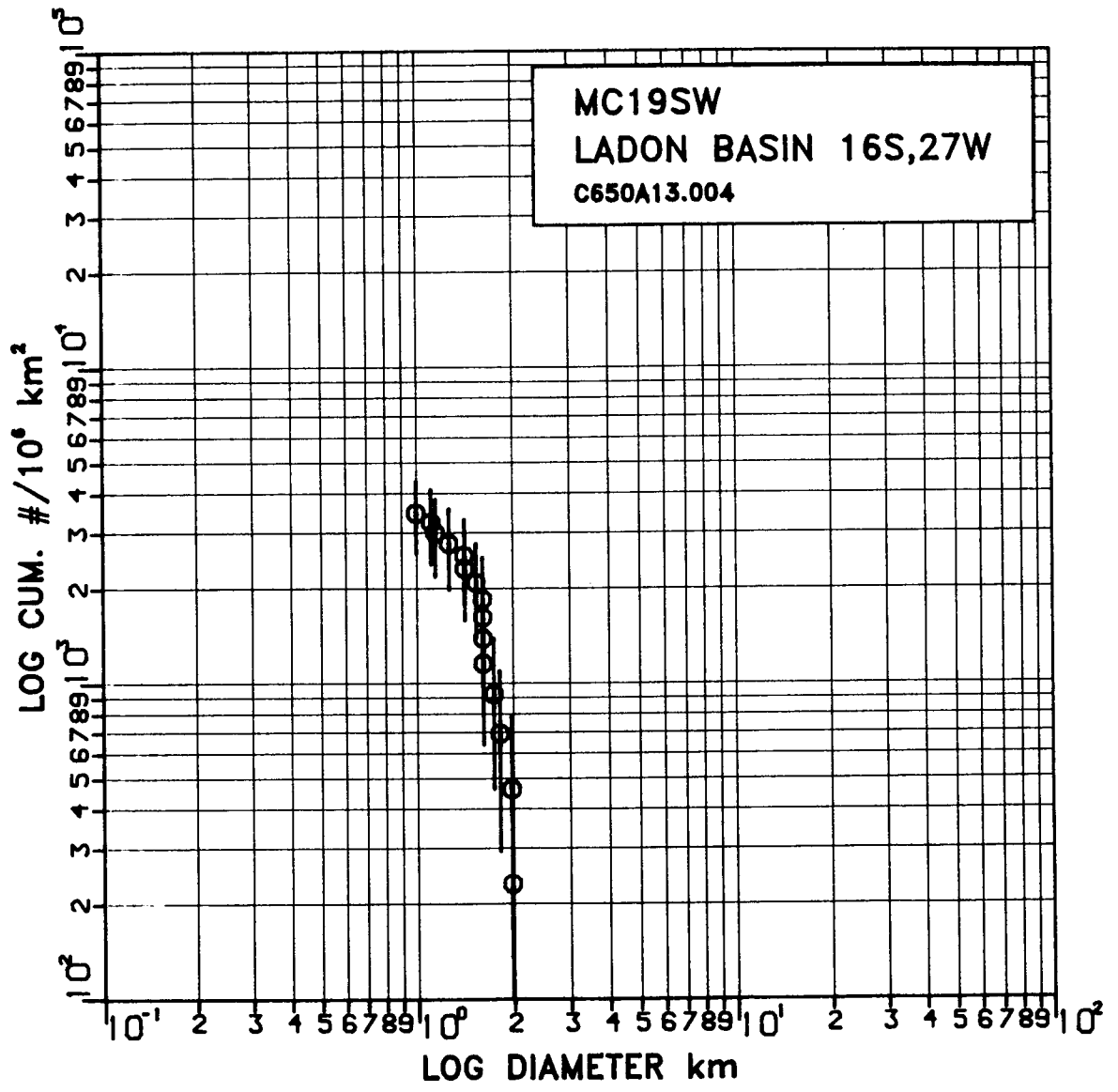


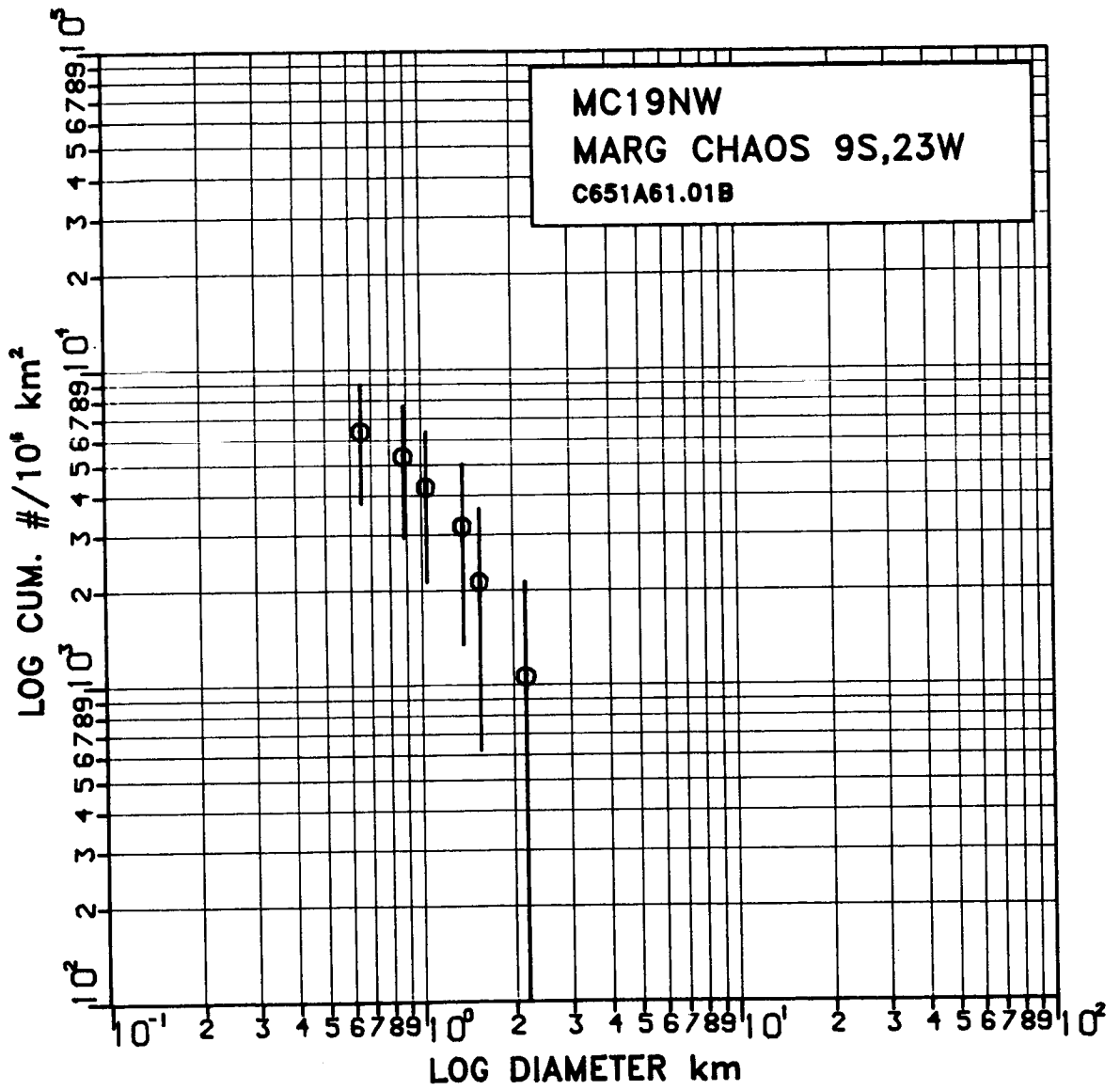


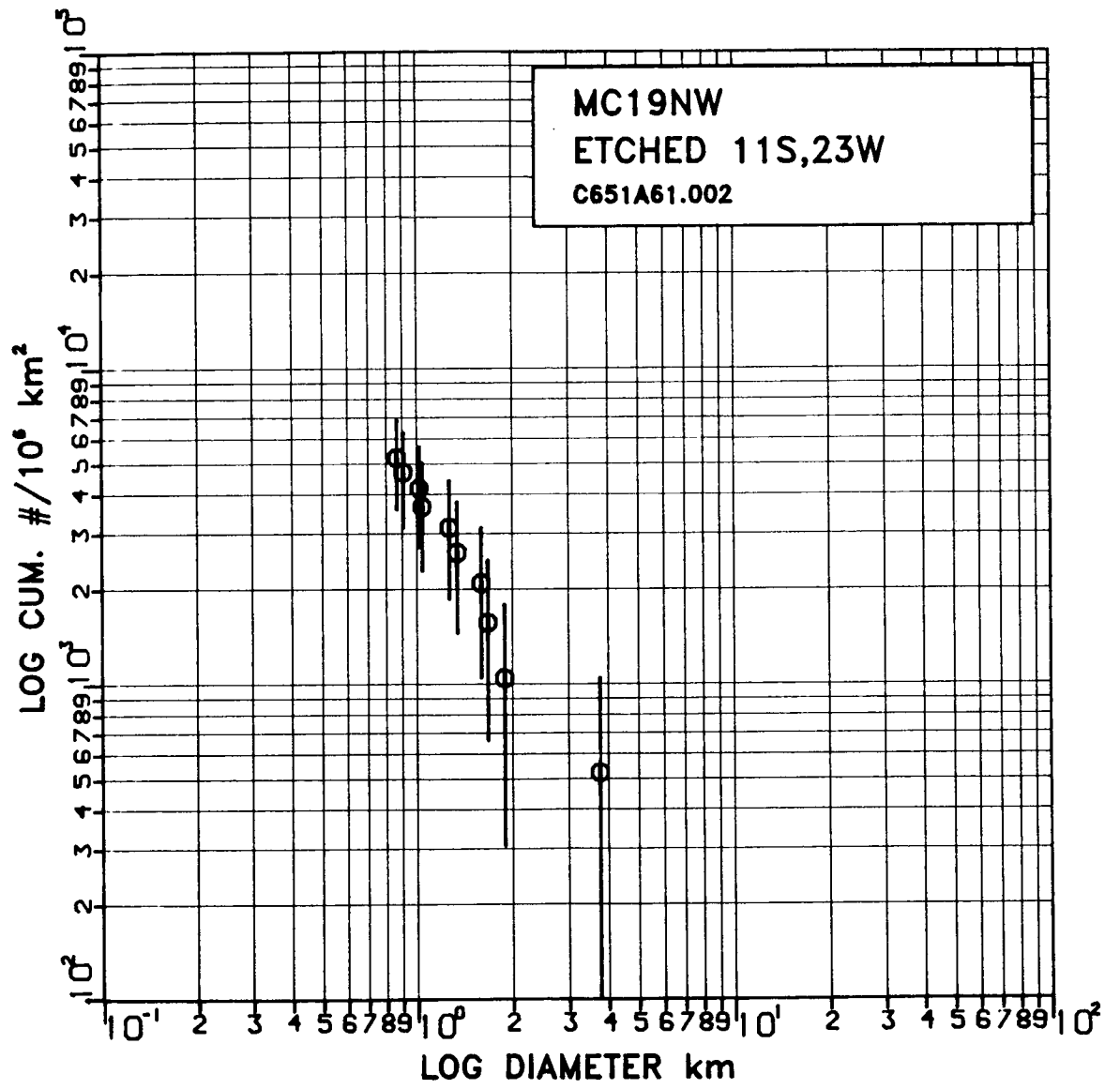


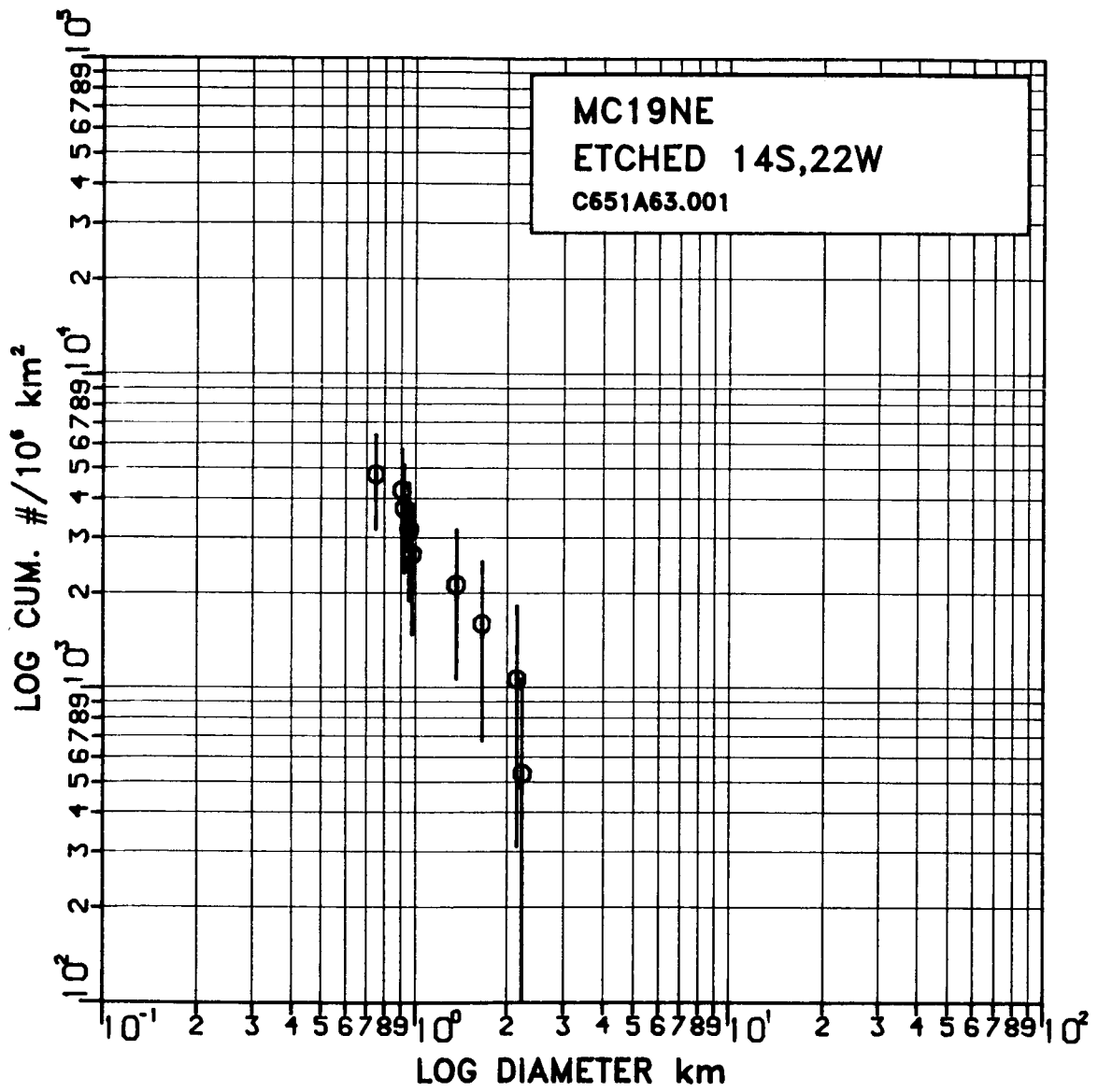


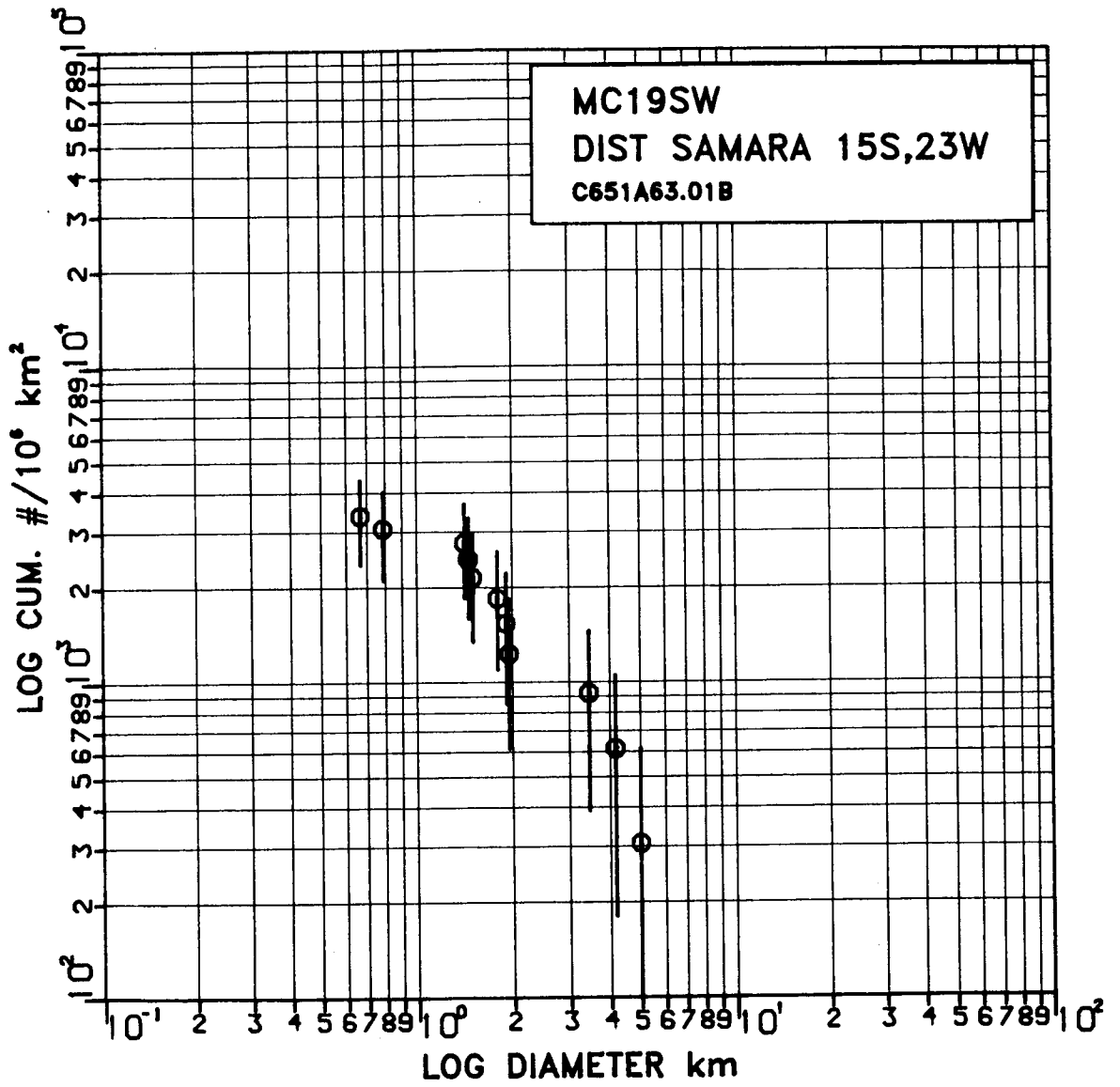
C-3

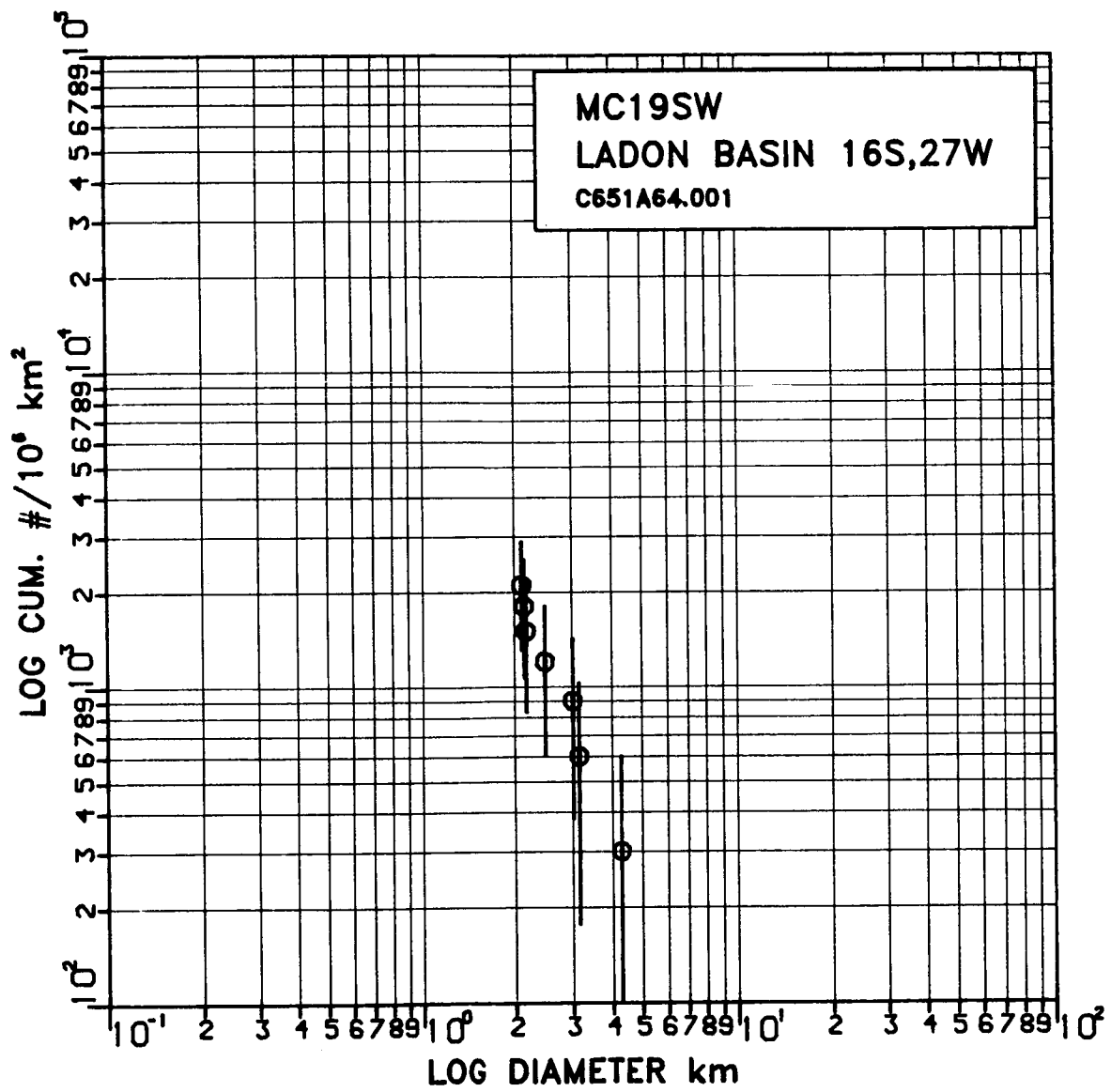


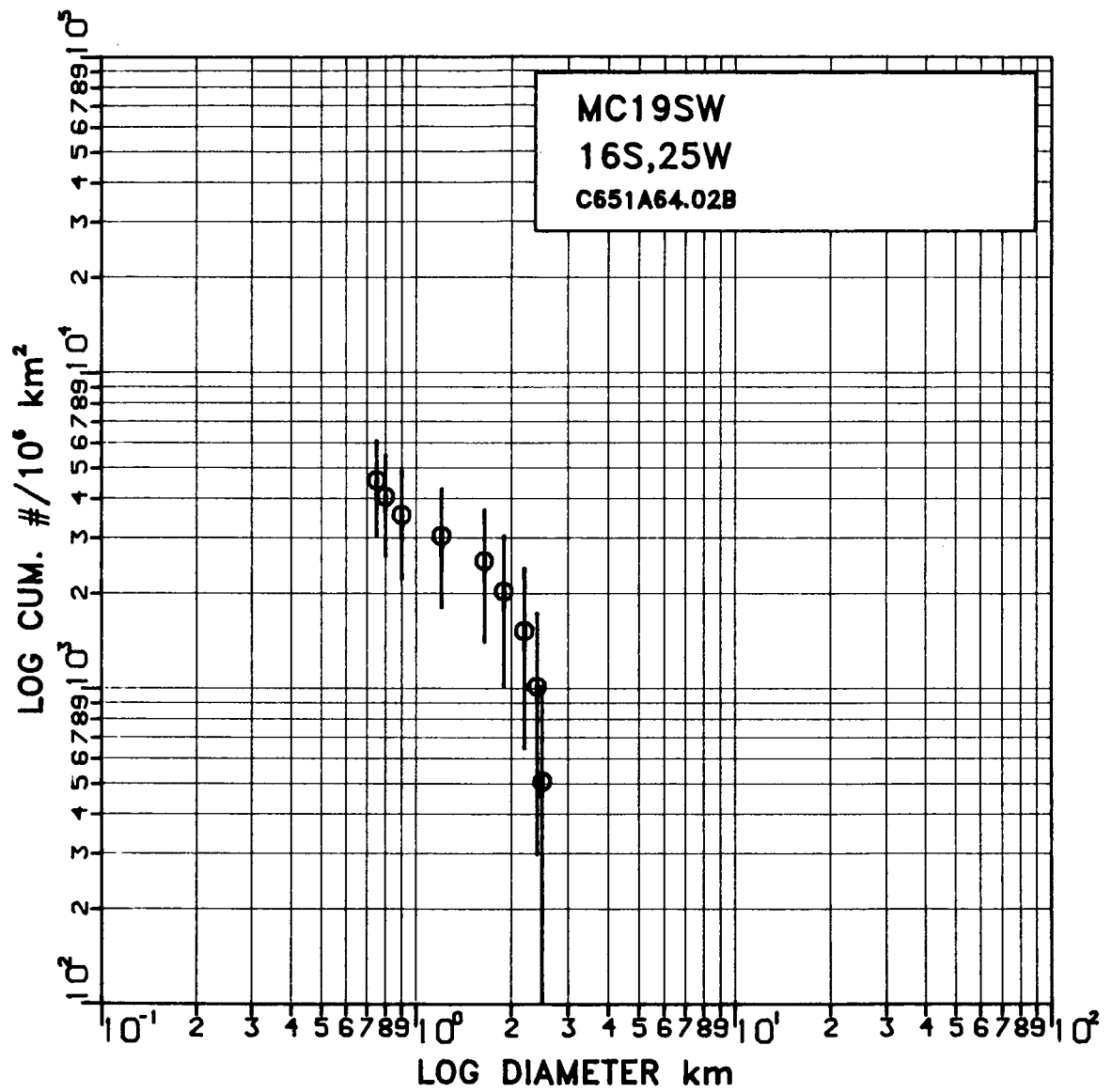


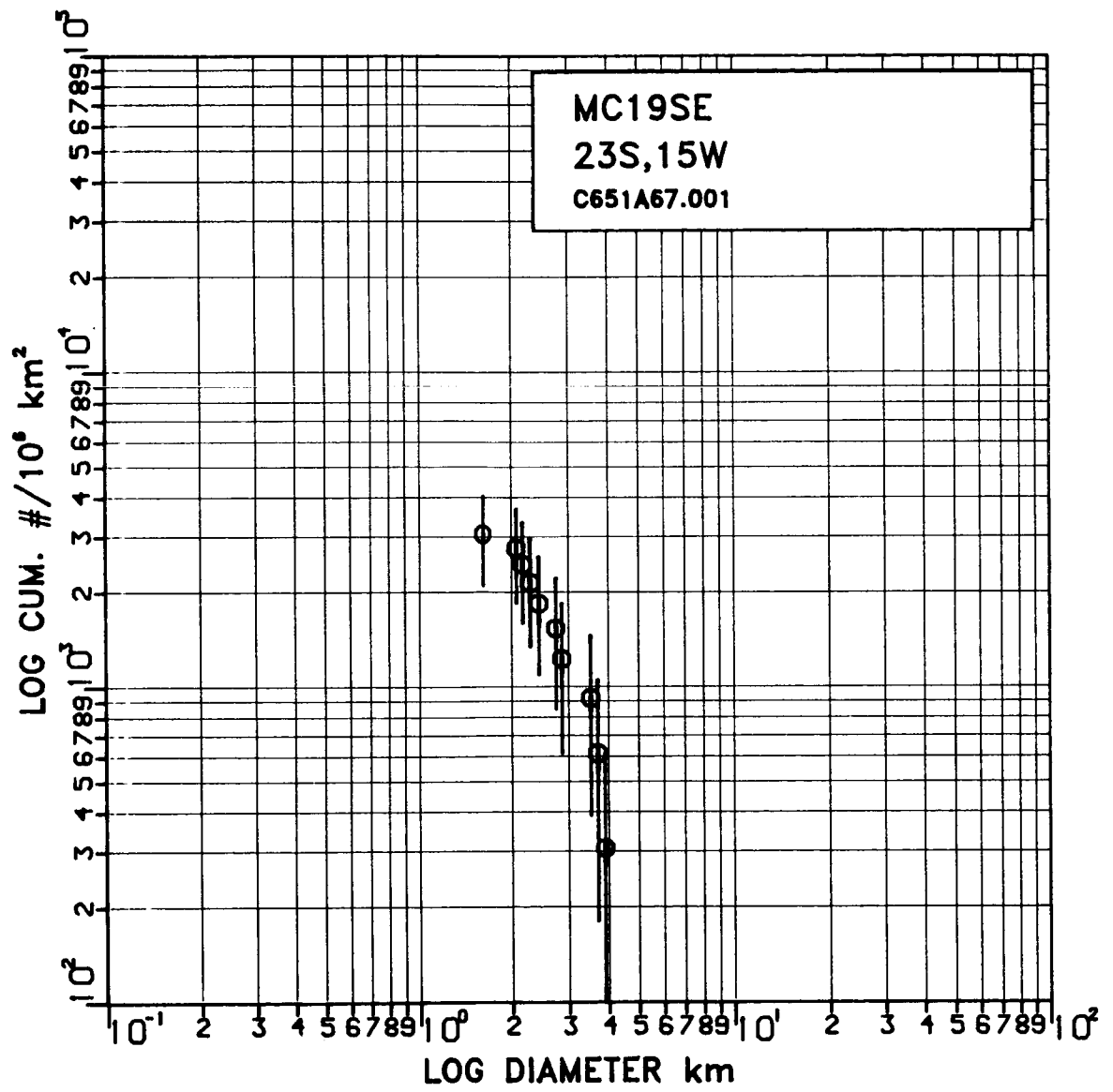


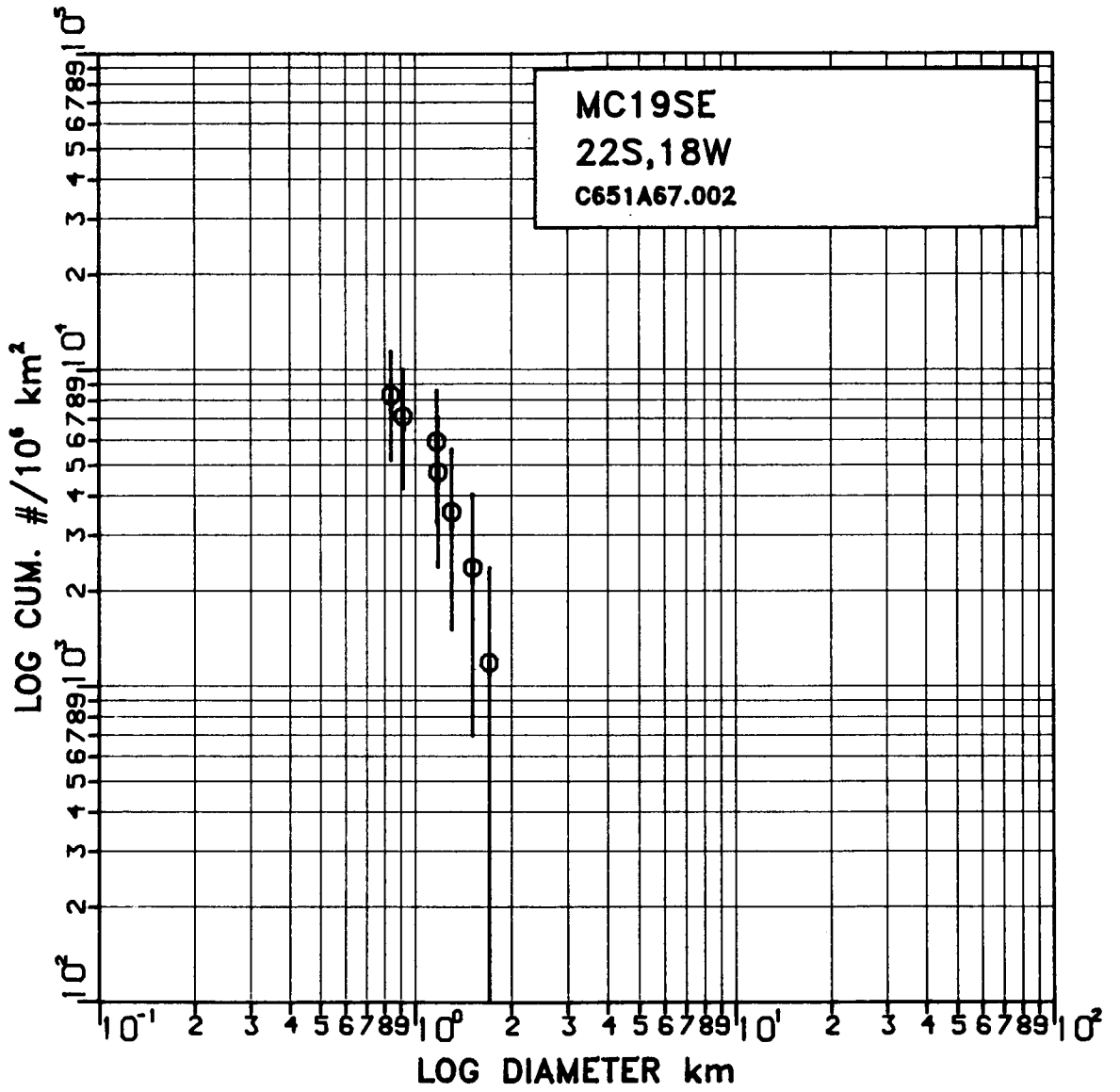


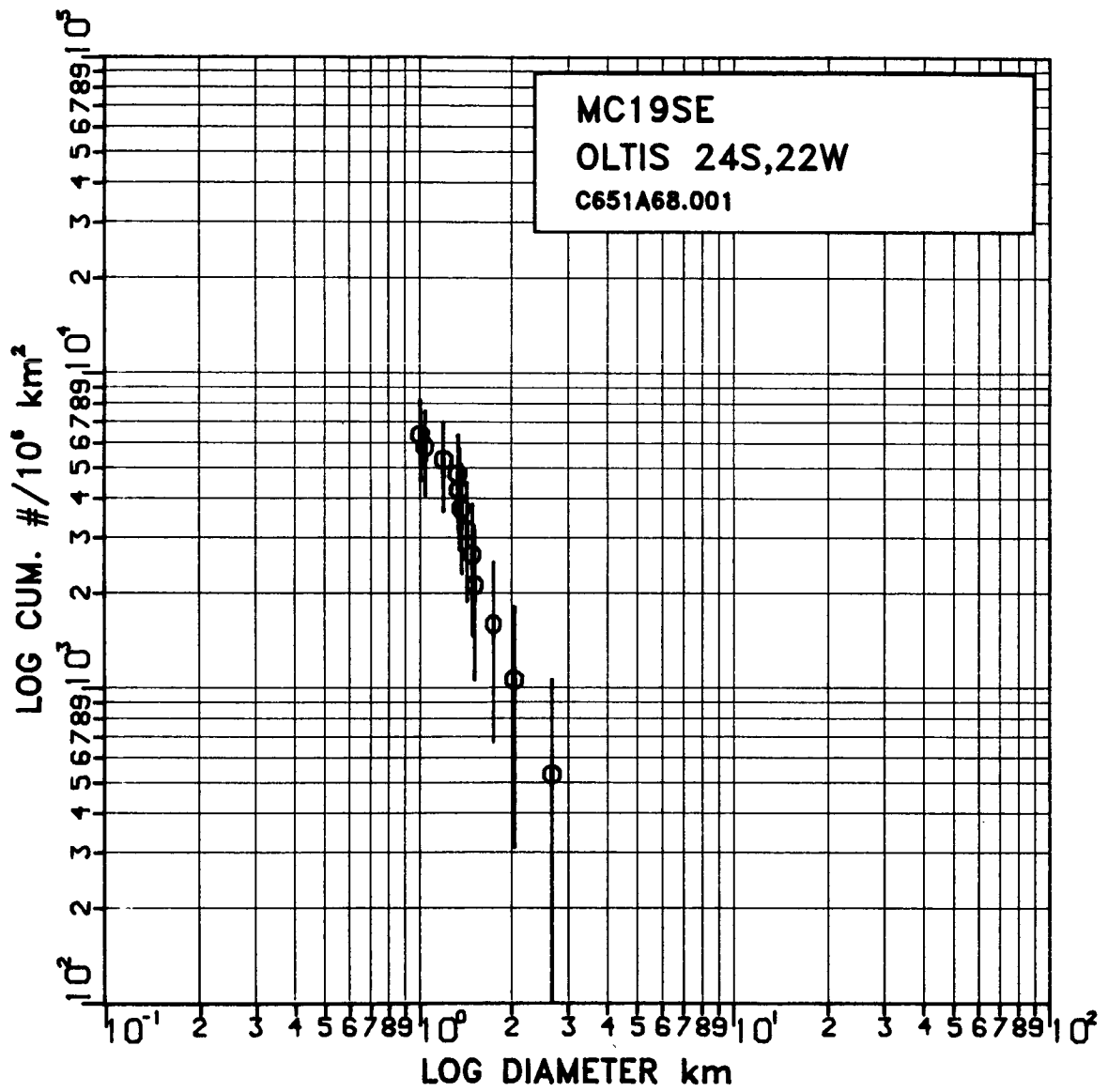


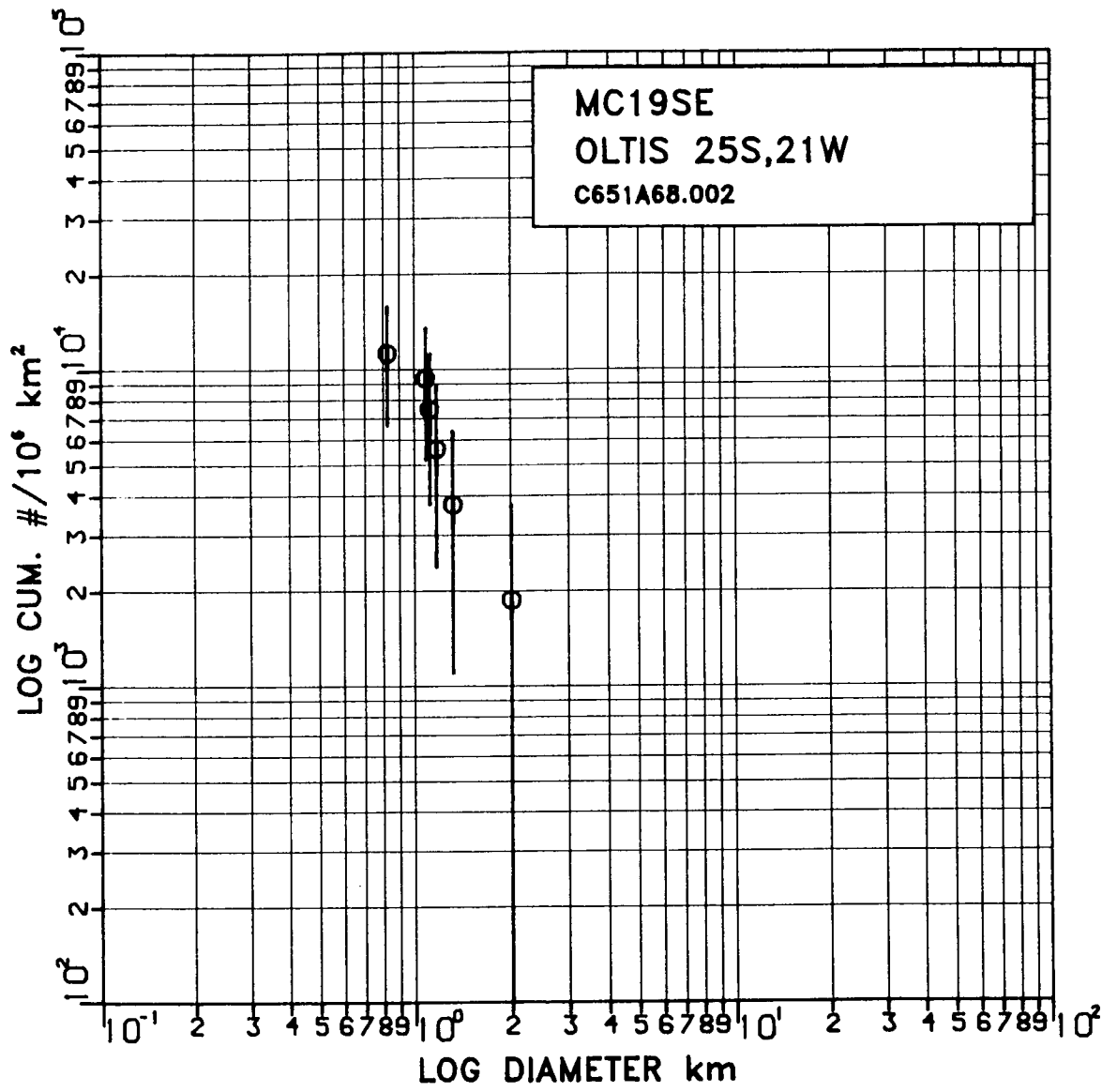


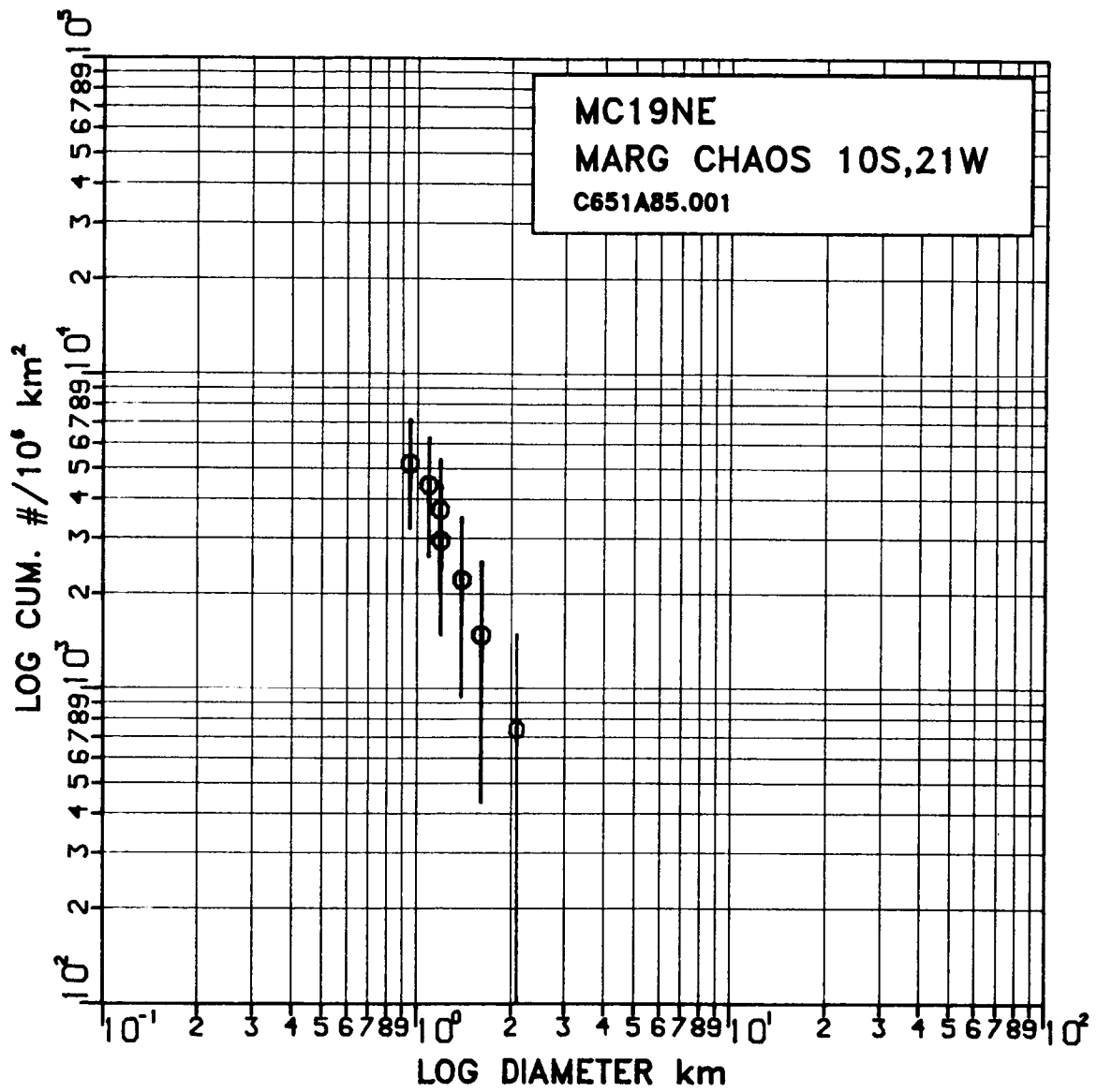


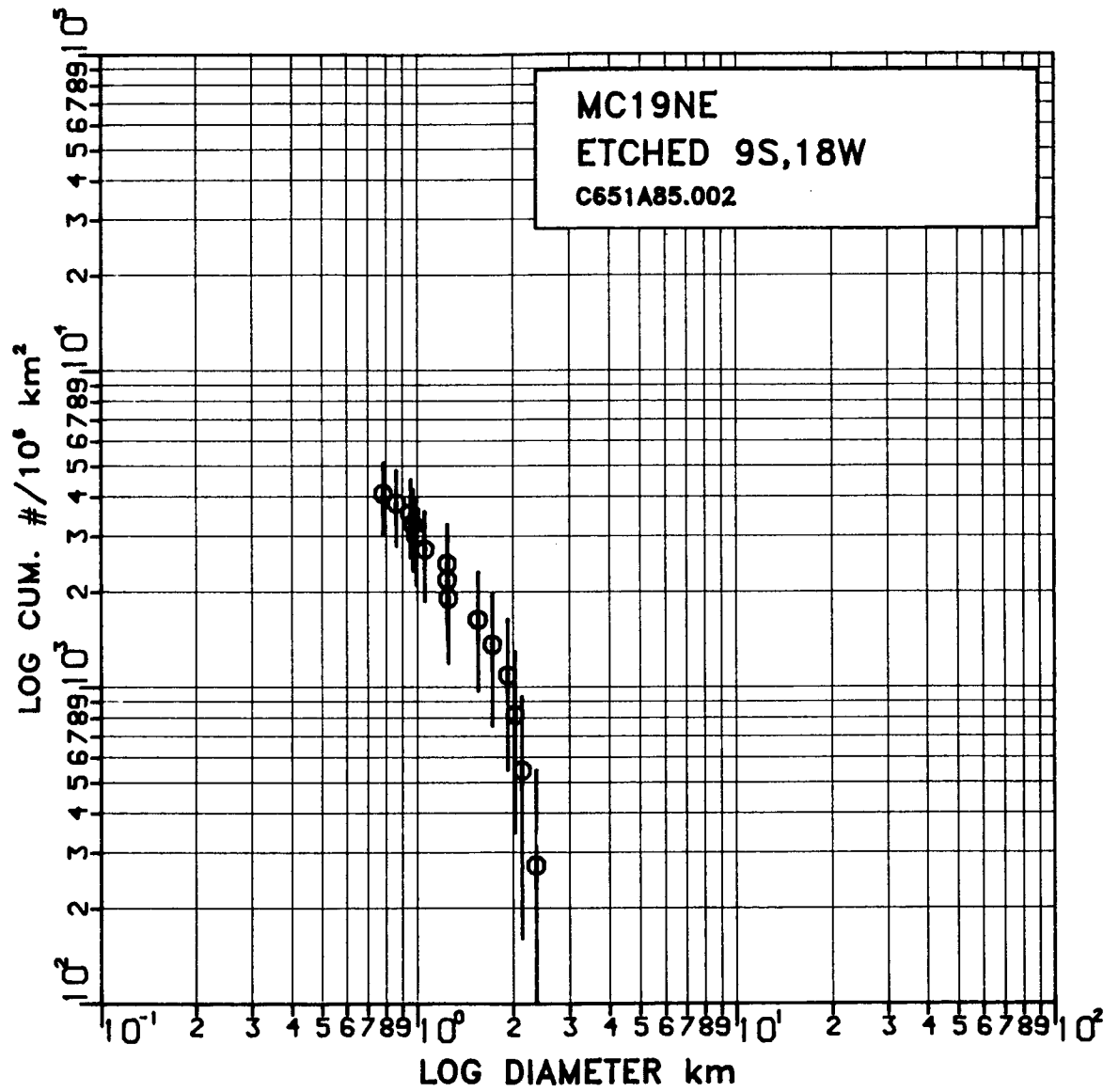


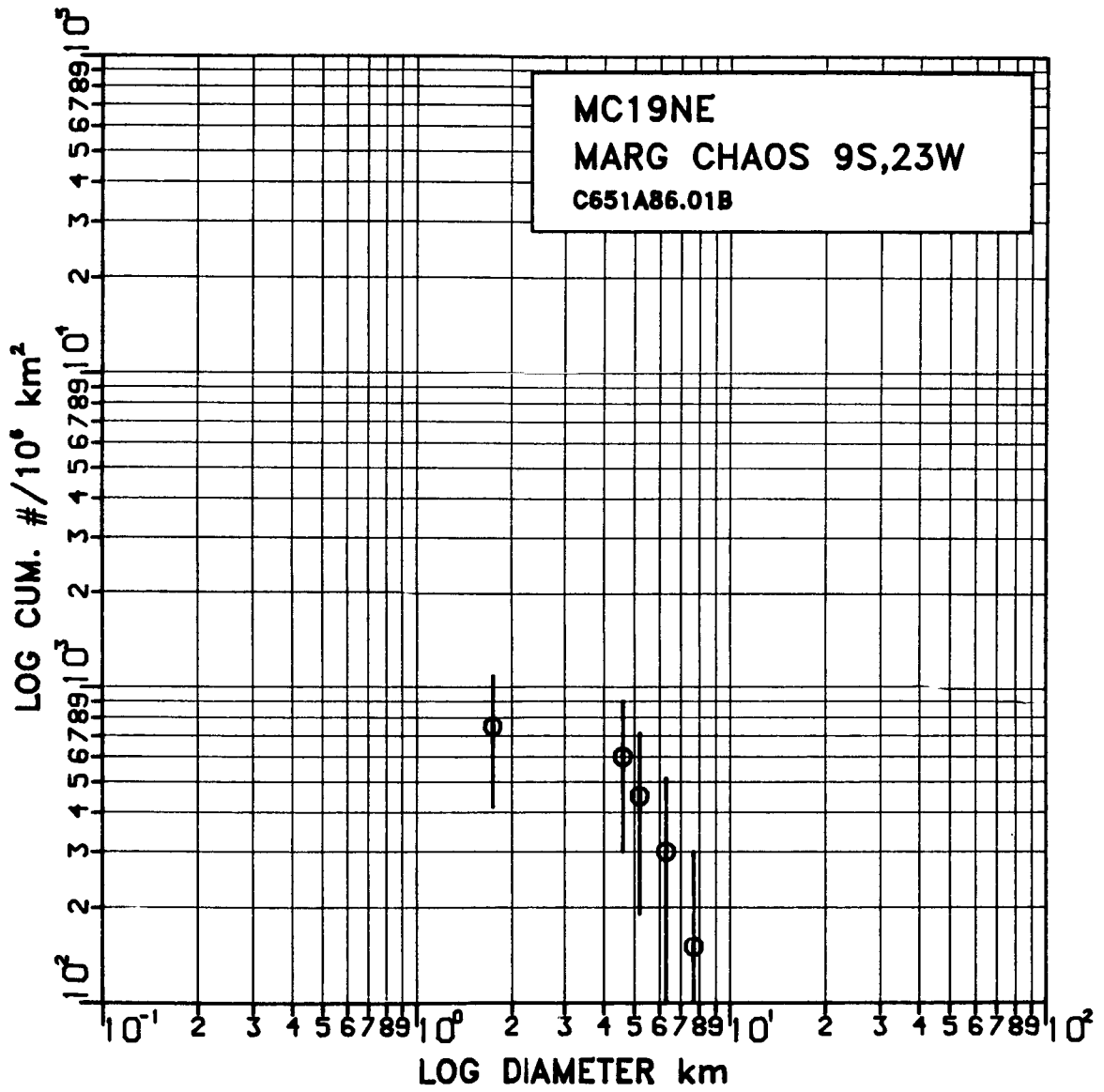


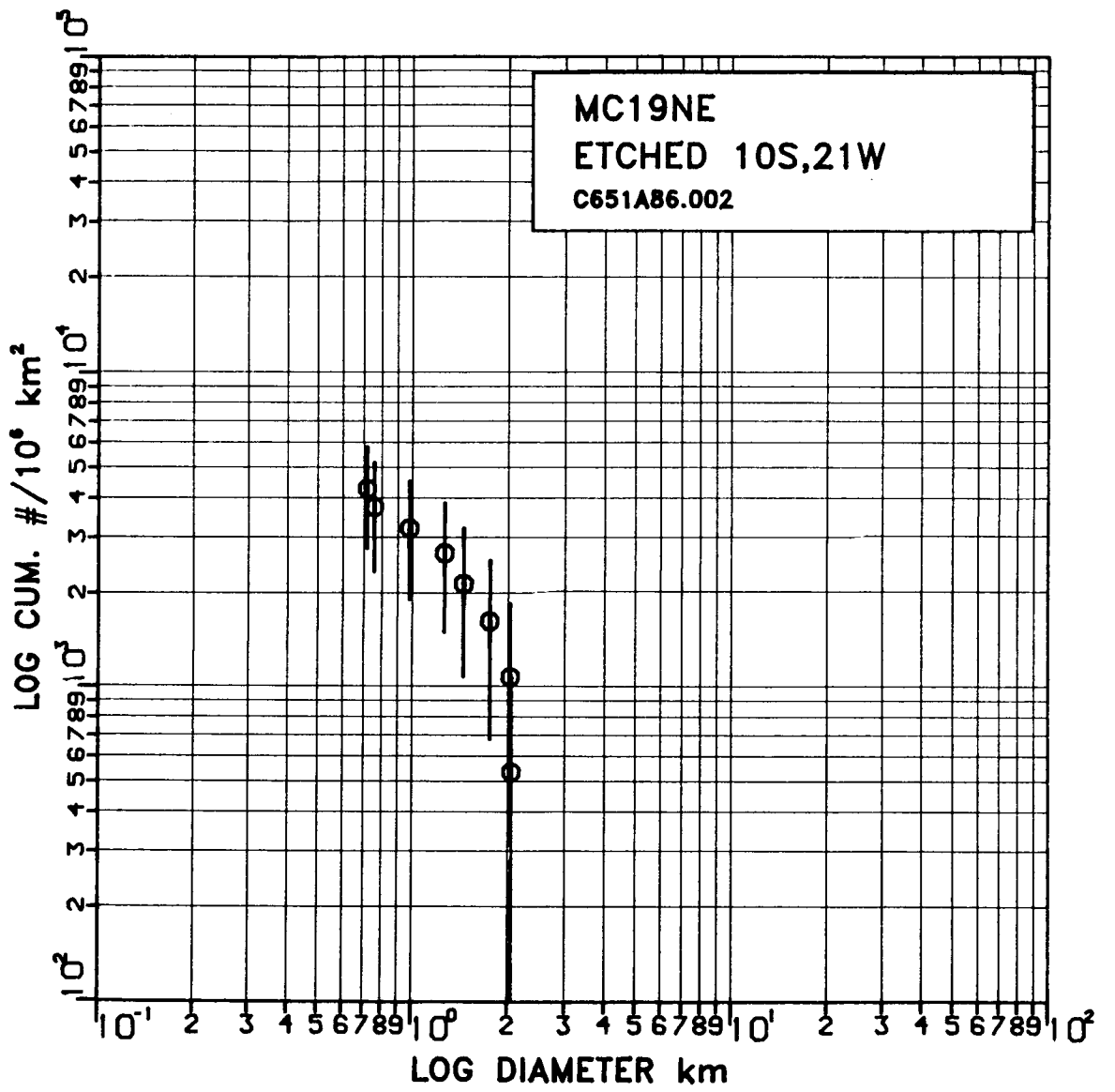


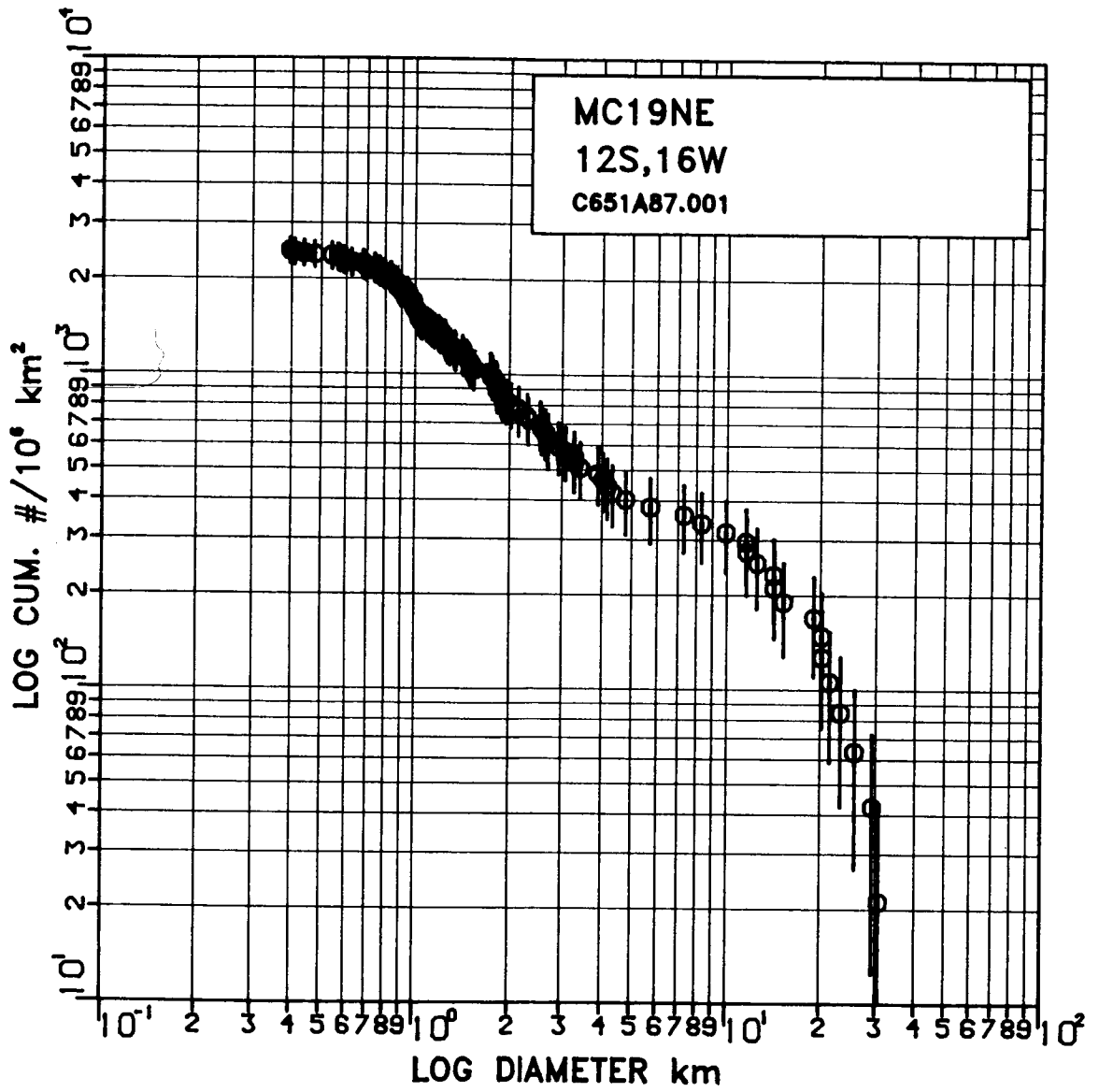


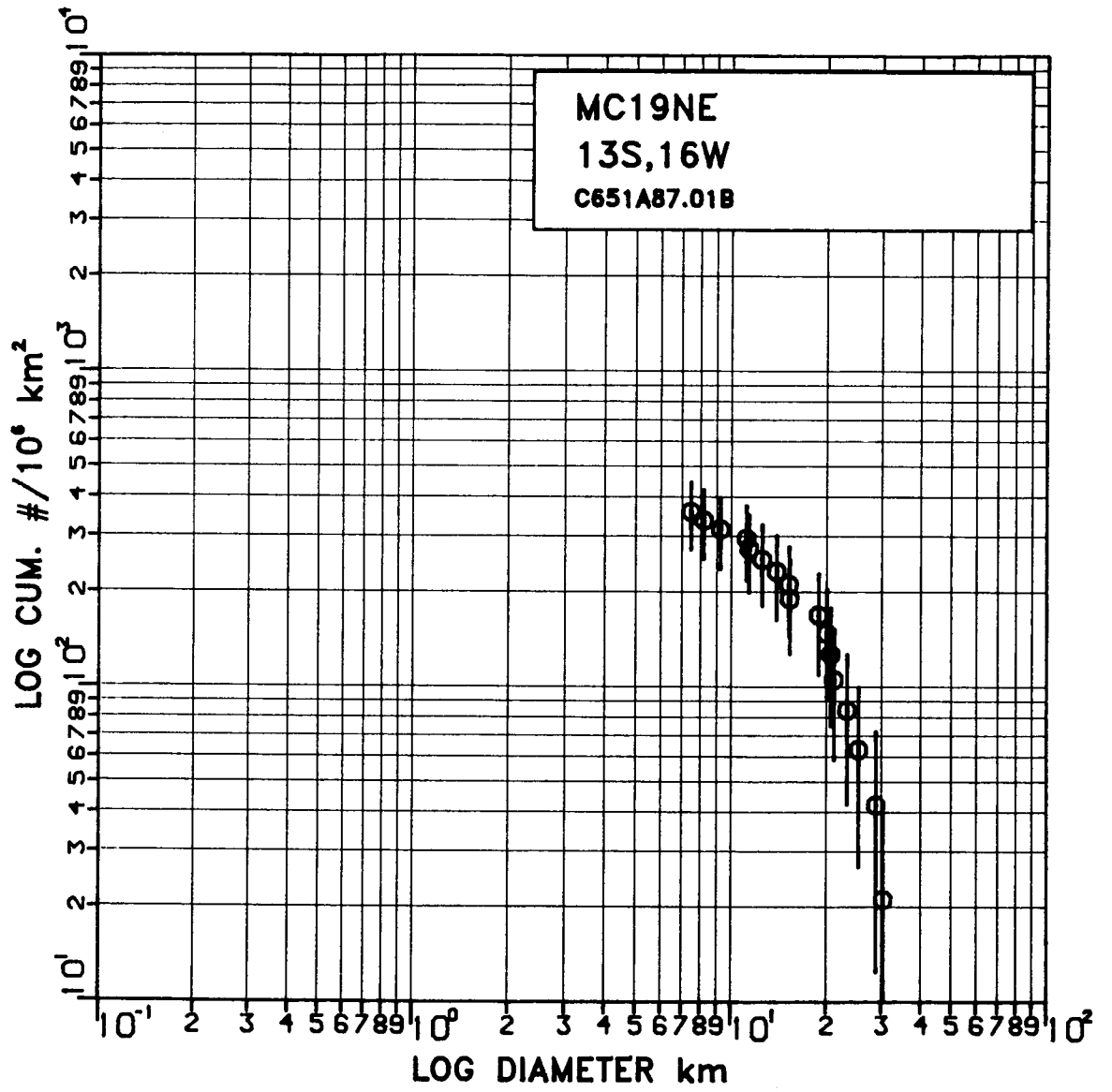


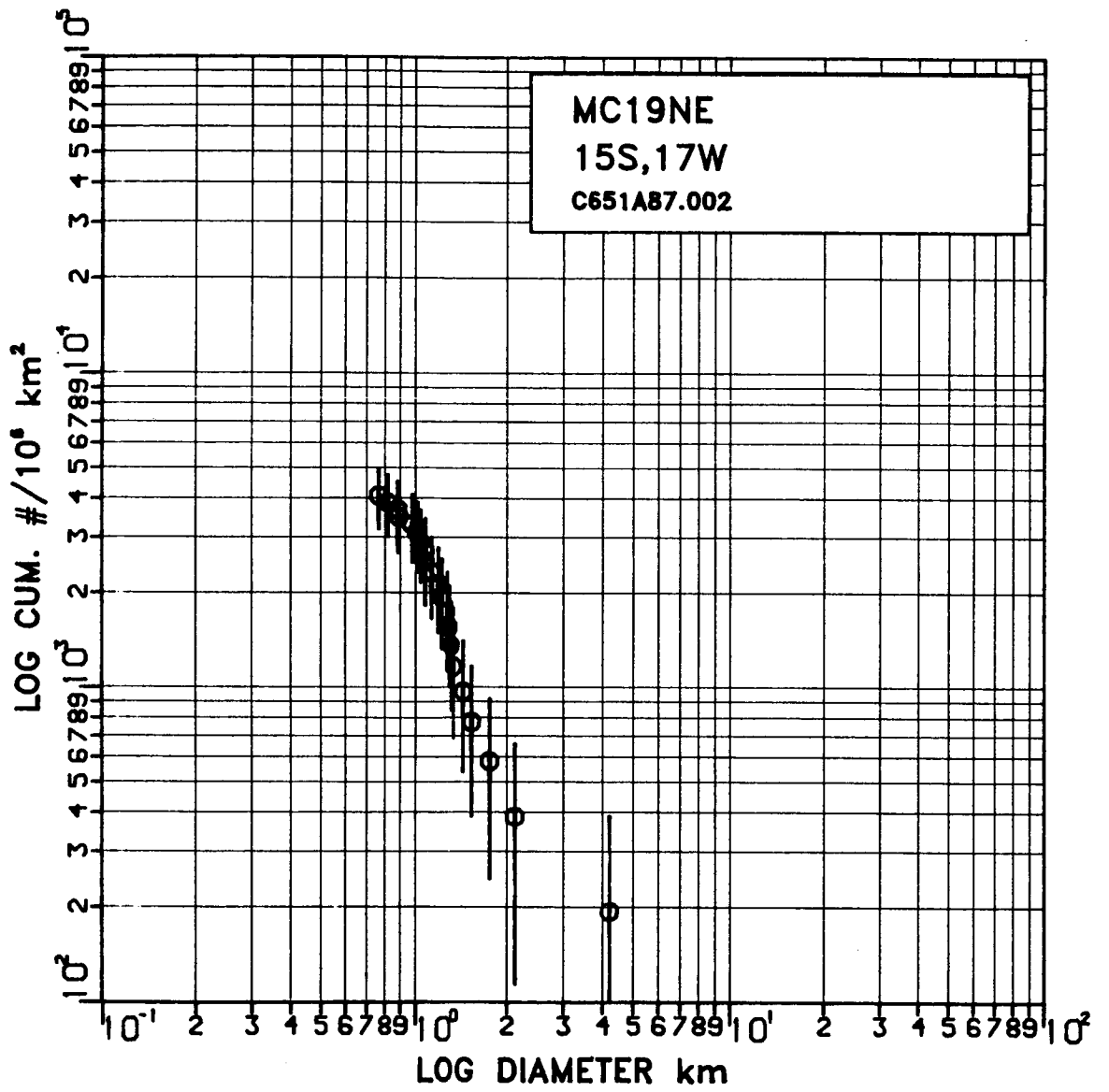


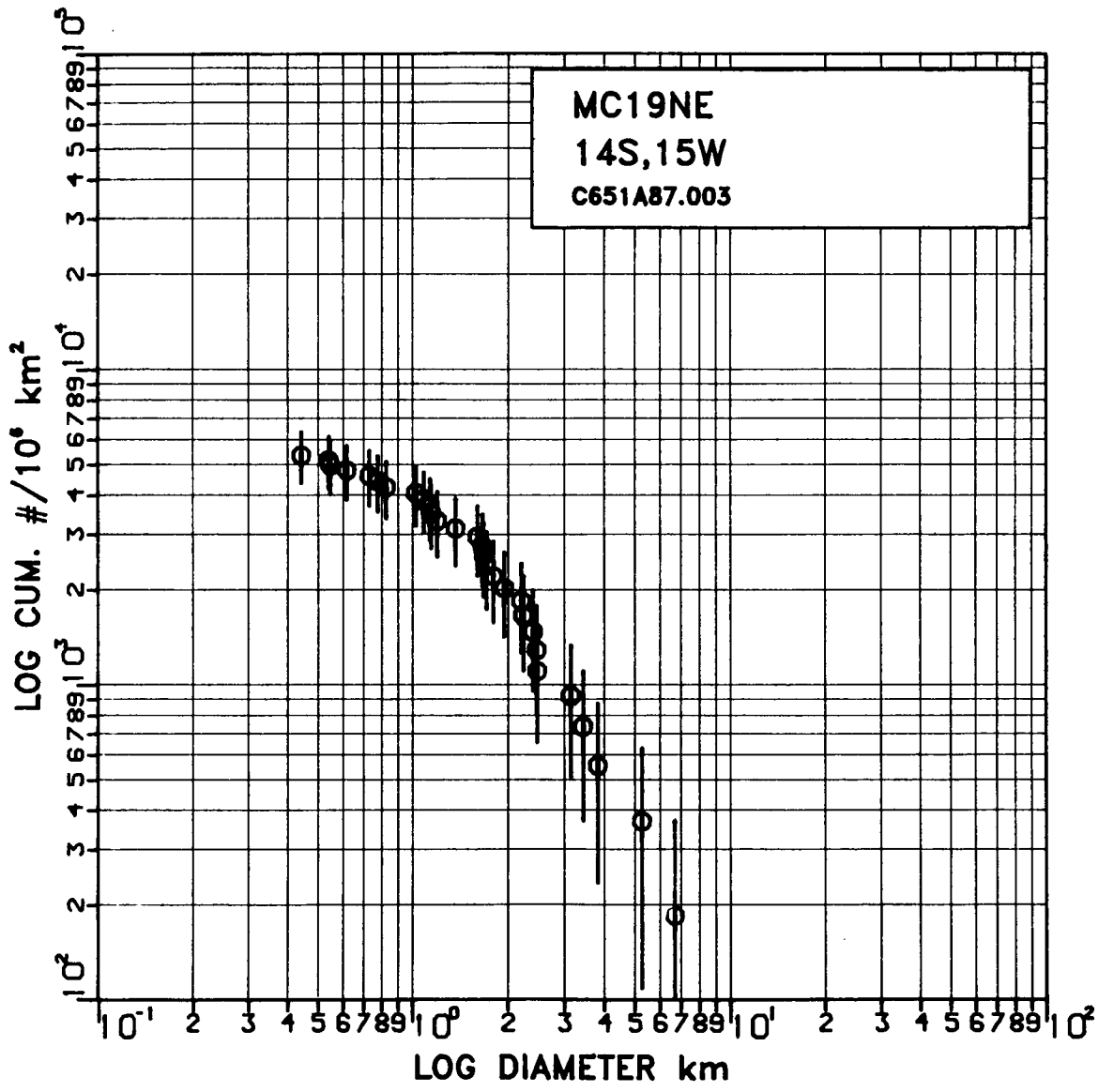


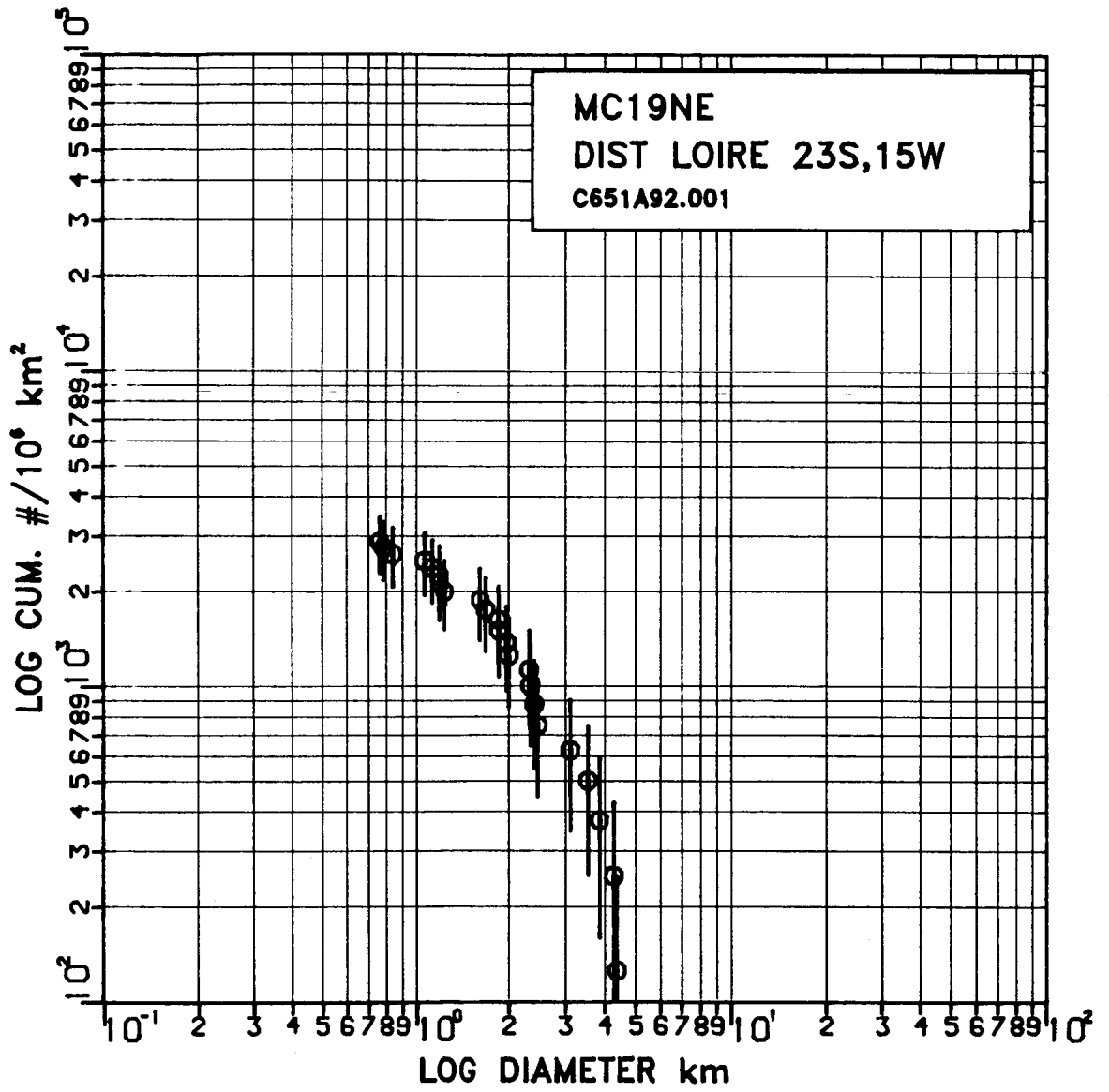


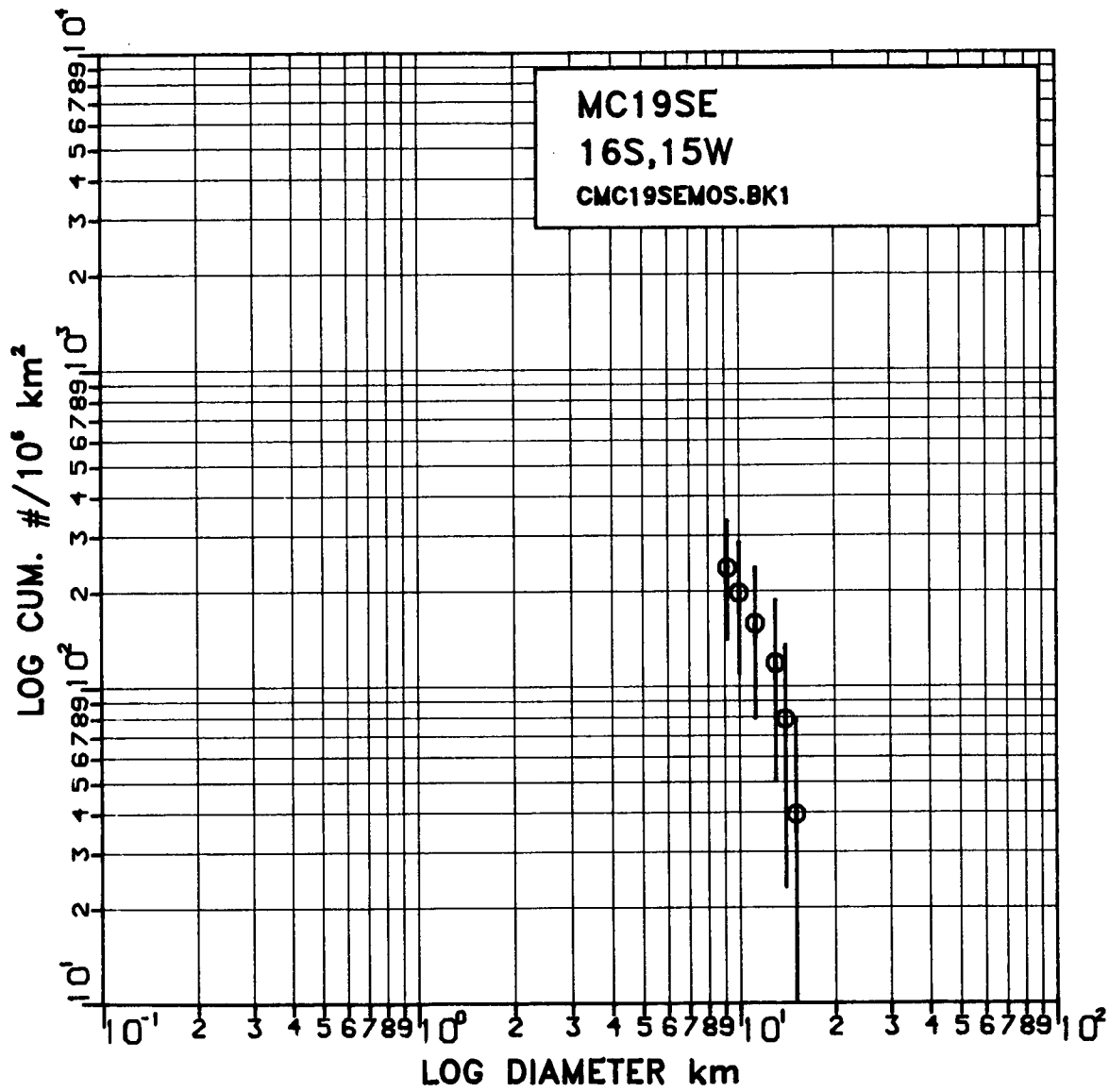


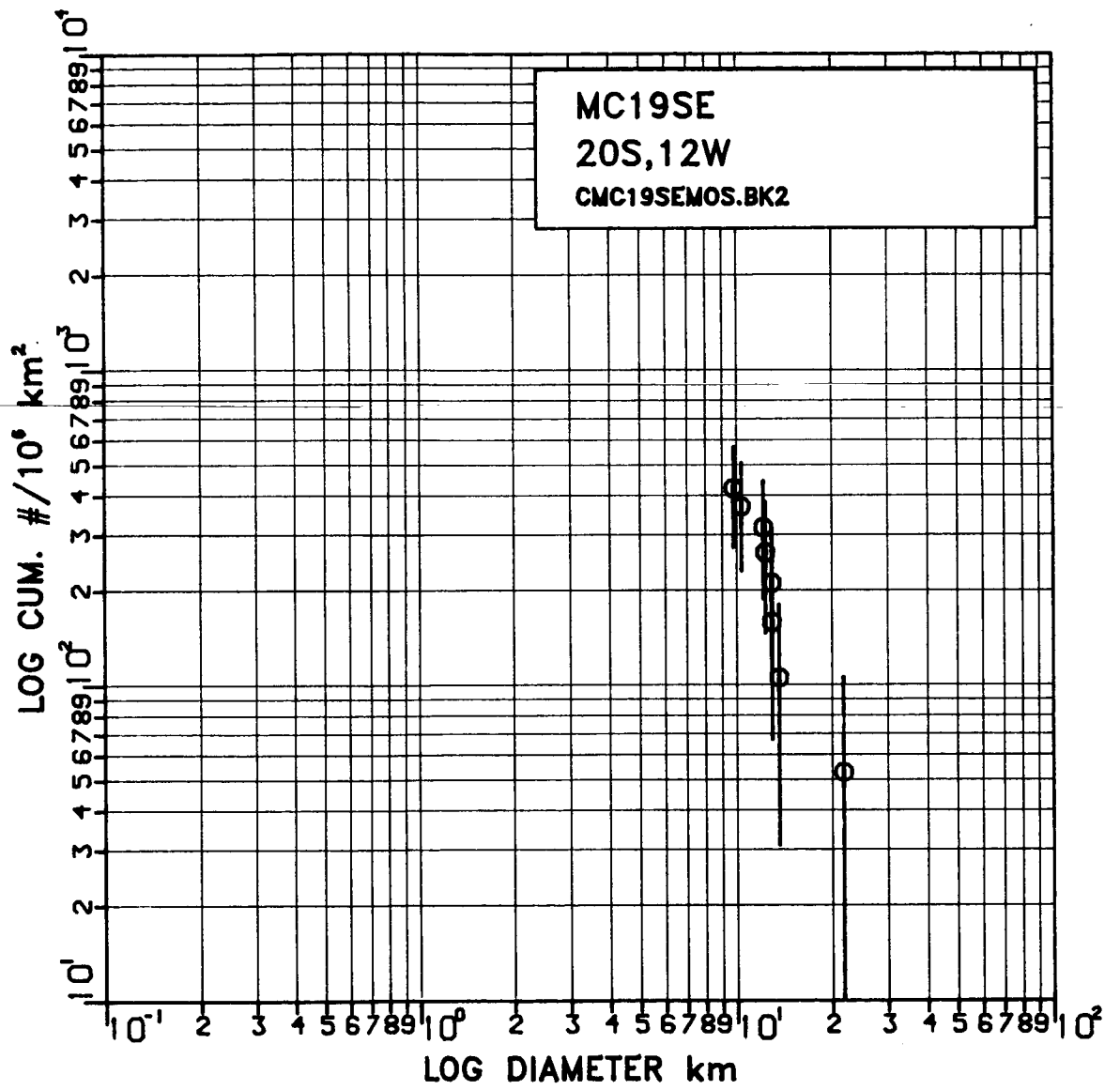


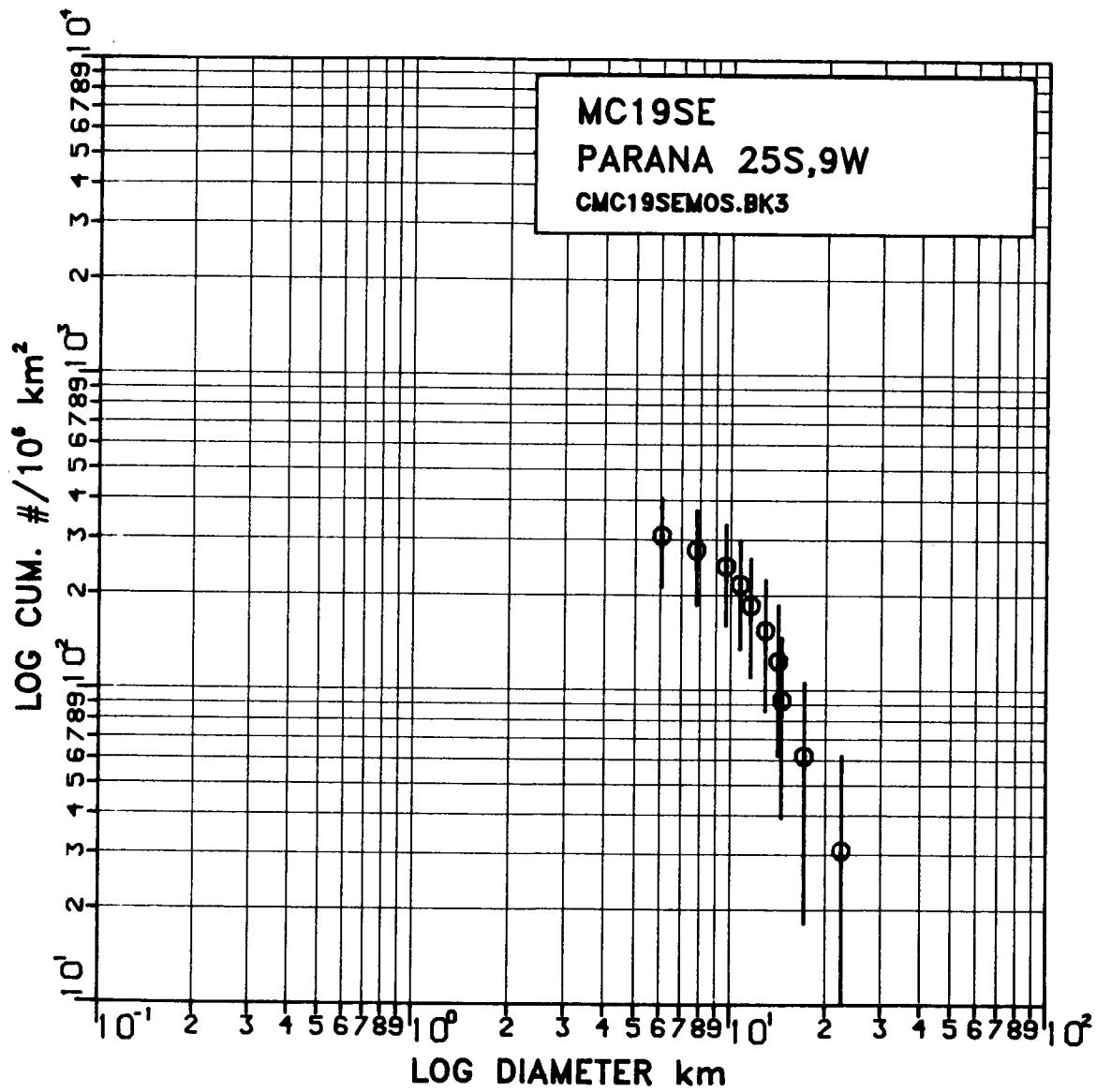


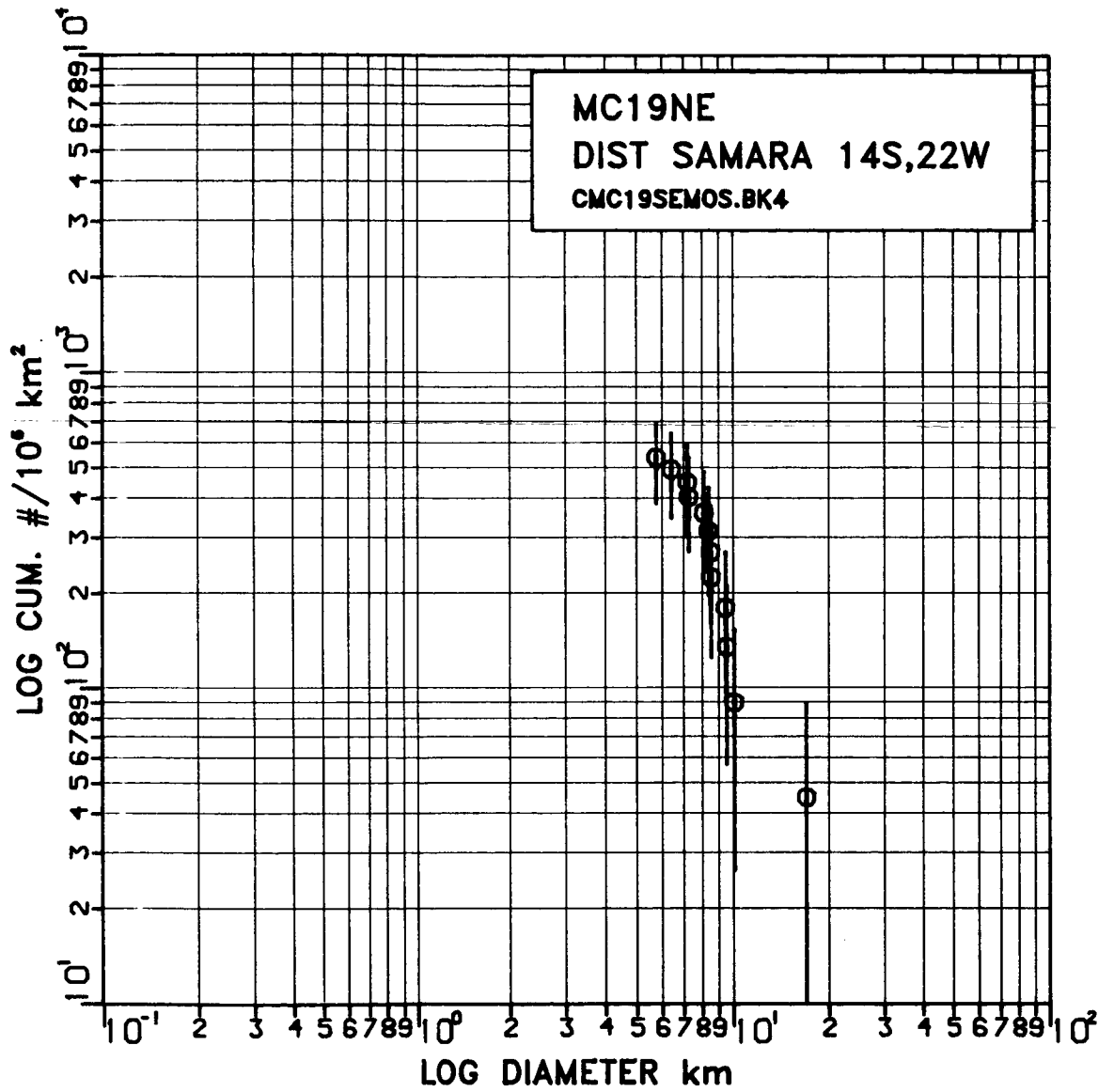


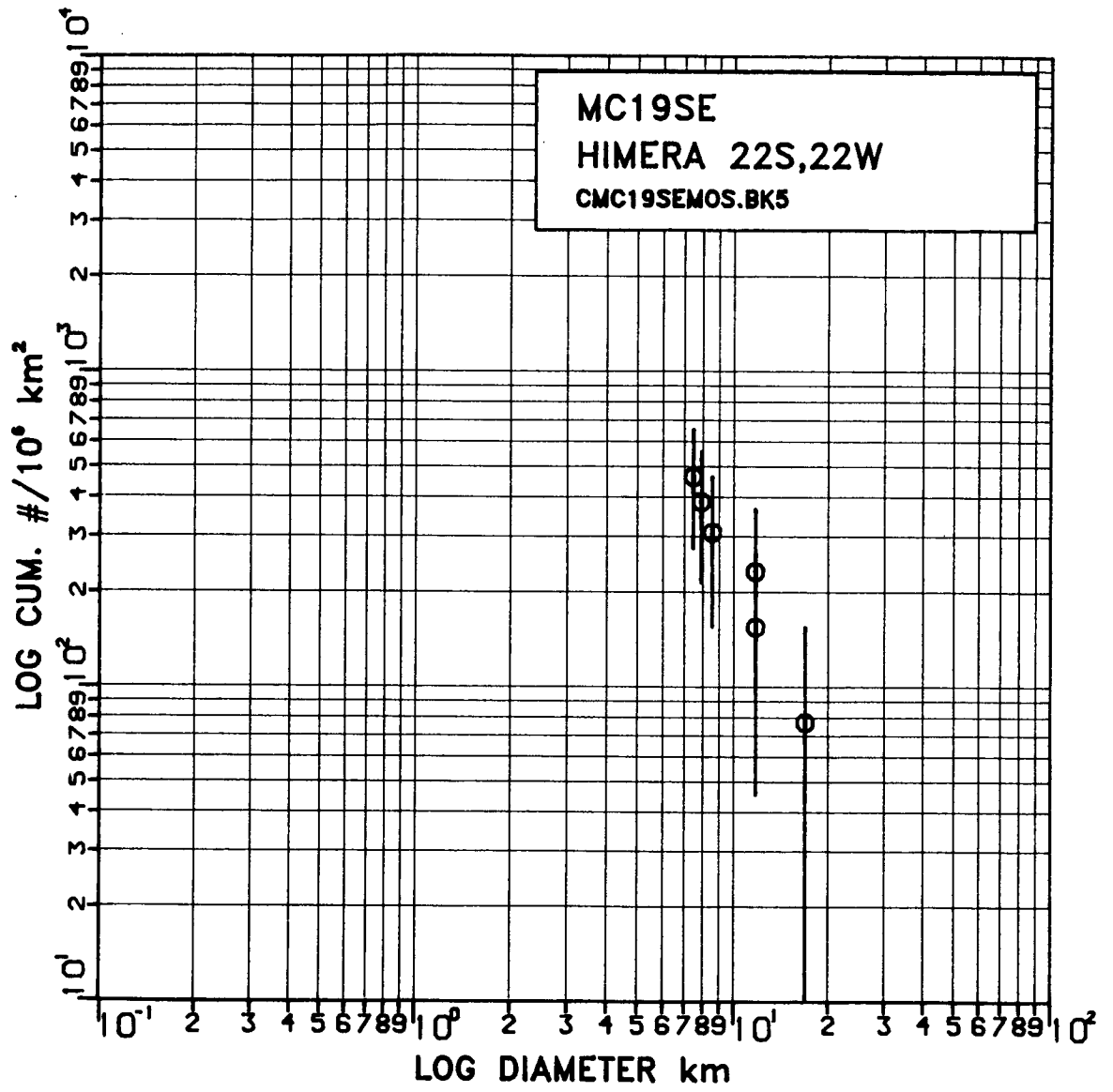


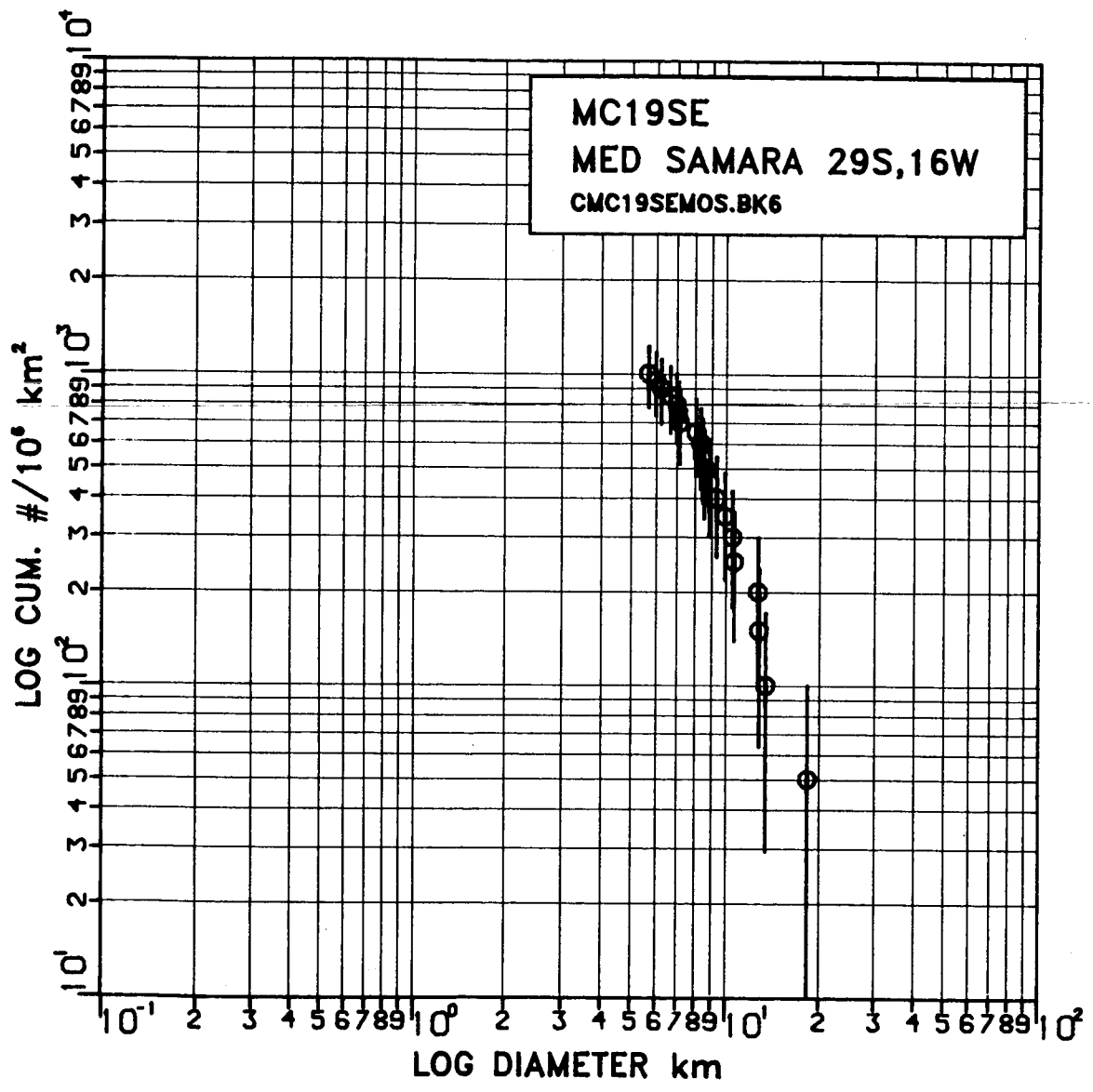


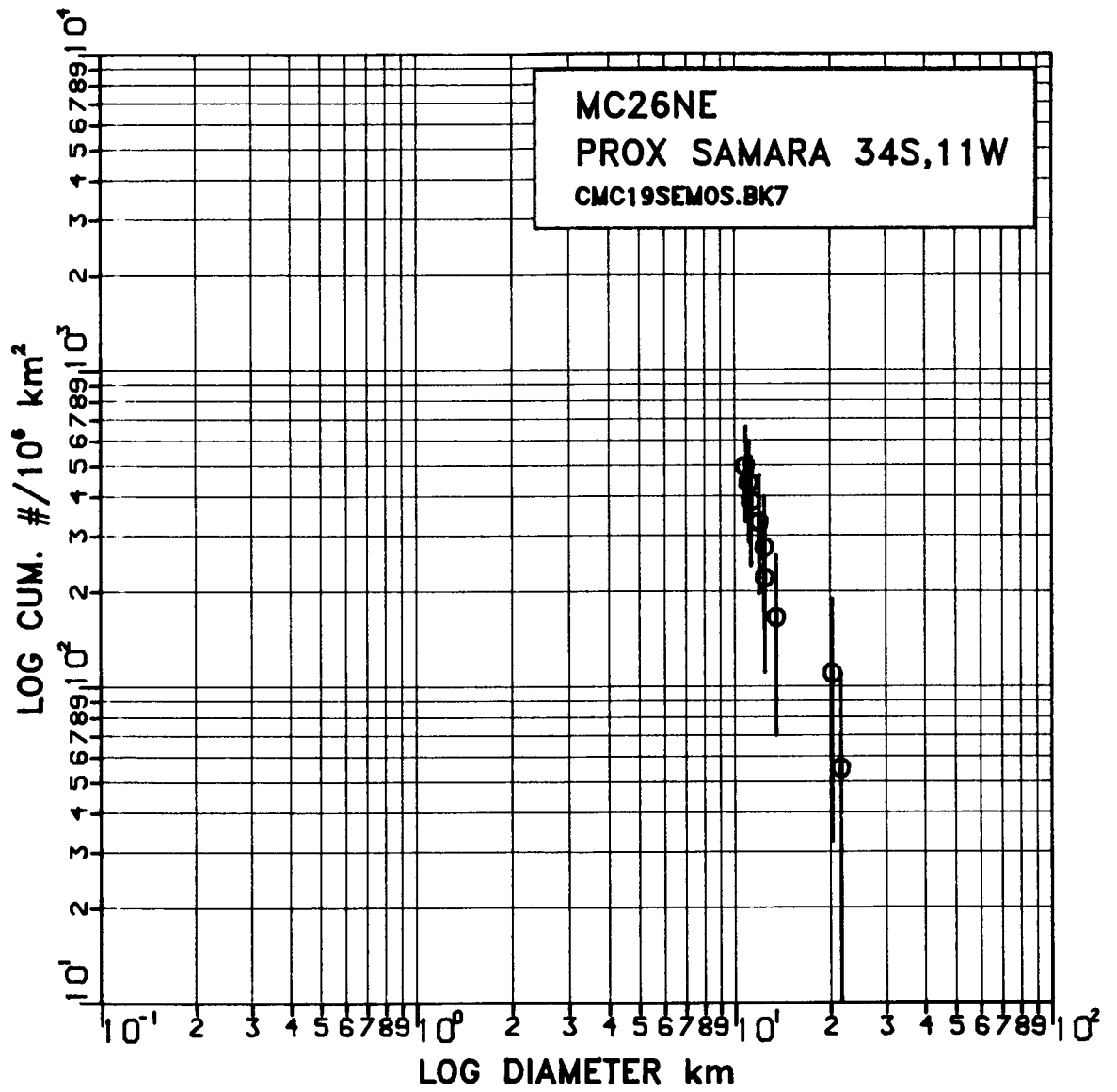


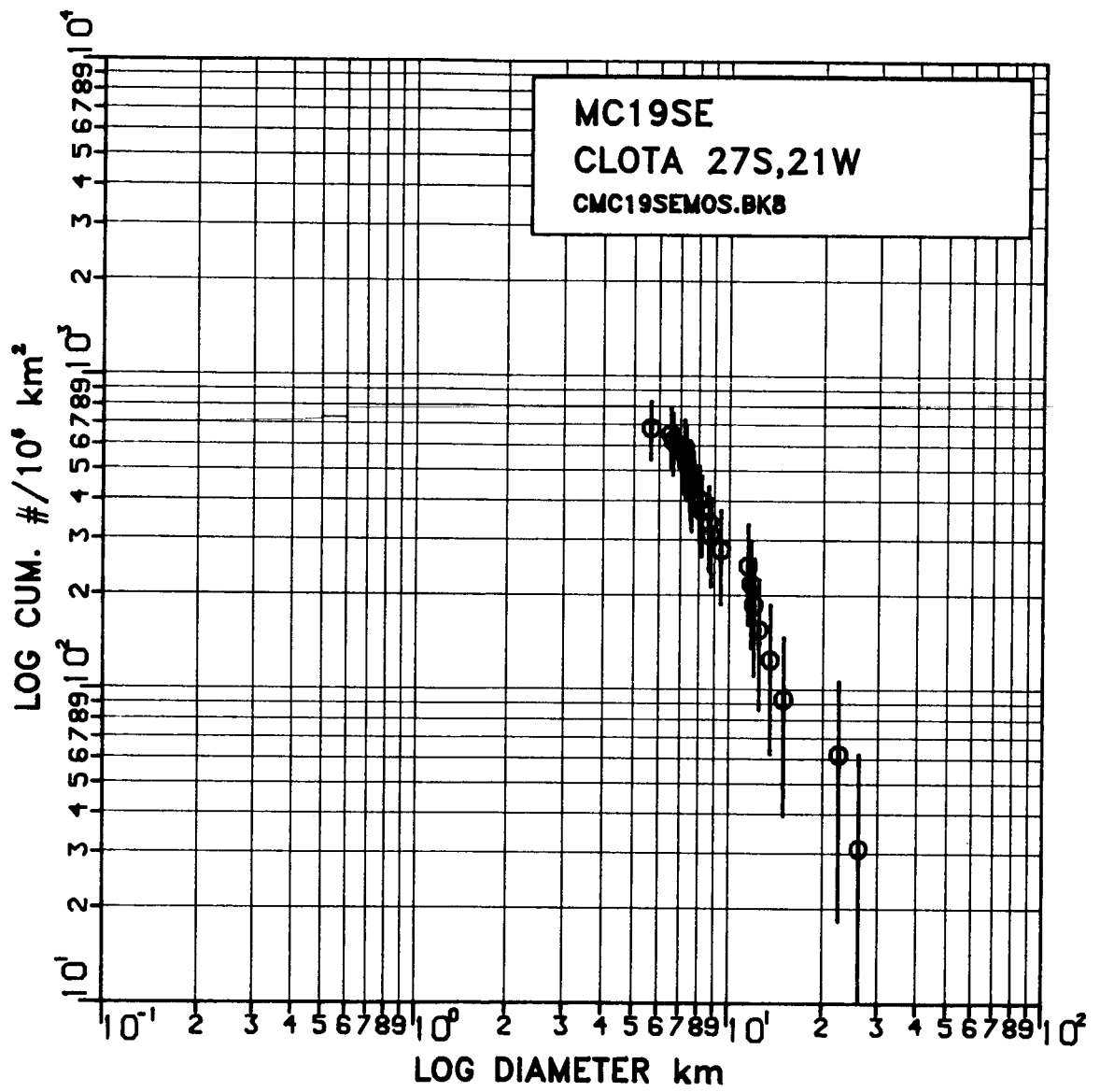


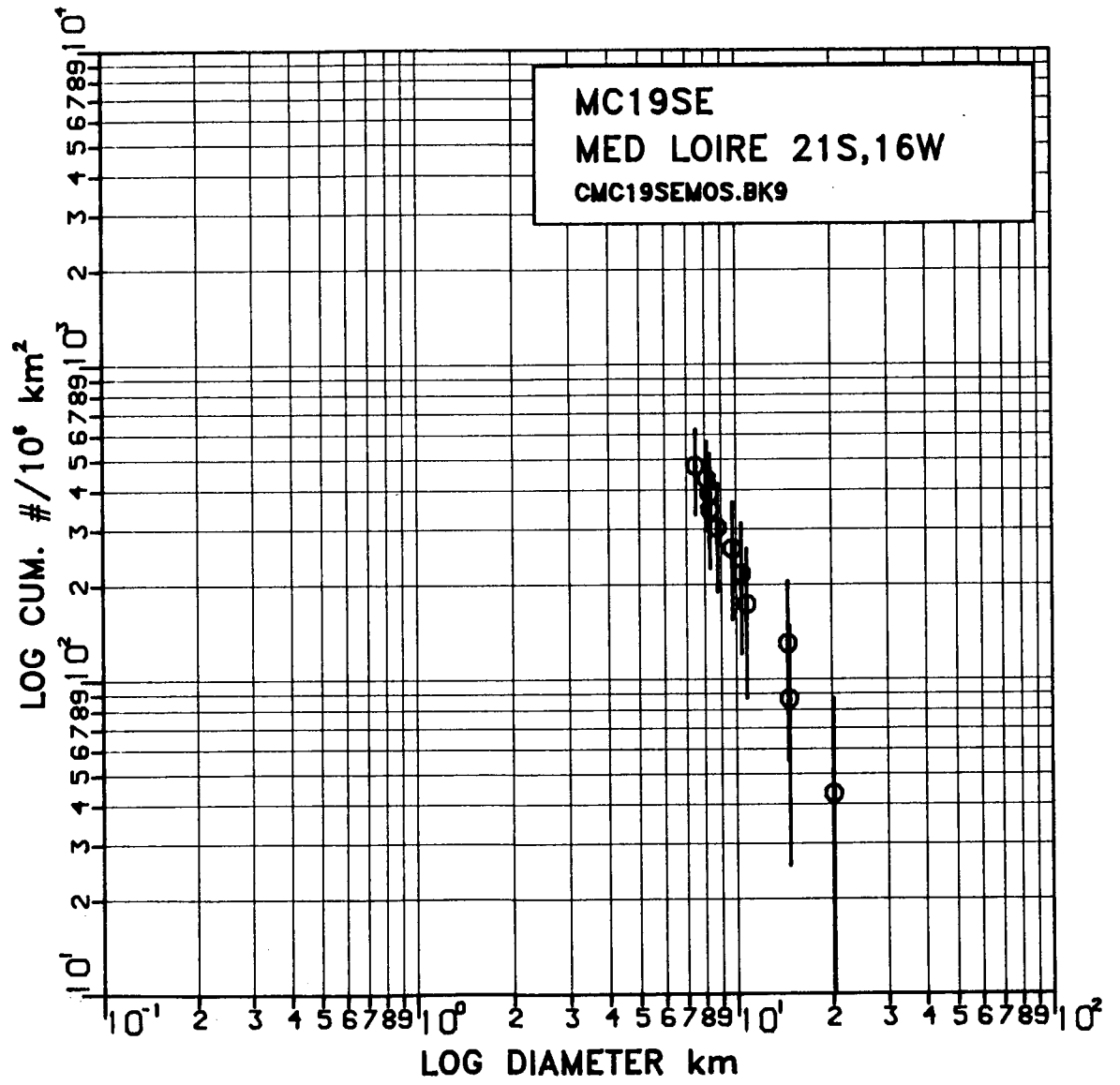


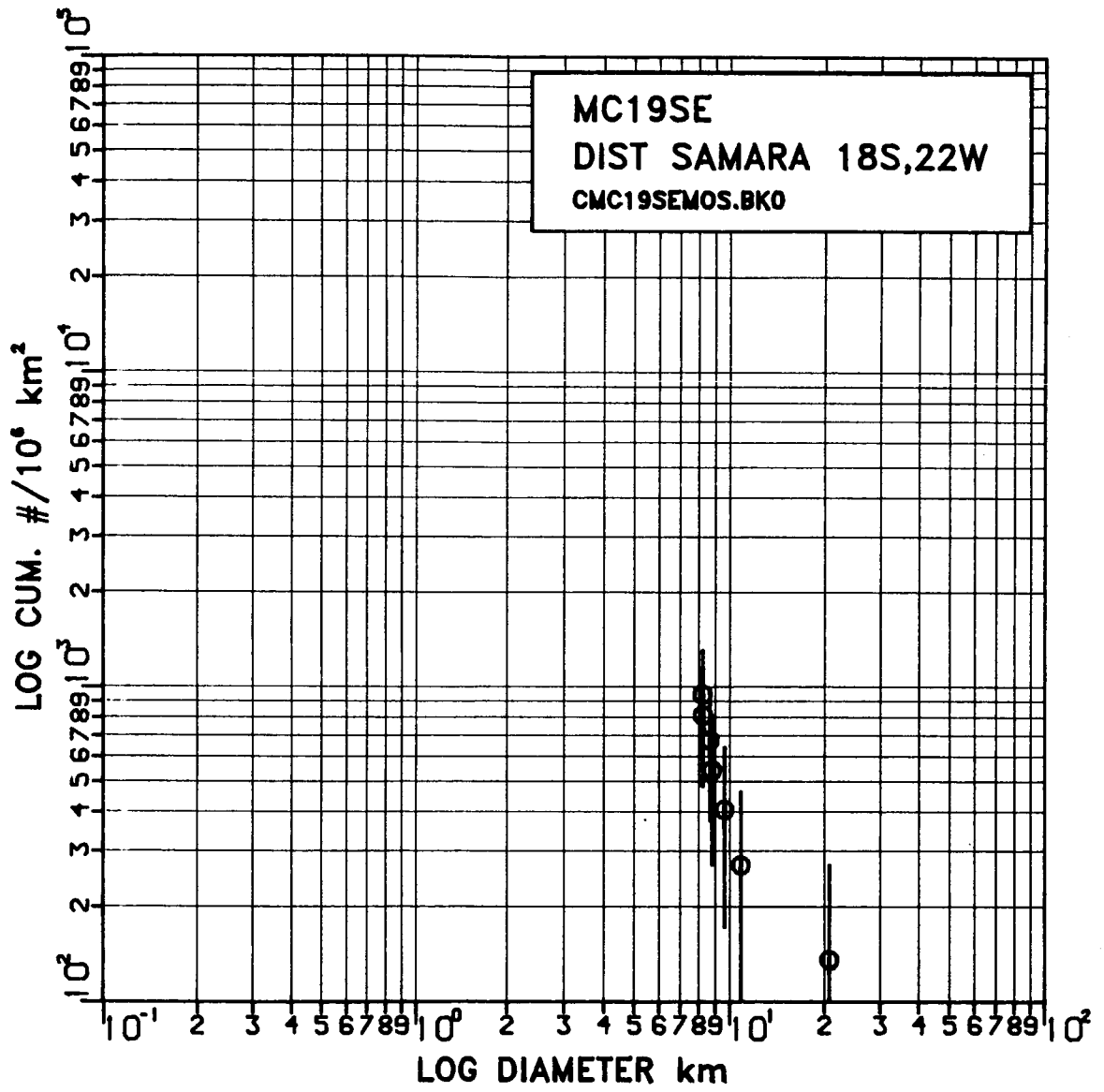


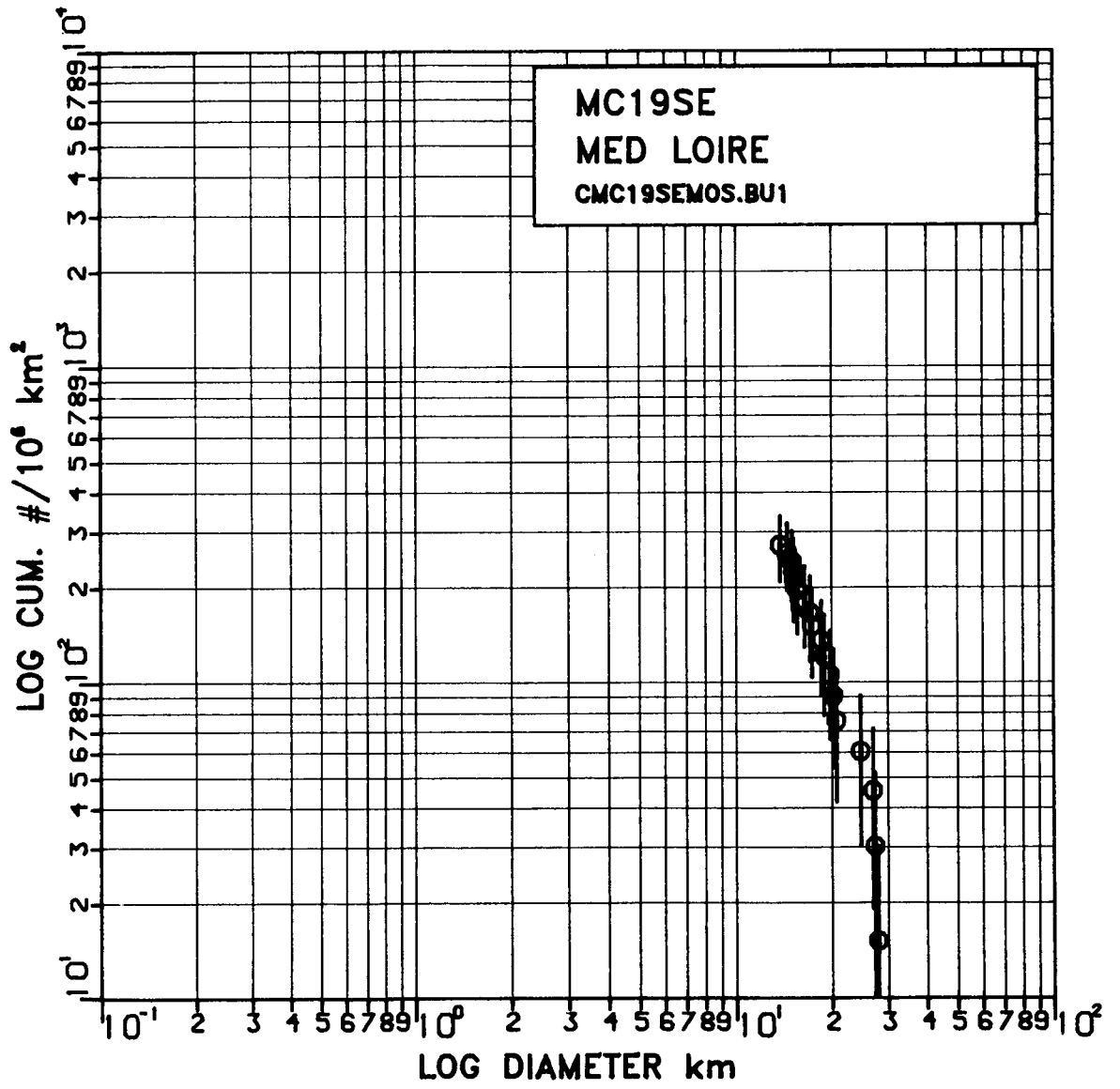


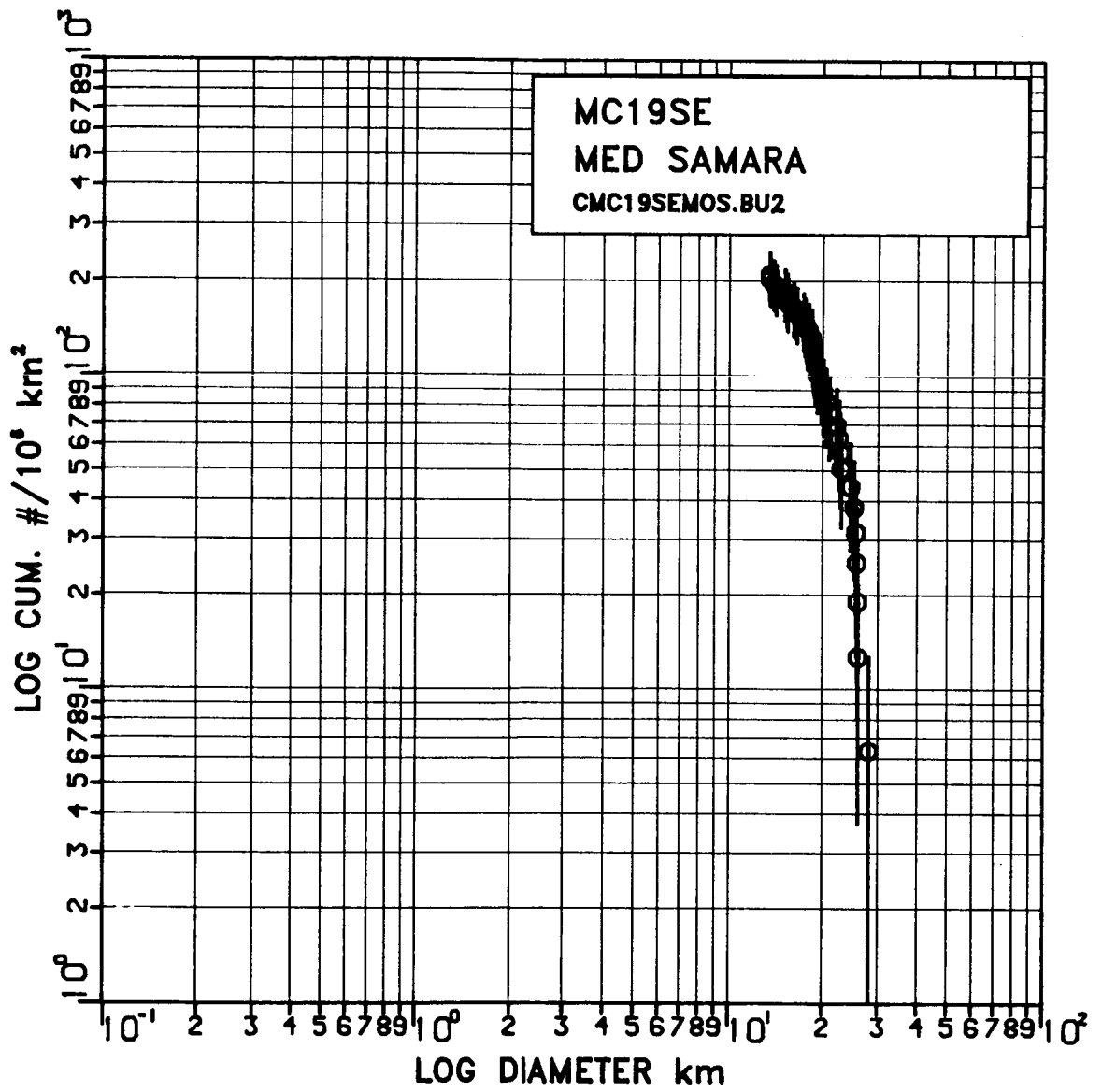


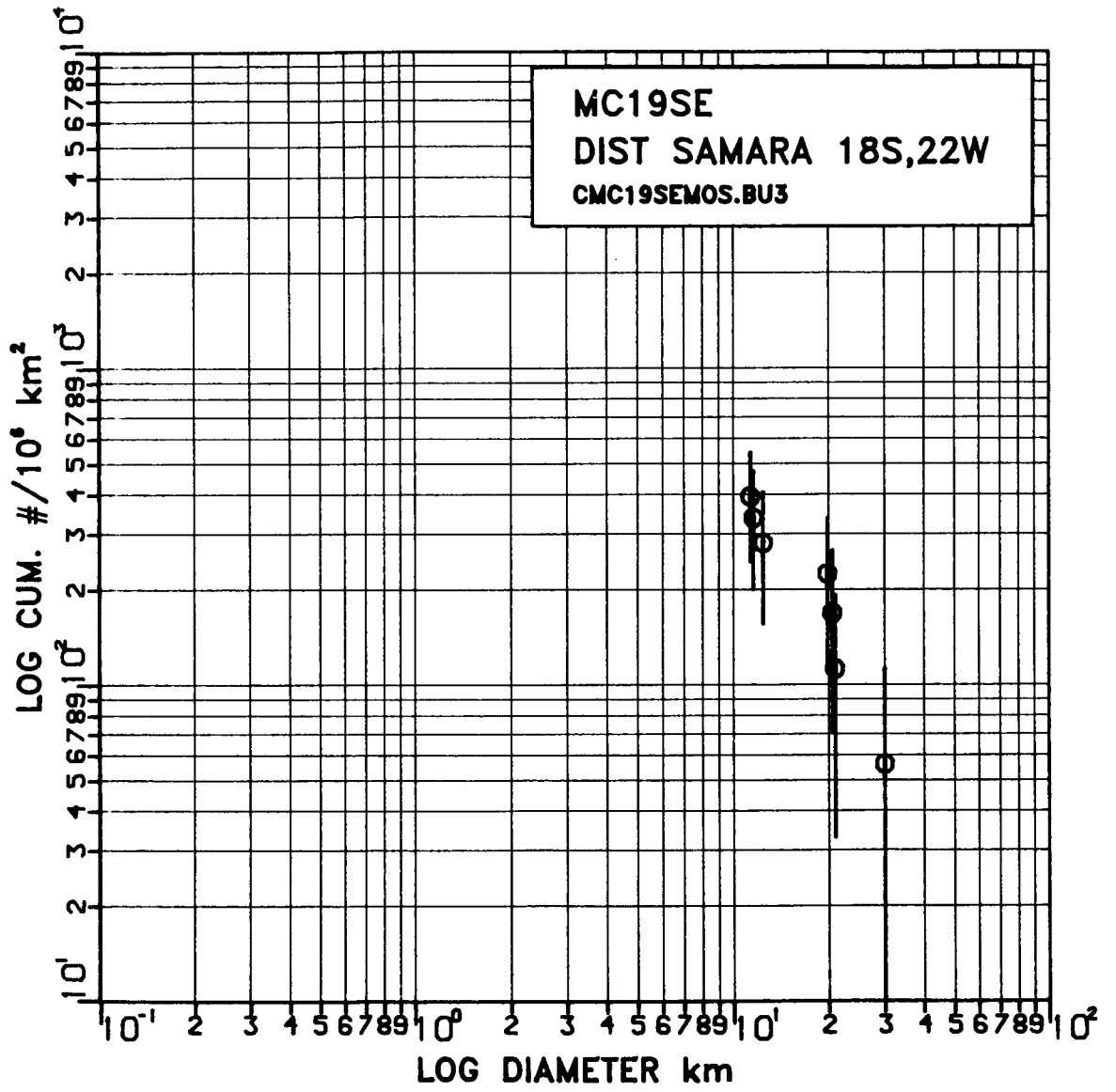


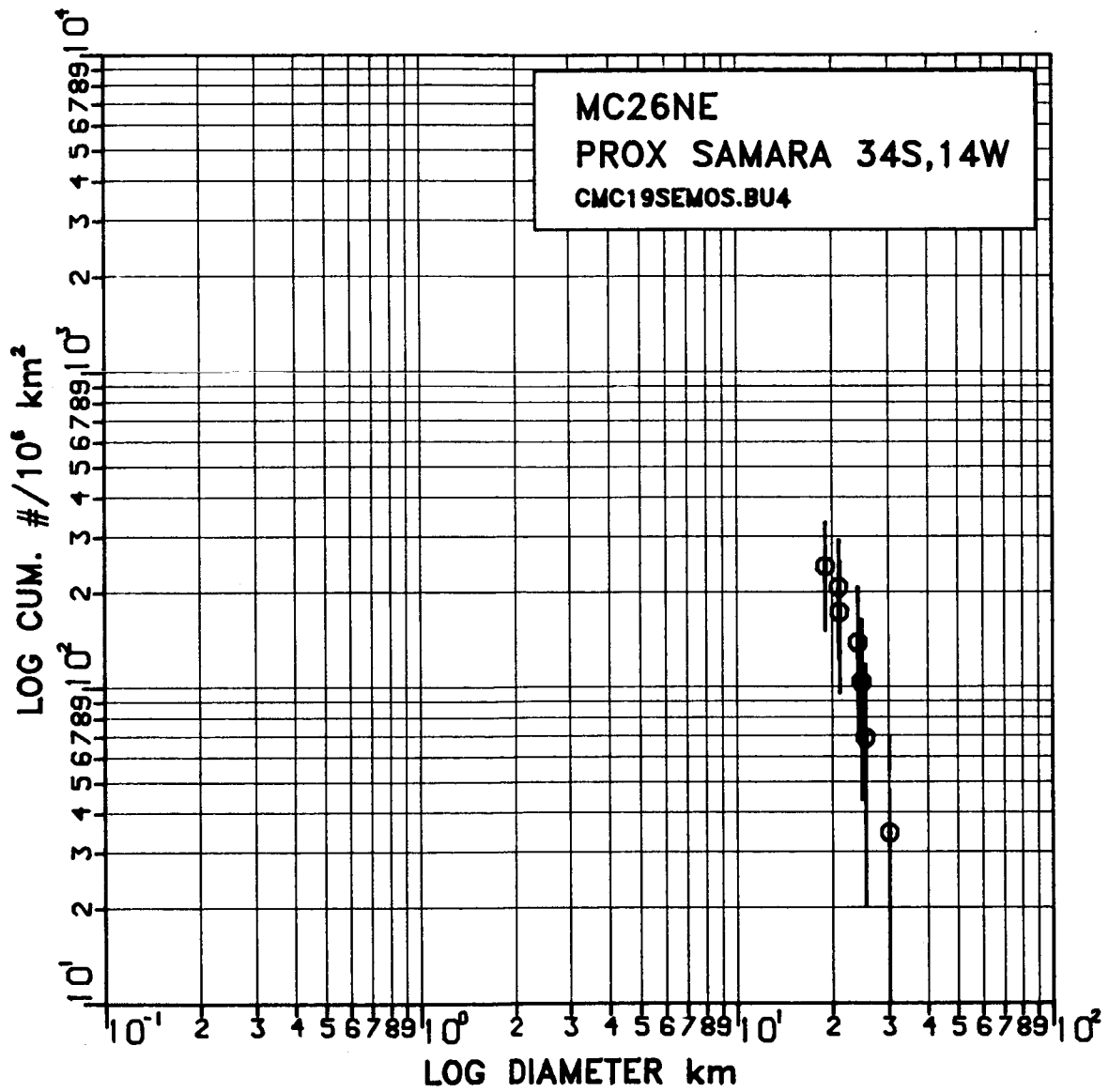


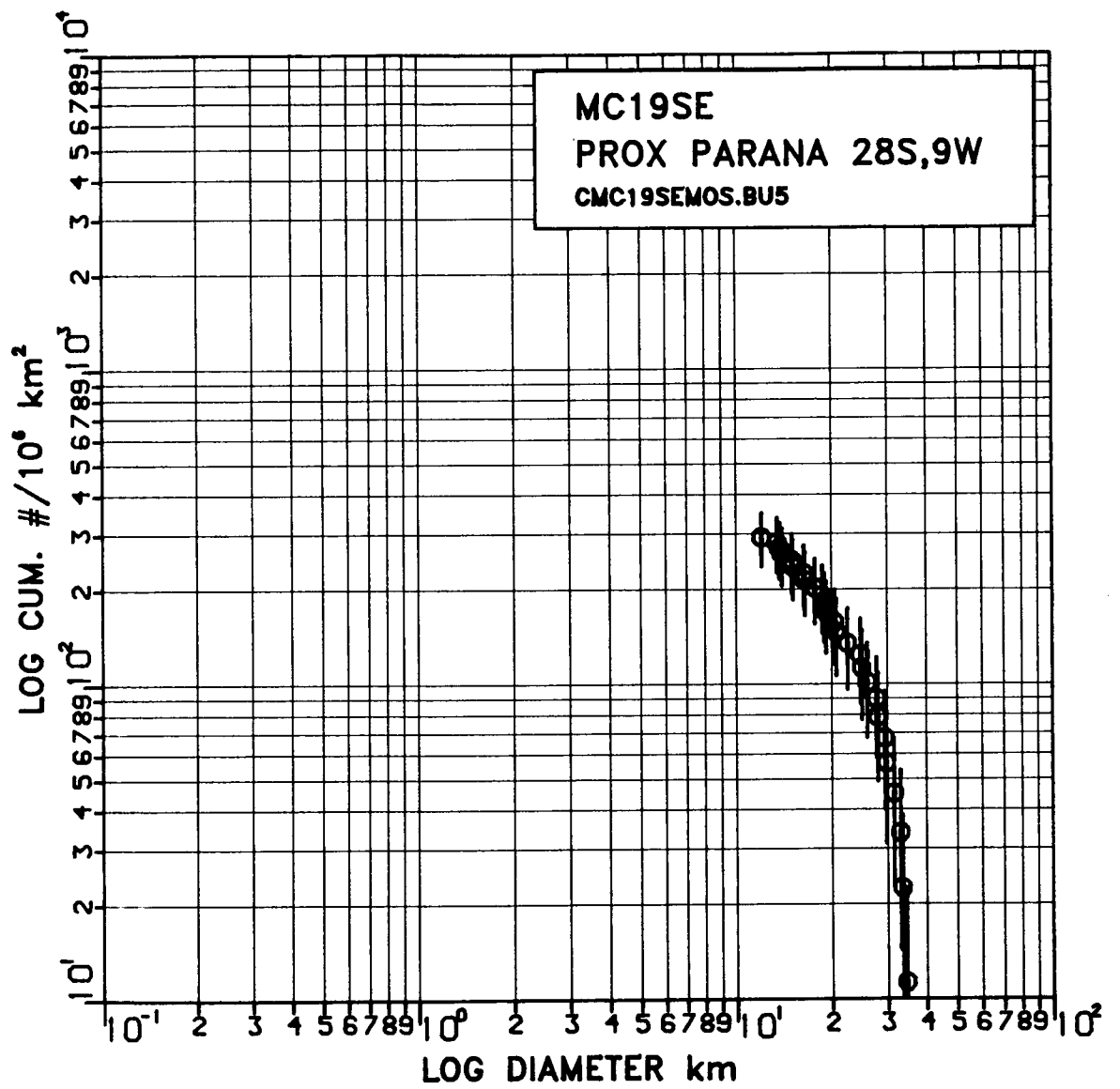


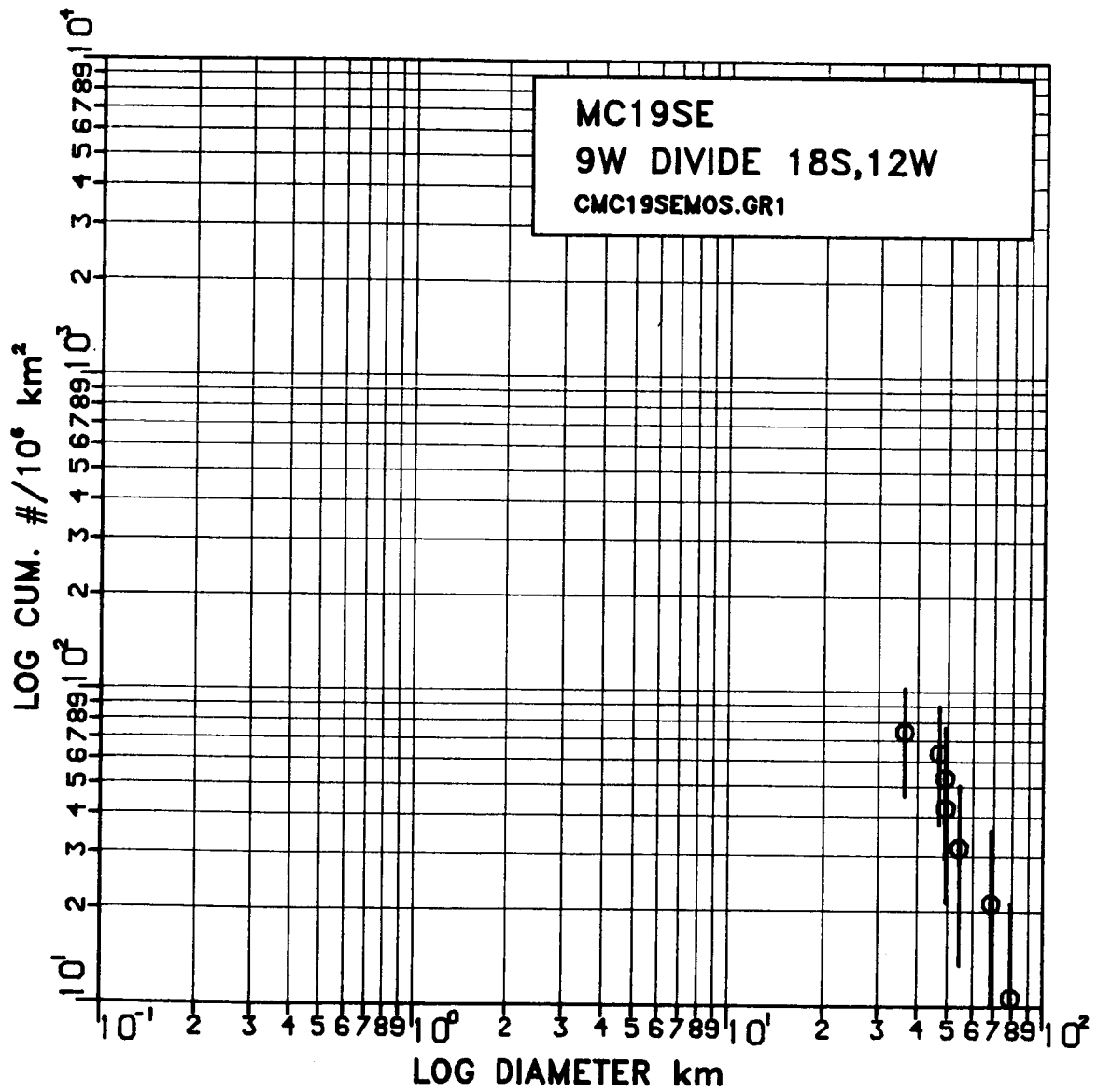


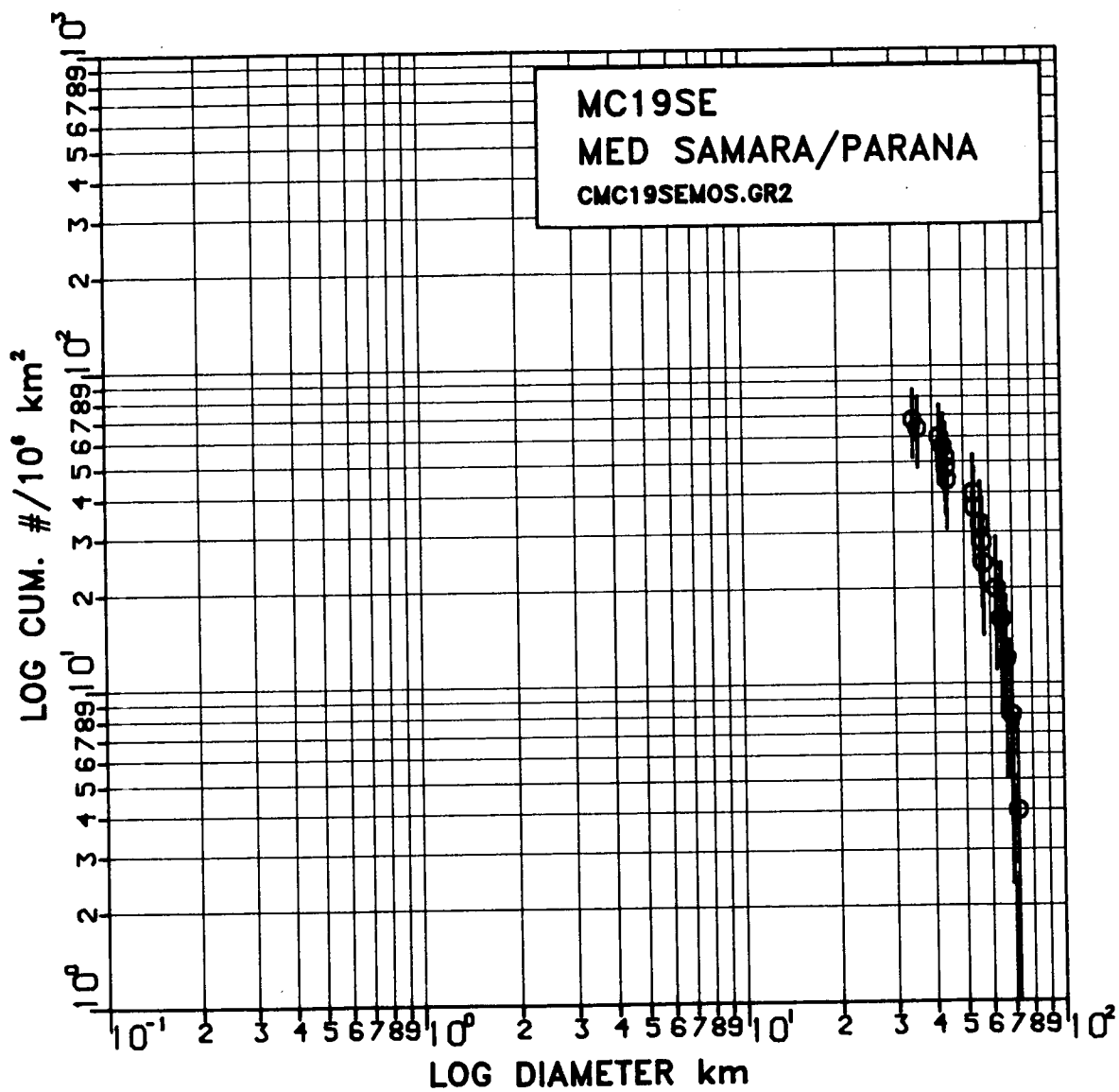


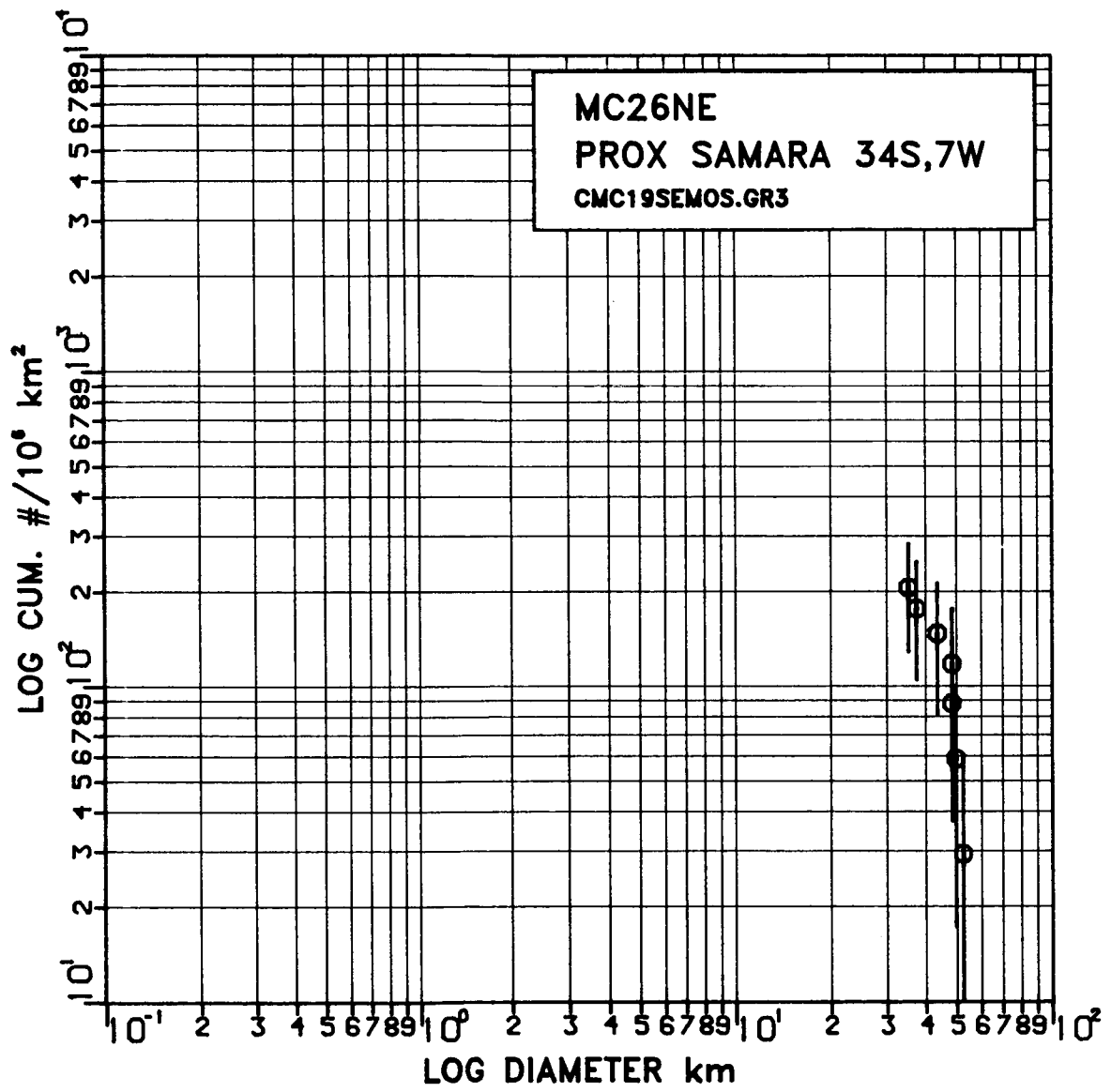


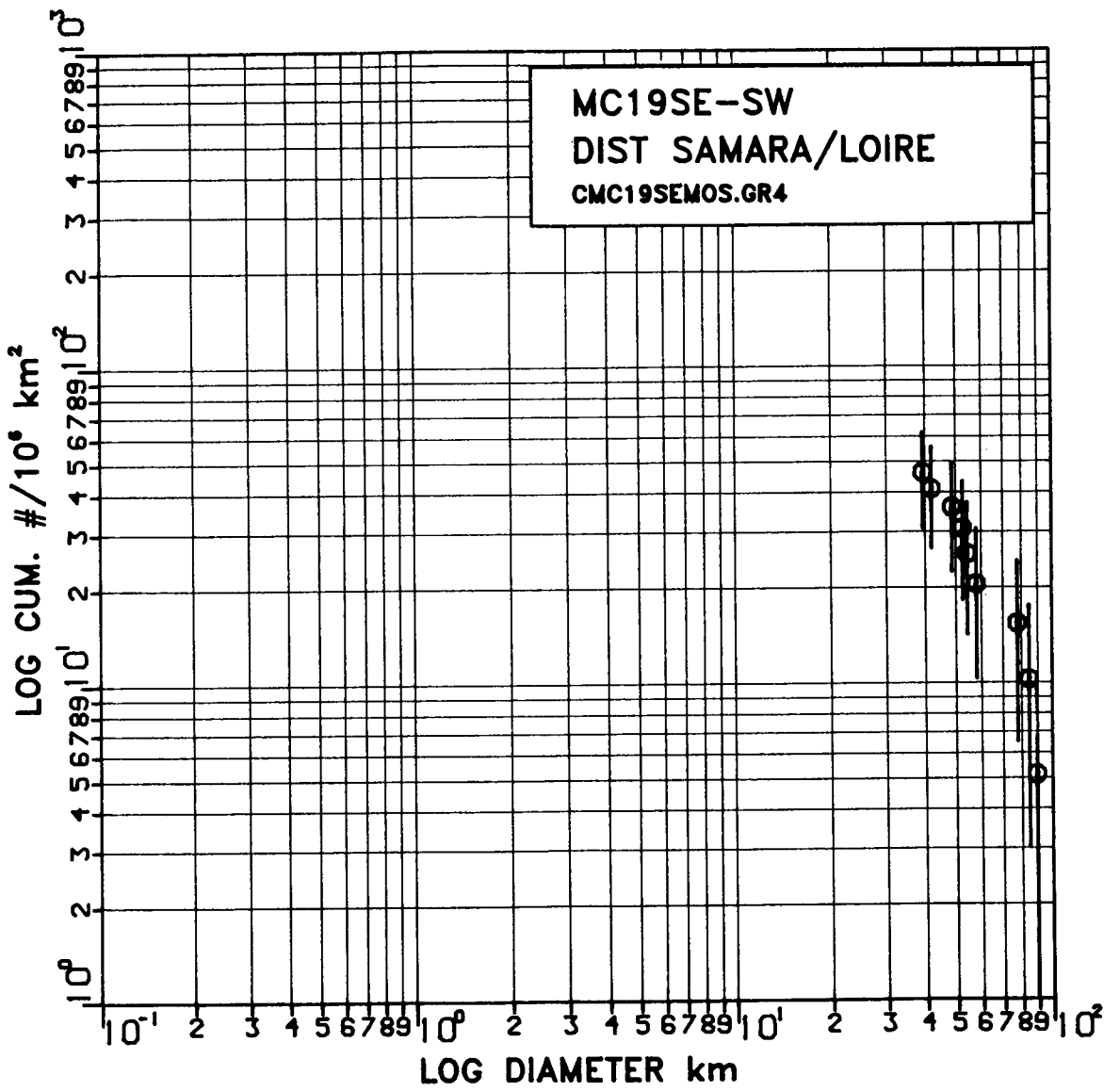


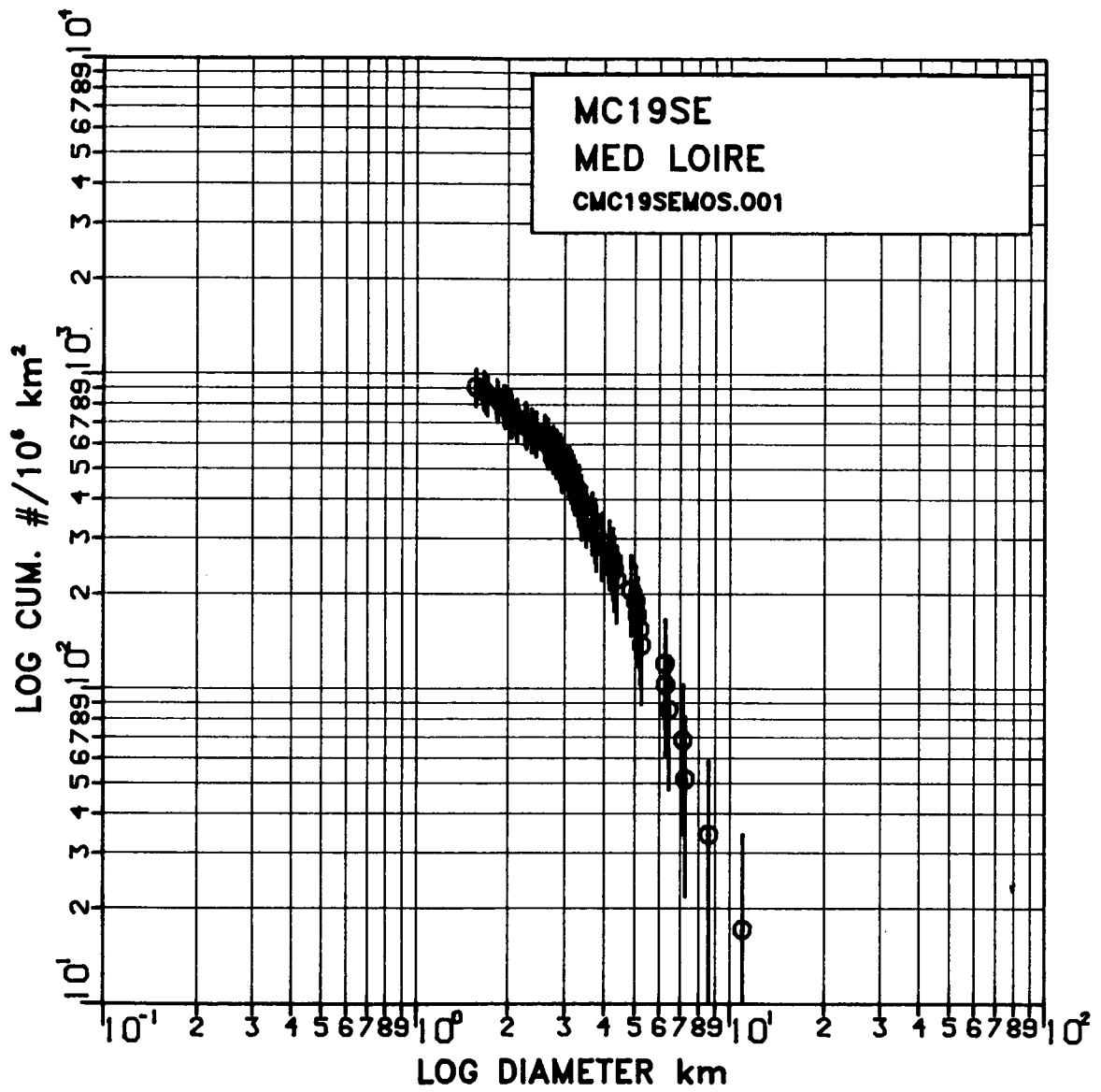


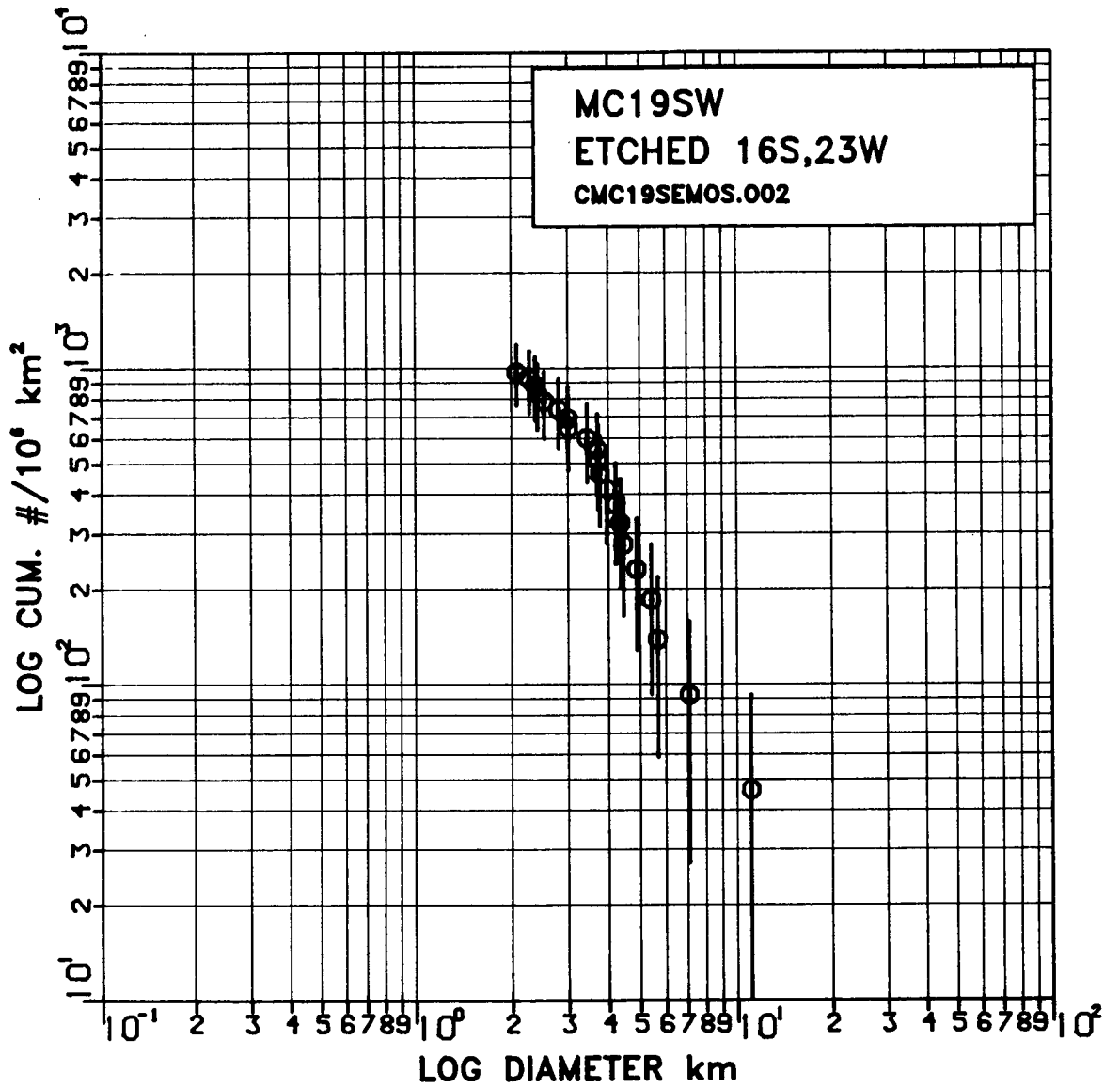


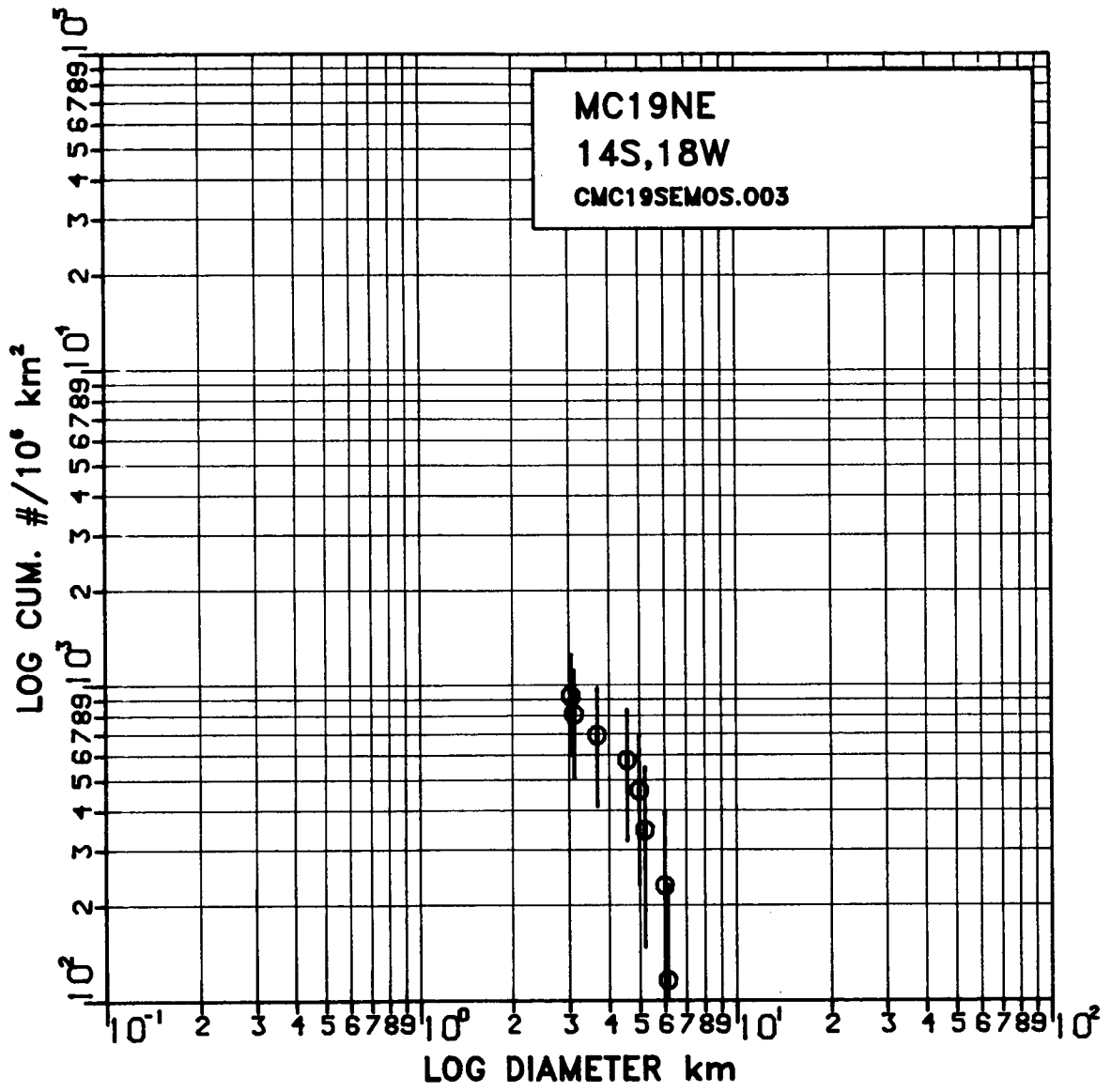


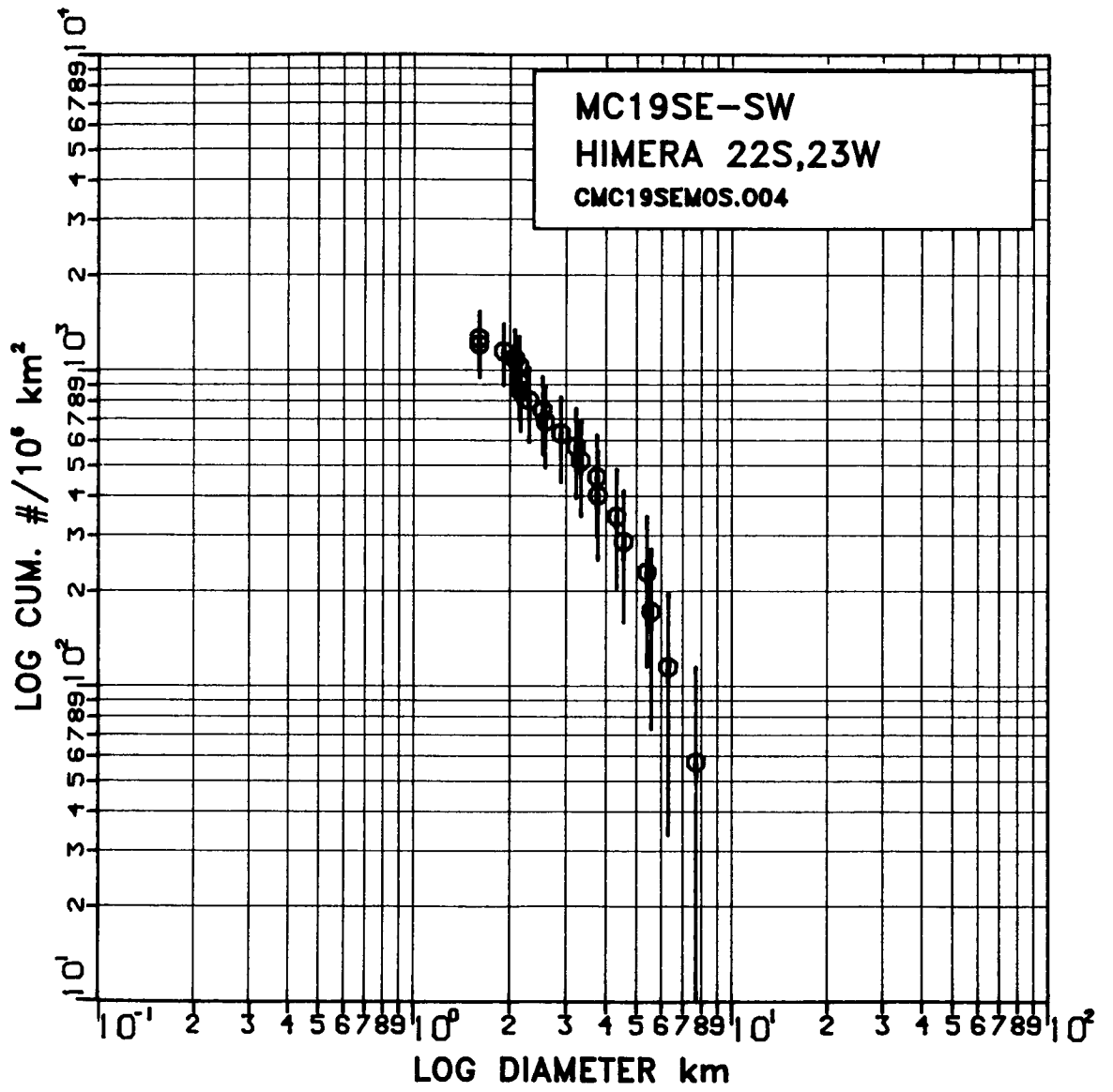


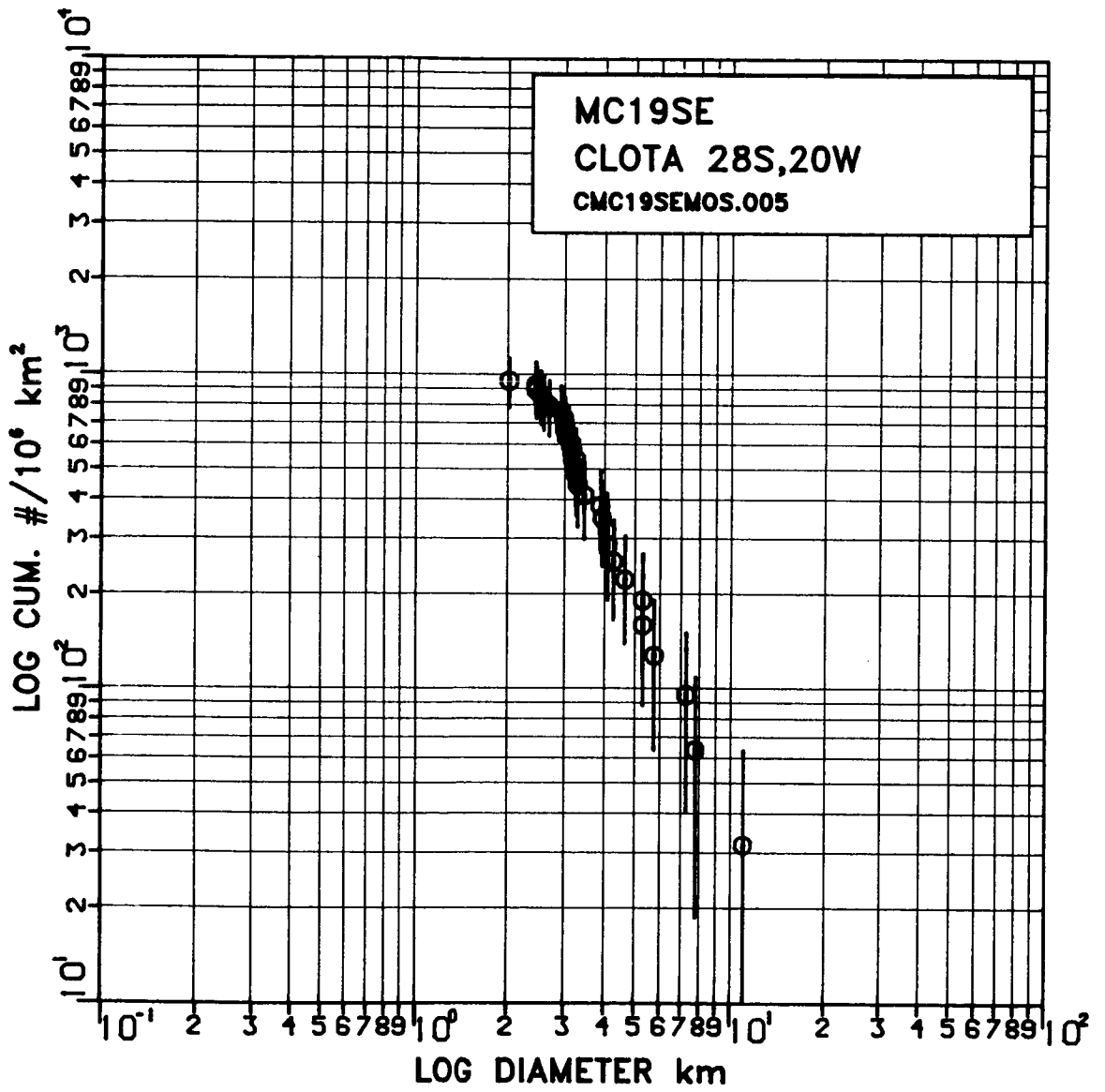


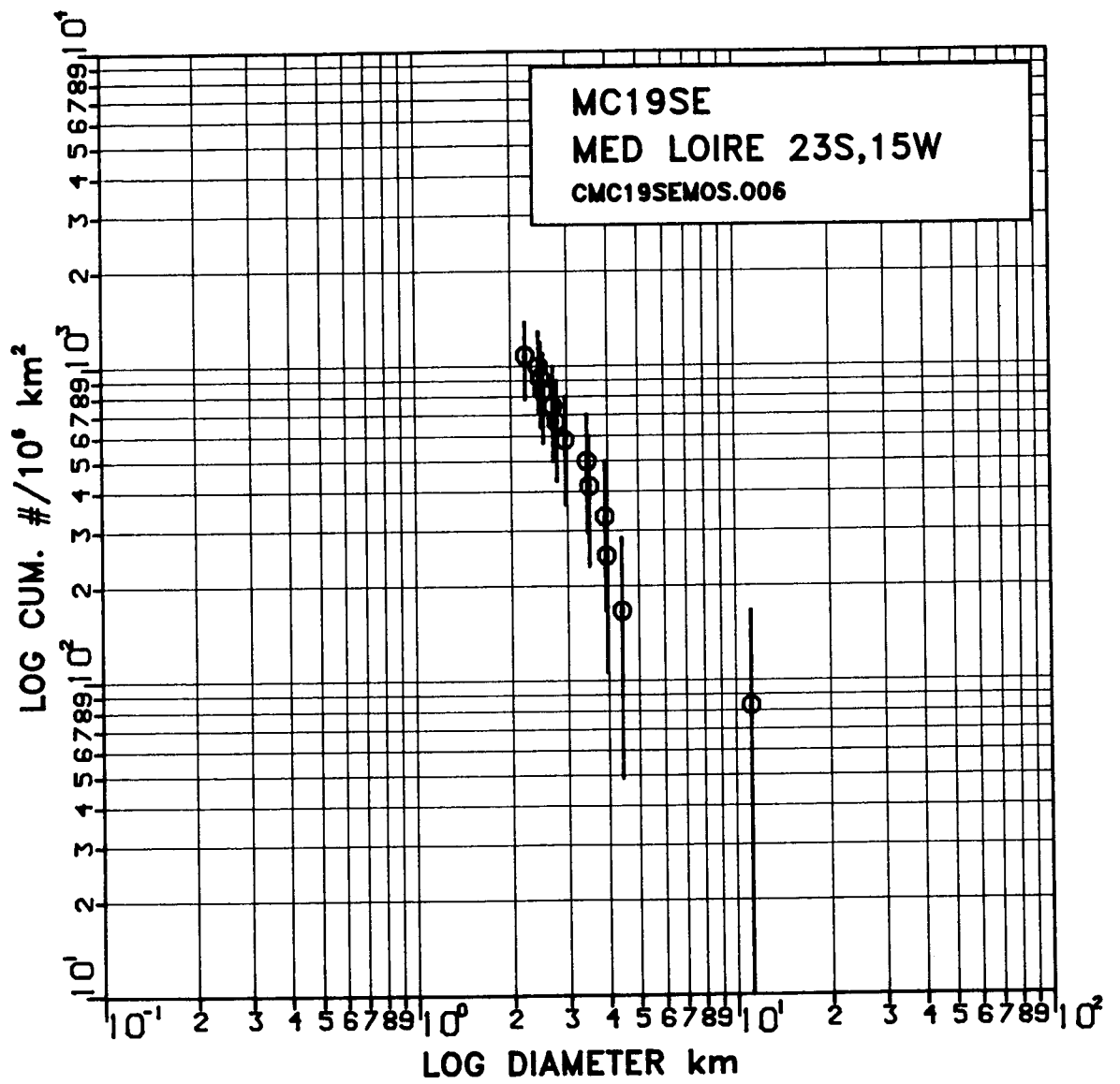


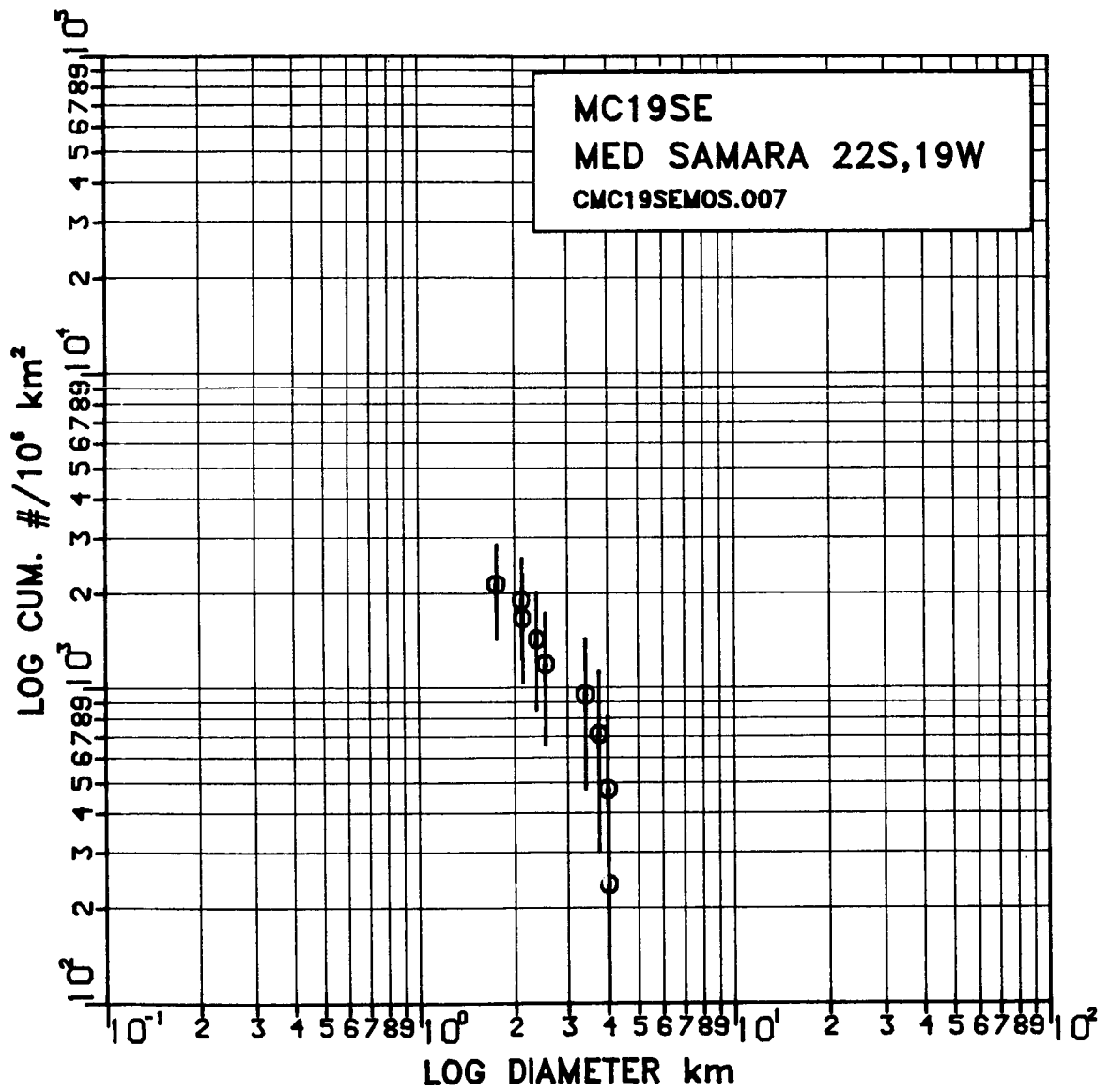


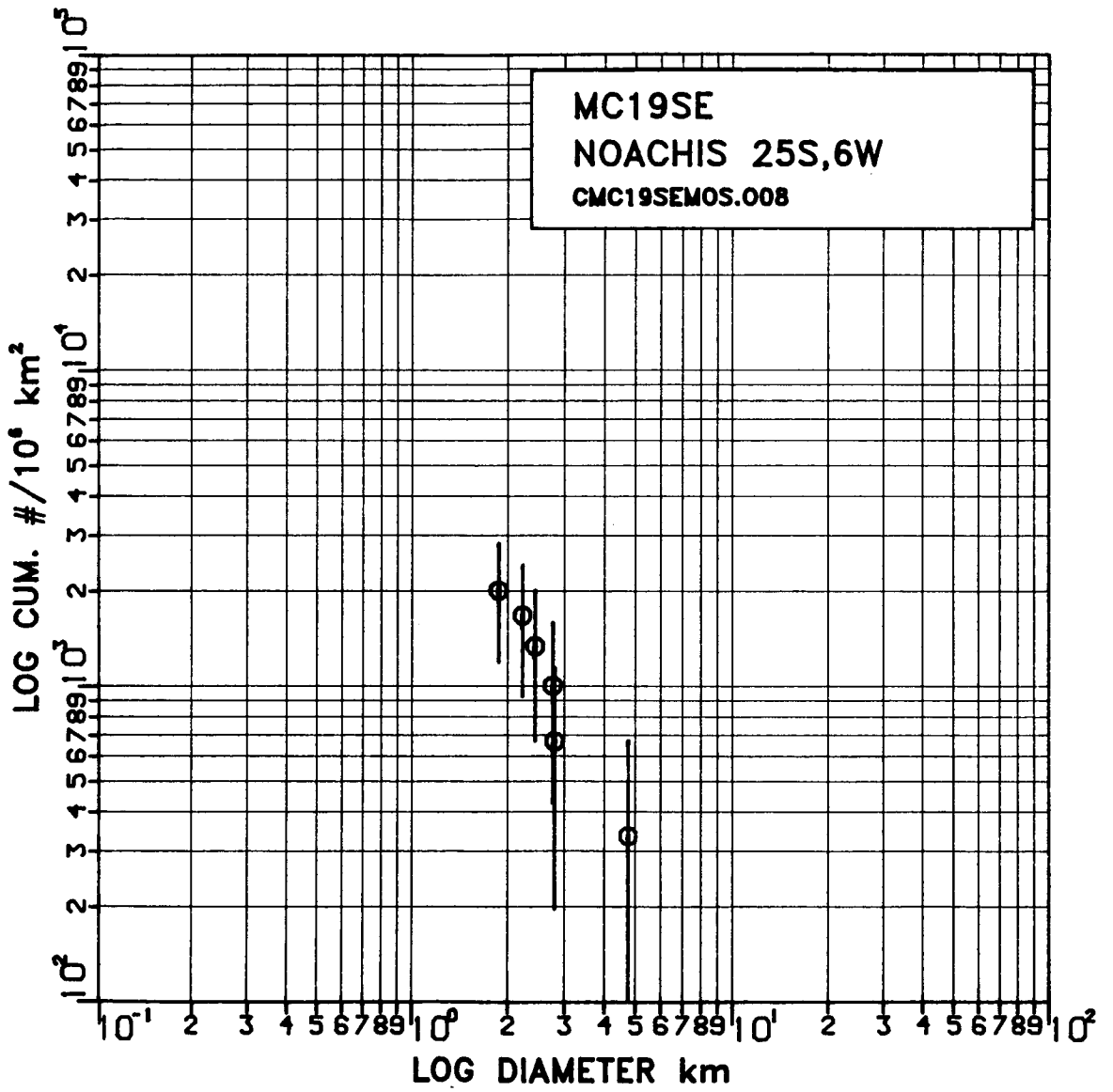


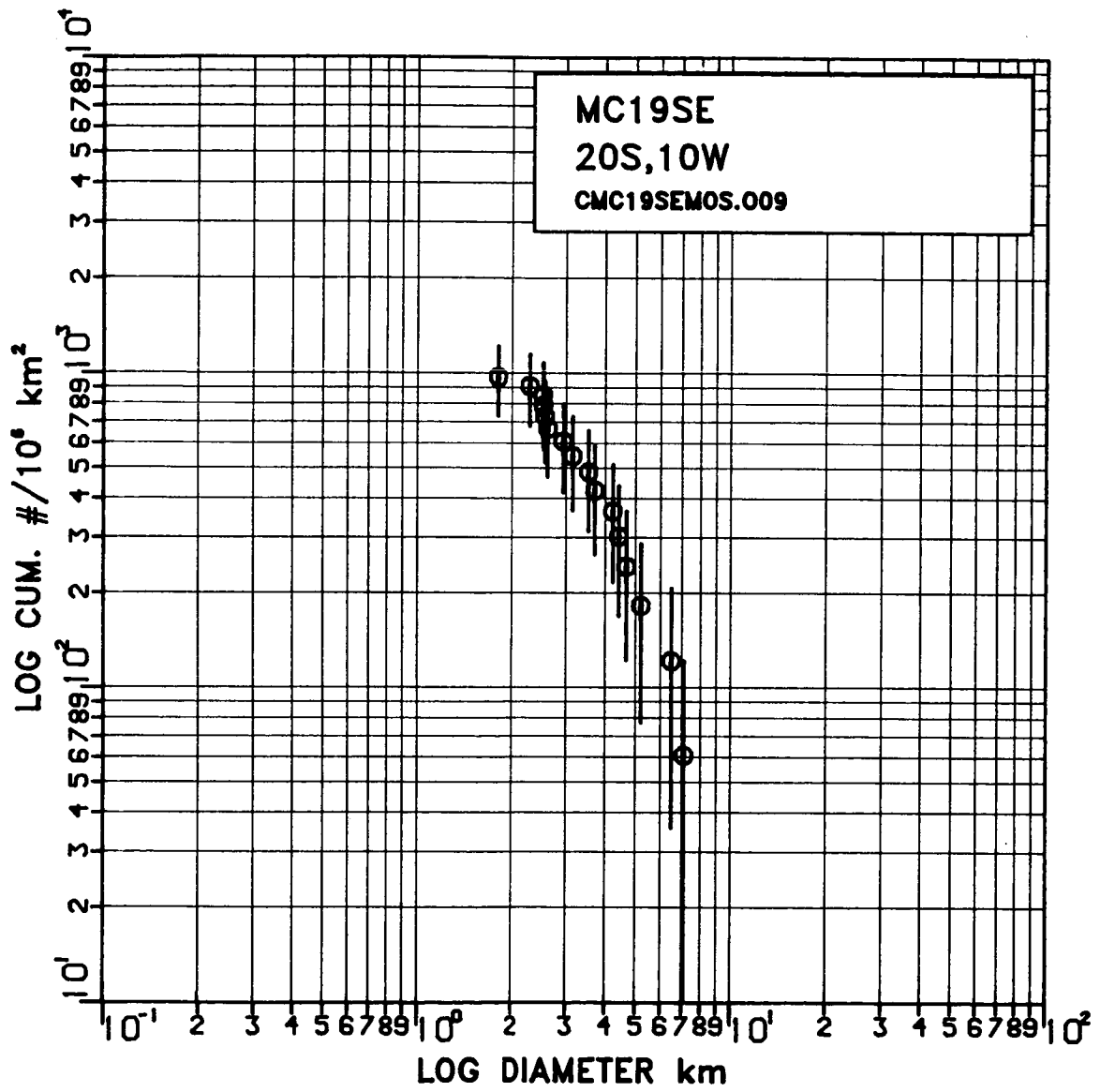


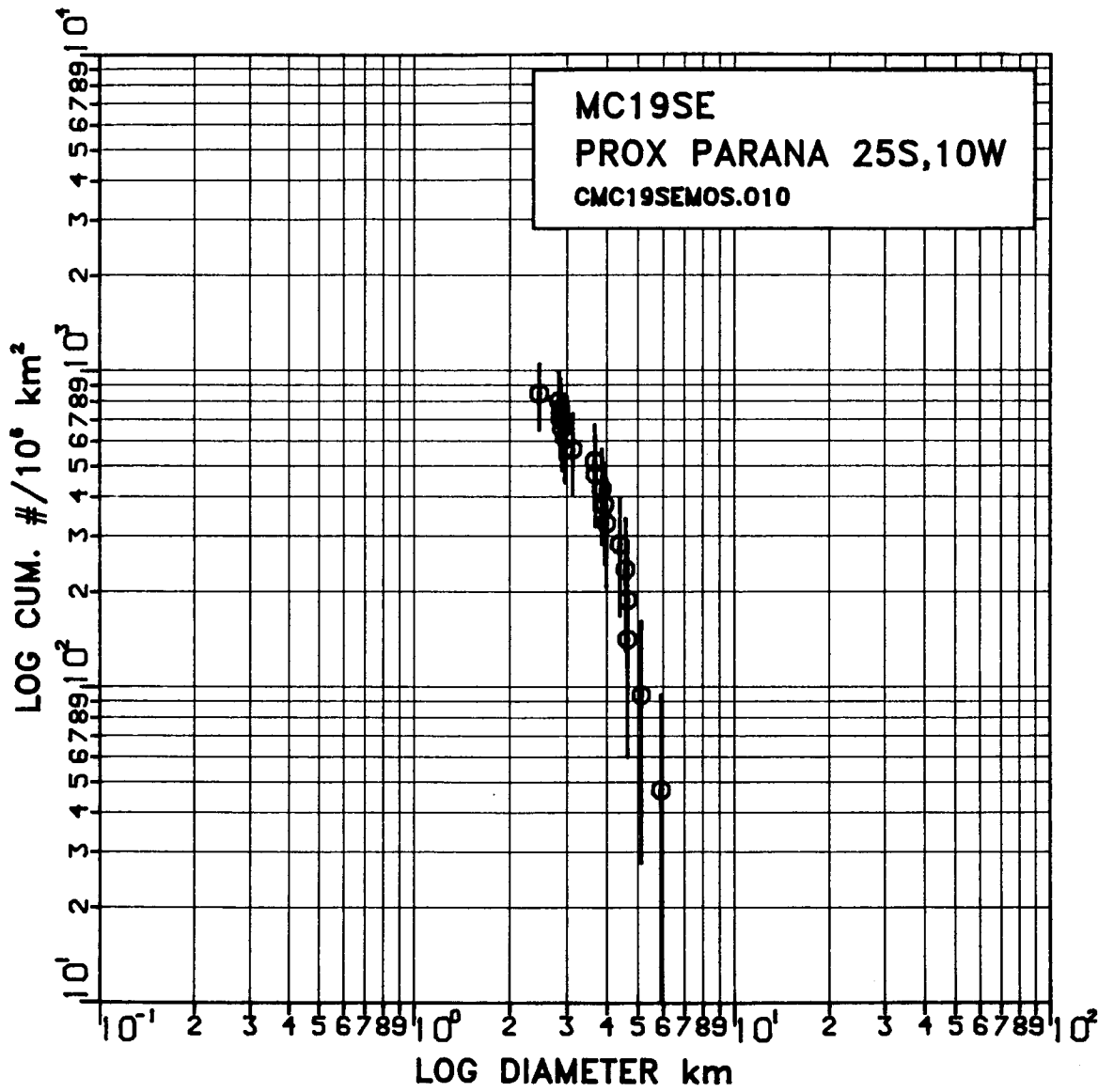


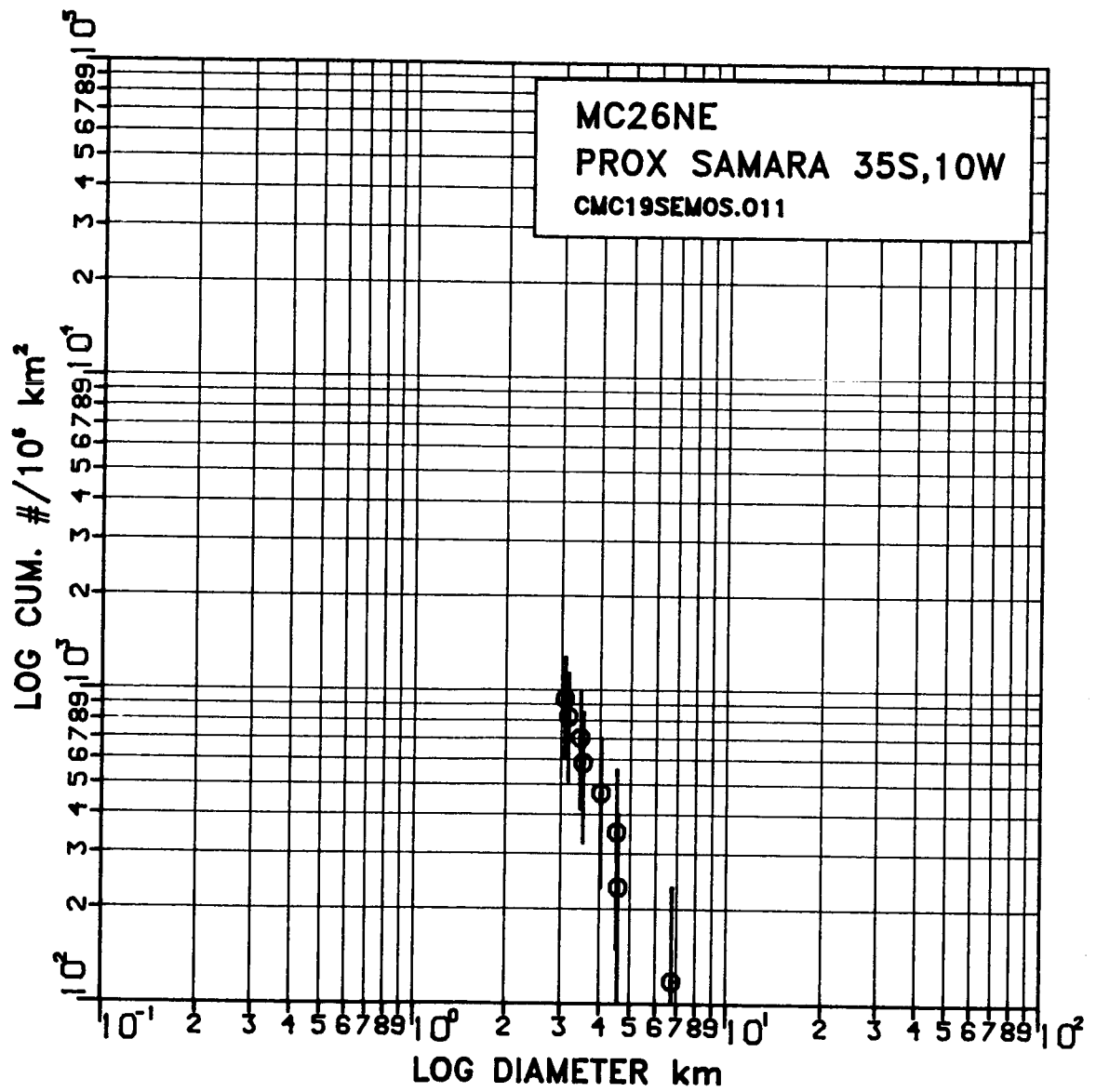


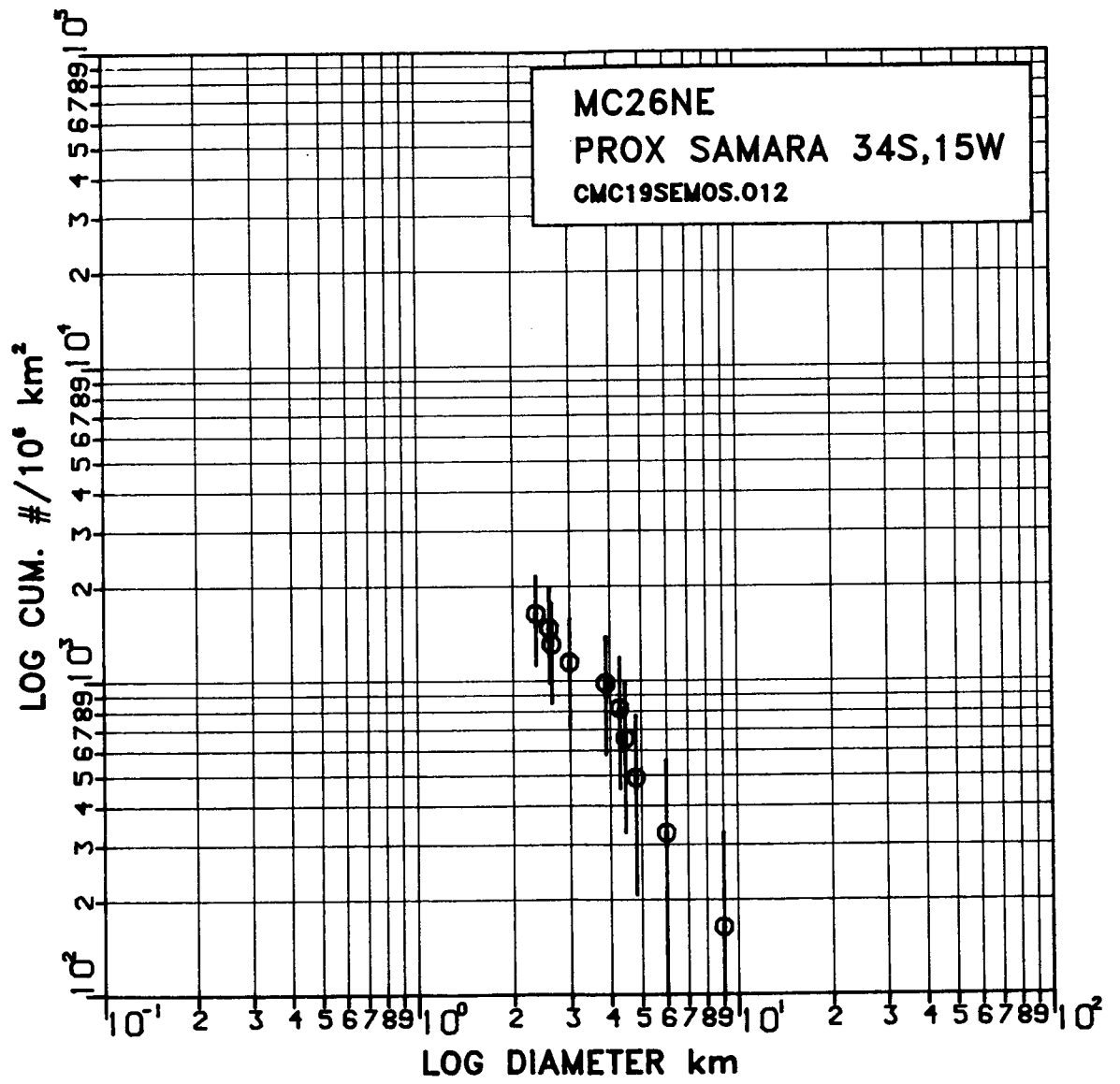


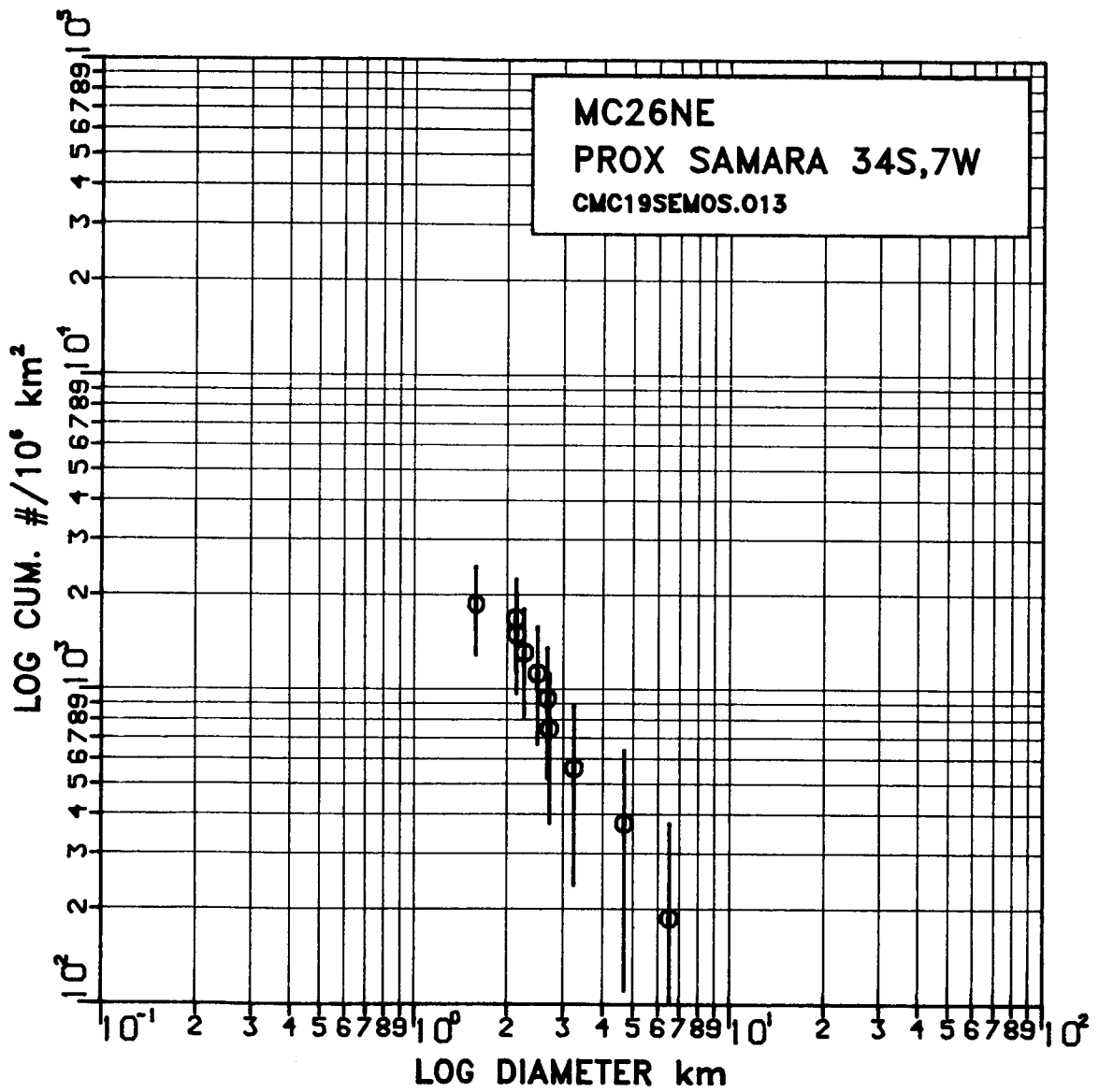


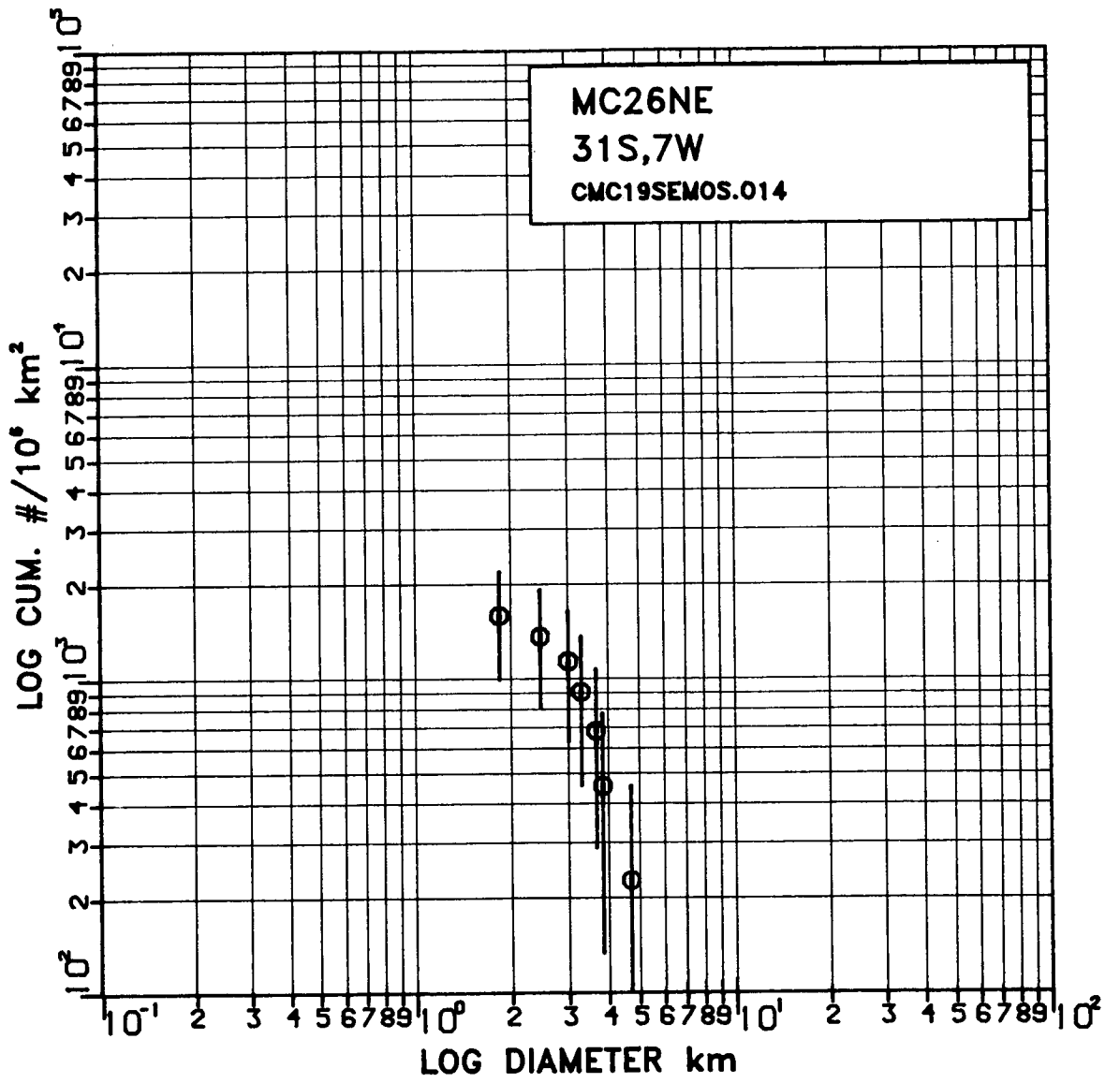


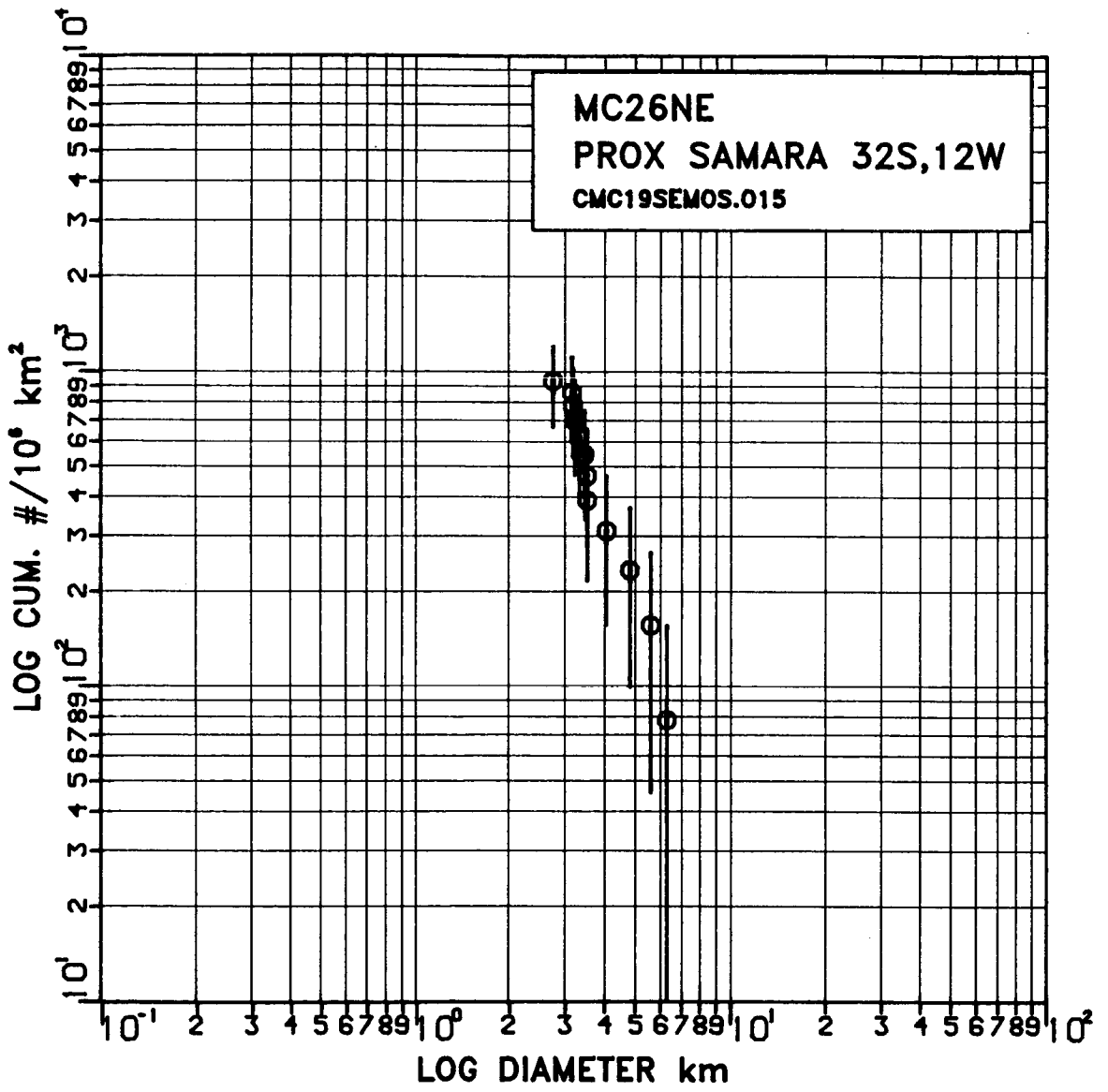


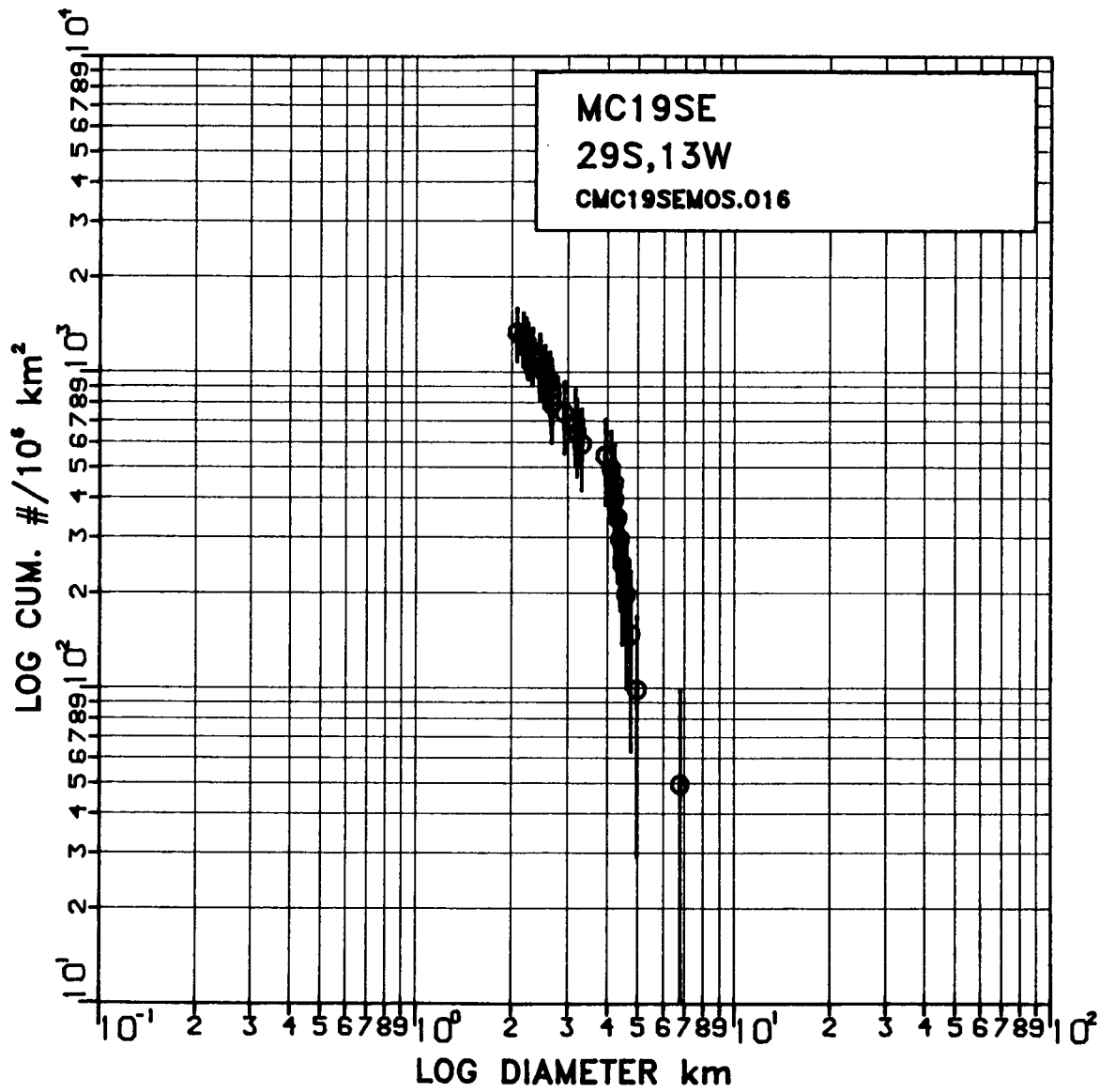


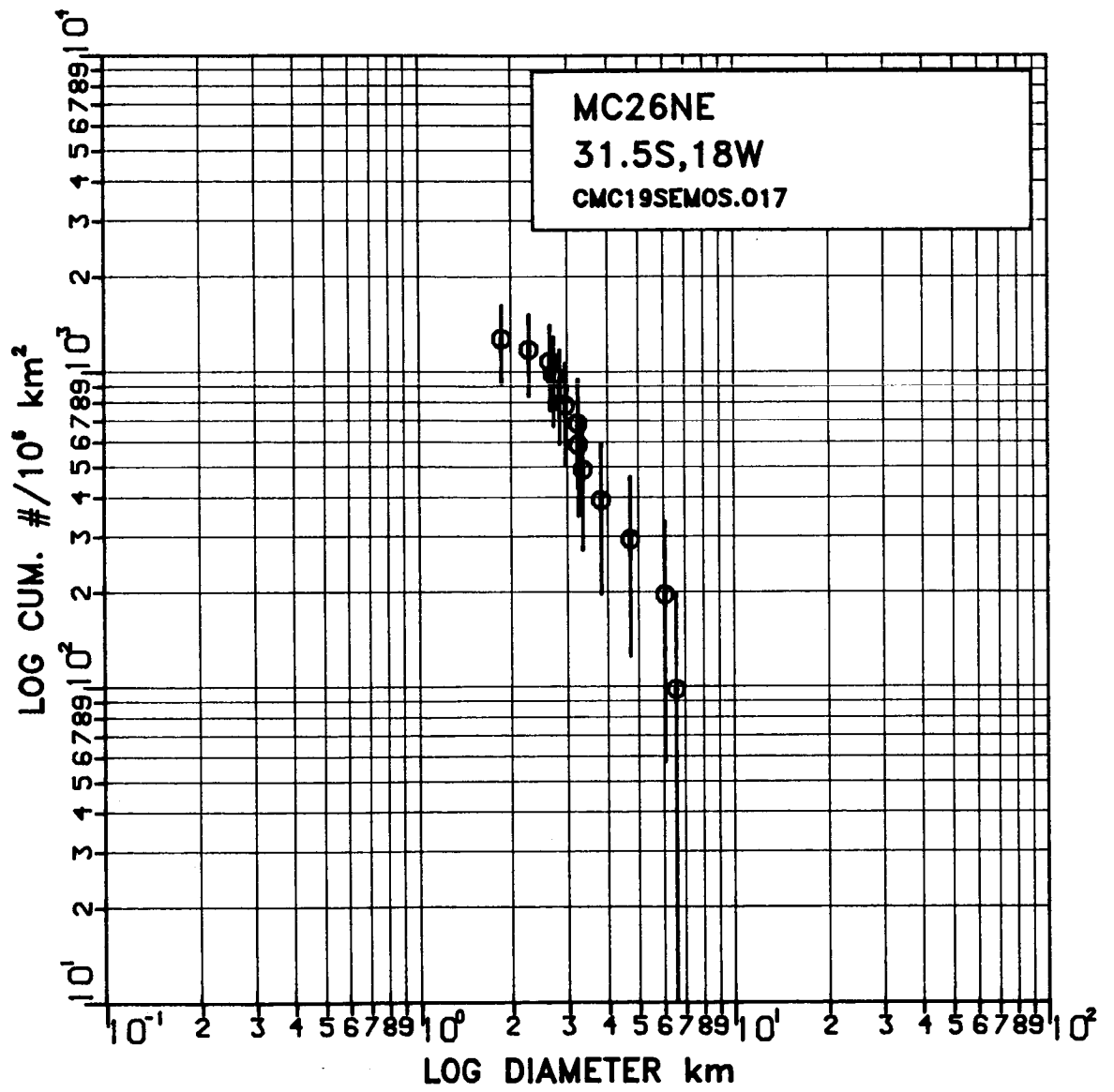


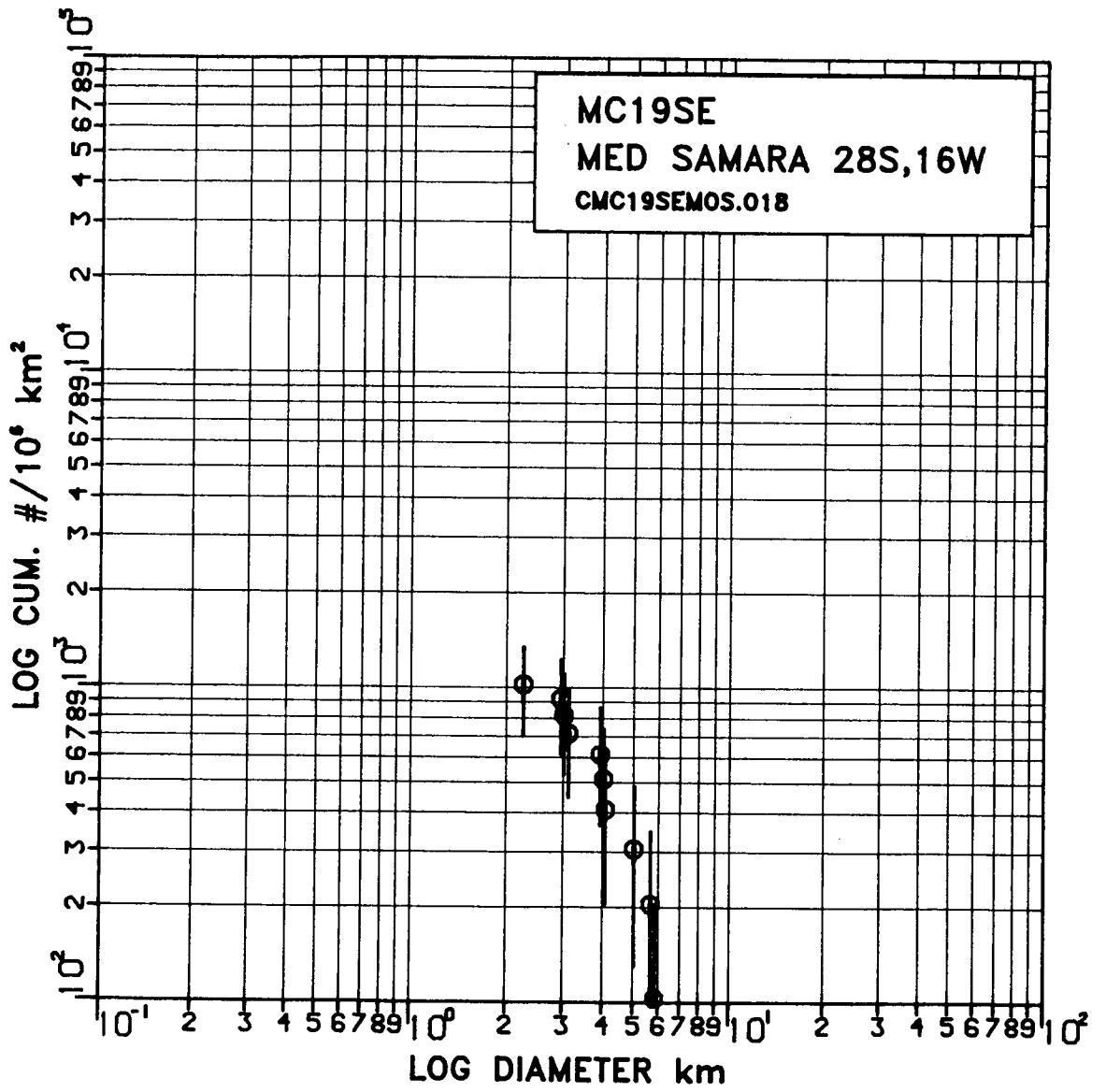


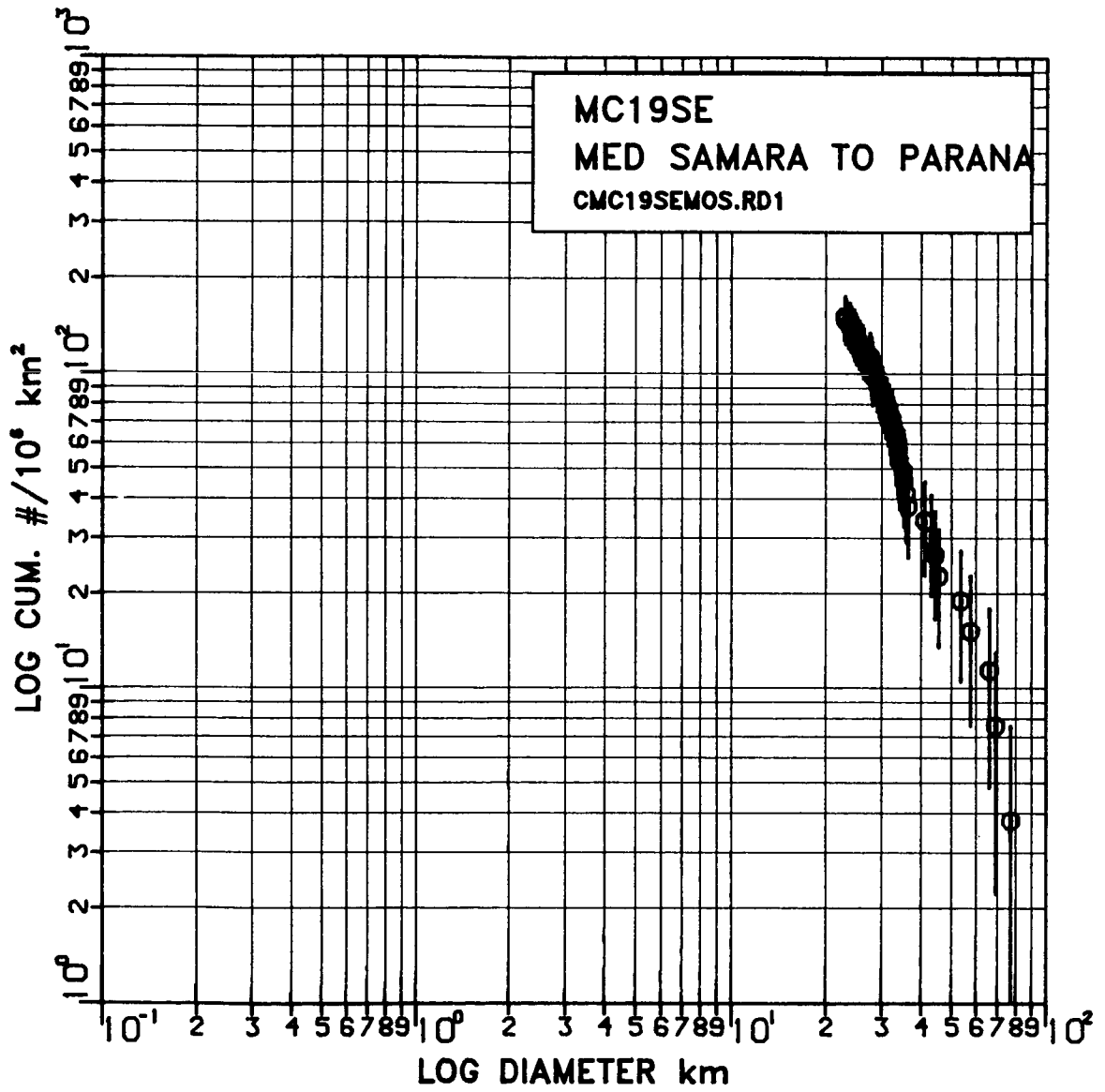


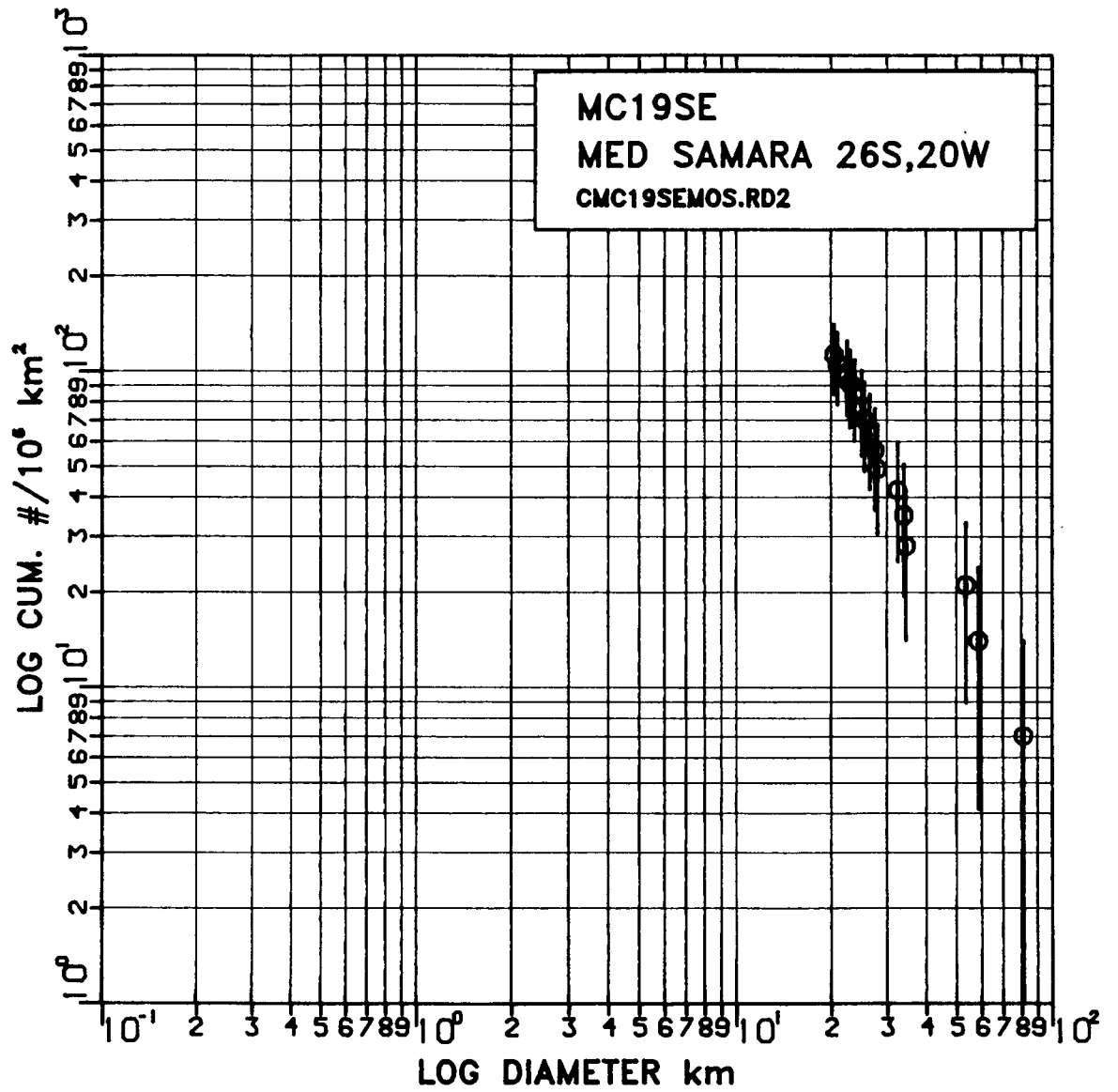


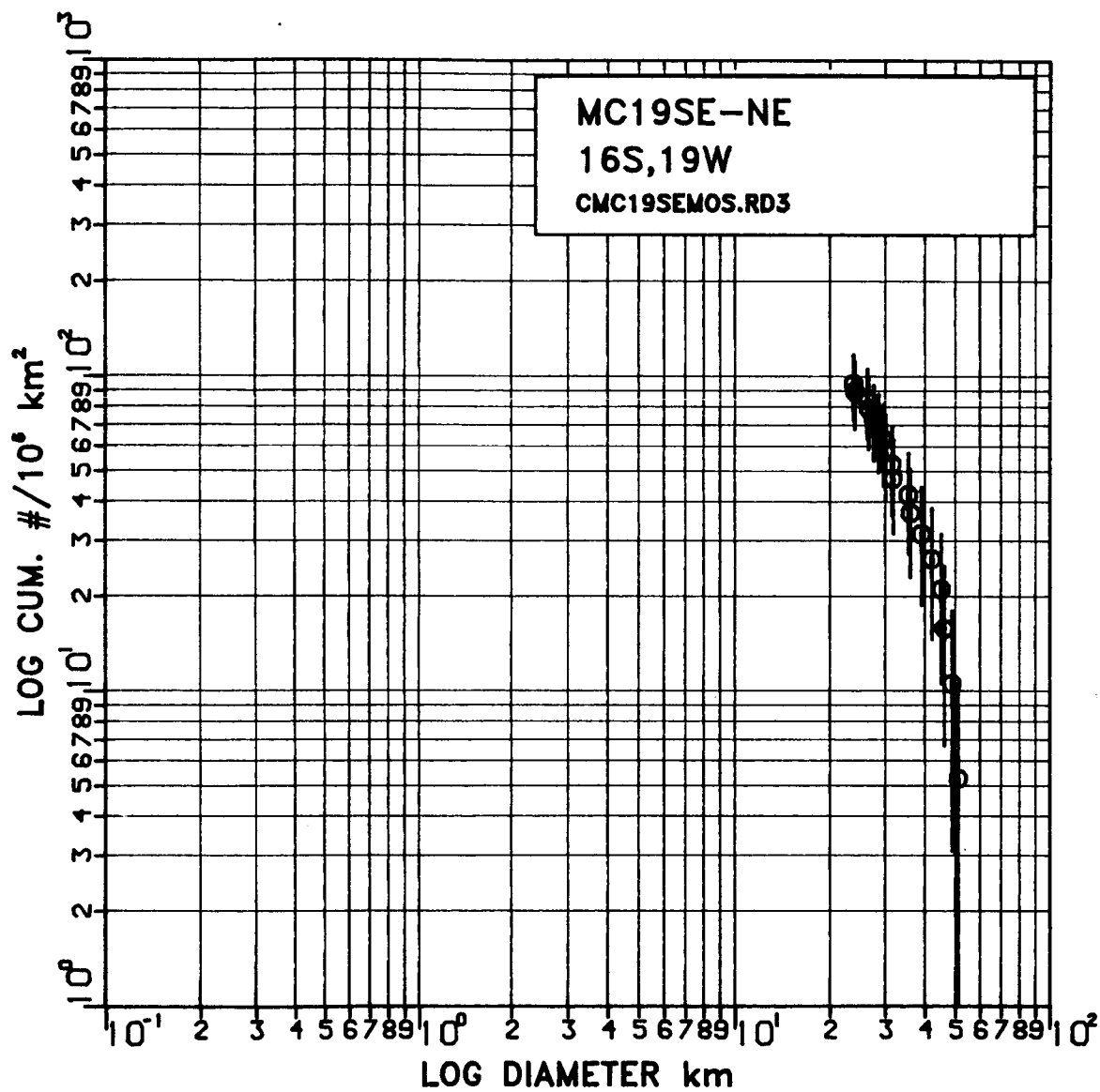












APPENDIX 4

STEREO PAIRS
USED FOR
DRAINAGE BASIN MAPPING

PRECEDING PAGE BLANK NOT FILMED

PAGE 262 INTENTIONALLY BLANK

Table 6 is a list of all stereo pairs used for drainage basin mapping. All images with >25% overlap are listed. The location given refers to the approximate center of overlap between two images. Footprints of images listed in Table 6 are given in Fig. 8. The number in () following an image number in Table 6 refers to the footprint number of that image in Fig. 8.

Table 6.-- STEREO PAIRS: images and location

(includes all images with >25% overlap)
 (* numbers in () refer to footprint locations in Fig. 26)

Stereo Pair		Location	
Image #	Image #	S Lat	W Long
MC19NW			
615A22 (7)	651A62 (3)	12	25
615A22 (7)	651A63 (10)	14.5	24
615A22 (7)	651A64 (6)	14	26
615A24 (8)	651A62 (3)	11	23
MC19NE			
451A06 (1)	451A08 (5)	4.5	18
451A06 (1)	651A83 (2)	5	20
451A08 (15)	651A83 (2)	5	20
451A08 (5)	651A85 (4)	8	18.5
615A23 (12)	651A88 (11)	14.5	21
615A24 (8)	651A62 (3)	13	22
615A24 (8)	651A88 (11)	12.5	21.5
651A25 (13)	651A87 (15)	14	18
651A25 (13)	651A88 (11)	14	19
651A26 (9)	651A85 (4)	10	19
615A26 (9)	651A87 (15)	12	18
651A27 (14)	651A87 (15)	12.5	10
MC19SW			
084A38 (31)	650A15 (32)	28	22.5
651A41 (25)	650A17 (22)	25	23
650A17 (22)	651A63 (23)	23	23
MC19SE			
084A38 (31)	650A22 (43)	29.5	22
084A38 (31)	084A40 (34)	27.5	21
084A39 (45)	084A41 (48)	29.5	18
084A39 (45)	650A15 (32)	29.5	20
084A40 (34)	084A42 (36)	27	18.5
084A40 (34)	650A15 (32)	27	19.5
084A40 (34)	615A62 (35)	27	19.5
084A40 (34)	651A70 (33)	27	18
084A41 (48)	579A42 (49)	29	15.5
084A41 (48)	615A61 (44)	29	18
084A41 (48)	615A63 (47)	29	16
084A41 (48)	650A15 (32)	28.5	18
084A41 (48)	651A69 (53)	28	15
084A41 (48)	651A70 (33)	28	17
084A41 (48)	651A72 (46)	29	16.5
084A42 (36)	615A43 (27)	24	18
084A42 (36)	615A62 (35)	26.5	18
084A42 (36)	651A67 (26)	24	18
084A42 (36)	651A69 (53)	26	16
084A42 (36)	651A70 (33)	26	18
084A43 (51)	579A42 (42)	28	14.5
084A43 (51)	615A63 (47)	28	14.5

Table 6.-- STEREO PAIRS (cont'd)

084A43 (51)	651A69 (53)	27	14
084A43 (51)	651A72 (46)	28.5	15
084A44 (38)	615A45 (28)	22.5	15
084A44 (38)	651A67 (26)	23.5	16
084A44 (38)	651A69 (53)	25	14.5
084A44 (38)	651A92 (24)	22.5	15
084A44 (38)	651A94 (56)	23.5	13.5
084A45 (52)	579A46 (54)	26	10
084A45 (52)	084A47 (25)	25	10
084A45 (52)	651A69 (53)	26	12
084A46 (40)	084A48 (42)	21.5	11.5
084A46 (40)	615A47 (29)	20.5	12
084A46 (40)	651A92 (24)	22	13.5
084A46 (40)	651A94 (56)	23	12
084A47 (57)	579A48 (55)	24.5	8
084A47 (57)	615A66 (39)	23.5	10.5
084A47 (57)	615A68 (41)	22.5	9
084A47 (57)	651A94 (56)	24.5	9.5
084A48 (42)	615A47 (29)	20	11
084A48 (42)	615A49 (30)	19	9
084A48 (42)	615A68 (41)	21	9
084A49 (58)	579A48 (55)	23.5	7
084A49 (58)	615A68 (41)	22	8
579A42 (49)	615A63 (47)	28.5	14.5
579A42 (49)	651A72 (46)	29.5	15
579A44 (50)	615A63 (47)	28	13.5
579A46 (54)	579A48 (55)	22.5	8.5
579A46 (54)	651A94 (56)	26	10
579A48 (55)	651A94 (56)	25	8.5
615A23 (12)	615A25 (13)	15.5	20.5
615A23 (12)	651A63 (23)	15.5	22
615A23 (12)	651A65 (17)	18	21
615A23 (12)	651A88 (11)	15	21
615A23 (12)	651A90 (19)	16.5	20
615A25 (13)	651A90 (19)	15.5	18.5
615A27 (14)	651A90 (19)	15	17.5
615A41 (25)	615A62 (35)	25.5	20.5
615A41 (25)	650A17 (22)	25	22.5
615A41 (25)	651A63 (23)	23.5	22
615A42 (16)	651A63 (23)	21	22
615A42 (16)	651A65 (17)	19.5	21.5
615A43 (27)	651A67 (26)	23	18.5
615A44 (18)	651A65 (17)	19	19
615A44 (18)	651A90 (19)	18	18.5
615A45 (28)	615A66 (39)	22	13
615A45 (28)	651A67 (26)	22	16
615A45 (28)	651A92 (24)	22.5	14
615A46 (20)	651A92 (24)	18.5	14.5
615A46 (20)	651A90 (19)	17	16.5
615A47 (29)	615A68 (41)	20.5	10.5
615A47 (29)	651A92 (24)	20.5	13
615A48 (21)	615A49 (30)	17	10
615A63 (47)	651A69 (53)	27	14.5

Table 6.-- STEREO PAIRS (cont'd)

615A63 (47)	651A72 (46)	29.5	15.5
615A64 (37)	651A69 (53)	25.5	15.5
615A66 (39)	615A68 (41)	22	11
615A66 (39)	651A92 (24)	22	13.5
615A66 (39)	651A69 (53)	24.5	13
615A68 (41)	651A94 (56)	23	9.5
650A15 (32)	651A72 (46)	29	18
651A65 (17)	651A90 (19)	18.5	19
651A67 (26)	651A92 (24)	22	16
651A69 (56)	579A44 (50)	27	12.5
651A69 (56)	579A46 (54)	27	11.5
651A69 (56)	651A94 (56)	26.5	12
651A88 (11)	651A90 (19)	15	19

MC26NE

084A39 (45)	650A22 (43)	31	19.5
084A39 (45)	615A61 (44)	30.5	19
084A39 (45)	651A72 (46)	31	17.5
084A41 (40)	615A61 (44)	30	17.5
579A24 (65)	579A26 (66)	34	9.5
579A26 (66)	651A71 (64)	32.5	9
579A41 (60)	579A43 (61)	31.5	13.5
579A41 (60)	651A72 (46)	32	15
579A43 (61)	579A45 (62)	31	10.5
579A43 (61)	650A23 (67)	32.5	12
579A43 (61)	651A71 (64)	31	12
579A43 (61)	651A72 (46)	31	13.5
579A45 (62)	651A72 (46)	30	4
615A61 (44)	650A22 (43)	31	20
650A23 (67)	579A24 (65)	34	11
650A23 (67)	650A24 (59)	35	14
650A23 (67)	579A26 (66)	34	8.5